Apoplast acidification in growing barley (*Hordeum vulgare* L.) leaves

Tamás Visnovitz (‘Okleveles Biológus’; MSc)

The thesis is submitted to University College Dublin in fulfilment of the requirements for the degree of Doctor of Philosophy

School of Biology and Environmental Science

Head of School: Prof. Thomas Bolger

Principal Supervisor: Dr Wieland Fricke

Members of the Doctoral Studies Panel: Dr Paul McCabe & Prof. Bruce Osborne

August 2011

Contents

Contents ii

List of figures v

List of tables viii

Abstract x

Statement of Original Authorship xi

Collaborations xii

Acknowledgements xiii

1 General Introduction - 1 -

1.1 Plant growth - 1 -

1.1.1 Plant cell expansion - 1 -

1.1.1.1 Cell wall - 1 -

1.1.1.2 Solutes - 3 -

1.1.1.3 Water - 4 -

1.1.2 pH conditions in the apoplast - 4 -

1.1.3 'Acid growth' theory - 5 -

1.1.3.1 'Acid growth' and effect of auxin and fusiccoccin on growth - 5 -

1.1.3.2 Experimental systems using coleoptiles - 6 -

1.1.3.3 Acid growth of coleoptiles - 6 -

1.1.3.4 Acid growth of dicotyledonous leaves - 8 -

1.1.3.5 Acid growth of roots - 9 -

1.1.4 Potassium uptake and 'acid growth' - 10 -

1.2 Plasma membrane H^+-ATPase - 11 -

1.2.1 Isoforms of PM-H^+-ATPase - 12 -

1.2.2 Structure of PM-H^+-ATPase - 14 -

1.2.3 Catalytic cycle of P-type ATPase and H^+ transport mechanism - 15 -

1.2.4 Control of PM-H^+-ATPase - 15 -

1.2.5 Fusicoccin-dependent PM-H^+-ATPase activation - 17 -

1.3 Barley - 18 -

1.3.1 The two weeks old barley seedlings and their advantage - 18 -

1.3.1.1 Morphology of developing barley leaves - 19 -

1.3.1.2 Anatomy of developing barley leaf - 20 -

1.3.2 Growth and potassium uptake of barley - 21 -

1.4 Technical approaches - 22 -

1.5 Objectives of the present study - 23 -

2 Materials and Methods - 24 -

2.1 Plant material - 24 -

2.1.1 Plant growth for study of leaves - 24 -

2.1.2 Plant growth for study of coleoptiles - 25 -

2.2 Apoplast pH measurements - 25 -

2.2.1 In-vitro gel system - 26 -

2.2.2 Microelectrode measurements - 27 -

2.3 Confocal microscopy - 29 -

2.3 LVDT measurements - 30 -

2.3.1 Leaf growth measurements - 30 -

2.3.2 Analysis of cell wall properties - 31 -

2.4 Expression analyses - 32 -
2.4.1 Plant harvest - 32 -
2.4.2 RNA extraction and cDNA synthesis - 33 -
2.4.3 PCR - 34 -
2.4.4 qPCR - 36 -
2.4.5 Analysis of qPCR data - 37 -

2.5 Cell size and tissue ratio measurements - 38 -
2.5.1 Mesophyll and epidermis cell size - 38 -
2.5.2 Tissue ratio calculation in elongation zone and emerged blade - 38 -
2.5.3 Cell size and plasma membrane surface estimation for qPCR analysis - 38 -

2.6 Plasma membrane isolation - 39 -
2.6.1 Plant harvest - 39 -
2.6.2 Preparation of microsomal fraction - 39 -
2.6.3 Purification of plasma membrane vesicles - 40 -

2.7 Determination of the total protein content of plasma membrane vesicles - 41 -
2.7.1 Bradford method - 41 -
2.7.2 Densitometric analysis of Laemmli gels - 41 -

2.8 Polyacrylamide gel electrophoresis (PAGE) - 42 -
2.8.1 Gradient polyacrylamide gel electrophoresis (PAGE) - 42 -
2.8.1.1 Solubilisation of membrane protein - 42 -
2.8.1.2 Gradient PAGE gel system - 43 -
2.8.2 Linear (12 %) PAGE - 45 -

2.9 ATPase assay - 45 -

2.10 Approach for light microscopy - 46 -
2.10.1 Fixation of leaf tissue - 46 -
2.10.2 Dehydration and embedding - 46 -
2.10.3 Staining with toluidine blue - 47 -

2.11 Immunological methods for PM-H$^+$-ATPase detection - 48 -
2.11.1 Qualitative Western blot analysis - 48 -
2.11.2 Quantitative Western blot analysis - 49 -
2.11.3 Immunostaining of paraffin-embedded sections - 50 -

2.11.4 Densitometric analysis of Western blots - 51 -

2.12 Protoplast experiments - 51 -
2.12.1 Protoplast isolation - 51 -
2.12.2 Purification of protoplasts - 52 -
2.12.3 Calculation of size and surface of the protoplast - 52 -

2.13 Statistical analysis - 52 -

3 Results - 53 -

3.1 Apoplastic pH measurements - 53 -
3.1.1 In-vitro agarose gel system - 53 -
3.1.2 Microelectrode measurements - 57 -
3.1.1 Confocal microscopy - 60 -

3.2 LVDT analyses of growth responses to treatments - 65 -
3.2.1 Leaf elongation under different treatments - 65 -
3.2.2 Cell wall changes in response to treatments - 69 -

3.3 Expression analysis of PM-H$^+$-ATPase using qPCR - 70 -
3.3.1 Quality control of the standard required for absolute qPCR - 71 -
3.3.2 Calculation of cell number and membrane surface - 72 -
3.3.3 Gene expression data based on absolute qPCR method - 74 -

3.4 PM-H$^+$-ATPase activity and expression at protein level - 77 -
3.4.1 Optimization of membrane isolation and ATPase assay - 78 -
3.4.1.1 Plasma membrane isolation - 78 -
3.4.1.2 Determination of total protein content in plasma membrane vesicles - 79 -

3.4.1.3 ATPase assay - 79 -
3.4.2 Quality of plasma membrane fractions - 81 -
3.4.3 Quantitative analysis of PM-H^+-ATPase protein - 82 -
3.4.4 Activity of PM-H^+-ATPase - 83 -
3.4.5 Immunolocalisation of PM-H^+-ATPase - 83 -

4 Discussion - 85 -

4.1 Growth-associated apoplast acidification - 85 -
4.1.1 Apoplast pH difference between growing and non-growing leaf tissue - 85 -
4.1.2 Reliability of pH values measured in elongation zone and emerged blade - 85 -
4.1.3 Relation between apoplast acidification and leaf growth - 86 -

4.2 K^+ and apoplast acidification - 87 -
4.2.1 Potassium uptake and leaf growth - 87 -
4.2.2 High affinity potassium transporters and leaf growth - 88 -

4.3 PM-H^+-ATPase expression and leaf elongation - 89 -
4.3.1 PM-H^+-ATPase density in plasma membrane and leaf growth - 90 -
4.3.2 qPCR data - 91 -
4.3.4 Immunolocalisation of PM-H^+-ATPase - 92 -

4.4 Leaf growth and changes in cell wall properties - 92 -

4.5 'Acid growth' in barley leaves? - 93 -

4.6 Model of leaf growth in barley - 93 -

5 Conclusions and future work - 97 -

5.1 Conclusions - 97 -

5.2 Future works - 98 -

6 Literature - 99 -

7 Appendix - 109 -

7.1 Processing of qPCR data - 109 -

7.2 List of chemicals - 115 -

List of figures

Figure 1.1 Model how expansins might interact with other wall components ..... - 3 -
Figure 1.2 Fusicoccin and auxin effect on maize coleoptiles..... - 7 -
Figure 1.3 Root elongation growth rate (REGR) and apoplast pH changes ..... - 9 -
Figure 1.4 Trajectory of a root element ..... - 10 -
Figure 1.5 Potassium transport dependency of abraded maize coleoptiles ..... - 11 -
Figure 1.6 Structure of AHA2 without auto-inhibitory domain..... - 14 -
Figure 1.7 Catalytic cycle and H^+ transport of PM-H^+-ATPase..... - 15 -
Figure 1.8 Auto-inhibition of PM-H^+-ATPase ..... - 17 -
Figure 1.9 14-3-3 protein-fusicoccin-PM-H^+-ATPase complex ..... - 18 -
Figure 1.10 Two-week old barley seedling ..... - 20 -
Figure 1.11 Toluidine blue stained cross section of barley leaves from different developmental stage ..... - 21 -
Figure 2.1 Leaf pieces in pH sensitive agarose gel medium ..... - 27 -
Figure 2.2 Measurement of cell wall properties..... - 32 -
Figure 2.3 Thermal profile of the two step PCR reactions..... - 35 -
Figure 2.4 Thermal profile of qPCR reactions ..... - 36 -
Figure 2.5 Five purification steps during plasma membrane isolation. ..... - 41 -
Figure 2.6 Typical gel for the measurement of protein content of plasma membrane samples..... - 42 -
Figure 2.7 Coomassie Brilliant Blue R250 stained gradient PAGE gels which were loaded with plasma membrane protein solubilised in two different ways ..... - 43 -
Figure 3.1 Leaf growth and apoplast acidification as analysed through the agarose gel system ..... - 54 -
Figure 3.2 Time course of growth and acidification of in-vitro gel experiments .... - 55 -
Figure 3.3 Leaf growth and acidification in agarose gel under cold treatment..... - 55 -
Figure 3.4 Average rate of leaf elongation (A) and medium acidification (B) in leaves exposed to fusicoccin, vanadate and caesium treatments as tested through the agarose gel system ..... - 56 -
Figure 3.5 Effect of auxin on leaf growth and medium acidification using the in-vitro gel system ..... - 57 -
Figure 3.6 Growth effect of auxin when applied in liquid medium..... - 57 -
Figure 3.7 Microelectrode analyses of apoplast pH in the elongation zone and emerged blade-portion of leaf three of barley..... - 58 -

Figure 3.8 Growth rate of leaf three in response to K^+-treatments during micro pH measurements. ..... - 59 -
Figure 3.9 Microelectrode pH analyses in the leaf elongation zone of barley in response to sodium orthovanadate and fusicoccin treatments..... - 60 -
Figure 3.10 Growth rate of leaf three of barley in response to vanadate and fusicoccin treatments as analysed through different approaches..... - 60 -
Figure 3.11 Confocal microscopic analysis of apoplastic pH using acridine orange fluoresce pH sensitive fluorescence dye ..... - 62 -
Figure 3.12 Confocal microscopic analysis of apoplastic pH using 5(6)carboxyfluorescein fluoresce pH sensitive fluorescence dye..... - 63 -
Figure 3.13 Carboxyfluorescein and acridine orange accumulation pattern in elongation zone and emerged blade ..... - 64 -
Figure 3.14 Effect of pH sensitive dyes on leaf growth rate ..... - 64 -
Figure 3.15 pH sensitivity of fluorochromes ..... - 65 -
Figure 3.16 Testing the responsiveness of the LVDT setup to treatments which were expected to increase (37 ℃) or stop growth (1 M Na Cl)..... - 66 -
Figure 3.17 The effect of test reagents in the apoplastic bathing medium on leaf growth as measured with the LVDT setup..... - 67 -
Figure 3.18 Potassium dependency of the leaf growth response to fusicoccin (5 µM) and vanadate (500 µM) ..... - 68 -
Figure 3.19 Auxin effect on leaf elongation growth..... - 68 -
Figure 3.20 Cell wall changes under different treatments ..... - 69 -
Figure 3.21 Growth rate before and in response to an additional applied force ... - 70 -
Figure 3.22 reference genes for qPCR experiments ..... - 71 -
Figure 3.23 Digital PCR pattern of external standard DNA ..... - 72 -
Figure 3.24 Representative cross sections used for determination of the contribution of different tissues and air space to total leaf volume..... - 73 -
Figure 3.25 Expression of PM-H^+-ATPase using absolute qPCR..... - 75 -
Figure 3.26 PM-H^+-ATPase expression using absolute qPCR and relating expression data to total plasma membrane surface area..... - 76 -
Figure 3.27 Comparison of molecular biological data using leaf tissues or mesophyll protoplasts..... - 77 -
Figure 3.28 Impact on the quality of PAGE separation of washing steps during plasma membrane isolation ..... - 78 -

Figure 3.29 Protein measurement in plasma membrane vesicles using two different methods ..... - 79 -
Figure 3.30 Typical ATPase assay ..... - 80 -
Figure 3.31 Kinetics of P_i detection assay ..... - 80 -
Figure 3.32 Coomassie stained SDS polyacrylamide gel and Western blot of plasma membrane proteins from different leaf regions ..... - 81 -
Figure 3.33 PM-H^+-ATPase ratio in total membrane protein ..... - 82 -
Figure 3.34 ATPase activity of inside-out plasma membrane vesicles ..... - 83 -
Figure 3.35 PM-H^+-ATPase immunolocalisation on leaf cross and longitudinal sections ..... - 84 -
Figure 4.1 Supposed effect of the treatments on barley leaf cells ..... - 95 -
Figure 4.2 Model of leaf elongation in barley leaves ..... - 96 -
Figure 7.1 Typical calibration curve for converting Ct values into transcript copy number ..... - 110 -

List of tables

Table 1.1 Localisation of specific PM-H^+-ATPase isoforms in plant body - 13 -

Table 2.1 Composition of the ½ strength Hoagland solution for barley seedlings - 25 -

Table 2.2 Composition of the pH sensor for microelectrodes - 28 -

Table 2.3 Composition of the buffer solutions used for calibrating pH microelectrodes - 29 -

Table 2.4 DNase treatment and reverse transcription - 34 -

Table 2.5 Components of PCR reactions - 35 -

Table 2.6 PCR primers - 35 -

Table 2.7 Composition of the stock solution (5x concentrated) of TRIS base boric acid EDTA buffer (TBA) - 35 -

Table 2.8 Components of qPCR reaction - 36 -

Table 2.9 Composition of the homogenisation buffer used for membrane isolation - 39 -

Table 2.10 Composition of the phase buffer used for membrane isolation - 40 -

Table 2.11 Composition of the resuspension buffer used for membrane isolation - 40 -

Table 2.12 Composition of Bradford reagent - 41 -

Table 2.13 Composition of Laemmli buffer used for PAGE - 43 -

Table 2.14 Components of the gradient PAGE system - 44 -

Table 2.15 Components of the solutions for Coomassie Brilliant Blue gel staining - 44 -

Table 2.16 ATPase reaction buffer and colour development reagent - 46 -

Table 2.17 Fixation and embedding of leaf samples for immunohistochemistry - 47 -

Table 2.18 Staining embedded leaf sections with toluidine blue - 47 -

Table 2.19 Composition of blotting buffer used for Western analyses - 48 -

Table 2.20 Composition of TRIS buffer saline buffer (TBS) - 49 -

Table 2.21 Composition of Tween®20 TRIS buffer saline buffer (TTBS) - 49 -

Table 2.22 Protocol for immunostaining of embedded leaf sections - 50 -

Table 2.23 Composition of phosphate buffer saline (PBS; pH 7.4) - 50 -

Table 2.24 Composition of protoplast isolation buffer - 51 -

Table 2.25 Enzyme concentrations in protoplast isolation buffer - 51 -

Table 3.1 Water content of two different regions of leaf three in two cultivars of barley - 72 -

Table 3.2 The contribution of different tissues to total leaf volume in the elongation zone (EZ) and emerged blade (EB) of leaf three of barley. - 73 -

Table 3.3 Cell size calculation based on the present and literature data. - 74 -

Table 3.4 Ct values of PM-H^+-ATPase expression together with RNA content per cell in the elongation zone (EZ) and emerged blade (EB) of leaf three of barley. - 75 -

Table 3.5 RNA content and PM-H^+-ATPase expression in the elongation zone (EZ) and emerged blade (EB) of leaf three of barley (Golf, Jersey). - 76 -

Table 4.1 Summary of data for PM-H^+-ATPase when related to surface area of plasma membrane. - 89 -

Table 7.1 Example for qPCR calculation of Golf cultivar. -112-

Table 7.2 Example for qPCR calculation of Jersey cultivar. -113-

Table 7.3 Example for qPCR calculation of Jersey protoplasts. -114-

Abstract

Apoplast acidification associated with growth is well-documented in roots, coleoptiles and internodes but not in leaves. In the present project on barley (*Hordeum vulgare* L.) advantage was taken of the high cuticle permeability in the elongation zone of leaves to measure apoplast pH and growth in response to application of test reagents. The role of the plasma membrane H^+-ATPase (PM-H^+-ATPase) and K^+ in this process was of particular interest. An in vitro gel system with bromocresol purple as pH indicator, pH microelectrodes and pH-sensitive fluorescence dye combined with confocal microscopy were used to monitor apoplast pH. Growth was measured in parallel or in separate experiments using a linear variable differential transformer (LVDT). Test reagents which blocked (vanadate) or stimulated (fusicoccin) PM-H^+-ATPase, or which reduced (NH_4^+, Cs^+, tetraethylammonium) K^+ uptake were applied. Plasma membranes were isolated from growing and mature leaf tissue and used to determine the activity (ATPase assay) and abundance (Western blotting) of PM-H^+-ATPase protein. Protein localisation was studied by immunohistochemistry and expression of mRNA quantified using real time PCR (qPCR). Apoplast pH was by up to 1.0 pH unit lower in growing compared to non-growing leaf tissue. Depending on the K^+ concentration in the bathing medium used during electrophysiological analyses, apoplast pH in the elongation zone ranged from pH 4.8 (0.1 mM K^+) to pH 5.8 (10 mM K^+). In the emerged blade, apoplast pH remained at about pH 5.8 irrespective of the K^+ concentration in the bathing medium Growth was more responsive to test reagents than to changes in apoplast pH. Expression of PM-H^+-ATPase was comparable between growing and non-growing leaf regions when expression was related to per unit extracted RNA or cell number. However, when expression was related to per unit surface area of plasma membrane, expression of PM-H^+-ATPase was about twice as high in growing compared to non-growing leaf tissue. The same applied to the protein level and activity of PM-H^+-ATPase. Immunohistochemical analyses showed that PM-H^+-ATPase was present in all living leaf tissues, particular in those (guard cells, phloem, and xylem parenchyma) associated with high rates of trans-membrane solute transport. It is concluded that leaf cell expansion in barley depends on the activity of the PM-H^+-ATPase and K^+ transport processes. The higher surface density of PM-H^+-ATPase activity in growing barley leaf tissue aids apoplast acidification and growth. A H^+ / K^+ co-transport system may play a key role in linking growth with apoplast pH, H^+ pump activity and K^+-uptake.

Statement of Original Authorship

I hereby certify that the submitted work is my own work, was completed while registered as candidate for the degree of Doctor of Philosophy, and I have not obtained a degree elsewhere on the basis of the research presented in this submitted work.

…….

Tamás Visnovitz

Collaborations

(i) pH measurements using pH microelectrodes were carried out under the supervision of Dr Anthony J. Miller at the Department of Plant Pathology and Microbiology of Rothamsted Research (Harpenden, Hertfordshire AL5 2JQ, UK). Towards the end of this project, Dr Miller moved to the John Innes Centre (Norwich Research Park, Colney, Norwich, NR4 7UH, UK), which is similar to Rothamsted Research a BBSRC (Biotechnology and Biological Sciences Research Council) funded institute.

(ii) Plasma membrane isolation, SDS PAGE, ATPase hydrolysis assays and part of the Western blot analysis was carried out in the laboratory of Dr Éva Sárvári and Dr Ilona Rácz with the help of Ádám Solti at the Department of Plant Physiology and Molecular Plant Biology, Institute of Biology, Faculty of Science, Eötvös Loránd University (Pázmány Péter sétány 1/C, Budapest, Hungary, H1117).

Acknowledgements

- First of all I want to thank my supervisor **Dr Wieland Fricke** for his expert guidance and advice in all aspect during the three years. He not just guided my steps in science, he gave the opportunity to plan my research workflow, experiments and test my own ideas.
- I would like to thank the help to everybody who worked with me in our research group **Matthieu Besse**, **Thorsten Knipfer**, **Mostefa Touati**, **Ehsan Bijanzadeh** and **Shimi Suku** who helped me a lot and we could spend great time in the lab together.
- Many thanks for the technical assistance and help to **Brendan**, **Eugen**, **Francis**, **Gwyneth**, **Eileen** (UCD), **Sue** (Rothamsted), **Györgyi** and **Zsuzsa** (ELTE). **Damian Egan** and **Eric Callaghan** helped me especially a lot, and special thanks to Eric for his critical reading of the thesis.
- I would like to thank **Prof. Jeremy C. Simpson** for access to the confocal microscopy unit and **Dr Gavin Stewart** and **Caragh Walpole** for their help with Western blotting at UCD.
- I never will forget the days in Rothamsted, thanks a million for **Dr Tony Miller** for his help in all aspect and I hope I will have the chance to work together in the future.
- At Eötvös University I had extremely big help from **Dr Éva Sárvári**, **Dr Ilona Rácz**, **Dr Szabolcs Rudnóy** and from **Prof. Zoltán Szigeti**. Without the guides of **Ádám Solti** the protein part of the work would not have been successful. **Dr György Csikós** helped a lot in immune histochemistry.
- Enormous thanks for my wife **Kriszti**. Without her help I would not able to finish this research and thesis. She was always with me when I was despondent and felt that I never will finish.
- Thank to all of my friends at UCD, Rothamsted and ELTE whose are not mentioned by name.
- Particular thanks to **IRCSET** (Irish Research Council for Science, Engineering and Technology) which made this PhD project possible through awarding me an EMBARK post-graduate fellowship.
- …és végül de nem utolsó sorban köszönöm a támogatást szüleimnek akik támogattak mindenben és elviselték, hogy Írországban éltem és doktoráltam.

1 General Introduction

1.1 Plant growth

Plant growth can be defined as an irreversible increase in the size of cells, tissues, organs or whole plants (Csiszár *et al.*, 2004). Cell expansion is generally considered to be caused by wall loosening and driven by turgor pressure (Christian et al., 2006). The term 'cell growth' mainly refers to the increase in size of proliferating cells in the cell cycle (meristematic cells), with increase in the total nucleic acid and protein content without vacuolization of the protoplast. In contrast, the term 'cell expansion' refers to the manifold increase in size of newly produced cells that is associated with the formation of a large central vacuole and finally leads to cell differentiation (Perrot-Rechenmann, 2010). While plants need to produce new cells to grow, it is cell expansion which leads to the physical increase in plant size and biomass.

1.1.1 Plant cell expansion

The enlargement of cells reflects increase in water content of cells. Irreversibility of this process is guaranteed by the plastic properties of the cell wall. From the biophysical view, plant cells need a wall which gives in to turgor pressure (mechanical driving force) and solutes which drive water uptake through osmosis. Therefore, cell expansion may be limited by the mechanical (yielding and extensibility) properties of the cell wall and the rate at which water and solutes are taken up or produced (solutes) by cells internally (Fricke & Flowers, 1998; Fricke & Peters, 2002).

1.1.1.1 Cell wall

It is a popular theory that expansion of leaf and root cells is controlled by cell wall properties. Based on the work of Green *et al*. (1971) on giant algae cells (*Nitella* sp.) and Lockhart's (1965) theoretical considerations, a growth model was developed which relates the growth rate (GR) to extensibility properties (m), yield threshold of cell wall where no cell expansion occurs (Y) and cell turgor (P):

$$GR = m \cdot (P-Y)$$

The impact of the mechanical properties of the cell wall for plant growth was found in many studies both in roots and shoots (Cosgrove, 1993; Pritchard, 1994; Cosgrove,

1998; Hsiao & Xu, 2000). The implication of these studies is that the rate of cell expansion, and therefore plant growth, may be regulated by altering the mechanical properties of the wall, making it 'softer' (more growth) or 'harder' (less growth). One way to alter wall properties is through changes in wall (apoplast) pH.

Acidification can affect growth through cell wall loosening (Rayle & Cleland, 1970) and different theories have been proposed to explain this phenomenon. One hypothesis suggested that H^+ directly affects non-covalent bonds between β-glucan within the cell wall, causing wall loosening (Hohl *et al.*, 1991). Another hypothesis suggested that due to H^+ excretion Ca^{2+} ions are displaced in the cell wall and that this leads to a more flexible cell wall (Arif & Newman, 1993). A breakthrough in our understanding of pH-related wall loosening came in 1992 when two proteins were extracted from cucumber hypocotyls which were capable of inducing extension in isolated, heat-inactivated cell walls of several plant species. These 'wall loosening' proteins were termed 'expansins'. The pH optimum of these proteins was pH3.5 - 4.5 (McQueen-Mason *et al.*, 1992) and this may explain at least in part why apoplast acidification increases the growth rate of plant organs.

Expansins are specifically expressed in growing tissues of monocotyledons and dicotyledonous plants. They are highly conserved in size and amino acid sequence (Cosgrove, 1996). However, studies on fescue suggest that another group of wall proteins, xyloglucan endotransglycosylases, may be more involved in regulation of cell expansion than expansins (Reidy *et al.*, 2001).

Expansins do not induce wall extension through simple polymer hydrolysis. They mainly disrupt hydrogen bonding not just in-vivo, in a paper sheet as well and reengineering the cell wall structure facilitating plant growth (McQueen-Mason, 1995). Promoting cell wall relaxation is necessary for expansion of plant cells (Cosgrove, 1993). An overview of expansin action is given in Fig. 1.1.

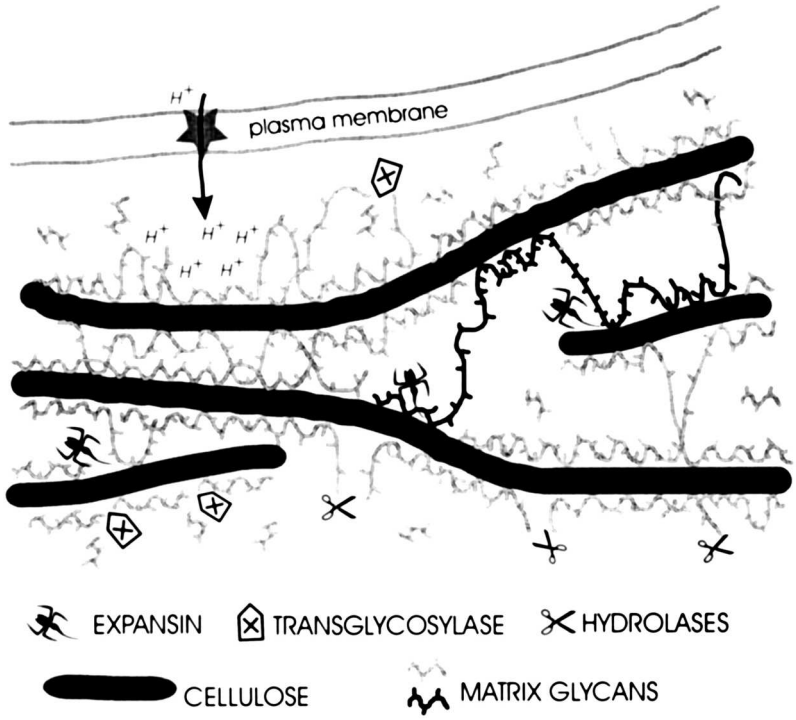

Figure 1.1 Model how expansins might interact with other wall components

Expansins might cause a transient release of short segments of matrix hemicelluloses glycans attached to cellulose microfibrils. Wall hydrolyses cut matrix glucans into shorter segments leading to weakening but not to creep of the cell wall. Transglycosylases are recombining glycans into shorter or longer pieces. PM-H^+-ATPases may lower the wall pH and control enzymes by their pH optima. Reprint from Cosgrove (1998) based on open access policy of www.plantphysiology.org with copyright American Society of Plant Biologists.

1.1.1.2 Solutes

Based on the original growth model described above (Lockhart, 1965; Green *et al.*, 1971), turgor pressure and solute uptake should have significant impact on cell expansion and growth. The availability of solutes seems to co-limit growth especially under water (Frensch, 1997; Hsiao *et al.*, 1998) and salt stress (Fricke & Peters, 2002).

Osmolality and turgor pressure change little along the elongation zone of cereal leaves (Fricke *et al.*, 1997; Fricke & Flowers, 1998; Martre *et al.*, 1999; Fricke, 2002a) and roots (Pritchard, 1994). The implication of a constant turgor pressure in expanding cells might be that cells instantly deposit solutes to maintain osmolality as the osmotic force driving water uptake while they expand and cell contents become diluted (Fricke, 2002a).

1.1.1.3 Water

In barley, it has been suggested that the rate of tissue-water transport might limit cell expansion in leaves (Fricke, 2002b). Similar conclusions have been made for soybean hypocotyls and maize leaves by the work of Boyer and colleagues who coined the term ‘growth-induced water potentials’ (Boyer, 2001; Tang & Boyer 2008). The mere existance of significant gradients in water potential between growing tissue and water source suggests that the conductance of the pathway between the two is limiting water transport. In a multi-layered tissue e.g. in roots, the radial hydraulic conductance can be one to three orders of magnitude larger under transpirating than under non-transpirating conditions (Steudle, 2000). Recent studies showed that in barley roots water uptake occurred along a pathway which involved crossing of membranes. It was not clear whether osmotic forces were sufficient to support water uptake (Knipfer & Fricke, 2011). Aquaporins have an essential role in the water transport at cellular level (Hachez *et al.* 2008). Aquaporins also may play essential role in elongation growth of barley leaves (Besse *at al.*, 2011).

1.1.2 pH conditions in the apoplast

The present analyses did not, or did little distinguish between cell wall space and apoplast. The latter also comprises intercellular spaces and middle lamellae. Therefore, and for simplicity, it is referred to ‘apoplast’ throughout the present work. The apoplast of higher plants occupies typically 5 % or less of the total tissue volume. This applies in particular to living tissues. The apoplast determines ionic conditions around the cells; it affects transport solutes into and out of cells, provides a diffusion barrier in speciliased cases (e.g. Casparian bands) and defines mechanical and osmotic conditions – conditions which may be or may not be compatible with cell expansion. The latter applies in particular to the pH of the apoplast. Using different methods (pH indicators in agar, microelectrodes and fluorescence probes) a huge variety in apoplast pH has been reported for roots of different plant species. Values ranged from pH 4.0 to pH 7.0 with most values being in the region pH 5.0 to pH 6.5 (Grignon & Sentenac, 1991). Dicotyledonous plants have generally a higher (less acidic) pH than monocotyledonous plants have, and apoplast pH is lower in gymno- compared to angiosperms (Grignon & Sentenac, 1991).

In fully developed barley leaves an apoplast pH of pH 5.0 was measured using microelectrodes (Felle, 2006). The pH varied in dependence of oxygen availability

(anoxia) (Felle, 2005; Felle *et al.*, 2005; Felle, 2006). Similar pH values have been reported for maize leaves using microelectrodes and fluorescence probes (Pitann *et al.*, 2009a; Ehlert *et al.*, 2011).

1.1.3 'Acid growth' theory

'Acid growth' originally was discovered by Bonner in 1934 when he described that the growth rate of *Avena* coleoptiles in pH 4.1 buffer was significantly higher than in pH 7.2 buffer (Kutschera, 1994). Later this effect was re-discovered and characterised in more detail by Rayle & Cleland (1970) and Hager *et al.*, (1971). Although in the literature 'acid growth' is mainly mentioned in relation to growth effects caused by the phytohormone auxin and the fungal toxin fusicoccin, which permanently activates PM-H^+-ATPase, linked plant growth, acid growth is a more general phenomenon and can be induced by other factors (Vesper & Evans, 1979). In 'acid growth', acid related cell 'wall-loosening' may constitute the initial event (Rayle & Cleland, 1970; Cosgrove, 1993). During the past decades, the 'acid growth' theory, or parts of the underlying mechanistic model, has been questioned repeatedly (Kutschera & Schopfer, 1985a; Kutschera, 1994; Grebe, 2005), However, with some limitation it is 'alive and well' (Lüthen *et al.*, 1990; Hager *et al.*, 1991; Rayle & Cleland, 1992; Kutschera, 2006). An alternative theory for 'acid growth' is the 'facilitated solute uptake' theory. This theory states that it is not the secreted H^+ which are causing directly the increased growth rate through alteration of wall properties, but that a proton-coupled transport mechanism across the plasma membrane is stimulated (Brummer *et al.*, 1984).

1.1.3.1 'Acid growth' and effect of auxin and fusiccoccin on growth

Almost at the same time, Darwin and Sachs proposed the theory that growth and development of plants is controlled by hormones (Darwin, 1880; Kutschera 1994). Using *Avena sativa* coleoptiles, Darwin, in 1880, showed that coleoptiles were bending towards the light source and once the tip of the coleoptiles was covered or cut, the coleoptiles were unable to produce this bending effect. In 1909, Fitting showed that coleoptile bending was a result of the non-homogeneous distribution of some factor, possibly a hormone (Katsumi, 2007). With gelatine cubes and glass pieces Boysen-Jensen (1913) proofed that this factor was transported from the tip to basal end of the coleoptile (Csiszár *et al.*, 2004). Paál (1918) could induce coleoptile bending without light, changing the orientation of coleotile tips (Paál, 1918; Csiszár *et*

al., 2004). Finally, in 1937, Went discovered the hormone (auxin) and showed that if the hormone was in gelatine cubes the tip was not necessary for coleoptile bending (Kutschera 1994). Heyn in 1940 proposed that auxin (in its physiological form indol acetic acid - IAA) promotes growth by enhancing cell wall extensibility. In 1934 and 1970 the 'acid growth' theory was born to explain auxin related plant growth (Kutschera, 1994). Fusicoccin, a phytotoxin of the fungus *Fusicoccum amygdale*, was discovered as 'super-auxin' a few years latter (Marré, 1979) and is still used today in many plant growth studies.

1.1.3.2 Experimental systems using coleoptiles

Coleoptiles of monocotyledon plants have widely been used as a model system to study plant growth. Coleptiles can be obtained on plants which need to grow for only a few days, are well characterised in terms of their phototropic or gravitropic response, show defined regions of growth and auxin production, are simple in anatomy and are easy to handle and cut. The main disadvantage, however, of coleoptiles is that their cuticle provides a permeance barrier to applied test reagents and diffusion barrier for protons and that this causes difficulties for applying treatments and measuring apoplastic pH (changes). In different laboratories this problem has been solved in different ways by peeling off part of the outer epidermis (Rayle, 1973), abrasion of coleoptiles with wet emery cloth prior to cutting (Kutschera & Schopfer, 1985a), abrasion with distilled water and SiC powder (Lüthen et al., 1990) or using dry polishing cloth for abrasion of coleoptiles before excision of segments (Schopfer, 1989). None of these methods were free from artefacts; however the results have been informative.

In most experiments, the incubation medium in which pH measurements were conducted was slightly buffered to prevent pH changes as a result of changes in CO_2 content of the atmosphere e.g. Rayle (1973); Stahlberg & Van Volkenburgh (1999) and Felle (2006). At the same time, the buffer capacity of the medium may affect pH measurements. Probably the best system for pH measurement was the method of ionostat (Döring *et al.*, 1996), because the incubation medium was not buffered and changes in H^+ efflux were measured rather than pH.

1.1.3.3 Acid growth of coleoptiles

Using maize coleoptiles, which were SiC-abraded in water and analysed using a computer controlled pH stat, both auxin and fusicoccin treatments affected growth in

a way which supported the ‘acid growth’ theory (Fig. 1.2). Neutral and alkaline solutions partly inhibited auxin- and fusicoccin-induced growth, whereas fusicoccin-induced growth under constant pH conditions. Fusicoccin and auxin did not show any additive effect (Lüthen *et al.*, 1990). Cell wall pH and growth rate were in close temporal correlation indicating co-regulation of apoplast solute composition (Peters *et al.*, 1998).

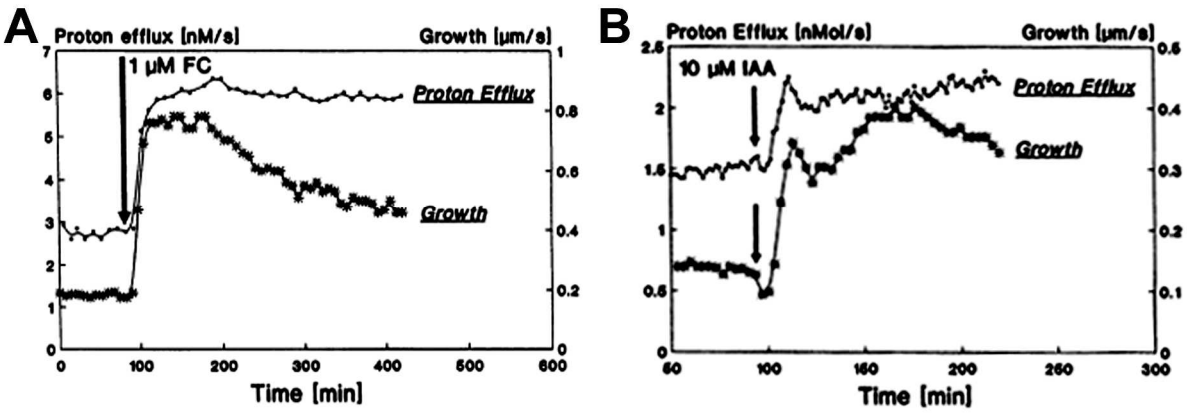

Figure 1.2 Fusicoccin and auxin effect on maize coleoptiles

Typical trace of fusicoccin (A) and auxin (IAA) effect (B). Dots represent the proton secretion while asterisks the coleoptiles growth rate. Experiments were carried out using SiC abraded maize coleoptile segments and a pH stat to maintain pH. Reprint from Lüthen *et al*. (1990) based on open access policy of www.plantphysiology.org with copyright American Society of Plant Biologists.

Other studies suggested that fusicoccin, but not auxin, caused ‘acid growth’. Using the wet emery cloth abrading technique and buffered incubation medium, fusicoccin-induced growth was totally inhibited by alkaline solutions (Kutschera & Schopfer, 1985b) while auxin-induced growth was not affected (Kutschera & Schopfer, 1985a). The difference between these and the above-mentioned results might have been caused by the experimental set ups. The abrading technique was different and the solution was buffered in case of Kutschera & Schopfer (1985ab), while Lüthen *at al*. (1990) could use unbuffered solutions. Difference in cation composition might have impacted too, with 10 mM KCl and 1 mM Ca^{2+} used by Lüthen *et al.* 1990), while Kutschera & Schopfer (1985ab) used Ca^{2+} in the incubation medium and K^{+} at minimal concentrations (discussed in Lüthen *et al*., 1990).

It is possible that extension growth of multi-tissue organs such as roots, coleoptiles and leaves is limited mechanically by the extension of one component tissue. This idea, which dates back to the 19th century (Kutschera, 1994), is proposed in particular for the epidermis of round, compact organs (containing little intercellular

air space) such as hypocotyls and coleoptiles. Therfore the wall of the epidermis may be important for growth, and it is possible that ‘acid growth’ may occur in all tissues of an organ or only in the epidermis or in all tissue but the epidermis. This could explain discrepancies in results obtained between researchers and for different organs and species. Peeling off just part of the epidermis of coleoptiles might cause immediately changes in growth conditions but also experimental artefacts (Kutschera, 1994). It was assumed that fusicoccin may interact with proton pumps of inner coleoptile tissues whereas auxin affects H^+ secretion of epidermal cells. Peeling off the epidermis caused 80 % less proton excretion of coleoptiles compared when coleoptiles were abraded with wet emery cloth (Kutschera *et al.*, 1987). These results are supported by immunolocalisation results. Fusicoccin sensitive plasma membrane H^+-ATPase (PM-H^+-ATPase) proton pumps were found mainly in mesophyll cells rather than in the epidermis (Villalba *et al.*, 1991); other authors, using electrophysiology, showed that auxin-induced H^+ pump activity did not depend on the presence of epidermal cells in maize coleoptiles (Peters *et al.*, 1992).

1.1.3.4 Acid growth of dicotyledonous leaves

The ‘acid growth’ theory has been tested much less in detail on dicotyledonous compared to monocotyledonous plants (coleoptiles) and the results in the literature are in part confusing. The validity of the acid growth theory appears to depend on the species tested. Light-induced leaf expansion of bean (*Phaseolus vulgaris*) and silver birch (*Betula pendula*) clearly showed an ‘acid growth’ type response. Apoplast pH decreased within 5 - 15 min of illumination, parallel to an increase in growth. Exogenous acidic buffer induced loosening of the cell wall and stimulated leaf growth whereas buffer at neutral pH inhibited growth. Fusicoccin stimulated both leaf growth and apoplast acidification (Van Volkenburgh & Cleland, 1980; Taylor & Davies, 1985; Cosgrove, 1996). In contrast, leaf expansion of sycamore (*Acer pseudoplatanus*) and tobacco (*Nicotiana tabacum*) could not be explained through ‘acid growth’. Apoplast acidification was not related to auxin-induced growth, yet fusicoccin-related ‘acid growth’ was present in tobacco leaves and independently of any auxin effect (Taylor & Davies, 1985; Keller & Van Volkenburgh, 1998). Growth related acidification in dicotyledonous leaves seems controlled by light and follows a partially independent pathway from photosynthesis as experiments with pea (*Pisum sativum*) leaves showed (Stahlberg & Van Volkenburgh, 1999). In tobacco leaves, some mechanistic link between light-stimulated leaf growth, H^+ excretion and K^+ uptake (Stiles *et al.*,

2003; Stiles & Van Volkenburgh, 2004) was observed. The role of K^+ could be to provide electrical counterbalance of H^+ rather than to provide an osmolyte for uptake (Stiles & Van Volkenburgh, 2004).

1.1.3.5 Acid growth of roots

Early results suggested auxin linked 'acid growth' in roots (Moloney *et al.*, 1981). However, more recent data showed that auxin increased growth of shoot and coleoptiles yet equally rapidly inhibited root growth (Christian *et al.*, 2006). Positive 'acid (pH 4.0) growth' has been not recorded in root elongation and at pH 3.5 organ elongation is reduced (Kutschera, 2006). In contrast with these results correlation was found between cell wall acidity and root elongation. Fusicoccin-induced H^+ efflux and growth rate of maize roots rather than auxin that reduced both H^+ efflux and root elongation (Lüthen & Böttger, 1988).

Using pH microelectrodes in the elongation zone of 4 day old maize primary roots a lower pH was recorded than in the non-growing zone when the pH was higher than pH 5.0 of the incubation medium (Fig. 1.3 and Fig. 1.4). Relative elemental growth rate and surface acidity were eliminated by auxin and cyanide treatments, respectively (Fig. 1.3) (Peters & Felle, 1999; Peters, 2004).

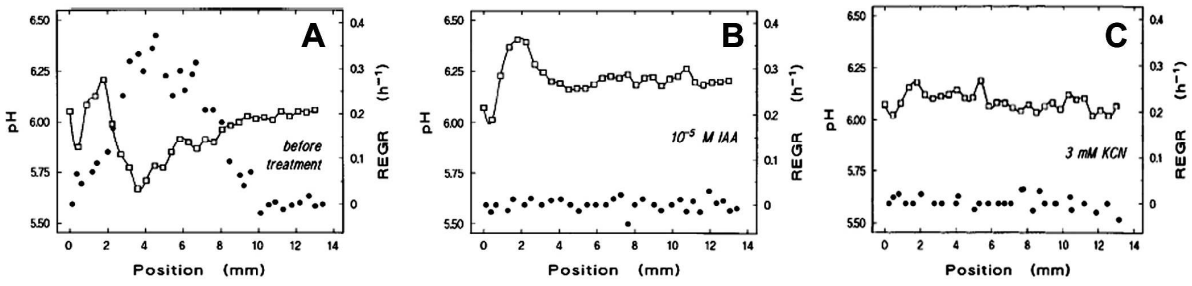

Figure 1.3 Root elongation growth rate (REGR) and apoplast pH changes

Profile of surface pH (□) and REGR (•) along the apical 12 mm of a growing maize root measured in pH 6.75 medium (A) and after 10 µM IAA treatment (B) or 3 mM KCN treatment (C). Position 0 refers to the tip of the root cap. Reprint from Peters & Felle (1999) based on open access policy of www.plantphysiology.org with copyright American Society of Plant Biologists.

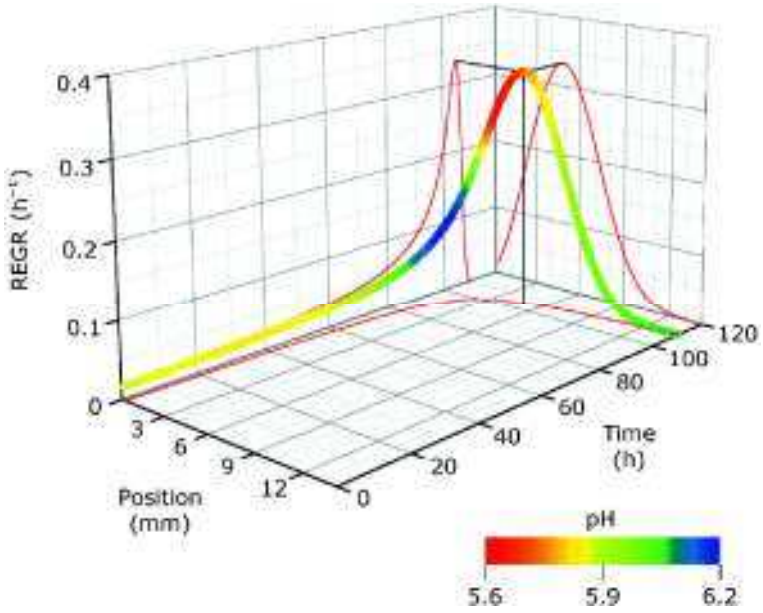

Figure 1.4 Trajectory of a root element

The figure shows the relation of the parameter time, position on the root, relative elemental growth rate (REGR) and surface pH (colour-coded) in growing maize root. The element considered is located at 0.2 mm above root apex at 0 time point. Reprint from Peters (2004) with the permission of the publisher (Licence No: 2693010825600, 'John Wiley and Sons')

Amtmann *et al.*, (1999) using different experimental systems had similar results on barley roots. They found that H^+ excretion could have crucial role in activation of inward K^+ channels. Changes in cytosolic pH and K^+ might be significant factors which contribute to the root growth response to changes in K^+ supply.

1.1.4 Potassium uptake and 'acid growth'

Potassium is the main inorganic solute used by most plant cells to generate osmotic pressure. Its cytosolic concentration is tightly regulated. Therefore, one would expect that changes in the PM-H^+-ATPase pump activity affect growth not only through changes in wall properties, but also through changes in K^+ uptake. Recent data show that 'acid growth' and K^+ uptake are related processes. Auxin and fusicoccin-induced growth was not present in absence of K^+ (Claussen *et al.*, 1997; Tode & Lüthen, 2001).

Claussen *et al.* in 1997 observed for abraded maize coleoptiles that auxin-induced growth and K^+ uptake were related processes. For auxin-induced growth the K^+ concentration in the medium was essential. In absence of K^+ an effect of auxin on growth was not observed, whereas when K^+ was added to the medium, auxin-related growth was immediately measured. The K^+ channel blocker triethylammonium (TEA)

also suppressed the growth response to auxin, and when the blocker was removed, growth recovered as shown in Fig. 1.5 (Claussen *et al.*, 1997). In a related study, a similar K^+-dependency was observed for fusicoccin-induced growth (Tode & Lüthen, 2001).

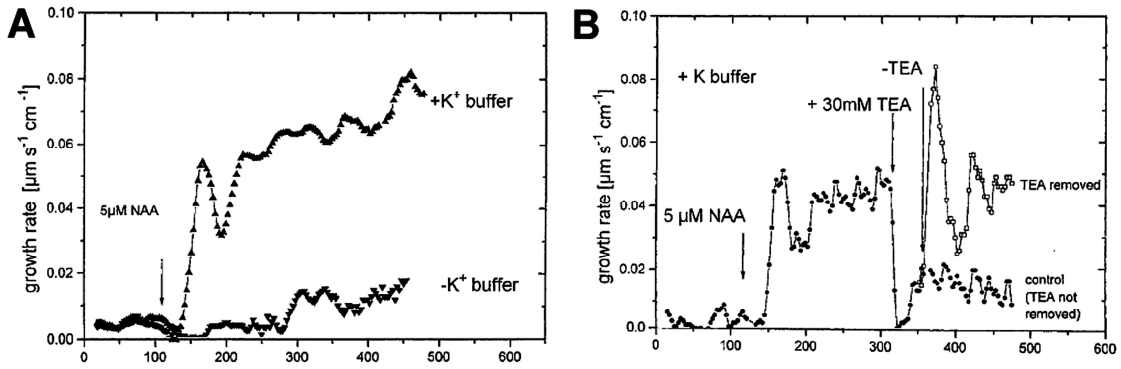

Figure 1.5 Potassium transport dependency of abraded maize coleoptiles

Potassium dependency of growth of coleoptiles was tested using a medium which contained 10 mM K^+ or no added K^+ (A). TEA, a K^+ channel blocker, inhibited auxin-induced growth; the blockage was completely reversible (B). When TEA was removed and replaced by incubation medium containing 10 mM K^+ and NAA, the growth rate recovered at the level before TEA treatment. Reprint from Claussen *et al.* (1997) with the permission of the publisher (Licence No: 2693030934022, 'Springer')

ZMK1 and ZMK2 K^+ channels genes from maize were tested from the viewpoint of coleoptile growth. ZMK1 seemed to be growth related, acidification immediately increased channel activity and auxin increased its expression but acidic pH did not changed the expression pattern (Philippar *et al.,* 1999). Over- expression of ZMK1 leads to K^+ independent growth (Philippar *et al.*, 2006). Similar results have been obtained for the *Arabidopsis* K^+ channel AtKAT1 in growing hypocotyl and flower stalk (Philippar *et al.*, 2004).

1.2 Plasma membrane H^+-ATPase

Plasma membrane H^+-ATPase (PM-H^+-ATPase) was first discovered in 1946 when acid dependent glucose transport was described during the fermentation of the yeast *Saccharomyces cerevisiae* (Conway & O'Malley, 1946). Cyanide and sodium azide caused plasma membrane potential decreases in *Neurospora crassa* within seconds, which also suggested an ATP-dependent H^+ pump activity (Slayman, 1965). The enzyme from fungi *Schizosaccharomyces pombe* and *S. cerevisiae* was isolated and shown to be a proton-pumping ATPase creating -150 to -300 mV plasma membrane potential in plants and fungi (Morth *et al.*, 2011).

PM-H^+-ATPase is a single polypeptide with a molecular mass of ~ 100kDa (Michelet & Boutry, 1995). ATPase activity is usually between 1 - 2 μmol P_i min^{-1} mg^{-1} in purified plasma membrane (Morsomme & Boutry, 2000). The enzyme is essential for living plant cells as it constitutes, to the best of our current knowledge, the primary ion pump which generates the electrochemical potential across the plasma membrane. This electrochemical gradient is responsible for ionotropic signalling, secondary transport, nutrient uptake, pH homeostasis, salt tolerance, stomatal and leaf movements and cell growth (Palmgren, 2001; Moran, 2007; Duby & Boutry, 2009). The PM-H^+-ATPase protein is a member of the family of P-type ATPases. Other members of this family include the Na^+,K^+-ATPase, the principal ion pump in animals and humans (Morth *et al.*, 2011).

1.2.1 Isoforms of PM-H^+-ATPase

Using the model plant *Arabidopsis thaliana* twelve PM-H^+-ATPase isoforms were identified from the genome (AHA1-12). The AHA12 isoforms carries two large deletions and is possibly a pseudogene (Palmgren, 2001). AHA1 and AHA2 are virtually expressed in all tissues and organs and function as housekeeping gene (Gaxiola *et al.*, 2007) while other PM-H^+-ATPase isoforms show some tissue specificity of expression (Morsomme & Boutry, 2000; Palmgren, 2001; Gaxiola *et al.*, 2007). Tissue-specific localization of PM-H^+-ATPase is summarised in Table 1.1, based on information provided in (Palmgren, 2001).

There is only one isoform of PM-H^+-ATPase known in full detail for barley (*Hordeum vulgare*) based on nucleotide and protein data bases (NCBI, http://www.ncbi.nlm.nih.gov/ and UniProt http://www.uniprot.org/). However, MS / MS results suggest that there exist at least two different PM-H^+-ATPase isoforms in barley (Hynek *et al.*, 2006).

Table 1.1 Localisation of specific PM-H^+-ATPase isoforms in plant body (Palmgren, 2001)

Tissue	PM-ATPase protein	Plant
Seedlings:		
Cotyledon	PMA1, PMA2, PMA4	*N. plumbaginifolia*
Primary root	PMA1, PMA4	*N. plumbaginifolia*
Root:		
Cortex parenchyma	PMA2, PMA3, PMA4	*N. plumbaginifolia*
Extension zone	PMA4	*N. plumbaginifolia*
Lateral root initials	PMA2, PMA4	*N. plumbaginifolia*
Lateral roots	PMA4, PMA9	*N. plumbaginifolia*
Root hair and epidermis	PMA1, PMA3, PMA4 MHA2	*N. plumbaginifolia* *Zea mays*
Root cap	PMA2, PMA4	*N. plumbaginifolia*
Stele (central cylinder)	PMA2, PMA3, PMA4	*N. plumbaginifolia*
Stem:		
Axillary buds	PMA2, PMA4, PMA9	*N. plumbaginifolia*
Cortex parenchyma	PMA1, PMA2, PMA4	*N. plumbaginifolia*
Pith	PMA4	*N. plumbaginifolia*
Vascular tissue	PMA2, PMA3, PMA4, PMA9	*N. plumbaginifolia*
	MHA2	*Zea mays*
	AHA3	*A. thaliana*
Leaf:		
Guard cells	PMA2, PMA4	*N. plumbaginifolia*
	VHA1, VHA2	*Vicia faba*
	MHA2	*Zea mays*
Mesophyll	PMA2, PMA4	*N. plumbaginifolia*
	VHA1, VHA2	*Vicia faba*
Trichomes (long)	PMA4	*N. plumbaginifolia*
Trichomes (short)	PMA6	*N. plumbaginifolia*
Vascular tissue	PMA2, PMA3, PMA4	*N. plumbaginifolia*
	MHA2	*Zea mays*
	AHA3	*A. thaliana*
Flower:		
Carpel	PMA2	*N. plumbaginifolia*
Ovules	PMA1, PMA2, PMA3, PMA4, PMA6, PMA9	*N. plumbaginifolia*
	AHA3, AHA10	*A. thaliana*
Nectaries	PMA2	*N. plumbaginifolia*
Stamen; pollen	PMA1, PMA2, PMA3, PMA4, PMA6, PMA6	*N. plumbaginifolia*
	AHA3, AHA9	*A. thaliana*
Style	PMA1, PMA3, PMA4	*N. plumbaginifolia*
Vascular tissue	PMA1, PMA2, PMA3, PMA4, PMA6	*N. plumbaginifolia*
	AHA3	*A. thaliana*

1.2.2 Structure of PM-H$^+$-ATPase

The crystal structure of AHA2, a PM-H$^+$-ATPase from *Ababidopsis thaliana*, has recently been described (Fig. 1.6). The protein contains a transmembrane domain with ten helices (M1-10) and three cytosolic domains: a nucleotide-binding domain (N), a phosphorylation domain (P) and an actuator domain (A). ATP is bound with the adenosine part at the N domain and its triphosphate group protruded towards the P domain. ATPase binding site was determined using 5'-(β,γ-methlene)-triphosphate (AMPPCP) a non-hydrolysable analogue of ATP (Pedersen *et al.*, 2007).

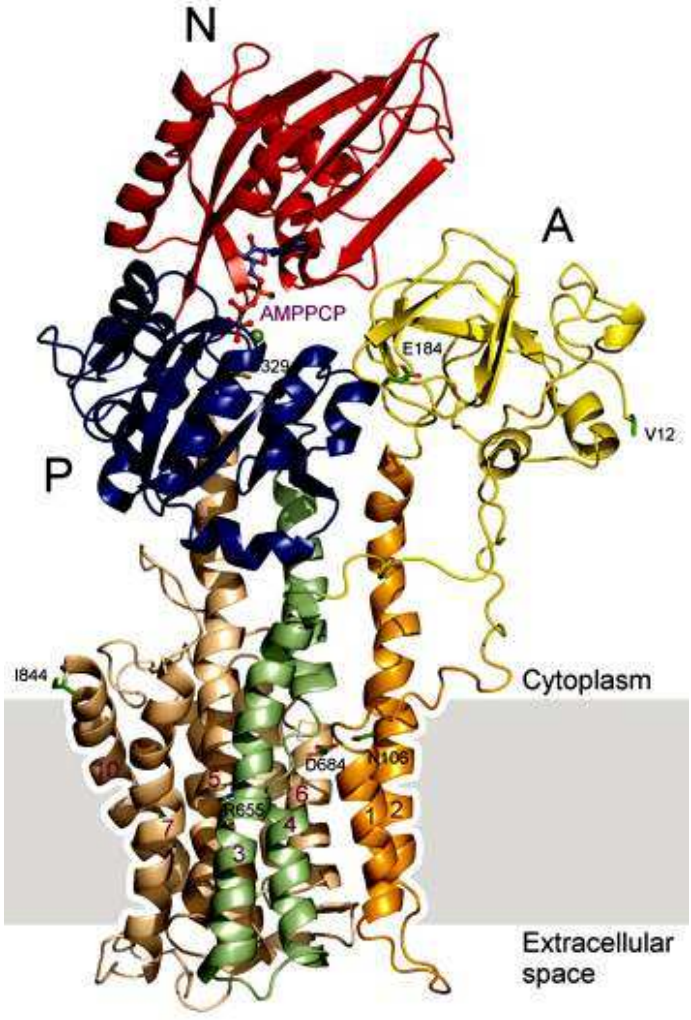

Figure 1.6 Structure of AHA2 without auto-inhibitory domain

AHA2 contains ten transmembrane helices (orange, green and brown); a nucleotide binding domain (N), red; a phosphorylation domain (P), blue; and an actuator domain (A); yellow. AMPPCP is shown as ball-and stick representation. The grey box represents the location of the plasma membrane; reprinted from Pedersen *et al.* (2007) with the permission of the publisher (Licence No: 2693040963163, 'Nature Publishing Group').

1.2.3 Catalytic cycle of P-type ATPase and H^+ transport mechanism

PM-H^+-ATPase undergoes conformational changes during each catalytic cycle. The enzyme has two distinct conformational states termed E1 and E2. The two conformation states differ in reactivity at the nucleotide binding site, which can be phosphorylated by ATP in the E1 form or by free P_i in the E2 form. E1 is the form that binds ATP and H^+. The catalytic cycle is shown in details in Fig 1.7 (Morsomme & Boutry, 2000; Pedersen *et al.*, 2007).

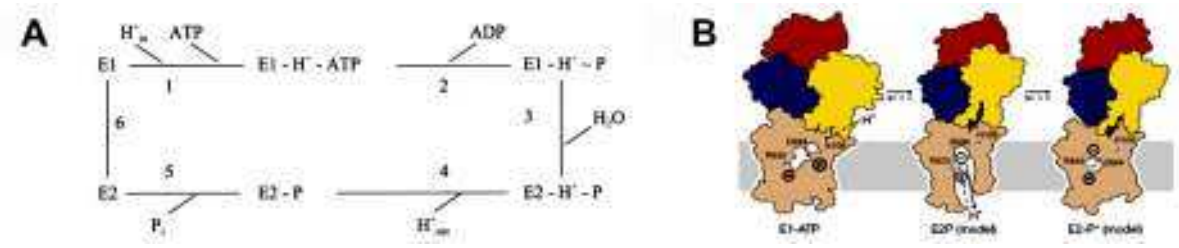

Figure 1.7 Catalytic cycle and H^+ transport of PM-H^+-ATPase

Originally the catalytic cycle was proposed for Ca^{2+} ATPase (subfigure A) E1 form binding ATP and H^+ (1), then a high energy intermediate is formed while ADP is released (2). Conformation of the enzyme is changing from E1 to E2 (3). Proton release to cell exterior (4), finally P_i is released (5) and conformation of the enzyme returning to form E1 (Morsomme & Boutry, 2000). The E1 form binds H^+ and ATP better than the E2 binds these substances, as subfigure B shows; reprinted from Pedersen et al. (2007) with the permission of the publisher (Licence No: 2693040963163, 'Nature Publishing Group').

1.2.4 Control of PM-H^+-ATPase

Activity of PM-H^+-ATPase is modulated by several physiological signals (such as temperature and salt stress). In comparison, there exists little evidence of a regulation of PM-H^+-ATPase activity through changes at the transcriptional or protein level. Moderate PM-H^+-ATPase expression changes have been describe for high aluminium treatment, (Shen *et al.*, 2005), iron deficiency (Santi *et al.*, 2005), in presence of high sugar concentration (Mito *et al.*, 1996) and high salt treatment (Maathuis *et al.*, 2003) .

Higher (compared to the 'average' tissue) PM-H^+-ATPase protein concentrations have been found in guard cells, root epidermis, phloem xylem parenchymas (Bouche-Pillon *et al.*, 1994; Michelet & Boutry, 1995; Morsomme & Boutry, 2000; Palmgren, 2001; Gaxiola *et al.*, 2007) and motor organs of seismonastic plants (Fleurat-Lessard *et al.*, 1997; Moran, 2007).

Regulated exocytosis of vesicles that contains PM-H^+-ATPase molecules constitutes an alternative regulation pathway (Hager *et al.*, 1991), yet post-

translational modification of the enzyme seem the most common control mechanism for causing changes in PM-H^+-ATPase activity (Gaxiola *et al.*, 2007).

Phosphorylation / dephosphorylation are further mechanisms through which PM-H^+-ATPase can be regulated. Elicitor-induced dephosphorylation in tomato plants (*Lycopersicon esculentum*) resulted in an increase in PM-H^+-ATPase activity (Vera-Estrella *et al.*, 1994) while subsequent phosphorylation of the enzyme reduced its activity; although Ca^{2+}-dependent phosphorylation caused decreased H^+ pumping activity. Phosphorylation also activates PM-H^+-ATPase activity through the fusicoccin (and 14-3-3 protein) activation pathway (Morsomme & Boutry, 2000).

The C-terminal auto-inhibitor regulation domain (R) could be mainly responsible for rapid activity changes of PM-H^+-ATPase. Removal of the R domain from the enzyme by trypsin digestion activated PM-H^+-ATPase (Palmgren *et al.*, 1991). Structural information of molecular mechanism of the auto-inhibition is not available yet. In AHA2 neutralisation of the auto-inhibitory R domain by binding of 14-3-3 protein results in pump activation. Before the activation process, the penultimate Thr947 needs to be phosphorylated by a protein kinase which is induced by environmental factors such as light, nutrient status and pathogens. This phosphorylation can lead to the binding of 14-3-3 protein on the R domain complex. The Thr947 is not freely accessible to protein kinase activity, structural modification is necessary by ligand binding or kinase docking. Phosphorylation of Ser931 inhibits PM-H^+-ATPase and destroys the 14-3-3 protein binding site (Sze *et al.*, 1999; Morth *et al.*, 2011). It seems that phosphorylation of most residues within the C-terminal domain impacts on 14-3-3 binding. The enzyme regulation is controlled by distinct protein kinases and phosphatases allowing gradual increase and decrease of the activity of PM-H^+-ATPase (Speth *et al.*, 2010). More details are provided in Fig. 1.8.

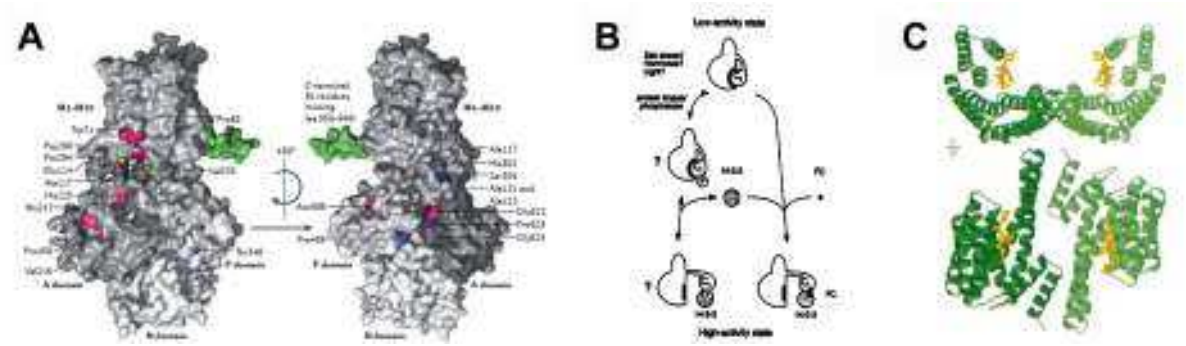

Figure 1.8 Auto-inhibition of PM-H$^+$-ATPase

On subfigure A residues are highlighted on the PM-H$^+$-ATPase (AHA2) that interact with the regulatory domain. Blue: present in yeast; red: present in plant; yellow: present in plant Ca^{2+}-ATPase.; green: 13 residue carboxy-terminal extension. Plant and fungal sites do not overlap, and it is likely that their pumps are inhibited by different mechanisms (Morth *et al.*, 2011). B: schematic summary of protein kinase/phosphatise-dependent and fusicoccin-dependent activation pathway of PM-H$^+$-ATPase. Subfigure C shows the ribbon plot of different orientation of dimeric tobacco 14-3-3c protein (green) bound to the C-terminal end (yellow) of PMA2 (tobacco PM-H$^+$-ATPase) (Würtele *et al.*, 2003). Figures are reprint from Morth *et al.* (2011) with the permission of the publisher, Licence No: 2693050346303, 'Nature Publishing Group' (A); Sze *et al.* (1999) based on open access policy of www.plantcell.org with copyright American Society of Plant Biologists (B) and Würtele *et al.* (2003) with the permission of the publisher, Licence No: 2693070537163, 'Nature Publishing Group' (C).

1.2.5 Fusicoccin-dependent PM-H$^+$-ATPase activation

Fusicoccin (a diterpene glycoside) is a phytotoxin, produced by the fungus *Fusicoccum amygdali*. The fungus is host specific, but isolated fusicoccin causes higher H^+ efflux in any higher plant tested so far (Marré, 1979). Recent structural studies show that fusicoccin is increasing H^+ pump activity by stabilising the interaction between 14-3-3 protein and auto-inhibitor R domain of PM-H$^+$-ATPase. Fusicoccin effective due binding its plasma membrane receptor (Olivari *et al.*, 1998) that is on the C-terminal of the R-domain of the PM-H$^+$-ATPase (Johansson *et al.*, 1993). This results in permanent binding of 14-3-3 protein to the regulation domain (Oecking *et al.*, 1994) and activates PM-H$^+$-ATPase permanently as shown in Fig. 1.8.

The toxin causes no major conformation changes; it fills a cavity between 14-3-3 protein and PM-H$^+$-ATPase (Fig. 1.9) and increases the stability of the complex about 90-fold (Würtele *et al.*, 2003).

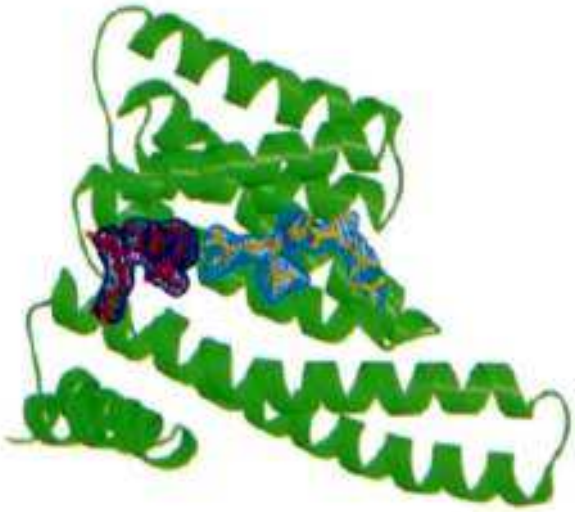

Figure 1.9 14-3-3 protein-fusicoccin-PM-H$^+$-ATPase complex

Ribbon diagram of a 14-3-3 protein monomer (green) with PM-H$^+$-ATPase peptide (yellow) and fusicoccin (orange). Blue represent the Van der Waals space of fusicoccin and PM-H$^+$-ATPase peptide (reprint from Würtele *et al.* (2003) with the permission of the publisher, Licence No: 2693070537163, 'Nature Publishing Group')

1.3 Barley

Barley (*Hordeum vulgare*) was domesticated 10,000 years ago and ranks fourth among cereals after maize (*Zea mays*), rice (*Oryza sativa*) and wheat (*Triticum aestivium*) in terms of global production. About two-thirds of the annual global barley production is used for animal feeding and the remaining third covers the needs of malting, brewing (beer) and distilling (whiskey) industries (Schulte *et al.*, 2009). The average annual production of barley in the world is about $1.24 \cdot 10^{11}$ kg and 62 % of this is harvested in Europe. The highest yield per hectar occurs in Ireland with 5.7 Mg ha^{-1} (Kim & Dale, 2004). In Ireland and Scotland brewing and distilling has a particularly big economic impact, not least because of the whiskey industry.

1.3.1 The two weeks old barley seedlings and their advantage

Barley seedlings at a developmental stage of two weeks old (between 14 - 17 days) present ideal research objects for leaf growth studies. At this stage leaf three is the main growing leaf and shows maximum or near-maximum growth rate (2 - 3 mm h^{-1}). Older leaves, which cause self-shading and reduce the potential biomass increase have not developed yet and younger seedlings are not yet fully dependent on the external medium for supply of mineral nutrients but still receive a considerable portion through seed reserves. The base 40 mm of leaf three that contains the leaf

elongation zone is enclosed by the sheath of the older leaves one and two (Fricke & Flowers, 1998; Fricke, 2002a). There are small quantities of cuticle waxes deposited on the epidermal surface along the base 20 - 30 mm of the elongation zone. This means that the permeance of the cuticle is much higher in the elongation zone compared to the emerged blade, which makes external application of test reagents to measurements of proton extrusion from the leaf apoplast comparatively easy without having to mechanically remove the cuticle (Richardson *et al.*, 2007).

1.3.1.1 Morphology of developing barley leaves

Barley leaves consist of two parts, the basal sheath and the leaf blade, separated by ligule and auricle. The sheath at the leaf base mechanically supports the blade which is the photosynthetic and transpirating active part of the leaf. The sheath also encloses the basal apical meristem, and any younger leaves emerge from within sheaths of older leaves. Leaves develop from the main meristem, which is located at the base. As a consequence, oldest tissues are at the leaf tip and youngest ones near the leaf base. The elongation zone of leaf three stretches to about 40 mm from the point of leaf insertion (‘leaf base’), with highest relative elemental growth rates between 10 - 30 mm (Fricke & Peters, 2002). In the elongation zone cells are elongating manyfold in size. Above the elongation zone is a zone which can be referred to as ‘non-elongation zone’. This zone extends to the point of emergence of the developing leaf from the sheath of leaf two and contains cells which are not elongating any more but can show some lateral expansion. The fully emerged leaf blade contains fully-differentiated cells, which are not dividing or expanding any more. Details are provided in Fig. 1.10.

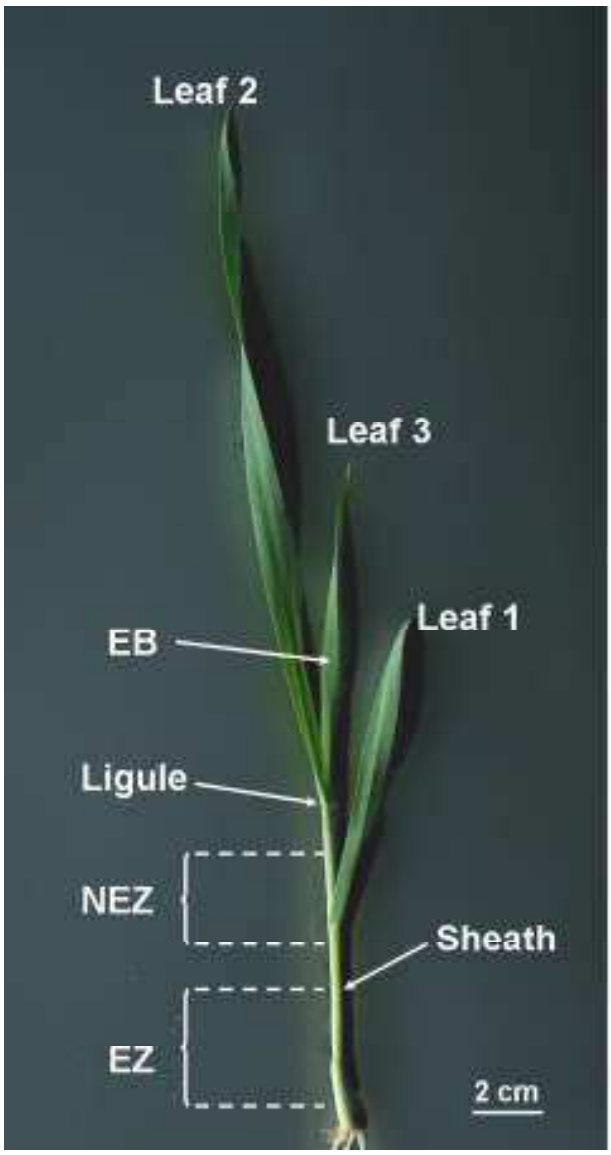

Figure 1.10 Two-week old barley seedling

The two-weeks old barley seedling has three leaves. Leaf one is the oldest leaf and leaf three is the youngest and main developing leaf. EZ: elongation zone; NEZ: non-elongation zone; EB: emerged leaf blade

1.3.1.2 Anatomy of developing barley leaf

Anatomical changes during leaf development can be visualised on cross sections of different parts of the leaf (Fig. 1.11). Cell size is increased manyfold in mature compared to immature tissue, although it is difficult to see this on cross sections, particularly in the epidermis, where elongation growth contributes most to cell enlargment. The most conspicuous difference between the different developmental stages is the specialisation of mesophyll cells for photosynthesis (chloroplast development), xylem (conductance of water and dissolved solutes) and increased intercellular spaces.

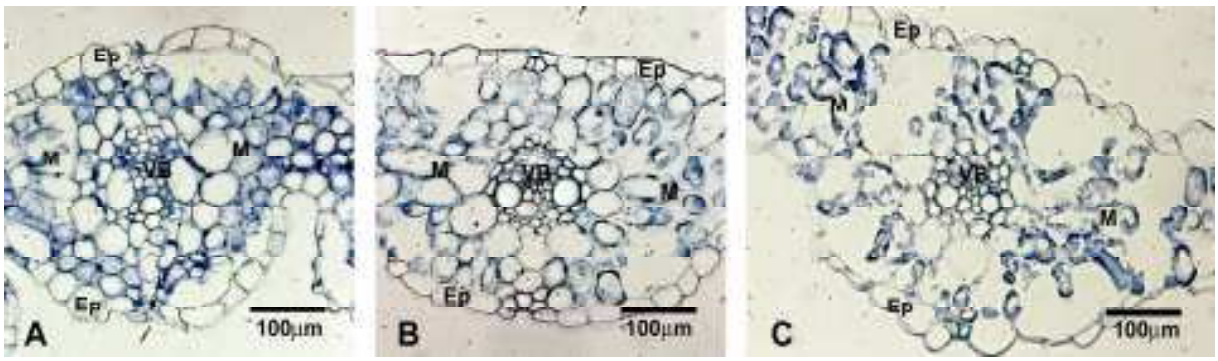

Figure 1.11 Toluidine blue stained cross section of barley leaves from different developmental stage

Cross sections from elongation zone (A) non-elongation zone (B) and fully emerged blade (C) of leaf three. Ep: epidermis; M: mesophyll cells; VB: vascular bundle.

1.3.2 Growth and potassium uptake of barley

The classical dual K^+ uptake mechanism has first been described for roots of barley (Epstein *et al.*, 1963). Further studies proofed the relevance of high affinity K^+ transporters for K^+ uptake; also H^+ / K^+ co-transport has a high significance in K^+ uptake of roots (Glass *et al*., 1981; Amtmann *et al*., 1999). For barley, four HAK genes have been described (HvHAK1-4). HvHAK1 was mainly expressed in roots, HvHAK3 in both shoots and roots while HvHAK4 was mainly expressed in shoots (Rubio *et al.*, 2000). HvHAK4 had significantly higher expression in the elongation zone of leaves compare with parts of barley seedlings (Boscari *et al.*, 2009). HvHAK1 is very similar to AtHAK5 and seems to be a high affinity K^+ transporters in contrast with HvHAK2, which facilitates K^+ uptake in a range of low or medium affinity (K_M of about 5 mM comparing with K_M of about10 µM for HvHAK1 (Rubio *et al.*, 2000; Senn *et al.*, 2001; Ashley *et al.*, 2006).

In previous studies on K^+ transport in barley it was concluded that apoplast K^+ must exceed 3 - 5 mM to allow growing leaf cells to take up K^+ through channels (Boscari *et al.*, 2009; Volkov *et al.*, 2009). Calculations showed that at 10 mM apoplast K^+, about 50 % of K^+ uptake was facilitated by time-dependent inward-rectifying currents typical of Shaker K^+ channels such as AKT1 or AKT2. The remaining 50 % was facilitated by instantaneous currents, which includes either or both, K^+ high-affinity transporters such as HAK / KUP / KT type K^+ / H^+ symporters or non-selective cation channels.

Potassium channels and transporters might study using different blockers of these proteins. Tetraethylammonia (TEA) inhibits K^+ transport through channels reversibly as K^+ analogue at the dehydration transition step (Lenaeus *et al.*, 2005).

Cs^+ ions as huge K^+ analogue block both channels and transporters (Rodriguez-Navarro & Rubio, 2006; Szczerba *et al.*, 2009) and NH_4^+ ions with competitive manner inhibit high affinity K^+ transporters (Spalding *et al.*, 1999; Kronzucker *et al.*, 2003; Rodriguez-Navarro & Rubio, 2006; Szczerba *et al.*, 2006; Britto & Kronzucker, 2008; Szczerba *et al.*, 2009; Britto *et al.*, 2010; Hoopen *et al.*, 2010)

1.4 Technical approaches

(i) Cell wall acidification was measured using three independent methods (pH sensitive fluorescence probe, micro pH electrode technique and in-vitro agarose gel system with bromocresol purple pH indicator. During these experiments leaf elongation was measured with a ruler (micro pH measurements) or image analysis tools (in-vitro gel experiments).

(ii) A linear variable differential transformer (LVDT) was used to determine the growth rate continuously and at micrometer resolution. This made it possible to record any rapid and short term response of leaf growth to application of test reagents to the apoplast of the leaf elongation zone.

(iii) Expression of PM-H^+-ATPase was determined by absolute qPCR technique and the PM-H^+-ATPase enzyme ratio in total purified plasma membrane protein was measured using Western blot analysis and densitometry on Coomassie Brilliant Blue stained SDS polyacrylamide gels. Activity of the enzyme was determined as vanadate sensitive ATPase hydrolysis activity of inside-out plasma membrane vesicles.

(iv) PM-H^+-ATPase tissue specific distribution was studied using immunolocalisation on paraffin embedded section and a commercially-available antibody of PM-H^+-ATPase isoforms.

1.5 Objectives of the present study

The aim of this project was to test whether apoplast pH differs between growing and non-growing leaf tissue of barley, how this acidification relates to growth and to which degree apoplast acidification relies on the activity, transcription and occurrence of PM-H^+-ATPase. The developing leaf three of barley was studied. Apoplastic pH and leaf elongation was measured together in the same experiments or in separate experiments. Differences in pH and leaf growth were followed using three independent techniques. Treatments affecting PM-H^+-ATPase activity (increase or decrease) or blockers of different type of K^+ transport (channel, transporter) were used to determine the physiological background of leaf elongation. Expression and activity of PM-H^+-ATPase was measured to test whether any higher acidity in the apoplast of the elongation zone originated from a higher expression of the enzyme or any other control mechanism, in particular post-translational modification. Finally tissue specific distribution of PM-H^+-ATPase was determined at different leaf developmental stages on cross sections.

2 Materials and Methods

2.1 Plant material

2.1.1 Plant growth for study of leaves

Barley seeds (*Hordeum vulgare* L. cv. Golf; and *Hordeum vulgare* L. cv. Jersey) were imbibed overnight in water, germinated in dark on approx. 0.5 mM $CaSO_4$ for 3 days and exposed to light for a further 3 days while remaining on $CaSO_4$ solution. On day seven, four seedlings were transferred into 1 l borosilicate glass beakers wrapped in tin foil (containing 0.8 - 0.9 l nutrient solution) on aerated ½ strength Hoagland solution (Table 2.1) and grown for a further 7 - 11 days at 70 - 80 % relative humidity and 300 – 350 µmol m^{-2} s^{-1} photosynthetically active radiation at third-leaf level, during a 16 h / 8 h, 21 ℃ / 15 ℃ day / night cycle in a growth chamber (I MAGO F3000, Snijders Scientific). Nutrient solution was not replaced during plant growth. These were the growth conditions at University College Dublin, where most experiments were carried out. Some experiments, including plant growth, were also carried out at Rothamsted Research (UK) and Eötvös University (Hungary). Plants were analysed when they were 14 - 18 d old.

At Rothamsted Research (pH microelectrode measurements) the growth temperature was different (constantly 20 ℃ during day / night). At Eötvös University (plasma membrane isolation) plants were grown under a 14 h / 10 h day / night period (150 µmol m^{-2} s^{-1}) with 20 / 18 ℃ day / night temperature. These alterations in growth conditions were due to local availability of growth facilities and the seedlings achieved the leaf three development stage about 2 - 3 d later at Eötvös University and 1 - 2 earlier at Rothamsted Research compared with Dublin.

The barley Golf cultivar was used for most experiments. Towards the end of the study, the availability of Golf seeds became limited due to vast demand by the laboratory in general, no further commercial (breeder) availability of this cultivar and due to limited availability of growth space at UCD to grow plants to the seeding stage. Therefore, experiments which were carried out towards the end of the study, in particular plasma membrane isolation, were performed on the barley cultivar Jersey. Both, Golf and Jersey are spring barleys.

Table 2.1 Composition of the ½ strength Hoagland solution for barley seedlings

Macronutrients (1 l each)	**Stock** (mM)	**Amount for 1 l stock** (g)	**Final concentration** (mM)	**Dilution**
(1) $NH_4H_2PO_4$	100	11.5g	0.5	200x
+ $(NH_4)_2HPO_4$	100	13.2	0.5	200x
(2) KNO_3	400	40.4	2.0	200x
(3) $MgSO_4x7H_2O$	100	24.7	0.5	200x
+ NaCl	100	5.84	0.5	200x
(4) $Ca(NO_3)2x4H_2O$	400	94,4	2.0	200x

Micronutrients (0.5 l each)	**Stock** (mM)	**Amount for 0.5l stock** (g)	**Final concentration** (µM)	**Dilution**
(a) H_3BO_3	25	0.775	6.25	4000x
(b) $CuSO_4x5H_2O$	0.5	0.0625	0.125	4000x
(c) $MnSO_4xH_2O$	2	0.169	0.5	4000x
(d) $Na_2MoO_4x2H_2O$	0.76	0.092	0.19	4000x
(e) $ZnCl_2$ (or $ZnSO_4$)	2	0.136	0.5	4000x
(f) Fe^{III}NaEDTA	36	6.606	27	1333x

2.1.2 Plant growth for study of coleoptiles

To grow coleoptiles for auxin sensitivity test Golf barley seeds were imbibed overnight in water and were germinated in the dark for 5 d in the growth chamber under the same temperature settings (16 h at 21 °C, 8 h at 15 °C) as described for seedlings. The apical 10 mm of the coleoptile tip was used and the first leaf developing inside the coleoptiles was removed (compare Sakurai & Masuda, 1978).

2.2 Apoplast pH measurements

Cell wall pH was measured through three independent approaches: an in-vitro gel system, electrophysiology and confocal microscopy. The in-vitro gel system involved incubating leaf segments in agarose which contained the pH indicator bromocresol purple. The advantage of this system was that it was easy to use. This made it possible to test many treatments and to directly relate changes in wall acidity to changes in growth rate. The pH microelectrode technique was used to obtain precise values of apoplast pH in growing and non-growing leaf regions. This technique, which was carried out at Rothamsted Research, required the most experimental effort and was used to a limited extent, due to limited funding for travel. Therefore only selected treatments were tested. Finally, intact plants were studied using

confocal microscopy, by loading plants with pH fluorescence probes added to the root medium. Epidermal peels were also studied as control material.

2.2.1 In-vitro gel system

The base 70 mm of leaf three was placed into a Petri dish which had been filled with agarose medium containing the pH indicator bromocresol purple (Tang *et al.*, 2004; Li *et al.*, 2007). The younger fourth leaf was removed from inside leaf three prior to experiments.

The agarose medium contained 10 mM, 1 mM $CaCl_2$, 0.5 % agarose (gelling temperature 38.3 °C) and 90 mg l^{-1} bromocresol purple. Any additional test reagents were added to the medium while it was fluid and the pH was adjusted to 7.0 using 3 mM KOH. The amount of K^+ added through this pH adjustment was negligible compared to the amount of K^+ added through 10 mM K^+. Leaf pieces were placed into the medium when it was almost semi rigid and had a temperature of between 28 - 32 °C. Petri dishes were incubated under the same conditions under which the plants had grown, except for cold-treatments, where dishes were incubated in the dark in a cold room (5 °C). At regular time intervals (every hour for the first 10 h of incubation), Petri dishes were photographed with a Canon EOS 350D digital camera. Two replicate pictures were made every hour. Final pictures were made after 24 h. Digital photographs were used to assess acidification of the medium and measure elongation growth of leaf pieces. ImageJ 1.41o software (http://rsbweb.nih.gov/ij) was used to measure the length of leaf pieces. Values were calibrated with the aid of graph paper which had been fixed to Petri dishes prior to the start of experiment. Due to the alkaline pH of the graph paper, the paper served as sort of an internal pH control as well since it gave the colour (bluish) of bromocresol purple in non-acidified medium. Acidic areas, which showed up as yellow in the purple-stained medium (see Fig. 2.1), were selected on pictures using the magic wand of Adobe® Photoshop® 7.0.1 (tolerance factor 10) and measured using Scion Image for Windows 4.0.3.2 (http://www.scioncorp.com, O'Neal *et al.*, 2002).

Preparation of leaf pieces and transfer to agarose medium resulted in an immediate, non-specific acidification of the medium, most likely as a result of unpeeling leaf three from the sheaths of leaves one and two. This non-specific acidification levelled off within 4 - 5 h. Preliminary experiments showed that the acid area value obtained after 1 h of incubation reflected the size of the exposed leaf surface of the individual plants therefore it was used as the reference point for the

start of experiment (A_1). Any areas measured at further time points 't' (A_t) were related to this reference point according to 'A_t / A_1'. Areas were expressed in mm^2.

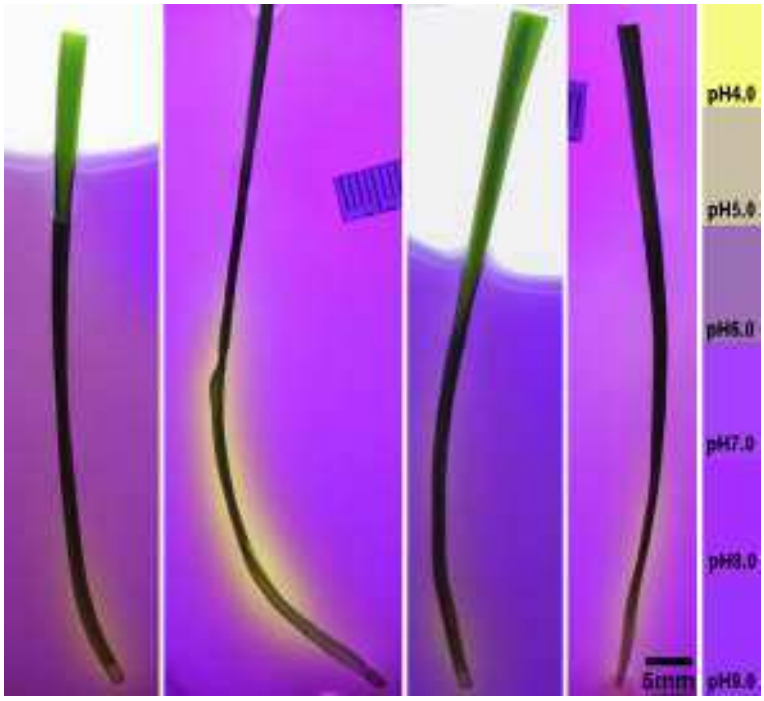

Figure 2.1 Leaf pieces in pH sensitive agarose gel medium

Agarose gels contained the pH indicator bromocresol purple pH. This pH indicator shows yellowish colour at acidic, purple at neutral and blueish colour at alkaline pH (see right column). Basal leaf segments were 70 mm long at the beginning of the experiments, and their tip end was sticking out from the medium. Graph paper was used as an internal alkaline control and to calibrate length of leaf segments to measure growth during the incubation period.

2.2.2 Microelectrode measurements

Apoplastic pH was measured with the aid of pH-sensitive microelectrodes. The elongation zone and emerged, mature portion of the developing leaf three of barley were analysed. The older leaves one and two were peeled back to expose the abaxial surface of the basal elongation zone of leaf three. The elongation zone was covered with wet tissue paper which had been soaked for the previous 24 h in distilled water. The latter was done to guarantee pH neutrality (which is not the case for tissue paper which is used 'fresh'). During experiments, the tissue paper was soaked in bath solutions, as specified in results, to alter the apoplastic environment of the leaf elongation zone. Due to the absence of a major permeability barrier (cuticle) in the elongation zone (Richardson *et al.*, 2007), apoplastic pH could be measured directly by bringing the microelectrode in close contact with the epidermal surface. Measurements were carried out at 20 - 30 mm from the base. In the fully-

cutinised emerged-blade portion of the developing leaf three, apoplastic pH was measured by inserting the microelectrode through stomatal pores (compare Fricke *et al*., 1994; Felle 2005;). Double-barrelled pH sensitive microelectrodes were prepared as described in Miller & Smith (1992) using the same setup and microelectrode cocktail as described in Dennis *et al.* (2009). The only difference was that in the present study a pH 5.0 rather than pH 3.0 calibration buffer was used and that an additional pH 8.5 calibration buffer was included. Calibration was performed before and after readings. The composition of the pH sensitive cocktail and calibration buffers is given in Table 2.2 and Table 2.3. Microelectrode outputs were analysed with Origin® 6.1 (OriginLab Corporation) software.

Analysis of one leaf region of one plant typically lasted between 2 - 6 hours, and between 1 - 6 pH recordings were taken for each leaf region under room temperature and humidity in the dark. To avoid too long exposure of plants on the microelectrode rig, recordings for elongation zone and emerged blade were obtained from different plants. Elongation growth of leaf three of plants mounted on the rig was measured by measuring the length of leaf three at the beginning and end of experiments using a ruler. Preparation of plants reduced leaf elongation growth by about 50-60 % compared to elongation growth of undisturbed plants in the growth chamber.

Table 2.2 Composition of the pH sensor for microelectrodes

Component of pH sensor	Amount of the component
Hydrogen Ionophore II Cocktail A	35 mg
High molecular weight PVC	16 mg
Nitrocellulose	6 mg
Tetrahydrofuran (THF)	Dissolve the other components

Table 2.3 Composition of the buffer solutions used for calibrating pH microelectrodes

pH	Composition of buffer
4.0	20 mM $KHC_8H_4O_4$ (potassium hydrogen phthalate) 120 mM KCl 10 mM $NaH_2PO_4x2H_2O$ Adjust pH using 1 N NaOH
5.0 and 6.0	20 mM MES (2-[N-Morpholino]ethanesulfonic acid) 120 mM KCl 10 mM $NaH_2PO_4x2H_2O$ Adjust pH using 1 N NaOH
7.0	20 mM MOPS (3-[N-Morpholino]propanesulfonic acid) 120 mM KCl 10 mM $NaH_2PO_4x2H_2O$ Adjust pH using 1 N NaOH
8.5	20 mM TAPS (N-tris[Hydroxymethyl]methyl-3-amino-propanesulfonic acis) 120mM KCl 10 mM $NaH_2PO_4x2H_2O$ Adjust pH using 1 N NaOH

2.3 Confocal microscopy

The pH sensitive fluorochromes 5(6)carboxyfluorescein (10 μM) and acridine orange (2.5 μM) were used. In contrast to carboxyfluorescein, acridine orange can be taken up into cells and has been widely used to monitor pH inside animal (Wieczorek *et al.*, 1991; Zoccarato *et al.*, 1999; Malnic & Geibel, 2000) and plant cells (Pope & Leigh, 1988; DuPont, 1989). Carboxyfluorescein is a large double-negative charged anion that can permeate the plasma membrane only in its non-fluorescing diacetate form (Babcock, 1983; Graber *et al.*, 1986). By using its anionic form, its presence in the apoplast and absence in the symplast was guaranteed. The application of acridine orange has some limitations (Palmgren, 1991) but with adequate controls these limitations can be overcome (Clerc & Barenholz, 1998; Manente *et al.*, 2008). The fluorescence intensity of carboxyfluorescein between pH 4.5 and 6.5 can be used to reflect changes in pH conditions in this pH range (Babcock, 1983; Graber *et al.*, 1986).

Dyes were added to the root medium of intact plants in the growth chamber. Plants were allowed to take up dyes into the apoplastic space of both roots and leaves and analysed after an incubation period of 24 h (carboxyfluorescein) and 48 - 72 h (acridine orange). Detached leaves, epidermal peels or leaves still attached to the remainder of the plant were examined with an Olympus FV1000 confocal microscope. Dyes were excited at 488 nm and fluorescence was detected between

500 - 550 nm (carboxyfluorescein) and 516 - 536 nm (acridine orange). To test how effective the uptake of dye into the leaf apoplast had been during the incubation period and how pH sensitive the approach was, epidermal strips were peeled from first leaves of incubated barley plants or from the elongation zone and emerged blade of leaf three. The strips were placed into buffers of specified pH for 30 min, before being examined under the confocal microscope. Calibration of fluorochromes was carried out with a Leica DMIL fluorescence microscope. The microscope's excitation filter was cut between 450 - 490 nm and the suppression filter at 515 nm. For pH calibration, 50 mM phthalate buffer (pH 4.0), 100 mM MES / KOH (pH 5.5, pH 6.5) and 100 mM TRIS-HCl (pH 7.5) was used. Digital images were analysed with ImageJ 1.41o software (http://rsbweb.nih.gov/ij) and Adobe® Photoshop® 7.0.1.

The pH dependence of fluorescence of 5(6)carboxyfluorescein and acridine orange were examined by recording fluorescence spectra at different pH using a FluoraMax-2® (Instruments S.A.) (pH 5.0; pH 5.5; pH 6.0 – 50 mM MES-KOH; pH 6.5 – 50 mM MES-BisTRIS and pH 7.0; pH 7.5 – 50 mM HEPES-HCl).

2.3 LVDT measurements

A linear variable differential transformer (LVDT) was used to measure changes in leaf length continuously and at micrometer resolution in response to treatments (compare Fricke, 2004; Fricke *et al.*, 2004). The setup could also be used to determine changes in cell wall properties.

2.3.1 Leaf growth measurements

Plants were prepared in the same way as for electrophysiological analyses to be able to relate the results from both types of experiments to each other. Leaves one and two were peeled back and the exposed elongation zone of leaf three was wrapped in washed (24 h in distilled water) tissue paper which was soaked in the respective test solution. The wet tissue paper guaranteed a humid microclimate and prevented the elongation zone from drying out; it also allowed application of test reagents to the apoplast of elongating tissue. The base 40 - 50 mm of leaf three was wrapped to provide sufficient mechanical support to allow the leaf to remain in an upright position. Above 50 mm from the leaf base, the cuticle is sufficiently developed preventing the leaf tissue from drying out (Richardson *et al.*, 2007). Roots were left in the same medium in which the particular plant had grown. The tip of leaf three was attached to fishing line and connected through cellotape to a LVDT (DFG 5.0; RS

Components, Corby, UK). A counterweight of 2 g was applied. The LVDT signal was digitalised with a Burster 92101 data logger module with ICP 100 software. Changes in voltage output were recorded on PC using Pfloek 1.09 software (LS Pflanzenökologie, Universität Bayreuth, Germany). The system was calibrated by replacing the plant with a micrometer screw. The rate of growth was calculated from LVDT outputs using Origin® 6.1 software (OriginLab Corporation) and Microsoft® Excel. Although leaf elongation rate was comparable between replicate plants and batches, values for treatments were expressed as percentage of the control to further minimise any plant-to-plant variation. The control value was the elongation rate of a particular plant attached to the LVDT before a treatment was applied. Typically, control plants had the elongation zone of leaf three wrapped with tissue paper soaked in either 1 or 0.1 mM KCl. It took up to 1 h for elongation rate to reach a steady level following attachment of plants to the LVDT. Application of vanadate and CsCl treatments required a similar period of stabilisation (about 1 h), while application of fusicoccin and ammonium treatments required leaf elongation rate to stabilise for up to 2 - 3 h. LVDT experiments were carried out at room temperature and humidity under ambient laboratory light.

To assess how much plant preparation affected the elongation rate of leaf three, intact plants which did not have leaves one and two peeled back, were attached to the LVDT. In addition, leaf elongation rate was determined for undisturbed plants in the growth chamber by measuring twice daily the increment in leaf length with a ruler.

2.3.2 Analysis of cell wall properties

Cell wall elasticity and plasticity was measured with the same LVDT system as described above by applying an additional 3 g counterweight for 10 min following the approach taken by Neumann (1993) (see also Chazen & Neumann (1994) and Sabrizhanova *et al.* (2005)). Plants were prepared and chemical treatments applied in the same way as for growth analyses. When the growth rate had stabilised (control, treatment), the additional 3 g counterweight was applied to the LVDT for 10 min and then removed; 30 - 40 min later, when growth rate had stabilised again, the experiment was repeated, and the average of these two measurements was used for calculations of wall properties. Elasticity and plasticity of walls and growth rate with and without the applied force (additional 3 g counterweight) was calculated from LVDT traces as detailed in Fig. 2.2.

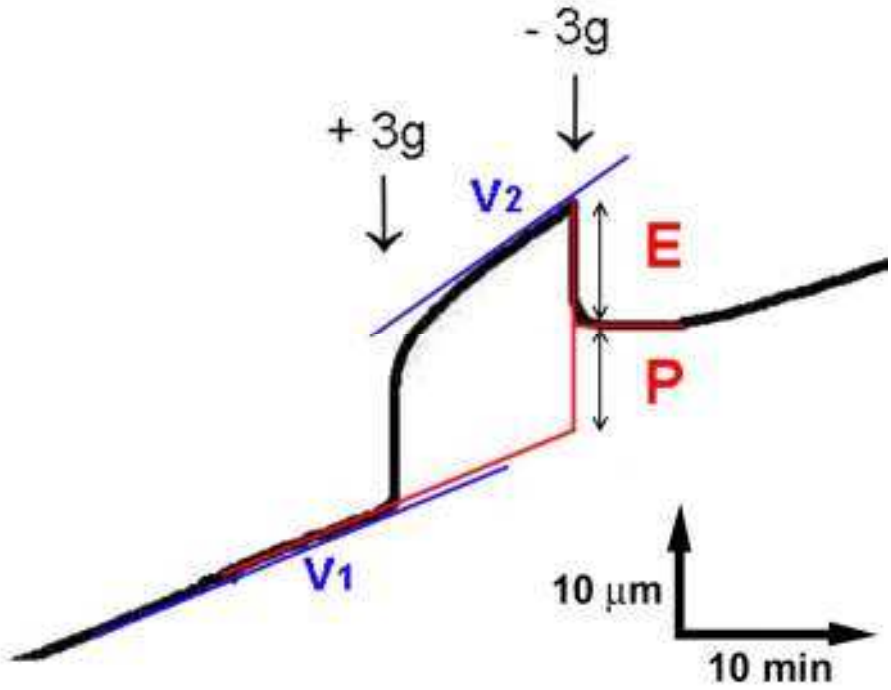

Figure 2.2 Measurement of cell wall properties

LVDT traces show the change in leaf length with time. LVDT traces before and after application of an additional 3 g counterweight (0.03 N of applied force), growth rates were calculated from the slope of the lines fitted to the stabilised part of traces (v_1 and v_2). The applied force caused an extension, part of which was reversible (elasticity, E) of wall) and part of which was irreversible (plasticity, P of wall).

2.4 Expression analyses

The aim of expression analyses was to test whether any elevated proton efflux in the leaf elongation zone was due to higher PM-H^+-ATPase expression.

2.4.1 Plant harvest

Plants were harvested 2 - 6 h into the photoperiod. Samples from the elongation zone were about 1 cm long and were cut from the mid-portion of the elongation zone (between 20 - 30 mm from the leaf base). Samples of the emerged blade were 1 - 2 cm long and taken from the mid-portion of the part of leaf three that had emerged from the sheath of leaf two. The leaf segments were weighed on a digital balance (Mettler Toledo, Sweden), immediately frozen in liquid nitrogen and stored at -80 ℃ until they were used for RNA extraction.

2.4.2 RNA extraction and cDNA synthesis

For RNA extraction, corresponding leaf segments from 3 - 4 plants were pooled; their combined fresh weight was between 0.04 - 0.07 g (Besse *et al.*, 2011) Total RNA was extracted using a QUIAGEN RNeasy kit following the manufacturer's instructions. RNA was eluted into 50 µl RNase free water. The concentration and quality of RNA was determined with Nanodrop® (ThermoFisher Scientific Inc., Waltham, USA).

After DNase treatment, following the manufacturer's instructions (Deoxyribonuclease I, Amplification Grade; Invitrogen Corporation, Carlsbad, California, USA), 1 µg RNA was used for cDNA synthesis. cDNA synthesis was performed as recommended by the manufacturer (SuperScriptTM II Reverse Transcriptase; Invitrogen Corporation, Carlsbad, California, USA) using anchor $oligo_dT_{16}$ primer. The final volume of cDNA was 20 µl. Details of the procedure and reagents used are provided in Table 2.4.

In some experiments, RNA was also extracted from protoplasts. RNA extraction from a protoplast suspension was carried out in a way similar to the one described above, with minor modifications. RNeasy lysis buffer (300 - 1000 µl) was added to 300 - 1000 µl protoplast suspension (~ 0.5 – 7 million protoplasts) or to 1 ml cell-free protoplast isolation medium. The latter was used as background control to reflect RNA released from broken cells or protoplasts into the isolation medium and was prepared by centrifuging the protoplast suspension at 30 g for 1 min and taking the supernatant and centrifuging it again at 12,000 g for 5 min. The final volume of RNA extract for protoplasts or isolation medium was 30 µl rather than 50 µl as obtained for leaf extracts.

Table 2.4 DNase treatment and reverse transcription

DNase treatment		Total volume
	1 µg (8 µl) RNA 1 µl 10x DNaseI Reaction buffer 1 µl (1 U) DNaseI Ampl. Grade enzyme	10 µl
	Incubation 15 min 25 ℃ 1 ml EDTA (25 µM)	11 µl
	Incubation 10 min 65 ℃	
Reverse transcription		
	11 µl sample from DNase treatment 1 µl anchor oligo-dT primer (100 µM) 1 µl $_d$NTP (10 mM)	13 µl
	Incubation 5 min 65 ℃ 4 µl 5x First-Strand Buffer 2 µl DTT (0.1 M)	19 µl
	Incubation 2 min 42 ℃ 1 µl SuperSript™ RT Enzyme (200U)	20 µl
	Incubation 50 min 42 ℃ then 70 ℃ 15 min	

2.4.3 PCR

Before cDNA samples were used for qPCR analysis, which required expensive reagents, the quality of cDNA, suitability of designed primers and optimum PCR conditions was tested through conventional PCR (G-Storm 482 thermocycler, Gene Technology). A GoTaq® Flexi DNA Polymerase (Promega Corporation, Madison, USA) kit was used in 25 µl total volume with 1 µl 200x diluted cDNA as template. A precise protocol of the PCR reaction is given in Table 2.5. Primers are listed in Table 2.6. The PCR was run in amplification two steps; after initial step (95 ℃; 30 s) through 35 cycle step one (95 ℃, 30 s) and step two (60 ℃, 60 s) were repeated and then a final step (72 ℃, 120 s) was used as Fig. 2.3 shows.

PCR products were separated on 1 % agarose gels in 0.5 strength TRIS base boric acid EDTA (TBA, see Table 2.7) buffer containing 1 µg ml^{-1} ethidium bromide and viewed under UV light (Image Master® VDS, Pharmacia Biotech, USA).

Table 2.5 Components of PCR reactions

Component	Volume	Final concentration
5x Green GoTaq® Flexi Buffer	5 µl	1x
MgCl Solution (25 mM)	2 µl	2 µM
dNTP (10 mM)	0.5 µl	0.2 µM each nucleotide
Forward primer (10 mM)	0.5 µl	0.2 µM
Reverse primer (10 mM)	0.5 µl	0.2 µM
GoTaq® DNA Polymerase (5 U / ml)	0.125 µl	0.625 U
Template cDNA (200x diluted)	1 µl	5000x diluted
Nuclease-Fee Water	15.375 µl	N/A
Total volume	25 µl	

Table 2.6 PCR primers

Primer name	Primer sequence
Anchor oligo$_d$T$_{16}$	5'NVTTTTTTTTTTTTTT3'
ATPase forward	5'ACATCGACACCATCAACCAA3'
ATPase reverse	5'ACAACTAGGGGCTGGTCAGA3'

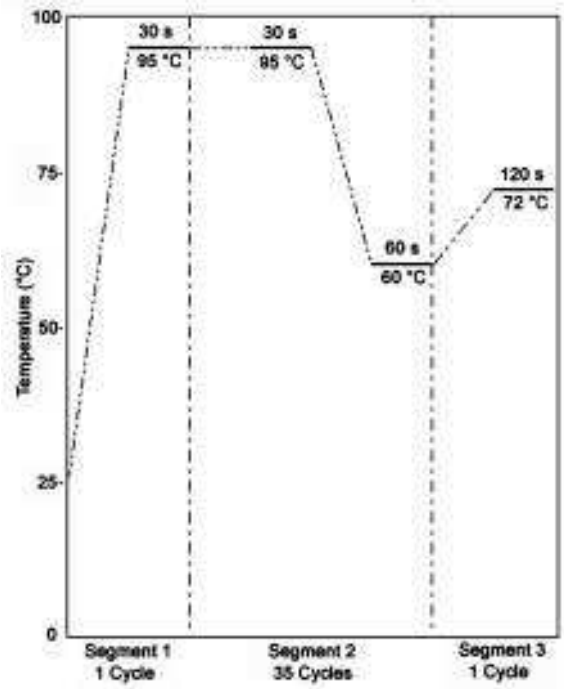

Figure 2.3 Thermal profile of the two step PCR reactions

Two step PCR protocol was used when quality of cDNA or primers were tested. This protocol was as similar as possible to the protocol used for qPCR analyses.

Table 2.7 Composition of the stock solution (5x concentrated) of TRIS base boric acid EDTA buffer (TBA)

Component	***Amount for 1 l***
TRIS base	53 g
Boric acid	27.5 g
EDTA (0.5 M, pH 8.0)	20 ml

2.4.4 qPCR

qPCR expression analysis was carried out on a real time thermal cycler STRATAGENE Mx3000P (Agilent Technologies, Inc., Santa Clara, USA), using a SYBRgreen master mix and following the supplier's instructions (SYBR®*Premix Ex Taq*™, Takara Bio Inc, Otsu, Japan) (see Table 2.8). The reaction mix was loaded onto 96-well plates (96 Multiply PCR plate natural, SARSTEDT AG & Co., Nümbrecht, Germany). Three technical and biological (independent batches of plants) replicates were run together with external standards (purified PM-H^+-ATPase PCR product; see below) on the same plate. Samples were maintained for 10 s at 95 ℃ as initial step, then 5 s at 95 ℃ and 30 s a t 60 ℃ through 45 cycles. After amplification, melting curves were recorded (95 ℃ 1 min then temperature gradient from 55 ℃ to 95 ℃ in 81 steps) to check product s ize and homogeneity, see also Fig. 2.4.

Table 2.8 Components of qPCR reaction

Component	Final Volume	Final concentration
SYBR®*Premix Ex Taq™*	6.25 µl	1x
Forward primer (10 mM)	0.25 µl	0.2 µM
Reverse primer (10 mM)	0.25 µl	0.2 µM
Rox Dye II	0.25 µl	N/A
Template cDNA (200x diluted)	1 µl	2500x diluted
Nuclease-Free Water	4.5 µl	N/A
Total volume	12.5 µl	

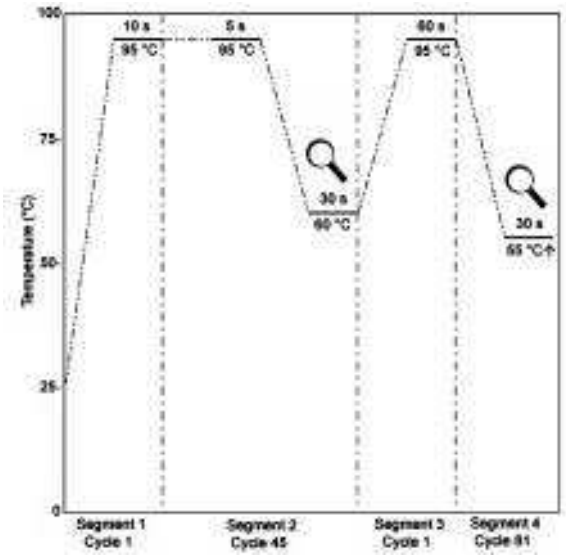

Figure 2.4 Thermal profile of qPCR reactions

Magnifying glass symbols indicate detection sites of SYBR Green fluorescence

To quantify the number of mRNA transcripts of the target gene (PM-H^+-ATPase), cDNA samples which contained known copy numbers of PM-H^+-ATPase cDNA molecules were required. This external standard was obtained by purifying PM-H^+-ATPase PCR product and a pCR®8/GW/TOPO construct that contained the ATPase PCR product as insert. Initially, the plasmids were used as an alternative external standard in addition to purified PM-H^+-ATPase. However, preliminary experiments showed that purification of plasmids from *E. coli* cells did not yield sufficiently pure product to use it as external standards.

To obtain purified ATPase PCR product, PCR was performed in 50 µl volume as described above using colourless reaction buffer. After the quality of PCR product was checked by running the samples on an agarose gel, the PCR product was cleaned with a NucleaSpin®Extract II PCR clean-up / Gel extraction kit (Macherey-Nagel GmbH & Co. KG, Germany) following the manufacturer's instructions. The purified DNA was eluted from the NucleaSpin®Extract II Column with nuclease free water. The DNA content was measured with Nanodrop® (ThermoFisher Scientific Inc., Waltham, USA) and the concentration / copy number of cDNA molecules was calculated from the expected molecular weight of the cDNA product for PM-H^+-ATPase (100,587 g mol^{-1}). From this purified stock, dilutions of 0.5, 5, 50, $5 \cdot 10^2$, $5 \cdot 10^3$, $5 \cdot 10^4$ and $5 \cdot 10^5$ copy μl^{-1} were prepared.

2.4.5 Analysis of qPCR data

An absolute quantification method was used to compare the PM-H^+-ATPase expression between elongation zone and fully developed emerged blade. This approach was chosen in favour of the conventional Δ-Ct approach (Pfaffl, 2001) because the generally most suitable reference gene of expression e.g. ubiquitin, gave more than one PCR product due to the existence of poly-ubiquitins. Using the Genevestigator (http://genevestigator.com) online application this problem (Hruz *et al.*, 2011) could not be solved.

To further relate the copy number of transcripts to a biologically relevant size, qPCR results were expressed per cell or per mm^2 plasma membrane surface. The total number of cells and plasma membrane surface contained in the plant material which was used for extraction was calculated based on the water content of leaf tissue, protoplast number and stereological electron and light microscopic analyses as detailed in section 2.5.

2.5 Cell size and tissue ratio measurements

Cell size and tissue ratio in different leaf regions (elongation zone and emerged leaf blade) were determined and data combined with published data to calculate the total number of cells which were contained in samples used for qPCR analysis.

2.5.1 Mesophyll and epidermis cell size

The diameter of mesophyll cells was measured on living protoplasts with the help of Scion Image for Windows 4.0.3.2 (http://www.scioncorp.com) software. The data were then combined with data obtained by Volkov *et al*. (2007, 2009) for the same barley cultivar (Golf) and data obtained by Kavanagh (2010) through stereological electron-microscopic analyses. Epidermal cell size was calculated based on stereological results of Kavanagh (2010) and a light-microscopic study of Fricke & Flowers (1998) on the same barley cultivar (Golf) studied.

2.5.2 Tissue ratio calculation in elongation zone and emerged blade

The percentage of cross-sectional leaf volume occupied by leaf tissues (epidermis; mesophyll including vascular parenchymateous bundle sheath; vascular bundles except parenchymateous bundle sheath) and intercellular air space was determined on paraffin-embedded toluidine blue-stained cross sections (few micrometers thick) with the help of Adobe® Photoshop® 7.0.1 and Scion Image for Windows 4.0.3.2 software. By assuming that intercellular air spaces did not contain any significant amount of liquid, but that almost all liquid was contained within tissues, it was possible to calculated the total water content (and approximate) volume of each tissue used for RNA extraction since the water content of leaf samples had been determined.

2.5.3 Cell size and plasma membrane surface estimation for qPCR analysis

Mesophyll cells volume and surface were calculated as they were spheres using the equation of $(\pi/6)d^3$ for volume and πd^2 for surface. Epidermis cells were treated as long rods. In the total cell volume different cell types were present as their corrected tissue share. Corrected tissue share was calculated as dividing the tissue share by (1-share of air space) because air space did not contains any living plant cell. The

whole calculation and data can find in the Results at section 3.3.2 and in the Appendix.

2.6 Plasma membrane isolation

Plasma membranes were isolated from barley seedlings following the approach developed by Kjellbom & Larsson (1984) and Yan *et al.*, (1998). All steps were performed under cold conditions. For each plasma membrane isolation between 1.5 – 6 g of plant material was required (elongation zone; emerged blade). Between 200 - 400 barley seedlings had to be grown and harvested in each experiment.

2.6.1 Plant harvest

Plant tissues, elongation zone (basal 40 mm without the lower 1 - 2 mm, containing meristematic zone) and emerged blade (leaf blade without the lower and upper 1 cm) of barley (cv Jersey) leaf three were harvested into 50 ml ice cold homogenisation buffer (all components are listed in Table 2.9). The tissues were gently vacuum infiltrated (3 times using a laboratory water jet vacuum pump) and used immediately for plasma membrane isolation.

Table 2.9 Composition of the homogenisation buffer used for membrane isolation

Component	***Final concentration***
Sucrose	500 mM
EDTA	2 mM (from 200 mM stock)
Glycerol	10 % (v/v)
BSA	0.5 % (w/v)
DTT	2 mM
PMSF	1 mM (prepared freshly from 12 mg ml^{-1} EtOH stock)
β-mercaptoethanol	5 mM
Non-soluble PVP	1 % (w/v)
Na-ascorbate	0.1 % (w/v) prepared freshly
HEPES-KOH	50 mM set to pH 7.8

2.6.2 Preparation of microsomal fraction

Tissues were homogenised in the homogenisation buffer with a razor blender (3 times 25 sec). The homogenate was filtered through four layers of gauze and one layer of Miracloths (Fisher Scientific). The filtrate was centrifuged at 11,500 g for 10 min at 4 ℃ (Sigma 3K15 and 3K10 bench top centrifu ge, fixed angle rotor). The supernatant was collected and centrifuged at 30,000 rpm (~82,000 g) in a

Beckman L7-65 ultracentrifuge for 40 min with a SW40Ti swinging bucket rotor. The resulting microsomal pellet was resuspended in phase buffer (Table 2.10).

Table 2.10 Composition of the phase buffer used for membrane isolation

Component	***Final concentration***
Sucrose	330 mM
KCl	3 mM
KH_2PO_4	5 mM
K_2HPO_4	5 mM
KOH	To adjust buffer to pH 7.8

2.6.3 Purification of plasma membrane vesicles

The microsomal fraction was further fractioned by a two-phase aqueous dextran T-500 and PEG-3350 system. From the polymers, 20 % (w/w) (dextran) and 40 % (w/w) (PEG) stock solutions were made in phase buffer. The final concentration of both polymers was 6.1 % (w/w) in the start tube, taking into account dilution through addition of phase buffer and resuspended microsomal fraction. The final weight of the tube was 12 g. The tube was mixed by inversion 30 times and the phase separation was carried out by centrifugation at 1,500 g at 4 °C (Sigma 3K15 and 3K10 bench top centrifuge with swinging bucket rotor) for 25 min. The upper phase was transferred into a new tube and completed to 12 g with fresh lower phase (prepared separately with the help of extraction funnel). The separation was done as before but for 15 min, and this purification step was repeated 3 - 4 times until the upper phase became clear and did not show any green colour (which would have been indicative of contamination with chloroplast membranes) (Fig. 2.5). The final upper phase was diluted 3 - 4x with phase buffer and ultracentrifuged (35,000 rpm, 1 h). The pellet was resuspended in resuspension buffer (Table 2.11) and washed by ultracentrifugation (35,000 rpm, 1 h) two times in resuspension solution. The final purified pellet was resuspended in 50 - 150 µl resuspension buffer and divided into aliquots, frozen in liquid nitrogen and stored at -80 ℃.

Table 2.11 Composition of the resuspension buffer used for membrane isolation

Component	***Final concentration***
Sucrose	330 mM
KCl	3 mM
KOH	To set pH 7.8

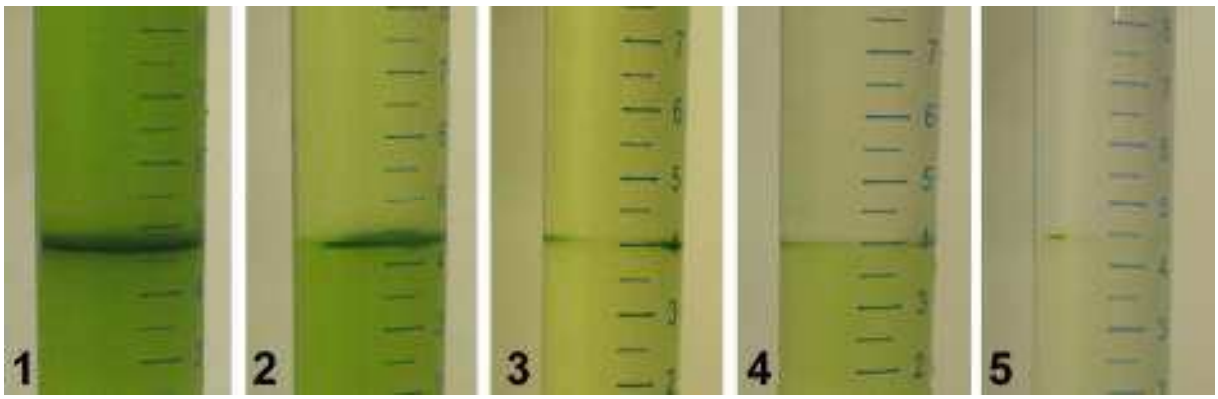

Figure 2.5 Five purification steps during plasma membrane isolation.

The upper phase becomes less and less green (indicative of thylakoid contamination). After the 5th step the upper phase is clear, no green colour is seen.

2.7 Determination of the total protein content of plasma membrane vesicles

2.7.1 Bradford method

The protein content of plasma membrane preparation was estimated using the method of Bradford (Kruger, 2002). The reagent was prepared and filtered through Whatman no. 1 filter paper. It was stored at room temperature in an amber bottle and used within weeks. The composition of the reagent is given in Table 2.12. The assays were carried out in duplicates in 1.1 ml final volume. For the calibration curve 0, 1, 2, 4, 6 and 8 μg bovine serum albumin (BSA) was used as standards. Absorbance was measured at 595 nm between 5 to 15 min following addition of Bradford reagent to samples (PerkinElmer Lambda25 UV/VIS Spectrophotometer)

Table 2.12 Composition of Bradford reagent

Component	***Amount of the component***
Coomassie Brilliant Blue G250	100 mg dissolved in 50 ml 95 % ethanol
Phosphoric acid 85 %	100 ml
Distilled water	Made up to 1 l

2.7.2 Densitometric analysis of Laemmli gels

The final values of protein concentration (used for ATPase assay, densitometry on polyacrylamide gels and Western blot analysis) were calculated from Laemmli gels (Sárvári et al, unpublished) using the modified protein solubilisation described below. Known volume of membrane vesicle sample (determined based on protein measurement using Bradford method, usually between 5 - 30 μl) were run on a gradient SDS polyacrylamid gel together with protein standards (Sigma). The amount

of total membrane protein was calculating by densitometry by Phoretix 4.01 software (Phoretix International). A typical gel photo is shown in Fig. 2.6.

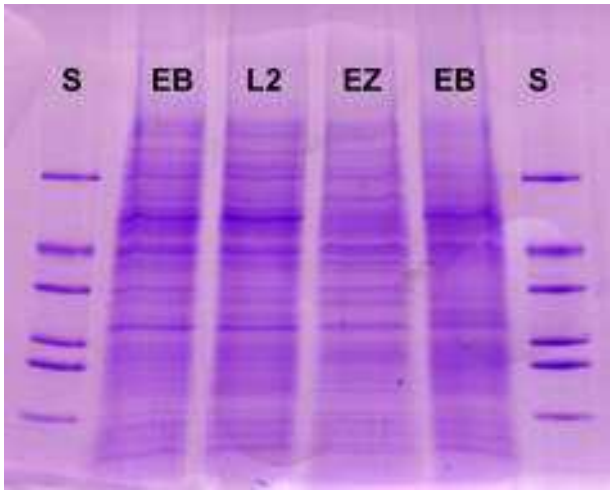

Figure 2.6 Typical gel for the measurement of protein content of plasma membrane samples

Coomassie Brilliant Blue R250 stained SDS gels were used to determine the total membrane protein content of different samples through a densitometric approach. EB – emerged leaf blade of leaf three; EZ – elongation zone of leaf three; L2 – mature blade of leaf two; S – Sigma protein standard, with a total protein content of 17.5 μg (2.5 μg each band) and proteins of molecular weights 66 (uppermost band), 45, 36, 29, 24, 20.1 and 14.2 kDa (lowermost band).

2.8 Polyacrylamide gel electrophoresis (PAGE)

Qualitative and quantitative analyses were carried out on isolated plasma membrane vesicles using polyacrylamide gel electrophoresis (PAGE).

2.8.1 Gradient polyacrylamide gel electrophoresis (PAGE)

A gradient polyacrylamide gel electrophoresis was performed based on (Laemmli, 1970), with some modification in the solubilisation of membrane protein, to check the quality of isolated plasma membrane fraction and quantify its (total) protein content.

2.8.1.1 Solubilisation of membrane protein

To optimise the solubilisation of plasma membrane protein, the approach taken by Kjellbom & Larsson (1984) was followed. TritonX®-100 detergent was added to the Laemmli buffer. Equal volumes of 0.1 % TritonX®-100 and plasma membrane suspension were mixed and vortexed. The mixture was then combined with an equal volume of Laemmli buffer (Table 2.13), incubated at room temperature for 30 min

and heated (90 °C) three times for 10 s each followed by vortexing. Non-solubilised protein was removed by centrifugation (5 min at 10,000 g) and the supernatant used for PAGE. With this modified solubilisation procedure, almost all protein was solubilised and no pellet was observed after centrifugation. In addition, gel bands stained with Coomassie Brilliant Blue R250 were much sharper and distinct (Fig. 2.7).

Table 2.13 Composition of Laemmli buffer used for PAGE

Component	***Concentration in the agent***	***Final concentration***
TRIS-HCl pH 6.8	2.3 % (w/v)	0.76 % (w/v)
SDS	7.15 % (w/v)	2.38 % (w/v)
Glycerol	30 % (v/v)	10 % (v/v)
DTT	5.5 % (w/v)	1.83 % (w/v)
Bromophenol blue	0,003 % (w/v)	0.001 % (w/v)

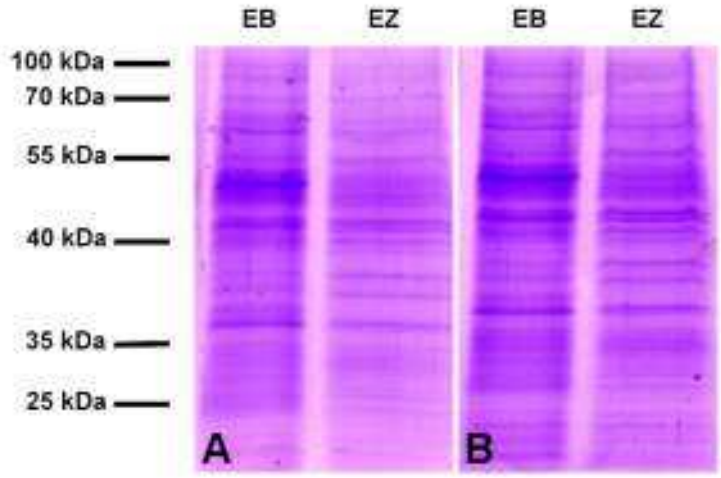

Figure 2.7 Coomassie Brilliant Blue R250 stained gradient PAGE gels which were loaded with plasma membrane protein solubilised in two different ways

Plasma membrane protein was solubilised using the conventional Laemmli solubilisation method (A) or a modification involving TritonX®-100 (B). The bands are sharper and more distinct using the modified solubilisation method. Samples were derived from the elongation zone (EZ) and emerged blade (EB) of leaf three of barley.

2.8.1.2 Gradient PAGE gel system

Solubilised proteins were separated on 7 cm long 10 - 18 % gradient gels in a MiniProtean (BioRad Laboratories, Inc.) gel running system based on Laemmli (1970) under 20 mA / gel at 4 °C until the bromphenol blue front exited the gel (after about 2 h). The components of the gel are listed in Table 2.14. The acrylamide / bis-acrylamide ratio was 30:0.8.

Table 2.14 Components of the gradient PAGE system

Stacking gel

Component	*Concentration in the gel*
Acrylamide	5 % (w/v)
TRIS-HCl, pH 6.8	125 mM
SDS	0.1 % (w/v)
TEMED	0.01 % (v/v)
APS (ammonium persulfate)	0.1 % (v/v)

Separation gel

Component	*Concentration in the gel*
Acrylamide	10 - 18 % (w/v) linear gradient
TRIS-HCl, pH 6.8	375 mM
SDS	0.1 % (w/v)
TEMED	0.013 - 0.017 % (v/v) gradient
APS	0.04 % (v/v)

Gel running buffer

Component	*Concentration in the buffer*
TRIS, pH 8.3	25 mM
Glycine	192 mM
SDS	0.1 % (w/v)

The polyacrylamide gel was stained overnight with Coomassie Brilliant Blue R-250 and washed 3 - 4 times with washing solution (Table 2.15) on a horizontal swinging table (BIOSAN Multi MR-12). After the final washing step the gel was placed into distilled water for 20 min and then scanned with an UMAX Aster-1220S gel scanner. Each gel was stored for longer-term use in 7 % acetic acid solution.

Table 2.15 Components of the solutions for Coomassie Brilliant Blue gel staining

Coomassie brilliant blue stain

Component	*Concentration*
Coomassie brilliant blue R-250	1 % (w/v)
Methanol	41.67 % (v/v)
Acetic acid	16.66 % (v/v)
Distilled water	41.67 % (v/v)

Washing buffer

Component	*Concentration*
Methanol	30 % (v/v)
Acetic acid	10 % (v/v)
Distilled water	60 % (v/v)

2.8.2 Linear (12 %) PAGE

For Western blotting at UCD, Dublin, linear (12 %) polyacrylamide gels were used for protein separation. Purified and solubilised plasma membrane samples were run on the polyacrylamide gels using a Hoefer^{TM} SE260 gel running system (Hoefer Inc, USA) at 240 V and 80 mA for 1.5 h using the same gel running buffer as described before (Table 2.14). For gel electrophoresis a 12 % separation and 4 % stacking gel were prepared following the instructions of the manufacturer (ProtoGel® 30 % Kit, National Diagnostics, U.S.A.). Each well was loaded with 5 µg total membrane protein. Gels were not stained, but separated proteins were blotted to nitrocellulose membrane to quantify PM-H^+-ATPase content of the samples by Western blot analysis.

2.9 ATPase assay

The ATPase assay was designed based on the method described by Sarkadi *et al*. (1992) and Pitann *et al.* (2009b). The ATP-dependent release of inorganic phosphate was followed. Precisely 3 µg total membrane protein was incubated in 100 µl reaction buffer (Table 2.16) at 28 ℃ for 60 min in a BIOSAN TS-100 Thermo Shaker. The reaction was stopped through addition of 50 µl 10 % (w/v) phosphate free SDS. For colour development, 400 µl colour developing reagent (Table 2.16), 1 ml ultra-pure water and 200 µl 1 % freshly made ascorbic acid solution were added in succession to each reaction tube. Colour development occurred at 37 ℃ and was completed within 20 - 30 min. Within 1 min following the end of colour development, the absorbance of samples was read at 880 nm using a PerkinElmer Lambda25 UV/VIS Spectrophotometer. Appropriate standards (0, 10, 20, 40, 60 nmol P_i per sample of K_2HPO_4) were always run in parallel to samples and used to convert absorbance readings into nmol P_i generated.

Table 2.16 ATPase reaction buffer and colour development reagent

ATPase reaction buffer

Component	*Concentration*
MES-KOH, pH 6.5	10 mM
$MgSO_4$	5 mM
Sodium ATP	5 mM
KCl	50 mM
KNO_3	50 mM
Brij58	0.02 % (w/v)
NaN_3	10m M

Colour developing reagent for ATPase reaction

Component	*Concentration*
H_2SO_4	2.5 M
Ammonium molybdate	1 % (v/w)
Potassium antimony (III) oxid tartrate	0.014 % (v/w)

2.10 Approach for light microscopy

2.10.1 Fixation of leaf tissue

Leaf pieces (1 cm in length) from the elongation zone and emerged blade were fixed in 4 % formalin (overnight, 4 ℃). To facilitate th e penetration of the fixative, samples were vacuum infiltrated (3 times for 10 sec) using a Millipore WP6122050 vacuum pump (Millipore, USA).

2.10.2 Dehydration and embedding

Dehydration of leaf tissue was achieved through an ethanol series, and tissues were cleared with Neo-clear® and embedded into paraffin wax. Details of the protocol are given in Table 2.17. Sections of 5 µm thickness were cut using a MicroTec® 4060 rotary microtome (MicroTec Laborgeräte GmbH, Germany). Sections were mounted on slides and dried at 37 ℃ (overnight) and staine d. For immunostaining, samples were mounted on APTES (3-aminopropyltriethoxysilane) coated slides, prepared based on the instruction of the supplier (Sigma-Aldrich), to prevent tissue damage during the overnight staining procedure. Slides were washed in absolute ethanol before coating and were immersed into 2 % APTES (dissolved in absolute ethanol) for 5 s, briefly rinsed in ethanol, washed in running tap water (5 min), rinsed in distilled water and dried overnight at 55 - 60 ℃.

Table 2.17 Fixation and embedding of leaf samples for immunohistochemistry

Fixation		
	Solution	***Duration***
	4 % Formalin	Overnight, 4 ℃
Dehydration		
	Solution	***Duration***
	30 % Ethanol	1 h
	50 % Ethanol	1 h
	70 % Ethanol	1 h
	90 % Ethanol	1 h
	96 % Ethanol	1 h
	Absolute Ethanol	2x 1 h
Clearing		
	50 - 50 % Ethanol Neo-clear®	Overnight, 4 ℃
	Neo-clear®	2x1 h
Infiltration		
	Neo-clear®-wax	30 min
	50 - 50 % Nea-clear®-wax	1 h, 65 ℃
	100 % wax	2x 1 h, 65 ℃

2.10.3 Staining with toluidine blue

Paraffin-embedded sections were rehydrated, stained with 1 % (w/v) aqueous toluidine blue, washed, dehydrated, cleared and mounted in Entellan® mountant (Table 2.18). Sections were examined with a Leica DMIL and Olympus BX60 microscope.

Table 2.18 Staining embedded leaf sections with toluidine blue

Rehydration		
	Solutions	***Duration***
	Neo-Clear® A	10 min
	Neo-Clear® B	10 min
	Absolute ethanol	5 min
	96 % ethanol	5 min
	70 % ethanol	2 min
	Running water	5 min
Staining		
	1 % aqueous toluidine blue	10 min
	Running water	5 min
Dehydration		
	70 % ethanol	Dip twice
	96 % ethanol	Dip four times
	Absolute ethanol 1	5 min
	Absolute ethanol 2	5 min
	Neo-clear® C	5 min
	Neo-clear® D	5 min
Mounting		
	Entellan®	Mount under cover slip

2.11 Immunological methods for PM-H$^+$-ATPase detection

2.11.1 Qualitative Western blot analysis

At Eötvös University the PM-H$^+$-ATPase content of the isolated membrane vesicles and identity and molecular weight of PM-H$^+$-ATPase protein was determined using Western blotting. Gradient SDS polyacrylamide gels were run as described above. Separated proteins were transferred onto nitrocellulose membrane (Hybound^{TM}-C Extra, Amesham-Pharmacia, USA) using the Mini Transfer Blot (BioRad Laboratories, Inc.) system. The composition of blotting buffer is given in Table 2.19. Protein transfer was carried out in an ice-cold buffer tank (4 ℃) at 90 V constant voltage (I < 0.4 A) for 2 - 3 h.

Table 2.19 Composition of blotting buffer used for Western analyses

Component	***Concentration***
TRIS-HCl, pH 8.3	25 mM
Glycine	192 mM
Methanol	10 % (v/v)
SDS	0.01 % (w/v)

The blotted and washed nitrocellulose membrane was blocked with 3 % (w/v) gelatine in TRIS buffer saline (TBS) for 1h (composition is given in Table 2.20). As primary antibody, plant PM-H$^+$-ATPase specific polyclonal rabbit IgG (Agrisera, Uppsala, Sweden) was used at 1,000x dilution in TBS buffer containing 1 % gelatine (overnight; room temperature). Non-bound antibody was removed by washing the membrane in Tween®20 TRIS buffer saline (TTBS) (Table 2.21), twice for 20 min, followed by two washes for 20 min each in TBS. Horseradish peroxidase (HRP)-labelled anti rabbit IgG produced in goat (BioRad Laboratories, Inc.) was used as secondary antibody. It was used at 3,000x dilution in TBS buffer (2 h). The membrane was washed in the same way as described for primary antibody and was then developed in developing solution (0.06 % (w/v) HRP Colour Development Reagent^{TM} (BioRad Laboratories, Inc.)). The colour development reagent contained 4-Cl-1-naftol as active component and was dissolved in -20 ℃ methanol and 0.015 % H_2O_2 in TBS. The bands were digitalized (HP Scanjet) before the membrane had dried out.

Table 2.20 Composition of TRIS buffer saline buffer (TBS)

Component	*Concentration*
TRIS-HCl, pH 7.5	20 mM
NaCl	150 mM

Table 2.21 Composition of Tween®20 TRIS buffer saline buffer (TTBS)

Component	*Concentration*
TRIS-HCl, pH 7.5	20 mM
NaCl	150 mM
Tween®20	0.005 % (w/v)

2.11.2 Quantitative Western blot analysis

Plasma membranes could only be isolated at Eötvös University, yet the more sensitive Western blot system was available at UCD, Dublin. Therefore, Western analyses of plasma membrane fractions were carried out not only at Eötvös University but also at UCD using plasma membrane vesicle samples which had been brought back (flight back from Hungary) on dry ice. The Western analyses system at UCD was the same one as described by Collins *et al*. (2011).

The separated proteins were blotted onto nitrocellulose membrane (Whatman® PROTRAN BA 85) using a Hoefer™ TE22 blotting system, at 40 V and 120 mA overnight at room temperature. The gel running buffer contained 20 % (v/v) methanol. Blotted nitrocellulose membranes were stained with Ponceau S stain (Sigma) and washed with washing buffer (0.2 % Tween®20 containing gel running buffer). Thereafter, membranes were blocked with 5 % skimmed milk powder in washing buffer for 1 h, at 30 rpm on a horizontal shaker. Primary antibody ($PM\text{-}H^+$-ATPase specific polyclonal rabbit IgG antibody; Agrisera, Sweden) was applied overnight at 2,500x dilution in washing buffer containing 5 % milk powder, at 30 rpm shaking. Non-bound primary antibody was removed through washing three times (10 min each; 70 rpm) in washing buffer. Peroxidase-labelled anti rabbit IgG produced in goat (Invitrogen Corporation, Carlsbad, California USA) was applied as secondary antibody at 10,000 x dilution in washing buffer containing 5 % milk powder (2 h; 70 rpm). After three final washes (10 min each) in washing buffer, bound secondary antibody was visualised through an EZ-ECL Chemiluminescence Detection Kit for HRP (Biologica Industries, Israel) and LAS-4000 Luminescence Image Analyser (Fujifilm, USA).

2.11.3 Immunostaining of paraffin-embedded sections

PM-H^+-ATPase tissue specific localisation was determined on paraffin-embedded samples using immunohistochemistry. The same PM-H^+-ATPase specific primary antibody was used as for Western blotting. Anti rabbit IgG alkaline phosphatase-labelled antibody, produced in goat (Sigma), was applied as secondary antibody as detailed in Table 2.22. Colour development was carried out with SIGMAFAST™ Fast Red TR / Naphthol AS-MX Tablets (Sigma) following the instructions of the manufacturer. Colour development was stopped with 7 % acetic acid. After a 5 min washing in running tap water, samples were mounted in 80 % glycerol in phosphate buffered saline (PBS, its composition is given in Table 2.23) under a cover slip.

Table 2.22 Protocol for immunostaining of embedded leaf sections

	Solutions	***Duration***
Rehydration		
	Neo-Clear® A	10 min
	Neo-Clear® B	10 min
	Absolute ethanol	5 min
	96 % ethanol	5 min
	70 % ethanol	2 min
	Running water	5 min
Blocking		
	5 % (v/v) goat serum in PBS	10 min
Staining		
	Primary antibody (100x diluted) in 2.5 % (v/v) goat serum in PBS	Overnight, 4 ℃
	Washing with PBS	3x 5 min
	Secondary antibody (30x diluted) in 2.5 % (v/v) goat serum in PBS	2 h
	Washing with PBS	4x 5 min
Colour development		
	SIGMAFAST™ Fast Red	2 - 10 min
	5 % (v/v) acetic acid	1 - 5 min
	Running water	5 min
Mounting		
	80 % glycerol in PBS	Mount under cover slip

Table 2.23 Composition of phosphate buffer saline (PBS; pH 7.4)

Component	**Concentration (mM)**	**Concentration (g / l)**
NaCl	137	8.00
KCl	2.7	0.20
$Na_2HPO_4x2H_2O$	8.1	1.44
KH_2PO_4	1.76	0.24

2.11.4 Densitometric analysis of Western blots

Densitometric analysis of Coomassie-stained polyacrylamide gels and Western blots was carried out with a Photetix 1D Advanced 4.01 system (Phoretix International, Newcastle, UK). Raw data were processed using Microsoft® Office Excel 2003 (Microsoft Corporation, USA) and Origin®6.1 (OrigiLab Corporation, USA) statistical software.

2.12 Protoplast experiments

2.12.1 Protoplast isolation

Protoplasts were isolated according to Volkov *et al.* (2007), with some modifications.

Osmolality of the isolation buffer, incubation time and shaking frequency were optimised. Cell walls and middle lamellae from tissue of the elongation zone were digested in 500 mOsm kg^{-1} isolation buffer with 90 rpm shaking frequency over a period of 2 - 3 hours in the dark, while pieces of the emerged blade were incubated in isolation buffer of 600 mOsm kg-1 osmolalility, over a 1 h period and at 160 rpm shaking frequency in the dark.

Cell wall digestive enzymes (Table 2.24) were dissolved in isolation medium (components are in Table 2.25) overnight, at 4 ℃, without any shaking or vortexing. Prior to use, enzyme solutions were centrifuged (5 min, 10,000 g, mini Spin plus, Eppendorf AG, Hamburg, Germany) and the supernatant was used for cell wall digestion.

Table 2.24 Composition of protoplast isolation buffer

Component	***Concentration***
Murashige and Skoog salt	4 g l^{-1}
MES	10 mM
Sorbitol	500 - 600 mOsm kg^{-1}
PVP K30	0.025 % (w/v)
BSA	0.1 % (w/v)
KOH	Used to adjust to pH 5.7

Table 2.25 Enzyme concentrations in protoplast isolation buffer

Enzyme	***Concentration***
Cellulase	1 % (w/v)
Driselase	0.5 % (w/v)
Pectolyase	0.05 % (w/v)

2.12.2 Purification of protoplasts

After enzymatic digestion of the cell wall, protoplast were passed through a 100 μm mesh and washed with 4 - 5 volume isolation buffer. Protoplasts were collected by centrifugation (30 g, 2 min; Eppendorf 5810 R, swinging bucket rotor) and resuspended in 0.3 – 1 ml volume using isolation buffer. Viability of protoplasts was tested using 0.001 % (w/v) fluorescein diacate (Larkin, 1976), which was prepared from a 0.1 % (w/v) acetone stock. Protoplasts were viewed with a Leica DMIL fluorescence microscope equipped with an excitation filter (450 - 490 nm) and suppression filter (515 nm).

Protoplasts were counted with a Neubauer ultra plane counting chamber (Hausser Scientific) under a Leica DMIL microscope. These data were used to relate expression values obtained through qPCR experiments to protoplast number.

2.12.3 Calculation of size and surface of the protoplast

The diameter of protoplasts was measured on micrographs taken with a Leica DMIL microscope with the help of Scion Image for Windows 4.0.3.2 software. From the diameter (d), the protoplast volume, $((\pi/6)d^3)$ and surface (πd^2) could be calculated,due to the almost perfectly spherical shape of protoplasts.

2.13 Statistical analysis

Statistical analysis was carried out with Origin® 6.1 (OriginLab Corporation) software, using paired and independent Student's t test and one-way ANOVA.

3 Results

3.1 Apoplastic pH measurements

Apoplast pH was measured through three independent approaches: in-vitro gel system, electrophysiology and confocal microscopy. The in-vitro gel system involved incubating leaf segments in agarose containing a pH indicator that made it possible to directly relate changes in apoplast acidity to changes in growth. With pH microelectrodes precise values of apoplast pH in growing and non-growing leaf regions could be obtained. Finally, confocal microscopy involved loading plants with pH fluorescence probes and had the advantage that intact plants could be studied.

3.1.1 In-vitro agarose gel system

The base 70 mm of leaf three was placed in agarose gel medium containing the pH indicator bromocresol purple. Growth was monitored parallel to acidification of the medium. The basic assumption underlying this experiment was that any changes in the extent of acidity of the medium adjacent to leaf tissue reflected similar changes in the net H^+ production rate (due to PM-H^+-ATPase activity) in the tissue's apoplast. 'Extent' of acidity can refer to either or both, changes in pH and changes in the area of medium which was acidic. Gel images of a typical set of experiments, involving application of fusicoccin and vanadate, are shown in Fig. 3.1 A-C.

There was a non-specific acidification of medium with a maximum acidification at the first hour following the placement of unpeeled leaf segments into the agarose. This acidification, which most likely reflected changes in apoplast pH caused by the unpeeling and which was not restricted to the base 40 mm (leaf elongation zone), disappeared within 4 - 5 h and then reappeared in a growth-dependent manner (Fig. 3.2 A and B). Growth dependency of acidification was also tested by applying an initial (0 - 24 h) cold treatment. There was no acidification of medium and no growth either during the cold treatment (Fig. 3.3). As soon as the cold treatment finished, growth resumed parallel to the acidification of medium (Fig. 3.3).

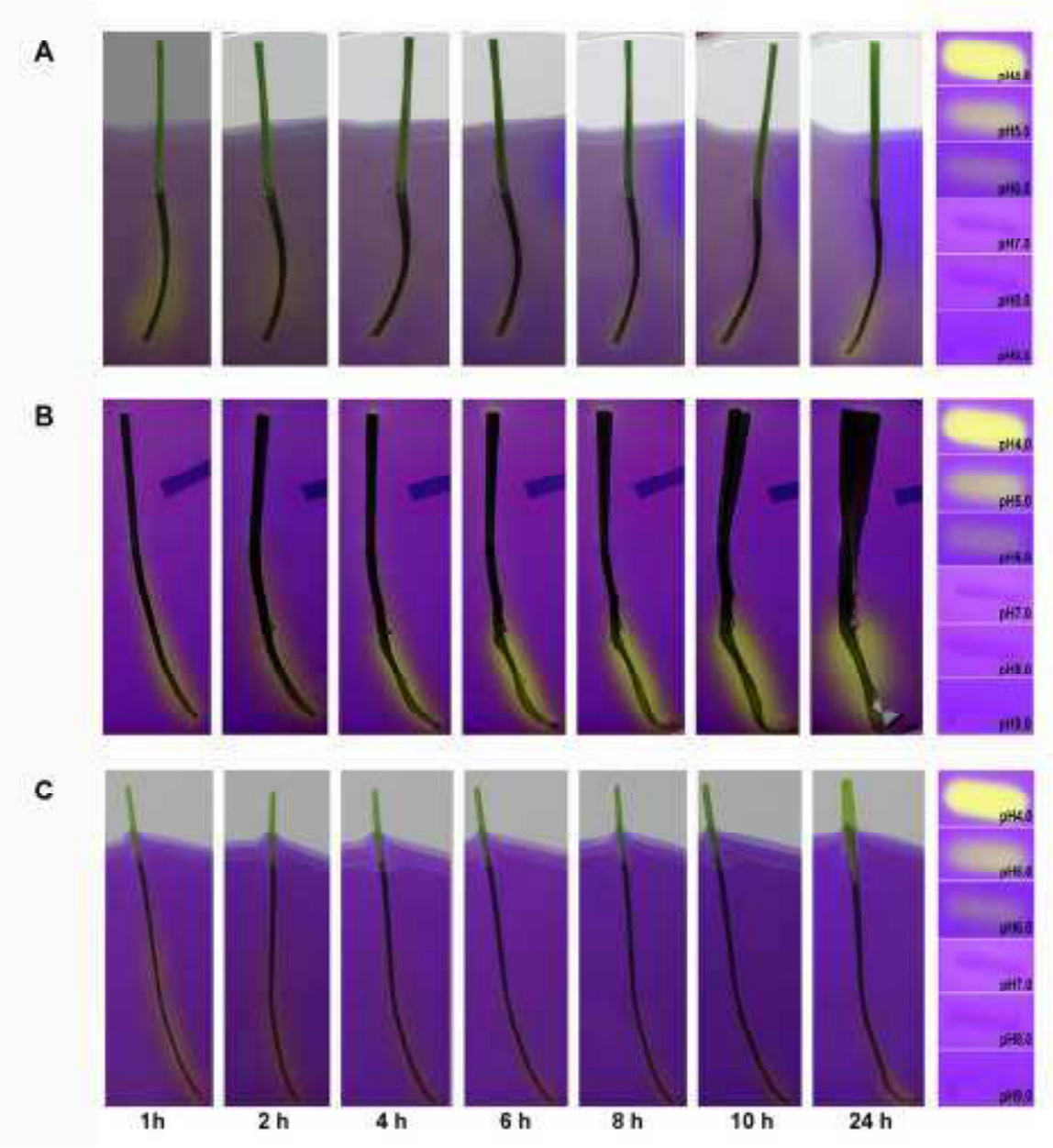

Figure 3.1 Leaf growth and apoplast acidification as analysed through the agarose gel system

Typical images of an experiment involving control leaves (A) and leaves which were placed in agarose containing 5 µM fusicoccin (B) and 500 µM vanadate (C). Scale bar is 1 cm long.

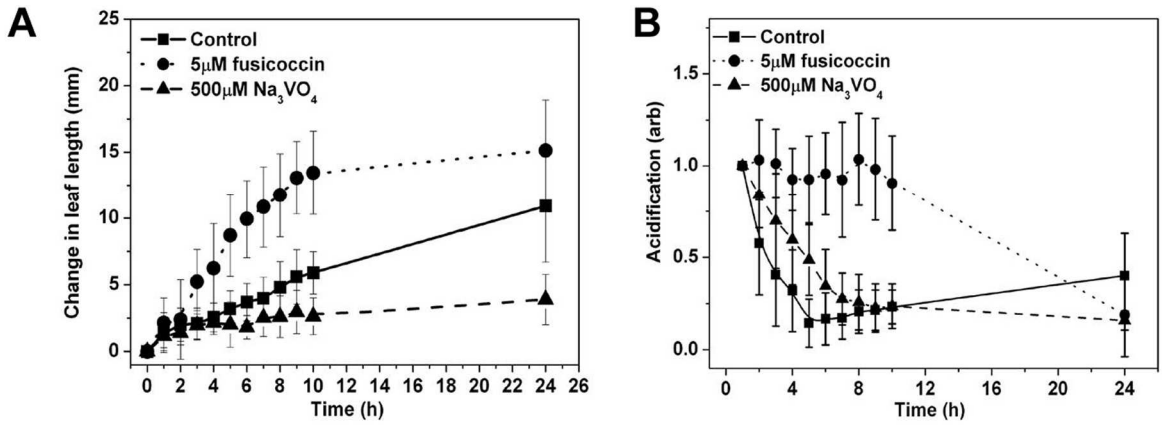

Figure 3.2 Time course of growth and acidification of in-vitro gel experiments

Typical time course of changes in leaf length (A) and medium acidification (B) in response to treatments are shown. Values are averages and standard deviations (error bars) of 27 (control) and 10 (treatments) plants.

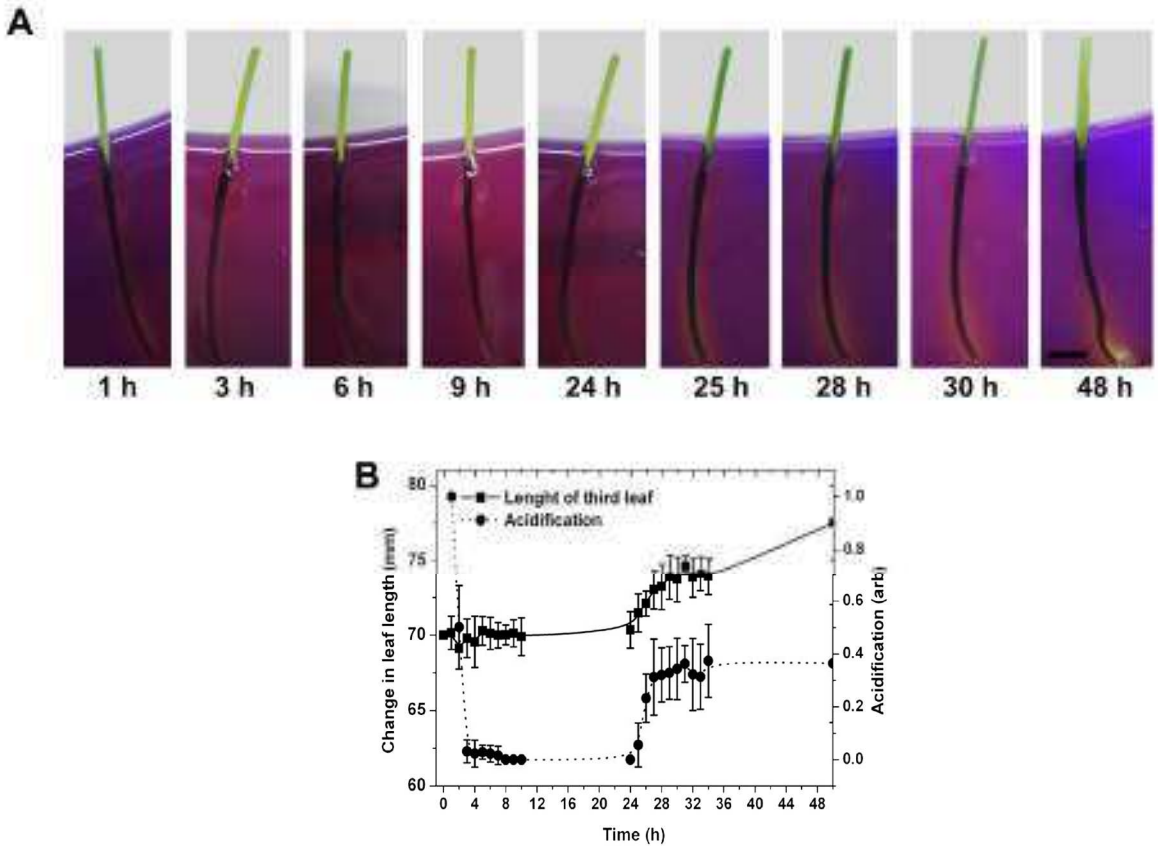

Figure 3.3 Leaf growth and acidification in agarose gel under cold treatment

Typical images of an experiment involving cold treated leaves 0–24 h and under control condition 24 - 48 h (A). Scale bar represents 1 cm. Response of medium acidification and change in leaf length (growth) to cold treatment and subsequent incubation in the growth chamber (B); values are averages and standard deviations (error bars) of 10 plants.

A range of treatments was tested for their effect on medium acidification and leaf growth (Fig. 3.4). Fusicoccin increased significantly leaf elongation rate and medium acidity. Vanadate caused the opposite effect, as did caesium, which inhibits K^+ channels (Szczerba *et al.*, 2009; Volkov *et al.*, 2009).

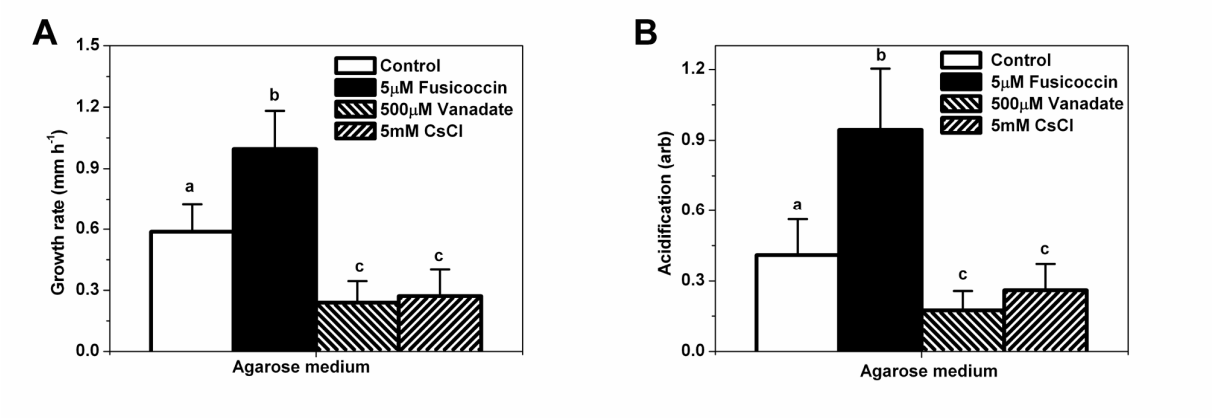

Figure 3.4 Average rate of leaf elongation (A) and medium acidification (B) in leaves exposed to fusicoccin, vanadate and caesium treatments as tested through the agarose gel system

All media contained 10 mM KCl and test reagents were applied at 5 μM (fusicoccin), 500 μM (vandate) or 5 mM (CsCl). Values are averages and standard deviations of 20 (control), 9 (fusicoccin), 7 (vanadate) and 14 (CsCl) plants. Different letters show a statistically significant difference at $p < 0.05$ (Student's t-test and ANOVA).

Although auxin-induced growth is often related to cell wall acidification and referred to as 'acid growth', no such stimulation of either growth or acidification was observed in the present study. Using in-vitro gel system and applying the artificial auxin, α-Naphthaleneacetic acid (NAA), growth did not change and acidification was similar to control. If anything, acidification of NAA treated plants continuously decreased whereas control plants started to slightly decrease after 5 h (Fig. 3.5).

Auxin-induced growth was not detected either when the experiment was carried out in liquid medium (10 mM KCl and 1 mM $CaCl_2$ without agarose and bromocresol purple) to check whether the absence of any auxin effect was due to conditions associated with the agarose gel. To check whether it was possible to induce any auxin-specific effects, coleoptiles were tested since these represent the classical 'acid growth' system. A significant increase in growth was measured (Fig. 3.6).

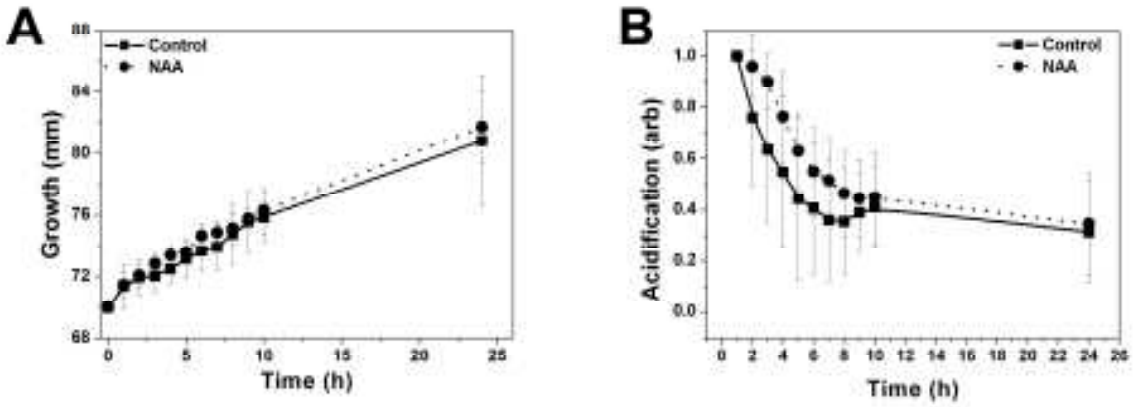

Figure 3.5 Effect of auxin on leaf growth and medium acidification using the in-vitro gel system

Difference in growth (A) was not found between 5 μM NAA treated and control plants. Medium acidification was similar in auxin-treated and non-treated (control) leaves (B). Traces are average of 10 - 27 plants, error bars represent standard errors.

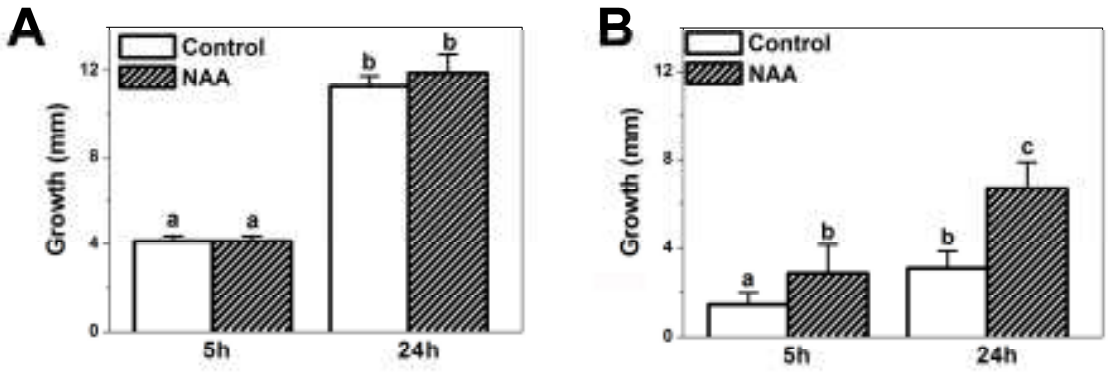

Figure 3.6 Growth effect of auxin when applied in liquid medium

NAA (5 μM) effect on growth was tested in liquid medium on leaf (A) and coleoptile pieces (B). Measurements were carried out at 5 h and 24 h of incubation. Values are averages and standard deviations (error bars) of 4 leaf pieces and 40 coleoptile segments. Different letters show a statistically significant difference at $p < 0.05$ using Student's t-test and ANOVA.

3.1.2 Microelectrode measurements

Microelectrode measurements of apoplastic pH in the growing leaf three showed that the pH in the elongation zone was by up to one pH unit lower than the pH in the emerged blade (Fig. 3.7 A). Apoplastic pH in the elongation zone depended on the K^+ concentration in the bathing medium which was in direct contact with the leaf surface during measurements. At the lowest K^+ concentration tested (0.1 mM), apoplast pH was 4.8. Apoplast pH increased with the K^+ concentration of the medium. At 10 mM K^+, apoplast pH in the elongation zone was 5.8 and

indistinguishable from the value in the emerged blade. In contrast to apoplast pH in the elongation zone, apoplast pH of the emerged blade did not change with bathing medium K^+. When the pH of the bathing medium was adjusted to pH 7.0 using KOH (final K concentration of 0.3 - 0.5 mM) apoplastic pH in the elongation zone was between 4.8 and 5.2. This proved that the lower apoplastic pH measured in the elongation zone was independent from the pH of the bulk (bathing) solution which was in direct contact with the apoplast, when the solution did not contain any buffer component. When the pH of the bathing solution was adjusted to pH 7.0 using 100 mM TRIS-HCl, including 0.1 mM KCl, the pH of the apoplast was 6.1 - 6.2 in both elongation zone and emerged blade (Fig. 3.7 B). Although this pH was lower by almost one pH unit than the pH of the bathing medium, this experiment showed that apoplast pH of the emerged blade was responsive to changes in the composition of the bathing medium and that the two were in direct contact. Bathing medium must have bypassed the cuticle and entered leaves through stomata. Growth of leaves on the microelectrode stage was not affected by K^+ treatments, despite the K^+-dependency of apoplast pH (Fig. 3.8).

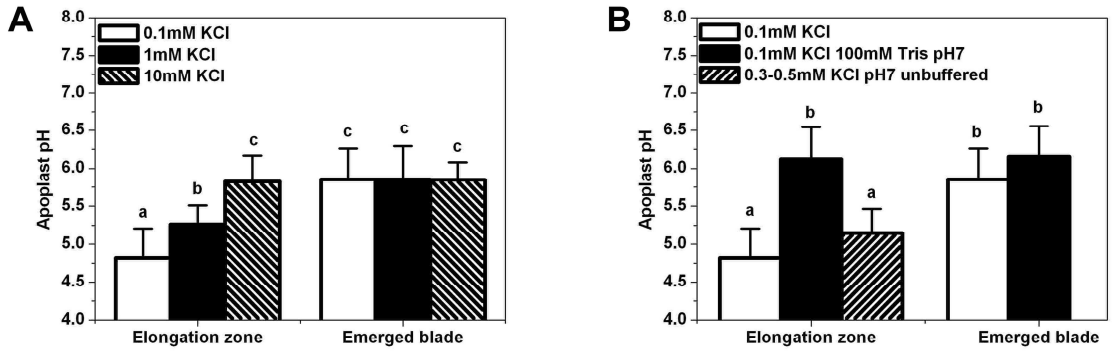

Figure 3.7 Microelectrode analyses of apoplast pH in the elongation zone and emerged blade-portion of leaf three of barley.

Apoplast pH was measured in dependence of the K^+ concentration (added as KCl) of the electrode bathing medium which was in direct contact with the leaf tissue analysed (A). Apoplast pH measured when buffered solutions were applied as bathing medium (B). Values are averages ±SD of 7 - 15 measurements obtained on 3 - 6 plants of each treatment. Different letters show a statistically significant difference at $p < 0.05$ (Student's t-test and ANOVA).

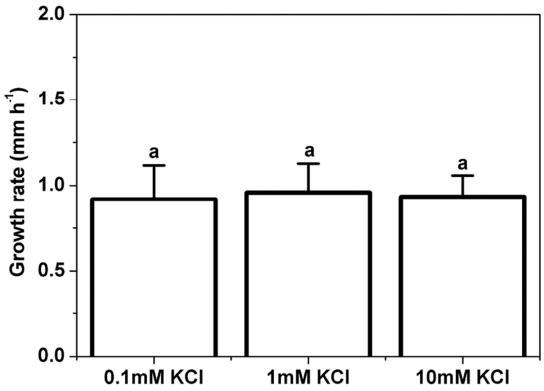

Figure 3.8 Growth rate of leaf three in response to K^+-treatments during micro pH measurements.

Values are averages ±SD of 7 - 15 measurements obtained on 3 - 6 plants of each treatment. Different letters show a statistically significant difference at $p < 0.05$ (ANOVA).

Vanadate (Na_3VO_4) and fusicoccin were added to the bathing medium to test whether the lower pH in the apoplast of the elongation zone was dependent on the activity of the PM-H^+-ATPase. Vanadate, which inhibits the PM-H^+-ATPase, was tested at a concentration of 500 µM in presence of 0.1 mM KCl. Apoplast pH in the elongation zone increased from pH 4.8 to pH 5.8, precisely the pH value observed in the emerged blade (Fig. 3.9). Fusicoccin, which stimulates the PM-H^+-ATPase (Marré, 1979; Würtele *et al*., 2003), was tested at a concentration of 5 µM in presence of 1 mM KCl. Apoplast pH was 5.2 and identical to the pH measured in absence of fusiccocin at 1 mM KCl in the bathing medium (Fig. 3.9). The rate of leaf elongation decreased in response to vanadate and increased in response to fusicoccin treatments (Fig. 3.10). This was observed for all experimental setups (Fig. 3.10).

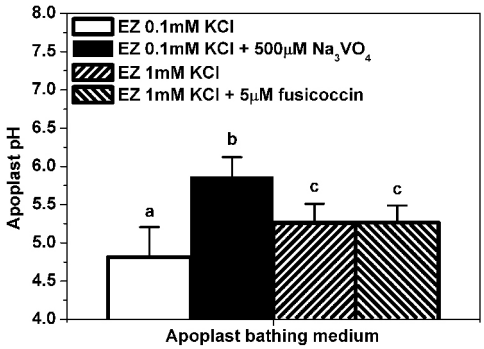

Figure 3.9 Microelectrode pH analyses in the leaf elongation zone of barley in response to sodium orthovanadate and fusicoccin treatments

The KCl concentration in the bathing medium was as indicated. Values are averages and standard deviations (error bars) of 12 (controls of 0.1 mM and 1 mM KCl), 4 (500 µM vanadate) and 4 (5 µM fusicoccin) datasets of between 3 - 6 different plants each. Different letters show a statistically significant difference at $p < 0.05$ (Student's t-test and ANOVA).

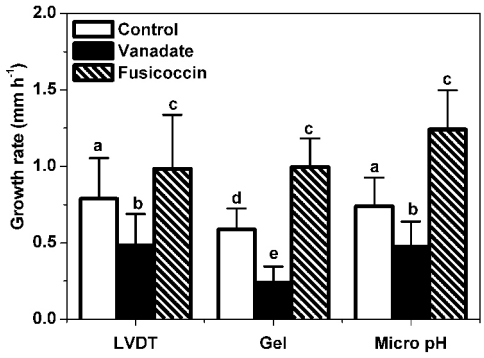

Figure 3.10 Growth rate of leaf three of barley in response to vanadate and fusicoccin treatments as analysed through different approaches

Values are averages and standard deviations (error bars) of 13 - 60 (control), 3 - 8 (vanadate) and 3 - 10 (fusicoccin) replicates. Different letters show a statistically significant difference at $p < 0.05$ (Student's t-test and ANOVA).

3.1.1 Confocal microscopy

Acridine orange and 5(6)carboxyfluorescein are pH sensitive fluorescence dyes. They were used to test whether the apoplastic pH was lower in the elongation zone compared with emerged blade in intact barley plants. First, the system had to be calibrated. This was achieved by peeling epidermal strips from plants which had been grown for 24 h in the presence of 5(6)carboxyfluorescein and 48 h in presence

of acridine orange in the root medium to allow sufficient uptake of dye into leaf tissue. Exposure of epidermal strips to solutions of different pH showed (i) that dye had been taken up into the leaf apoplast and (ii) that the fluorescence intensity of dye in the apoplast changed in the physiological pH range, in the same manner as observed for dye in free solution (Fig. 3.11 A, B for acridine orange and Fig. 3.12 A, B for carboxyfluorescein). Fluorescence decreased with pH. Optical sections from the epidermis of intact third leaves showed that the fluorescence intensity, and by implication pH, were considerably lower in the apoplast of the elongation zone than in the apoplast of the emerged blade (Fig. 3.11 C-F for acridine orange and Fig. 3.12 C-F for carboxyfluorescein).

It is possible that the difference in fluorescence intensity between leaf regions resulted not from differences in apoplast pH but from differences in the concentration of dye accumulated during the uptake period. This was tested by peeling epidermis strips from the elongation zone and emerged blade (leaf three) of dye-loaded plants and incubating the peels in pH 7.5 buffer solution. Peels were examined after a 30 min incubation period using a Leica epifluorescence microscope. The fluorescence intensity and by implication carboxyfluorescein and acridine orange concentration was similar in the epidermis of the two leaf regions; if anything, it was higher in the elongation zone (Fig. 3.13). This experiment showed that the lower apoplast pH in the epidermis of the elongation zone of intact, dye-loaded plants, was not the result of a lower fluorochrome concentration but reflected most likely a true difference in apoplast pH between the two leaf regions. Uptake of dyes through roots and accumulation in leaf tissue did not cause changes in leaf growth (Fig. 3.14 A, B).

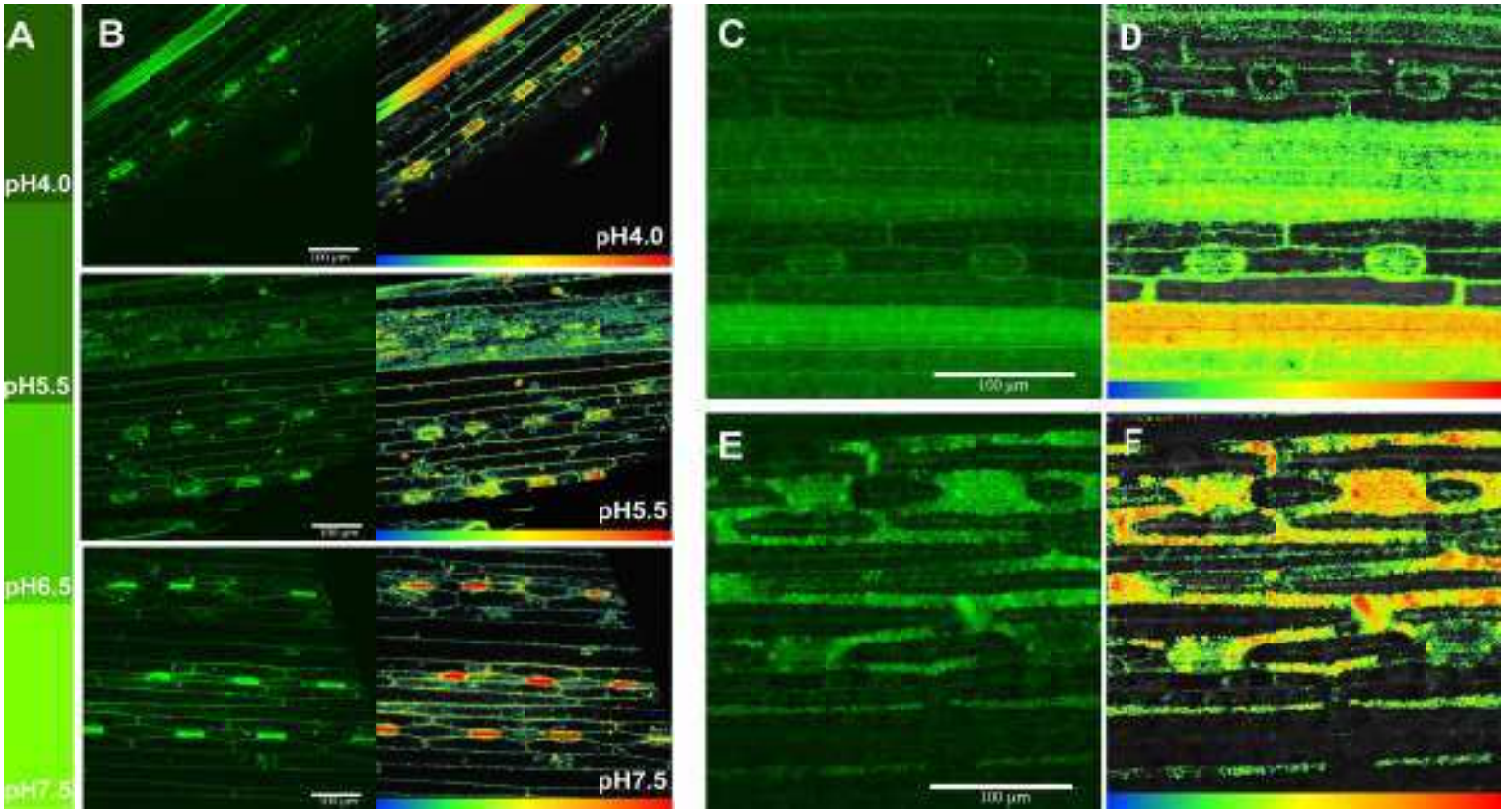

Figure 3.11 Confocal microscopic analysis of apoplastic pH using acridine orange fluoresce pH sensitive fluorescence dye

The pH sensitivity of fluorescence of dye as tested on sample droplets which contained 2.5 µM acridine orange and were buffered at the pH indicated (A). Confocal images of epidermal peels of the mature leaf one; following incubation of peels for 30 min in the solutions as shown in (B). Typical confocal images (C, E) and their heat map (D, F). Elongation (C, D) and emerged (E, F) region of leaf three of intact plants. Images containing scale bars show the original fluorescence image, while corresponding images without scale bars represent heat maps of images.

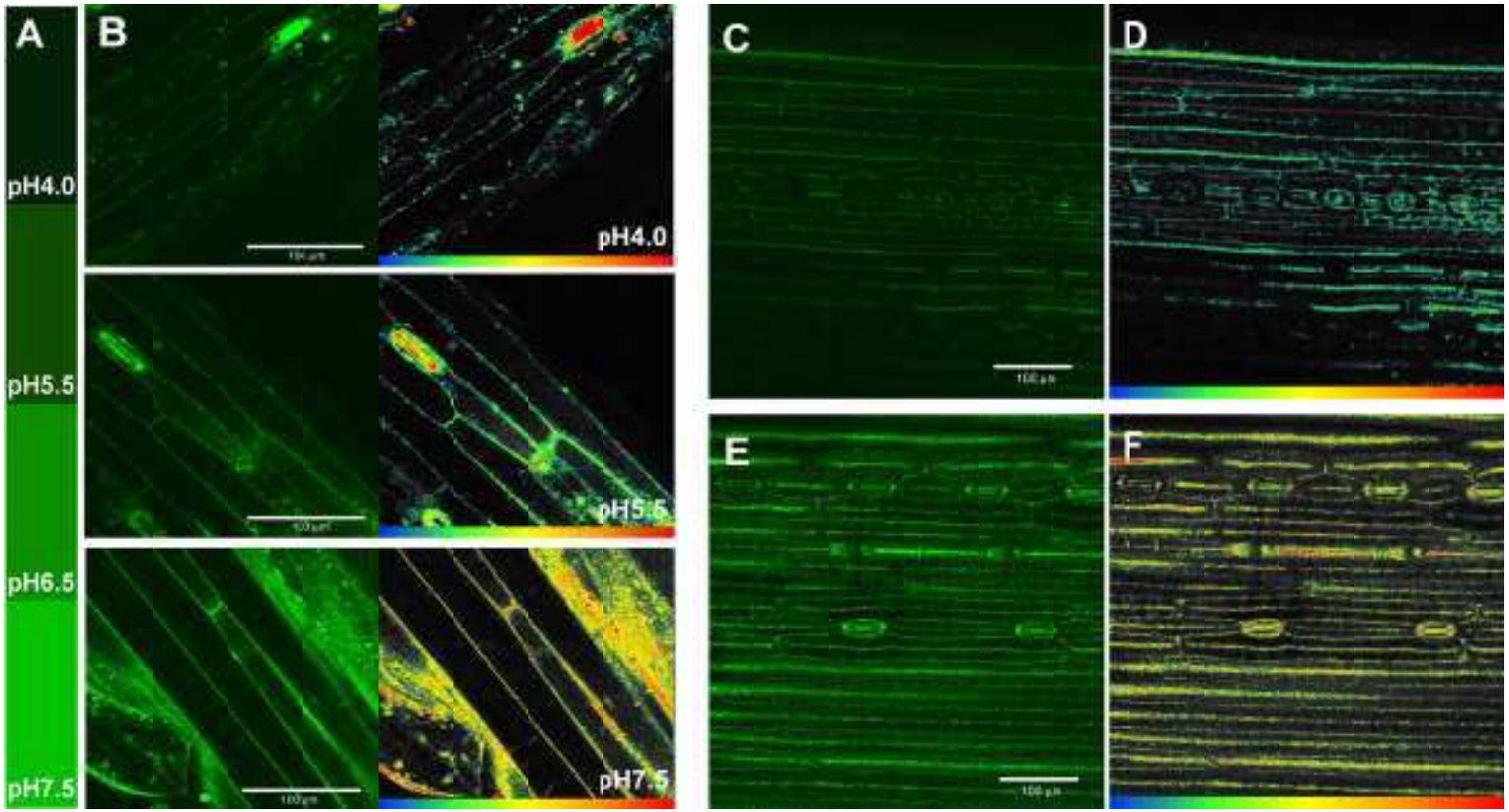

Figure 3.12 Confocal microscopic analysis of apoplastic pH using 5(6)carboxyfluorescein fluoresce pH sensitive fluorescence dye

The pH sensitivity of fluorescence of dye as tested on sample droplets which contained 10 µM carboxyfluorescein and were buffered at the pH indicated (A). Confocal images of epidermal peels of the mature leaf one; following incubation of peels for 30 min in the solutions as shown in (B). Typical confocal images (C, E) and their heat map (D, F). Elongation (C, D) and emerged (E, F) region of leaf three of intact plants. Images containing scale bars show the original fluorescence image, while corresponding images without scale bars represent heat maps of images.

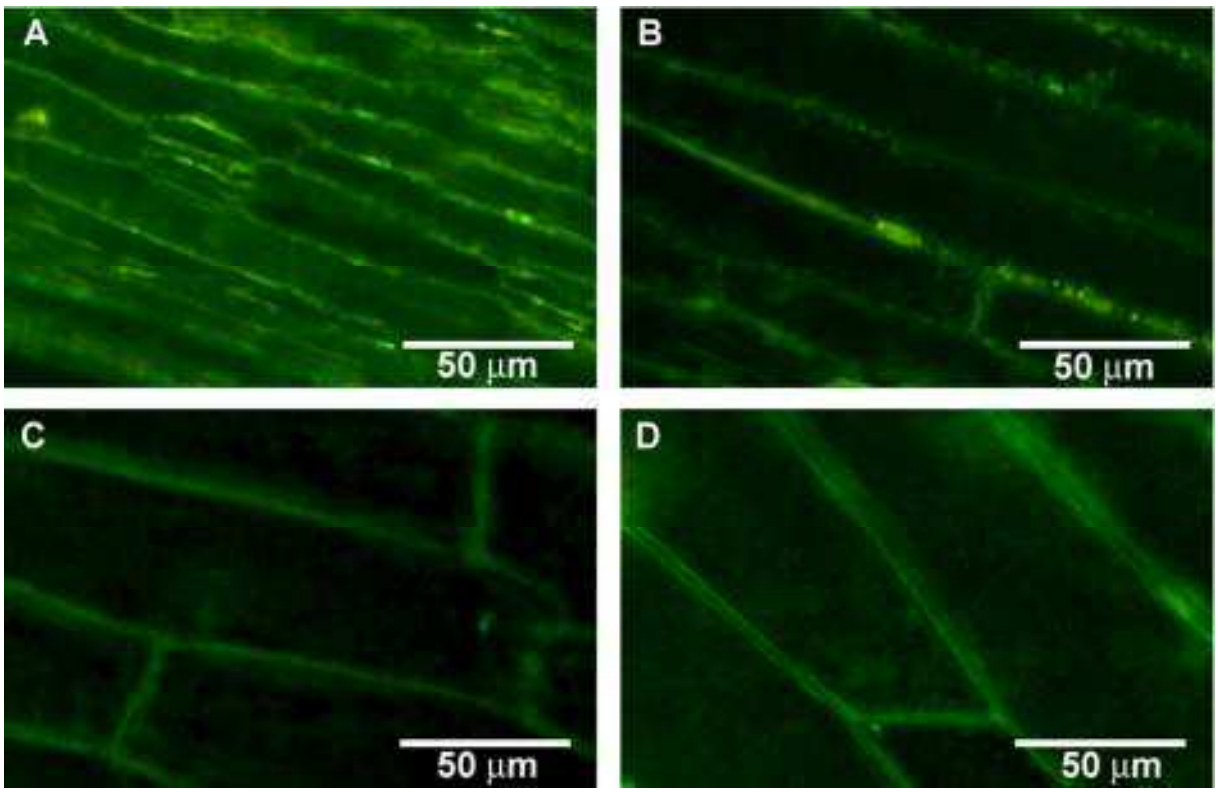

Figure 3.13 Carboxyfluorescein and acridine orange accumulation pattern in elongation zone and emerged blade

The distribution of the pH sensitive probes (5(6)carboxyfluorecein, A, C and acridine orange, B, D) appears to be similar in the elongation zone (A, C) and emerged leaf blade (B, D). The dye was taken up through the roots of intact plants and the epidermal strips of leaf three were incubated (30 min) in pH 7.5 buffer prior to be viewed under the microscope (Leica DMIL; 450 - 490 nm excitation filter and 515 nm suppression filter).

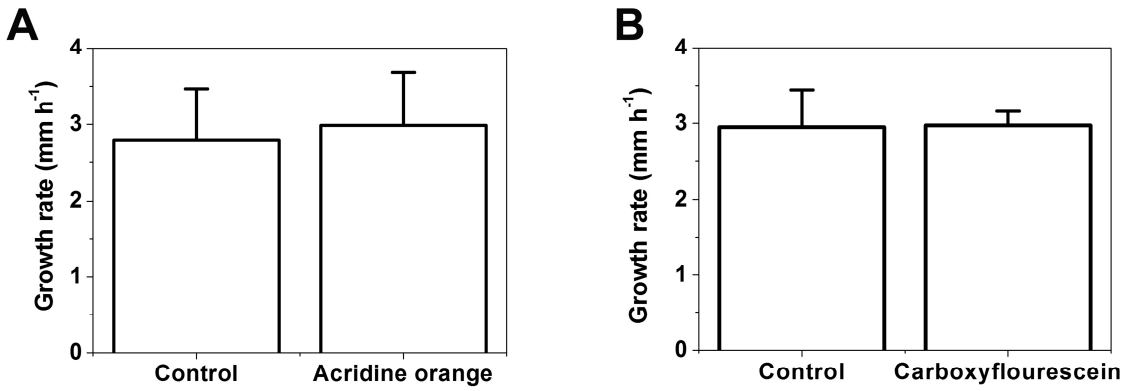

Figure 3.14 Effect of pH sensitive dyes on leaf growth rate

Growth, as measured with the LVDT on intact plants (unpeeled leaf three) did not change after 48 h incubation of plants in nutrient solution containing 2.5 μM acridine orange (A); the same was observed for plants after 24 h incubation in nutrient solution containing 10 μM carboxyfluorescein. Values are averages of 3 replicates, and error bars represent standard errors.

The pH sensitivity of fluorochrome 5(6)carboxyfluorescein and acridine orange was determined by fluorescence spectroscopy. Both fluorescein probes showed pH-sensitivity in the physiological pH range and had single peak spectra. Carboxyfluorescein showed a larger pH sensitivity in the pH range of interest compared with acridine orange (Fig. 3.15).

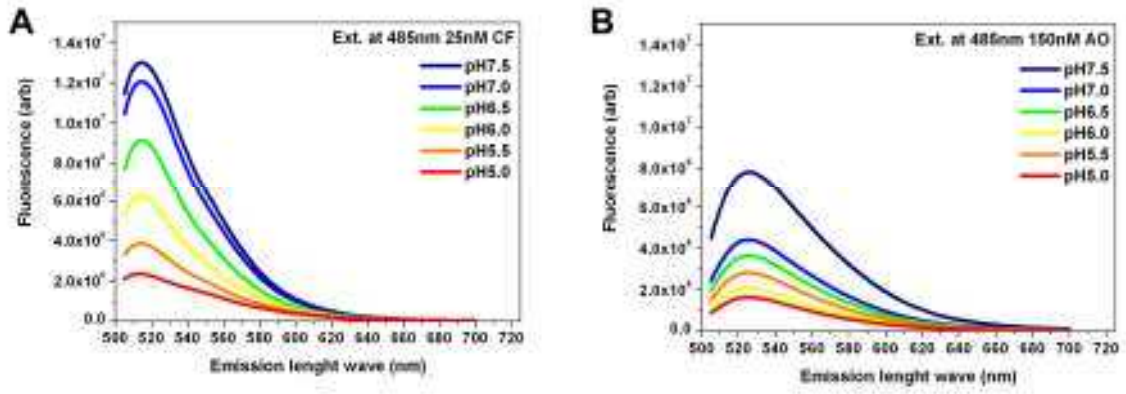

Figure 3.15 pH sensitivity of fluorochromes

Fluorescence spectra and pH sensitivity of 5(6)carboxyfluorescein (A) and acridine orange (B) was recorded. Both fluorochromes had pH sensitivity although carboxyfluorescein gave more explicit signal and better pH fidelity in the physiological pH range.

3.2 LVDT analyses of growth responses to treatments

3.2.1 Leaf elongation under different treatments

The basic assumption underlying LVDT experiments was that the wet tissue paper which was soaked in test solution and in direct contact with the surface of the elongation zone of leaf three allowed the test solution to diffuse into the apoplast. The responsiveness of setup to treatments was tested through two types of experiment, one designed to increase (37 ℃) and on e designed to reduce growth (1 M NaCl). Elongation growth of grass leaves responds little to changes in ambient temperature but to the temperature close to the basal meristem (Stoddart & Lloyd, 1986). Therefore, parts of a potato which had been heated to 37 ℃ in an incubator were placed round the leaf elongation zone without any direct contact between the potato and the barley seedling. Growth started to increase within minutes (Fig. 3.16 A, B). With time, the potato cooled down and leaf elongation rate decreased. When finally 1 M NaCl was added to impose a severe osmotic stress, growth stopped instantly and remained zero or close to zero (Fig. 3.16 A, B).

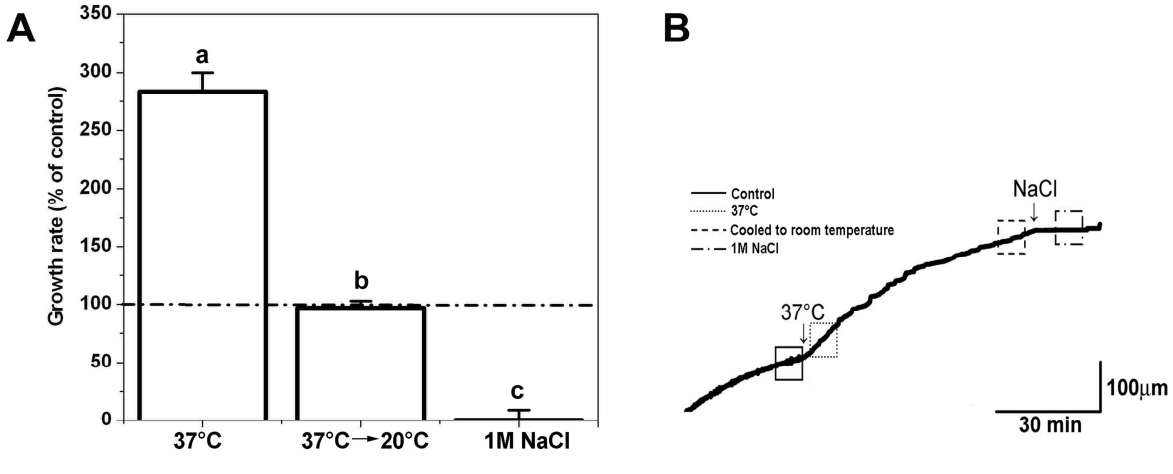

Figure 3.16 Testing the responsiveness of the LVDT setup to treatments which were expected to increase (37 ℃) or stop growth (1 M NaCl)

Average values (three plants) and standard deviations (error bars) (A) and a typical trace (B) are shown. The apoplastic bathing medium always contained 1 mM KCl. Different letters show a statistically significant difference at $p < 0.001$ (Student's t-test).

Having tested the responsiveness of the LVDT setup, treatments were applied. In presence of 1 mM KCl in the test solution fusicoccin (5 µM) increased leaf elongation rate to 160 % the rate observed in control plants. Vanadate, CsCl and CsCl–vanadate double treatments caused a 50 % decrease in growth rate (Fig. 3.17). The same was observed for the K^+ channel blocker tetraethylammonium (TEA) and ammonium, which blocks high-affinity K^+ transporters (NH_4^+; HAK-type transporters (Kronzucker *et al.*, 2003; Rodriguez-Navarro & Rubio, 2006; Szczerba *et al.*, 2006).

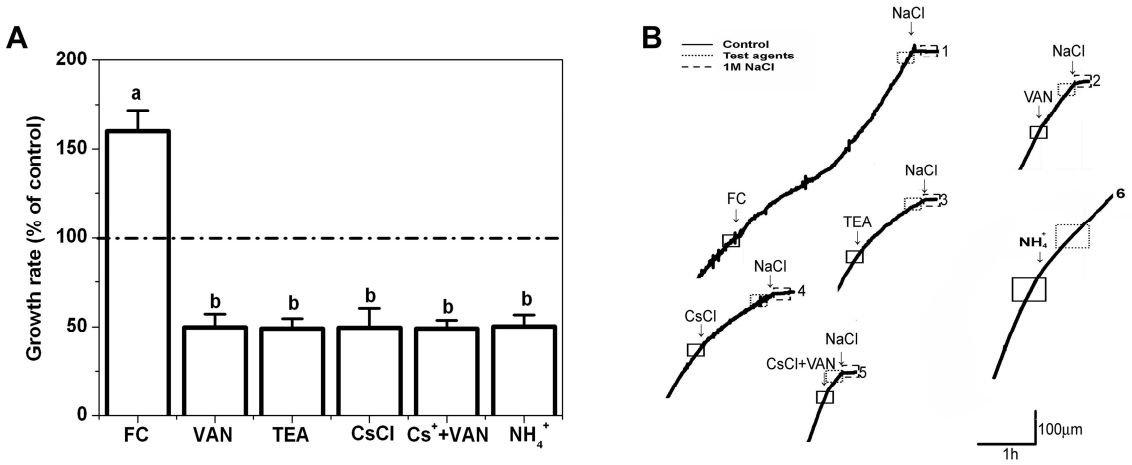

Figure 3.17 The effect of test reagents in the apoplastic bathing medium on leaf growth as measured with the LVDT setup

Average values and standard deviations of experiments (A) involving application of test reagents are shown (fusicoccin (5 µM, n = 3 plants), vanadate (VAN, 500 µM, 6 plants), tetraethylammonium chloride (TEA, 50 mM, 6 plants), CsCl (40 mM, 4 plants), CsCl+VAN double-treatment (40 mM / 500 µM, 3 plants), and $(NH_4)_2SO_4$ (20 mM, 3 plants)). Media always contained 1 mM KCl. Typical traces of experiments (B). Growth rates are expressed as percent of the respective KCl control, which contained only KCl but no test reagents in the apoplastic bathing medium. Different letters show a statistically significant difference at $p < 0.05$ (Student's t-test and ANOVA).

The effect of fusicoccin on elongation growth was dependent on the K^+ concentration in the bathing medium which was in direct contact with the leaf elongation zone (Fig. 3.18). The higher the K^+ concentration was, the larger was the stimulation of growth. In contrast, the inhibitory effect of vanadate on leaf elongation growth did not depend on the K^+ concentration in the bathing medium (Fig. 3.18). This experiment showed that changes in the K^+ concentration *per se* did not affect growth but required a functional PM-H^+-ATPase to affect growth.

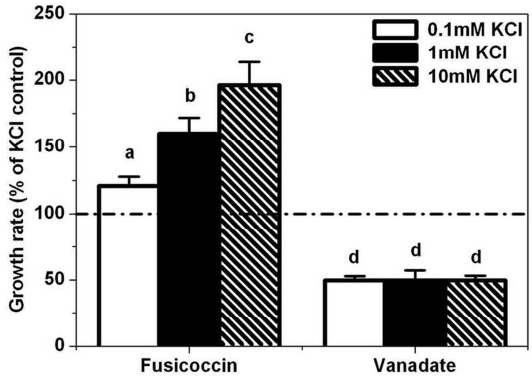

Figure 3.18 Potassium dependency of the leaf growth response to fusicoccin (5 µM) and vanadate (500 µM)

Values are averages and standard deviations (error bars) of 3 - 6 plants, and the K^+ concentration of apoplastic bathing medium was as indicated. Growth rates are expressed as percent of the respective KCl control, which contained only KCl and no test reagents in the apoplastic bathing medium. Different letters show a statistically significant difference at $p < 0.05$ (Student's t-test and ANOVA).

Short term (1 - 4 h) auxin-induced leaf growth was measured with the same LVDT set up. Treatments (5 µM NAA with 1 mM KCl) did not caused any significant increase in growth rate, moreover the leaf elongation rate slightly (but not significantly) decreased rather than increased (Fig. 3.19). These results suggested that leaf elongation can not be further increased by auxin treatments.

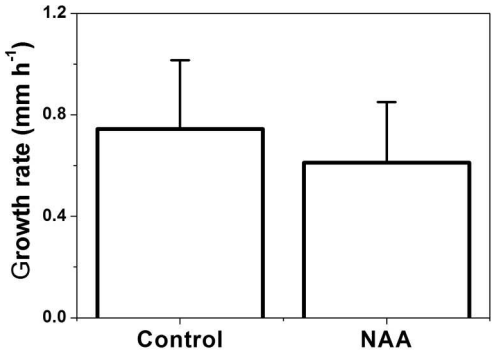

Figure 3.19 Auxin effect on leaf elongation growth

Elongation growth was monitored using the LVDT system. Growth in control (1 mM KCl) and NAA treated plants (1 mM KCl and 5 µM NAA) did not significantly differ from each other. Values are averages and standard deviations (error bars) of 3 replicates. The difference in growth between control and NAA treatment is statistically not significant (Student's t-test).

3.2.2 Cell wall changes in response to treatments

Changes in cell wall properties were tested for 500 µM vanadate, 40 mM CsCl and 5 µM fusicoccin treatments by applying an additional 3 g counterweight on the LVDT system. Control plants had 1 mM KCl in the apoplast bathing medium of the elongation zone. The elastic growth component significantly changed only in response to the fusicoccin treatment, whereas plasticity was affected significantly in response to CsCl (Fig. 3.20 A). Additional stress (0.03 N) on the cell wall did not change the relative growth rate compared with control (1 mM KCl, $\Delta\Delta v$), except in fusicoccin-treated leaves. Fusicoccin treatment caused a 50 % increase in $\Delta\Delta v$ compared with all other treatments and the control (Fig. 3.20 B).

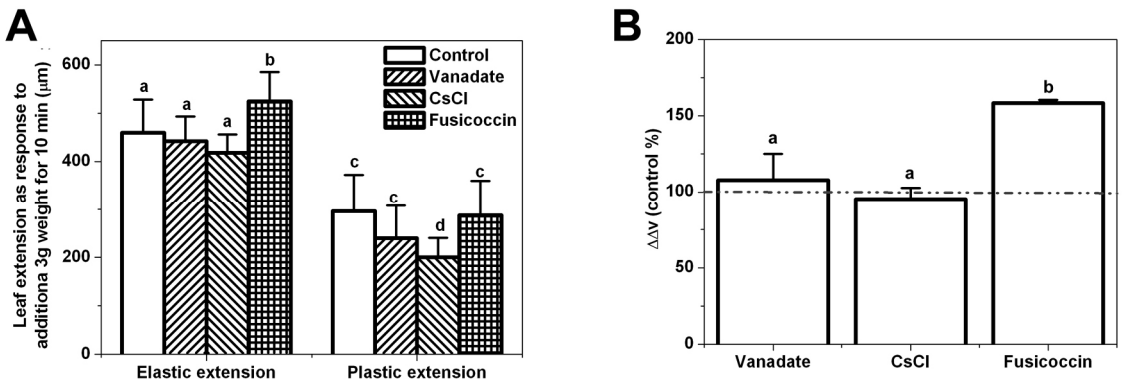

Figure 3.20 Cell wall changes under different treatments

Elastic and plastic growth (A) and 0.03 N stress caused growth rate (B) was measured on 3 independent plants in two replicates each. $\Delta\Delta v$ means the difference between $\Delta v_{control}$ and $\Delta v_{treatment}$ where Δv is the difference in growth rate before and under the applied additional stress (v_2-v_1 on Fig. 3.2). Different letters show statistically different values at $p < 0.05$ level with Student's t-test and ANOVA.

Growth rate before (v_1) and under (v_2) applied 0.03 N force was in agreement with previous effect of test reagents on growth (compare Fig. 3.17 and Fig. 3.21). The fusicoccin treatment caused a large increase in growth, although the increase was statistically not significant.

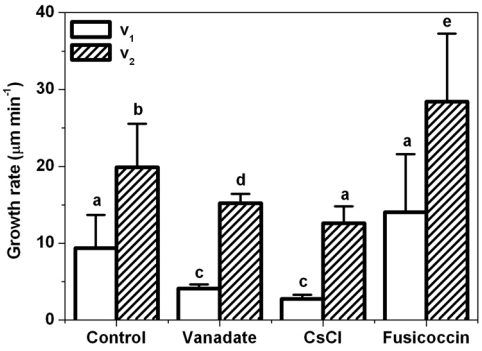

Figure 3.21 Growth rate before and in response to an additional applied force (0.03 N)

Growth rate before (v_1) and under (v_2) applied force (3 g) using different treatments as vanadate (500 μM), CsCl (40 mM) or fusicoccin (5 μM). Bath medium of control plants contained 1 mM KCl. Values are averages of 3 - 3 replicates. Different letters shows statistically different values at $p < 0.05$ level with Student's t-test and ANOVA.

3.3 Expression analysis of PM-H$^+$-ATPase using qPCR

PM-H$^+$-ATPase expression was analysed using qPCR. Altogether five reference genes (GADPH, cyclophilin, ubiquitin, HSP70 and PM-H$^+$-ATPase) were tested in the experimental system. Only ubiquitin and the two PM-H$^+$-ATPase (Ha1 and ATPase) primer pairs showed similar expression in the elongation zone and emerged blade (Fig. 3.22 A). Other, commonly used reference genes such as actin, tubulin, EF1, LHC were not suited because growing and non-growing leaf regions had to be compared (see Besse *et al*., 2011; Volkov *et al*., 2009). Ubiquitin could not be used as reference gene because the PCR product was not homogenous but produced more than one band as agarose gel analysis showed (Fig. 3.22 B). Applying Genevestigator bioinformatics application (www.genevestigator.com) could not solve the problem. Therefore, it was decided to carry out absolute qPCR quantification to determine PM-H$^+$-ATPase expression levels in the leaf elongation zone and emerged blade.

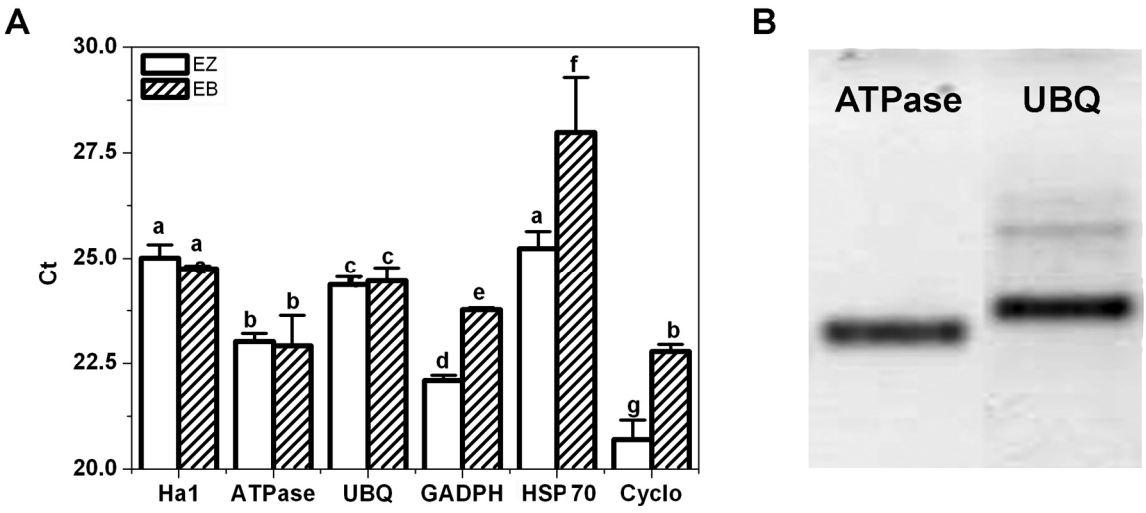

Figure 3.22 reference genes for qPCR experiments

500 pg total RNA-equivalent cDNA was used in each reaction well to check the qPCR profile of candidate reference genes. Expression, as shown as Ct-value, of the two PM-H^+-ATPase PCR primer pair (Ha1 and ATPase) and ubiquitin (UBQ) was similar between the two leaf regions, effectively qualifying them as reference genes of expression. In contrast, expression of glyceraldehyde-3-phosphate dehydrogenase (GADPH), heat shock protein 70 kDa (HSP70) and cyclophylin (Cyclo) differed significantly between leaf regions (A). Values are averages of 3 replicates and error bars represent SD. Different letters show significantly different values at $p < 0.05$ level using Student's t-test and ANOVA. Agarose gel picture of PM-H^+-ATPase (ATPase) and ubiquitin (UBQ) show that that ubiquitin shows more than one PCR product (B).

3.3.1 Quality control of the standard required for absolute qPCR

Quality of reference DNA (purified PM-H^+-ATPase PCR fragments) was validated using end point detection digital PCR technique (Vogelstein & Kinzler, 1999). The concentration of fragments was calculated as 0.5 copy μl^{-1} based on Nanodrop® measurements. From 40 PCR reactions 21 were PCR positive and 19 negative (Fig. 3.23). This suggested a concentration of 0.525 DNA copy μl^{-1} in the external standard and was just 2.5 % higher compared with the calculated copy concentration (0.5 copy μl^{-1}).

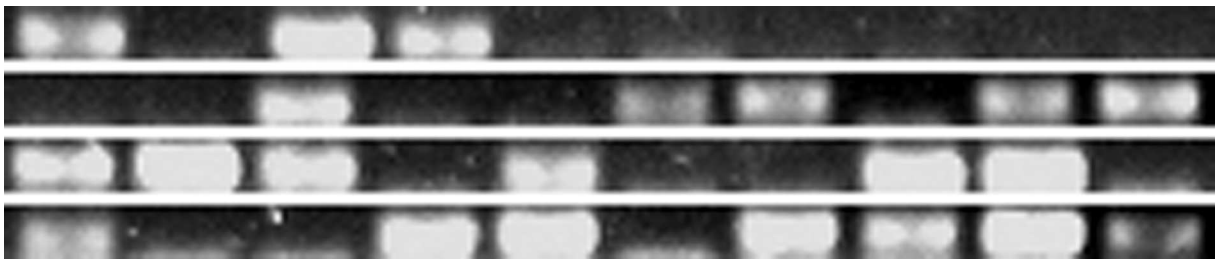

Figure 3.23 Digital PCR pattern of external standard DNA

Using digital PCR technique the concentration of the external standard for PM-H^+-ATPase expression was verified. The PCR positive / negative ratio was 21 / 19, which suggests a concentration of 0.525 copy of ATPase DNA in 1 µl of standard compared with the calculated 0.5. Therefore, the reliability of the standard was higher than 95%.

3.3.2 Calculation of cell number and membrane surface

Total cell volume of the leaf regions was calculated for the two barley cultivars using the water content of the plant material, cell dimensions and contribution of each tissue to total leaf symplast volume (Table 3.1). The water content differed significantly between the two leaf regions but not between the two cultivars.

Table 3.1 Water content of two different regions of leaf three in two cultivars of barley

Cultivar	Leaf part	No replicates	Water content (%)	SD
Golf	Elongation zone	3	92.06	1.57
	Emerge blade	3	86.78	2.25
Jersey	Elongation zone	7	93.78	3.12
	Emerge blade	7	87.78	1.07

The tissue volume ratio was measured on cross sections using light microscopy (Table 3..2 and Fig. 3.24) and average cell size was estimated from the present protoplast measurements and data published for Golf (Fricke & Flowers, 1998; Volkov *et al.*, 2007; Volkov *et al.*, 2009, Kavanagh, 2010) (Table 3.3). Mesophyll and epidermis cell size and surface area was calculated separately and the total number of cells and surface area was calculated from data on the contribution of each tissue to total leaf symplastic volume (not considering intercellular air space). Mesophyll cell size differed between growing and mature, emerged tissues around 2.2-fold and epidermis cells differed 4.6-fold, in each case being larger in emerged tissue. The surface was about 2.6-fold and 1.9-fold higher in the emerged blade for epidermis and mesophyll, respectively.

Table 3.2 The contribution of different tissues to total leaf volume in the elongation zone (EZ) and emerged blade (EB) of leaf three of barley. Values are given as % of the total leaf volume and are either not corrected or corrected for intercellular air space, effectively giving a contribution to total leaf symplastic volume.

	EZ		EB	
Epidermis (%)	24.85	± 1.54	23.37	± 2.94
Mesophyll (%)	61.75	± 1.93	51.61	± 4.36
Vascular bundle (%)	8.99	± 1.97	4.01	± 0.93
Intercellular air space (%)	4.40	± 1.32	21.01	± 4.29
Epidermis corrected (%)	26.00	± 1.28	29.59	± 3.72
Mesophyll corrected (%)	64.60	± 1.96	65.34	± 5.52
Vascular bundle corrected (%)	9.41	± 1.80	5.08	± 1.18

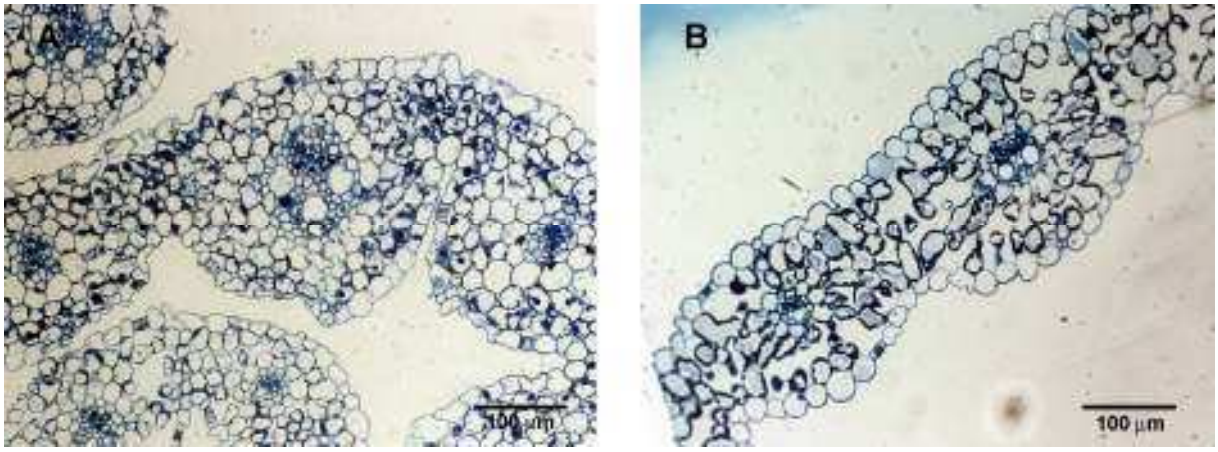

Figure 3.24 Representative cross sections used for determination of the contribution of different tissues and air space to total leaf volume

Toluidine blue stained cross sections were used to calculate the percentage of different tissues to total leaf and symplastic volume in the elongation zone (A) and emerged blade (B) of leaf three of barley.

Table 3.3 Cell size calculation based on the present and literature data. Values shown in bold were used for to relate ATPase expression and activity data to cell volume and surface area

	EZ		EB	
Cell volume	Average	SD	Average	SD
Epidermis cell size (Fricke & Flowers, 1998)	99.4		461	
Epidermis cell size average (pl)	**99.4**		**461**	
Mesophyll cell size (my protoplast results)	3.7		9.4	
Mesophyll cell size (Volkov *et al*., 2007)	8.9		24.4	
Mesophyll cell size (Volkov *et al*., 2009)	11.8		17.4	
Mesophyll cell size (Kavanagh, 2010)	2.08		8.11	
Mesophyll cell size average (pl)	**6.62**	± 4.52	**14.83**	± 7.59
Cell surface				
Surface of epidermis cell (Fricke & Flowers, 1998)	27100		65200	
Surface of epidermis cell (Kavanagh, 2010)	12308		34809	
Surface of epidermis cell average (μm^2)	**19,707**	± 10,459	**50,004**	±21,490
Mesophyll cell size (my protoplast results)	1,157		2,154	
Mesophyll cell size (Volkov *et al*., 2007)	2,077		4,068	
Mesophyll cell size (Volkov *et al*., 2009)	2,506		3,247	
Mesophyll cell size (Kavanagh, 2010)	788		1,952	
Surface of mesophyll cell (μm^2)	**1,632**	± 796	**2,855**	± 988

3.3.3 Gene expression data based on absolute qPCR method

Using the absolute qPCR method, together with cell size and tissue volume contributions it was found that PM-H^+-ATPase had a constant expression pattern in both elongation zone and emerged leaf blade; it was deemed to be a perfect reference gene in both Golf and Jersey cultivars (Fig. 3.25 and Table 3.4). The total RNA content was similar in the elongating zone and emerge leaf blade. This applied to both Golf and Jersey cultivars (Table 3.4).

Results expessed per plasma membrane surface unit were significant, being around 2 times higher PM-H^+-ATPase protein concentration as might be presumed in elongation zone compare with emerge blade in both barley cultivars. Absolute expression was 3 times higher in Golf compare to Jersey cultivar (Fig. 3.26). The calculation here presumed that protein translation from mRNA was linear and had equal probability in elongation zone and emerge blade. More details of the calculation can be found in the Appendix.

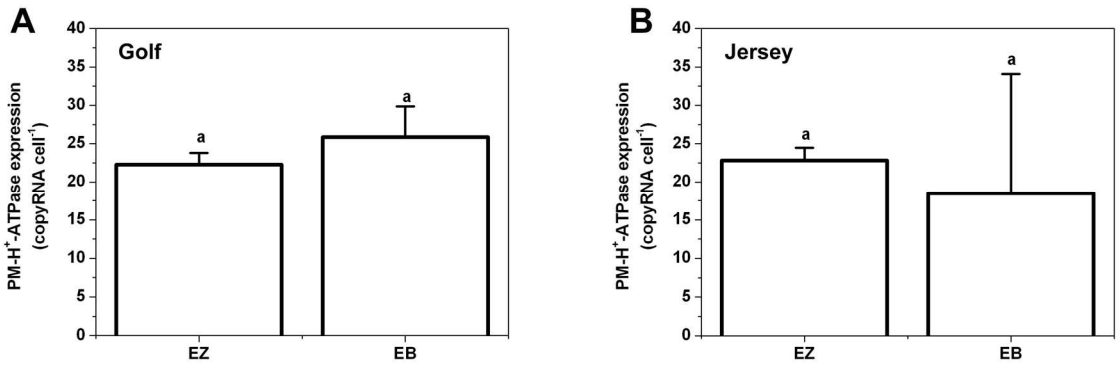

Figure 3.25 Expression of PM-H$^+$-ATPase using absolute qPCR

Using absolute qPCR, the total number of mRNA transcripts was determined for each cDNA sample. The amount of cDNA obtained from a given amount of leaf region (elongation zone, EZ; emerged blade, EB) was known, as was the number of cells for each region. This made it possible to express qPCR data as mRNA copy number per cell. Results are shown for the barley cultivars Golf (A) and Jersey (B) and represent averages and standard deviation (error bars) of three independent experiments (batches of plants). PM-H$^+$-ATPase expression (copyRNA cell^{-1}) did not differ significantly between elongation zone (EZ) and emerged blade (EB) in either Golf or Jersey (Student's t-test).

Table 3.4 Ct values of PM-H$^+$-ATPase expression together with RNA content per cell in the elongation zone (EZ) and emerged blade (EB) of leaf three of barley. Two barley cultivars were studied, Golf and Jersey, and three independent experiments were carried out.

	Ct	SD	RNA content (pg cell^{-1})	SD
EZ (Golf)	23.8	0.2	22.3	1.5
EB (Golf)	24.2	0.5	25.9	4.0
EZ (Jersey)	22.7	0.2	22.8	1.7
EB (Jersey)	22.8	0.2	18.5	15.6

Since the determination of cell number in a given leaf region involved large errors, an additional control experiment was conducted in which RNA was extracted from protoplast suspension of the Jersey cultivar. The number of protoplasts could easily be calculated. RNA yield of 300 - 1000 µl protoplast suspension (about 0.5 - 7 million cells) was 250 - 2,000 ng µl^{-1} and the 'background' protoplast medium which was taken as supernatant folowed gentle centrifugation of protoplasts, yielded virtually no extractable RNA (less than 1 - 10 ng µl^{-1}, which was below the measuring range of the Nanodrop® equipment). Results for protoplasts were expressed in copy number of PM-H$^+$-ATPase transcript protoplast^{-1} and in copy number of PM-H$^+$-ATPase transcript mm^{-2} protoplast plasma membrane surface area. These figures

were in the same range as results obtained for the Jersey cultivar when calculated cell number was used as reference system (see Fig. 2.25).

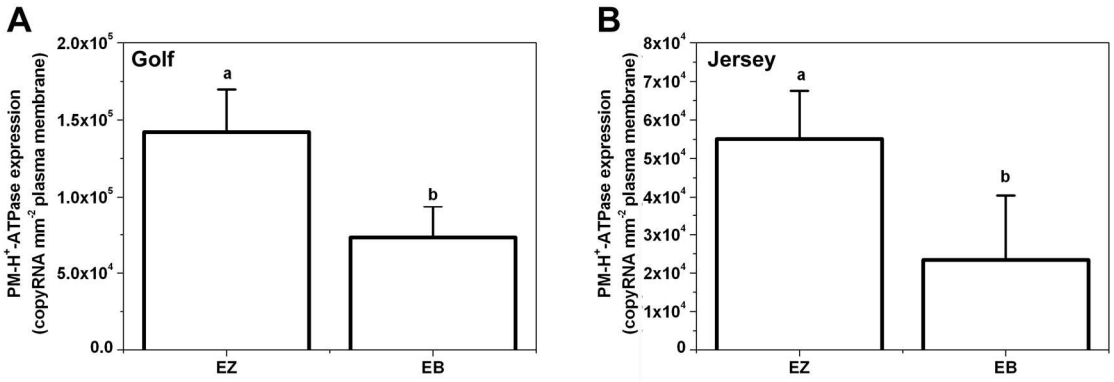

Figure 3.26 PM-H$^+$-ATPase expression using absolute qPCR and relating expression data to total plasma membrane surface area

PM-H$^+$-ATPase gene shows significantly (around 2 times) higher expression in the elongation zone (EZ) compared with emerged leaf blade (EB). Values for the Golf barley cultivar (A) were 3 fold higher than values for the Jersey barley cultivar (B). Results are averages and standard deviations (error bars) of three 3 independent experiments. Different letters shows statistically different values between leaf regions (student's t-test, $p < 0.05$).

Table 3.5 RNA content and PM-H$^+$-ATPase expression in the elongation zone (EZ) and emerged blade (EB) of leaf three of barley (Golf, Jersey). Different reference systems were used. Results are averages and SD of 3 - 6 independent experiments. Protoplasts were isolated only from the Jersey barley cultivar. PM, plasma membrane; protopl., protoplast.

	RNA (pg cell^{-1})		ATPase copy cell^{-1}		ATPase copy mm^{-2} PM (x 10^3)	
EZ (Golf)	22.3	± 1.5	300	± 60	142	± 28
EB (Golf)	25.9	± 4.0	260	± 70	73	± 20
EZ (Jersey)	22.8	± 1.7	120	± 30	55	± 12
EB (Jersey	18.5	± 15.6	80	± 60	23	± 17
EZ protopl.	18.7	± 17.5	50	± 30	38	± 23
EB protopl.	20.7	± 19.2	50	± 40	12	± 7

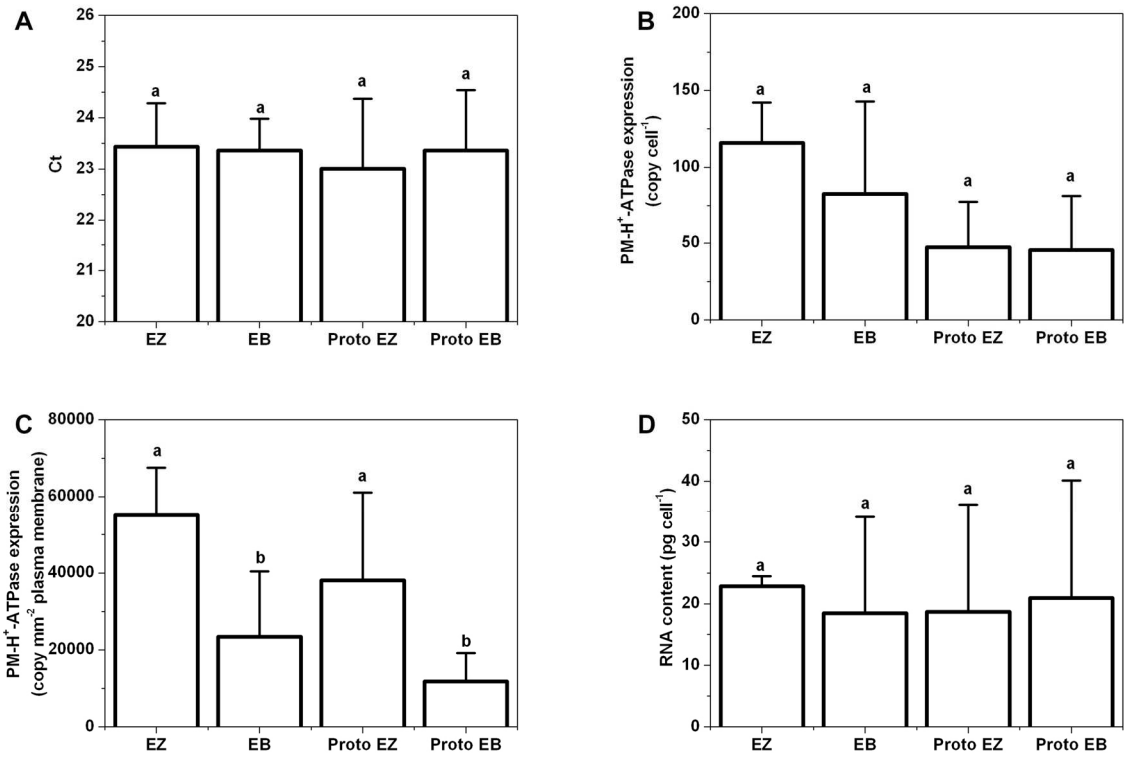

Figure 3.27 Comparison of molecular biological data using leaf tissues or mesophyll protoplasts

Ct values (A), PM-H^+-ATPase copy in a cell (B), per mm^2 plasma membrane (C) and total RNA content in a cell (D) was compared between experiments where RNA was isolated from whole leaf segments of the elongation zone (EZ) and emerged blade (EB) and from isolated mesophyll protoplasts of the elongation zone (Proto EZ) and emerged blade (Proto EB). Values are averages of 3 - 6 batches of plants. Different letters show statistically significant differences at $p < 0.05$ using Student's t-test and ANOVA. All experiments were conducted on the barley cultivar Jersey

3.4 PM-H^+-ATPase activity and expression at protein level

Data from qPCR experiments showed that the copy number of PM-H^+-ATPase transcripts per unit plasma membrane surface area was significantly higher in growing compared with non-growing leaf tissue. This could partially explain the lower apoplast pH in elongating tissue. To test to which degree changes in the activity of the PM-H^+-ATPase protein also contributed to the lower pH, plasma membrane fractions were isolated from growing and non-growing part of barley leaves and used to determine the activity of PM-H^+-ATPase. Due to the lack of availability of Golf seeds towards the end of this project, these experiments were carried out on the spring barley cultivar Jersey.

3.4.1 Optimization of membrane isolation and ATPase assay

Membrane isolation and ATPase assay had to be optimized. The original method had been described for a large amount of plant tissue (125 g) (Kjellbom & Larsson, 1984) however previous studies showed that with the method plasma membrane fraction might be purified from lower amout of plant material (Wei *et al.*, 2007). The P_i determination assay had been designed originally for animal membranes (Sarkadi *et al.*, 1992), with animal cells notably lacking any vacuolar ATPases.

3.4.1.1 Plasma membrane isolation

It was impossible to harvest more than 6 g leaf material from the elongation zone and emerged blade portion of leaf three, given the growth constraints (growth chamber, laboratory space) since this required already between 200 - 400 barley seedlings. Preliminary experiments were carried out to find the minimum amount of leaf tissue which was required for a two-phase separation system with 12 g final separation weight. These experiments showed that below 1 g initial leaf tissue virtually no membrane fraction could be obtained and above 10 g the plasma membrane fraction could not be separated from chloroplast membranes using 5 - 6 purification steps.

One washing step of the membrane fraction as recommended by Pitann *et al.* (2009b) was not enough to fully eliminate the rest of the polymers (dextran and PEG) from the purified membrane fraction. In the presence of one or both of these polymers PAGE could not be carried out properly and protein bands appeared blurred on the gel (Fig. 3.28).

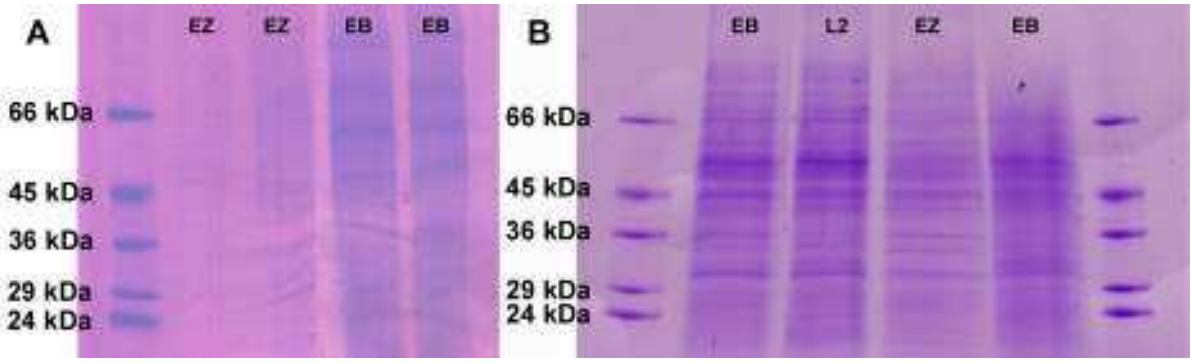

Figure 3.28 Impact on the quality of PAGE separation of washing steps during plasma membrane isolation

Residues of the polymers in plasma membrane fractions caused proteins to appear blurred on the polyacrylamide gel. One washing step was not enough to completely eliminate the polymers (A) while applying two steps (B) the blurring effect was not found on Coomassie stained gels. EZ – elongation zone, EB – emerged leaf blade and L2 – leaf blade of second leaf.

3.4.1.2 Determination of total protein content in plasma membrane vesicles

In studies where plasma membranes have been isolated, protein concentration has typically been quantified with the Bradford method or a modification of it (Yan *et al.*, 1998; Yan *et al.*, 2002; Zörb *et al.*, 2005; Pitann *et al.*, 2009b; Zhu *et al.*, 2009; Hatzig *et al.*, 2010; Wakeel *et al.*, 2010). Using this approach, it was found in the present study that protein concentration was grossly underestimated, compared to quantification of proteins through densitometry by Phoretix 4.01 software (Phoretix International) on Coomassie stained PAGE gels and calibration with protein standards (Sigma) of known protein content. (Fig. 3.29).

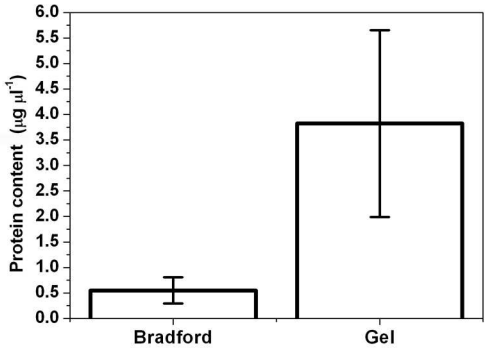

Figure 3.29 Protein measurement in plasma membrane vesicles using two different methods

The protein concentration of the plasma membrane vesicles was significantly lower when determined with the Bradford method than when determined through densitometry of samples run on PAGE gels. The difference in protein concentration between the two methods was statistically significant at $p < 0.05$ (Student's t-test).

3.4.1.3 ATPase assay

Optimization of ATPase assay was carried out to find the optimal reaction volume, detection method and membrane protein amount for the assay. Preliminary experiments showed that colour development was more reproducible in 1750 µl compared with 200 µl (microtiter plate). The optical density of the samples had to be measured within a minute of completion of colour development, together with the calibration curve. If this was not considered, the absorbance changed rapidly (Fig. 3.31). When 3 µg total membrane protein were used and the assay was run for 60 min at 28 ℃ reproducible and easy to measure amoun t of released (from ATP) amount of P_i could be measured A typical ATPase assay is shown in Fig. 3. 30.

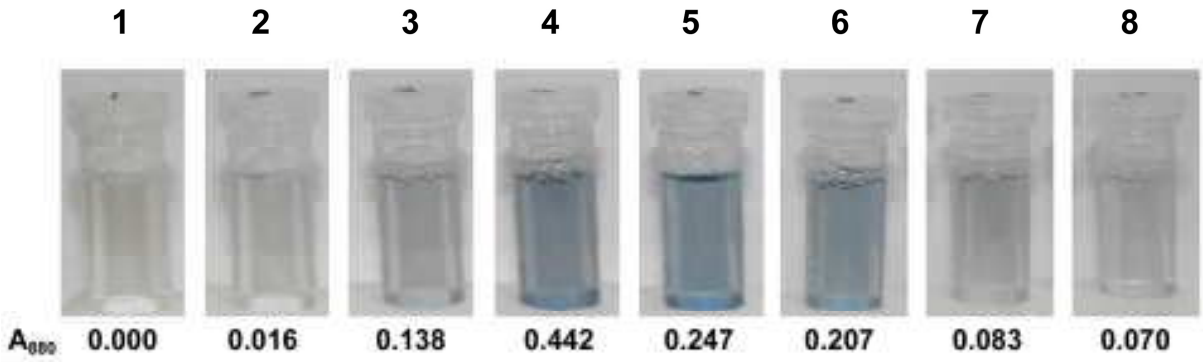

Figure 3.30 Typical ATPase assay

The concentration of P_i was determined by a blue colour reaction (detecting the absorbance at 880 nm) using calibration curve standards (1 - 4; with 0, 10, 30 and 60 nmol P_i per reaction. Without blocking bacterial and vacuolar type of ATPases (5) slightly more P_i could be measured compared with a reaction where these ATPase were blocked with 10 mM NaN_3 and 100 mM KNO_3 (6); 500 µM vanadate (7) blocked ATPase activity almost to the same extent as when total protein was denatured using SDS (8). Values below the tubes show the absorbance at 880 nm.

To determine the optimal detection time of the colour development reaction kinetics was recorded (Fig. 3.31). Between 20 - 30 min the absorbance was between 0.1 - 0.6 (arbitrary units) and could be measured with high reproducibility. In addition, the calibration curve was linear in this time range.

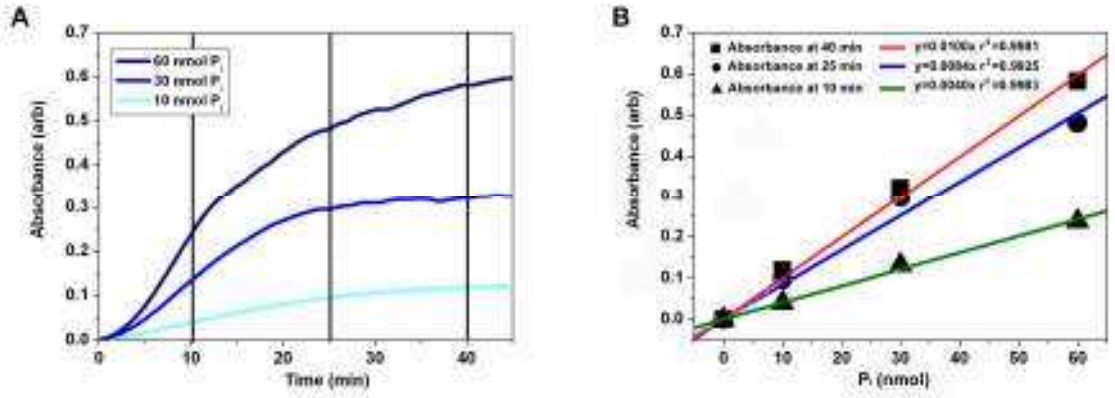

Figure 3.31 Kinetics of P_i detection assay

Kinetics of the P_i detection assay was recorded at 10, 30 and 60 nmol P_i concentration (A) and calibration curve at the time point 10, 25 and 40 min (B). Before 20 min the absorbance values were too low to be use reliably for measurements and the absorbance changed quickly. Between 20 to 30 min the reaction was slower and the values ideal for measurements whereas past 40 min of colour development absorbance values became too high and higher P_i concentrations resulted in errors.

3.4.2 Quality of plasma membrane fractions

The quality of plasma membrane fractions was checked on SDS PAGE gradient gels stained with Coomassie Brilliant Blue and on Western blots. Based on SDS gels the plasma membrane protein pattern of the emerged leaf blade (leaf three) and fully expanded blade (leaf two) was comparable whereas the elongation zone of leaf three and microsomal fraction (no plasma membrane purification) of emerged blade of leaf three differ from the other two (Figure 3.32 A). Western blot analysis confirmed the presence of PM-H^+-ATPase in the isolates (Figure 3.32 B), although based on these Western blots quantitative analysis of PM-H^+-ATPase density in the plasma membrane of different leaf regions could not be achieved. Subsequently, a more sensitive Western blot system (at UCD) was used to compare PM-H^+-ATPase content of plasma membranes between elongation zone and emerged blade.

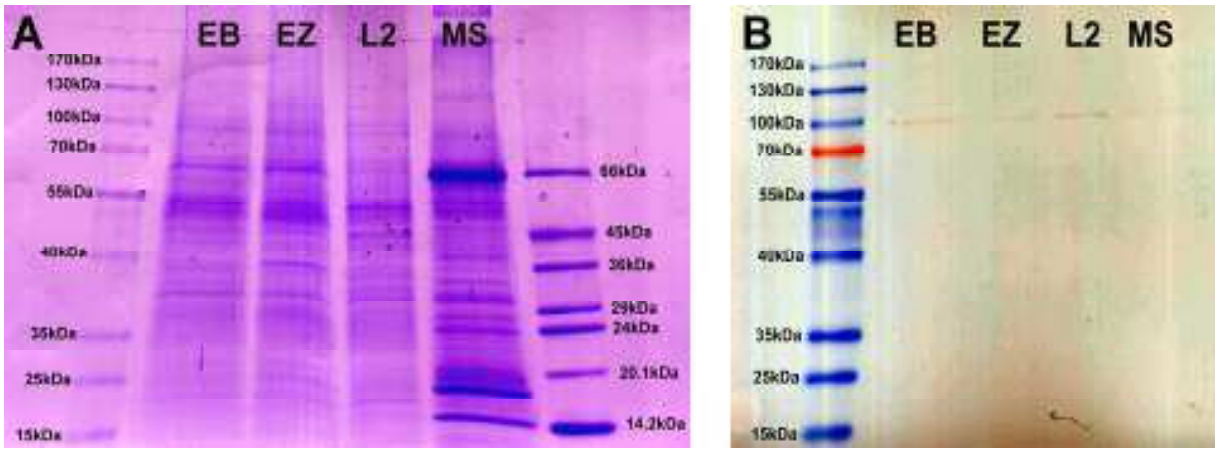

Figure 3.32 Coomassie stained SDS polyacrylamide gel and Western blot of plasma membrane proteins from different leaf regions

Gradient SDS polyacrylamide gel stained Coomassie Brilliant Blue R250 (A) shows the difference or similarity in membrane protein pattern of emerged leaf blade three (EB), elongation zone of leaf three (EZ), fully expanded leaf blade from leaf two (L2) and microsomal fraction from emerged leaf blade two (MS). Western blot (B) analysis demonstrated the presence of PM-H^+-ATPase in the isolates and also that the commercially available antibody recognised barley PM-H^+-ATPase (expected molecular weight of about 105 kDa). The band intensity was too weak to allow densitometric analyses of bands. This had to be done subsequently using a more sensitive detection system for the secondary antibody employed

3.4.3 Quantitative analysis of PM-H$^+$-ATPase protein

Sensitivity of the Western blot detection system at Eötvös University, where plasma membrane isolations and ATPase enzyme assays were carried out, was not enough to perform quantitative analysis on blots. Using the same samples in Dublin (having transported the samples on dry ice from Budapest) on thinner gels and chemiluminescence detection the proportion of PM-H$^+$-ATPase in total membrane protein was measured using a densitometric approach. The same amount of total membrane protein (5 μg) from the elongation zone contained 2.33 times higher concentration of PM-H$^+$-ATPase protein than non-growing leaf blade (Fig. 3.33 A). Densitometry of Coomassie stained gradient gels supported Western blot data. A higher PM-H$^+$-ATPase protein expression was measured in the elongation zone (Fig. 3.33 B) although the difference using the PM-H$^+$-ATPase band on SDS gels (identified based on molecular weight and Western blots) was lower with the ratio between the two leaf regions being 1.5 fold compared with 2.33-fold above.

The higher sensitivity of the second Western blot approach made it possible to detect a second band on the blot, at around 70 kDa. This might represents a fragment of the PM-H$^+$-ATPase enzyme (Fig. 3.33 C)

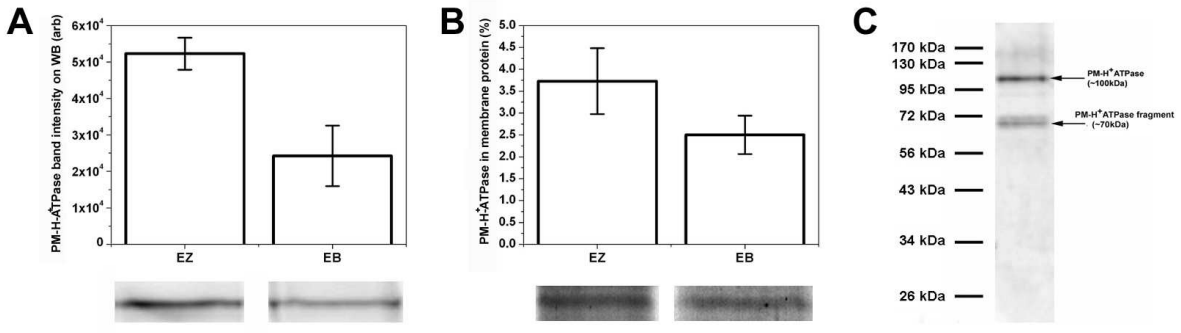

Figure 3.33 PM-H$^+$-ATPase ratio in total membrane protein

PM-H$^+$-ATPase protein, expressed on the basis of total plasma membrane protein applied onto gels (and entered into Western blots) was significantly higher in the elongation zone (EZ) compare with emerged blade (EB) (A); the same applied to densitometric analyses of Coomassie Brilliant Blue stained polyacrylamide gels (B). Results are significant using Student's t-test ($p < 0.05$). Using higher sensitivity on Western blots a second band was found which respresents most likely a 70 kDa fragment of the PM-H$^+$-ATPase (C).

3.4.4 Activity of PM-H^+-ATPase

Vandate-sensitive ATPase activity of membrane fractions was measured using inside-out plasma membrane vesicles and an ATP hydrolysis assay. Results were expressed in nmolP_i h^{-1} μg^{-1} total membrane protein at 28 °C. As Fig. 3.34 shows plasma membrane vesicles of the elongation zone had more than 2 times higher vanadate-sensitive ATPase activity compared with vesicles prepared from the emerged blade. Vacuolar and prokaryotic types of ATPases were blocked using high azide and nitrate concentration in the reaction mixture, and data were validated with vanadate sensitivity. The resulting enzyme activity represented PM-H^+-ATPase activity and this was two fold higher in the plasma membrane of the elongation zone compare with membranes prepared from the emerged leaf blade.

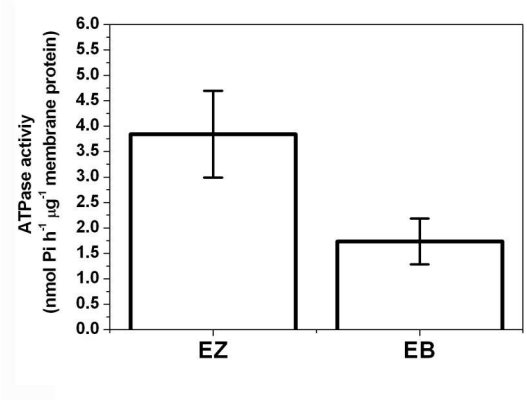

Figure 3.34 ATPase activity of inside-out plasma membrane vesicles

Vanadate-sensitive ATP hydrolysis activity of inside-out plasma membrane vesicles of the elongation zone (EZ) was more than two times higher than activity in the emerged blade of leaf three of barley (EB). Results are averages of four independent batches of membranes and 9 - 10 replicate activity determinations. Differences were statistically significant ($p < 0.05$) using Student's t-test.

3.4.5 Immunolocalisation of PM-H^+-ATPase

Paraffin-embedded sections were used to localise the tissue-specific distribution of PM-H^+-ATPase protein. Alkaline phosphatase-labelled secondary antibody with fast red detection was used. Reddish colour showed the location of PM-H^+-ATPase protein. There was no difference in PM-H^+-ATPase distribution between the elongation zone (Fig. 3.35 A) and emerged blade (Fig. 3.35 B). Higher expression of PM-H^+-ATPase was found in guard cells (Fig. 3.35 E), phloem, and xylem parenchyma. PM-H^+-ATPase was detected virtually on the plasma membrane of every living cell. Longitudinal sections of the elongation zone (Fig. 3.35 D) provided

further detail. Guard cells were easily identifiable. Dead parts of xylem tubes were free from red colour, whereas phloem and xylem parenchyma cells contained large amount of PM-H^+-ATPase. Negative control (Fig. 3.35 C), where primary PM-H^+-ATPase specific antibody was not applied, verified the selectivity of the assay as immunospecific staining was not present.

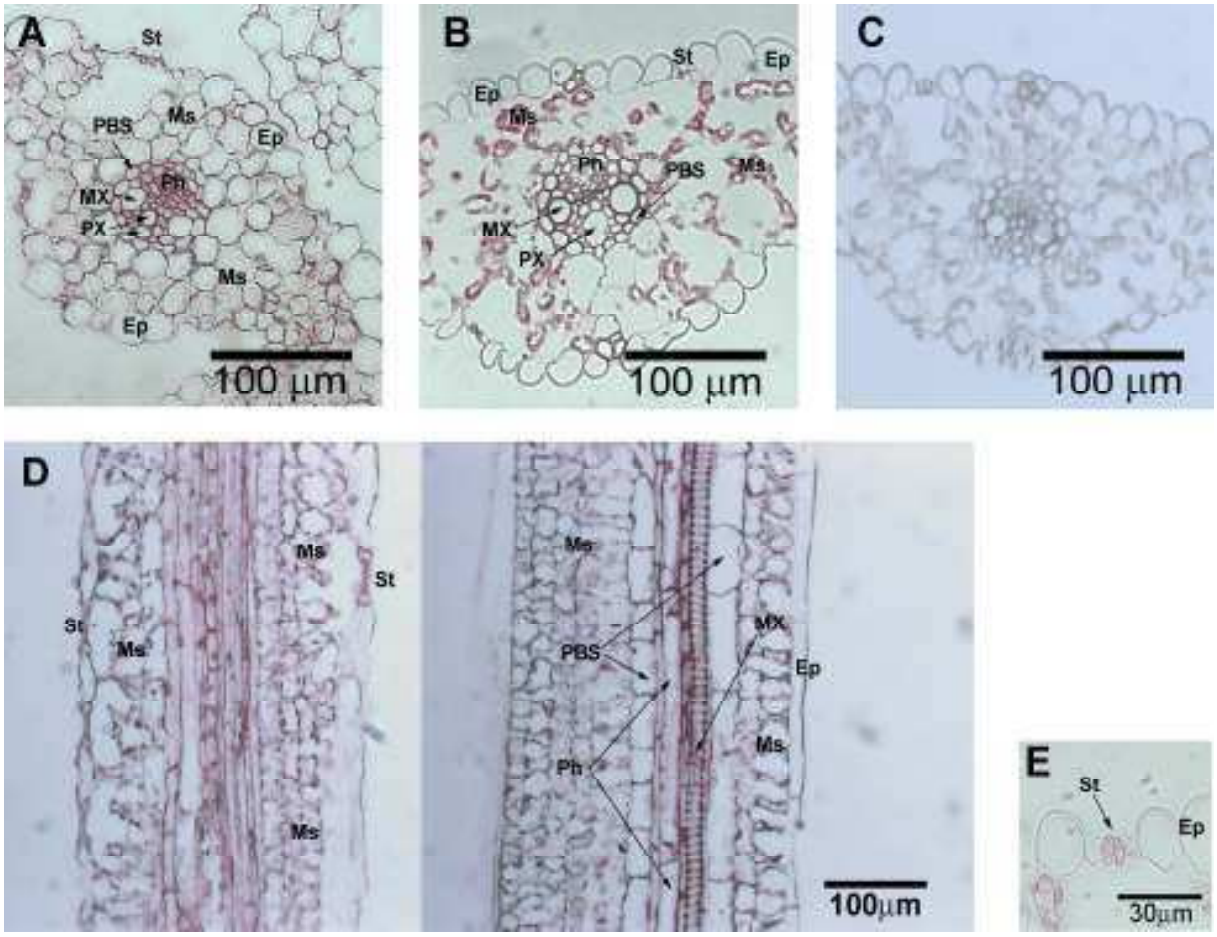

Figure 3.35 PM-H^+-ATPase immunolocalisation on leaf cross and longitudinal sections

PM-H^+-ATPase expression was detectable on all plasma membranes, both in the elongation zone (A) and emerged blade (B). Higher expression was present in guard cells (E), phloem and xylem and phloem subsidiary cells. Differences between elongation zone and emerged blade were not visible. Negative control (primary antibody was not applied) was free from immunolabelling (C). Longitudinal sections of elongation zones (D) were supporting observations from cross sections, stomata guard cells and vascular elements and subsidiary cells being heavily stained. Ep: epidermis; St: stomata; MX: metaxylem; PX: protoxylem; Ph: phloem; Ms: mesophyll cells; PBD: parenchymateous bundle sheath.

4 Discussion

4.1 Growth-associated apoplast acidification

Using different methods to measure or visualise apoplastic pH or H^+ transport activity into the intercellular space, a lower pH was recorded in the elongation zone compared with emerged blade of barley leaves. This observation is in agreement with the 'acid growth theory' which would predict a more acid apoplast pH in growing tissue.

4.1.1 Apoplast pH difference between growing and non-growing leaf tissue

Three independent approaches were used to analyse apoplast pH. Microelectrode pH measurements provided the most quantitative data. Also, similar to confocal analyses and contrary to the in-vitro gel system, microelectrode analyses measured pH in the actual wall or apoplast space. These measurements showed that the pH in the apoplast was by up to 1 pH unit lower and, therefore, the H^+ concentration up to 10-fold higher in elongating tissue. There do not exist any directly comparable studies on other grass leaves, although slightly different approaches have been taken for some species. When pH was measured in droplets placed on the exposed elongation zone of maize leaves a lower apoplastic pH compared with the emerged blade or elongation zone under non-growing conditions was measured; the absolute pH values in these droplets were significantly higher than the ones measured here, and the pH reading was not stable but drifted during recordings (Van Volkenburgh & Boyer, 1985; Neves-Piestun & Bernstein, 2001). Using 0.5 g of growing maize leaf segments in 2 ml unbuffered bathing medium, Neves-Piestun & Bernstein (2001) measured a pH of 4.8, a value which is very similar to the value recorded here for barley leaves.

4.1.2 Reliability of pH values measured in elongation zone and emerged blade

Microelectrode measurements revealed that apoplast pH in the leaf elongation zone depended on the bathing medium concentration of K^+. At the lowest K^+ concentration tested (0.1 mM) apoplast pH was 4.8, yet at 10 mM K^+, apoplast pH increased to 5.8

and was identical to the value in emerged tissue (Fig. 3.7). Since the emerged leaf contains at its surface a major permeance barrier (cuticle) to externally applied solution, this could mean that the difference in pH observed between leaf regions was an artefact and reflected differences in the access of bath solution between leaf regions. If, by chance, the K^+ concentration in the apoplast of the emerged blade of intact plants had been 10 mM, or at least higher than 1 mM, and if none of the external bathing solution had reached the apoplast, one would have predicted an apoplast pH of 5.8 based on measurements for elongating tissue at 10 mM K^+. Felle (2006) measured an apoplastic K^+ concentration of 2.6 mM in mature barley leaves. Also, if the apoplast K^+ concentration in the leaf elongation zone *in-planta* was close to 10 mM, one would not expect to find a difference in apoplast pH between the two leaf regions in intact, undisturbed plants. Recently, Ehlert *et al*. (2011) reported apoplast pH between 4.1 and 5.9 with average mean of 5.1 for elongating maize leaf tissue as analysed through pH microelectrodes.

Felle (2006) inserted pH microelectrodes through stomatal pores of mature barley leaves and measured a pH of 4.88. This pH is significantly lower than the pH reported here (pH 5.8) for emerged blade tissue. Possibly, the difference in results is due to use of 2 mM MES / TRIS buffer (pH 5.0) in the bathing medium in the study by Felle (2006). Also, measurements by Felle (2006) were carried out under illumination, stimulating PM-H^+-ATPase pump activity (Stahlberg & Van Volkenburgh, 1999), whereas the present measurements were carried out in the dark. In a natural setting, the mature blade is exposed to full, ambient light whereas the elongation zone receives less light, and this light is green-filtered due to subtending sheaths. Therefore, it is possible that the difference in apoplast pH between leaf regions in field-grown and -analysed plants is considerably smaller than the difference measured here with the microelectrode setup in a darkened laboratory environment or through confocal analyses on intact leaves. Vanadate experiments on detached leaves clearly showed that the lower apoplast pH in the barley leaf elongation zone depended on the activity of the PM-H^+-ATPase.

4.1.3 Relation between apoplast acidification and leaf growth

Acidification of the apoplast in the elongation zone of barley leaves generally coincided with growth, but there were notable exceptions. A positive relation was best visualised by cold treatment in the in-vitro gel system (Fig. 3.3). In the same system vanadate and fusicoccin treatments caused parallel changes in the growth

rate of leaves and acidification of medium adjacent to leaf apoplast (Fig. 3.1). Also, vanadate treatment in the microelectrode setup reduced growth and increased apoplast pH in the elongation zone to a value usually observed for mature tissue. However, when fusicoccin was applied in the pH microelectrode setup, growth increased while apoplast pH remained unchanged (Fig. 3.9 and 3.10). Also, changing the apoplast K^+ concentration from 0.1 to 1 or 10 mM significantly increased apoplast pH in the elongation zone, yet growth did not change (Fig. 3.7 and 3.8). Irrespective of the underlying mechanisms, these data show that there does not exist a simple, single relation of how apoplast pH relates to growth in the leaf elongation zone. The seemingly contradictory fusicoccin data obtained through the microelectrode and in-vitro gel setup could be explained through differences in what these two setups measured. The in-vitro gel system measured bulk effects on pH further away from the leaf surface and showed an increase in the acidified area and corresponding net production rate of H^+, and H^+ was titrated by the pH indicator bromocresol purple. In contrast, the microelectrode setup provided a point measurement of pH closer to the cell surface, irrespective of the rate at which H^+ diffused into surrounding bathing medium or was consumed through transport processes involving K^+. Thus, while fusicoccin will have stimulated H^+ pumping in both setups and led to increased diffusion, apoplast pH may not have changed in either setup.

4.2 K^+ and apoplast acidification

Potassium uptake coupled to H^+ uptake (symport) has been discussed as an alternative explanation for some of the effects associated with the 'acid growth' theory. For example, K^+ uptake and apoplast acidification were linked to growth in roots (Glass *et al.*, 1981; Ullrich & Novacky, 1990; Amtmann *et al.*, 1999) and coleoptiles (Claussen *et al.*, 1997; Tode & Lüthen, 2001; Christian *et al.*, 2006). The present data also suggest that K^+ transport and apoplast acidification are linked with each other in some way during elongation of barley leaf cells.

4.2.1 Potassium uptake and leaf growth

A previous patch-clamp study on K^+ transport in barley concluded that apoplast K^+ must exceed 3 - 5 mM to allow growing leaf cells to take up K^+ through channels (Boscari *et al*., 2009; Volkov *et al*., 2009). Calculations showed that at 10 mM apoplast K^+, about 50 % of K^+ uptake was facilitated by time-dependent inward-rectifying currents typical of Shaker K^+ channels such as AKT1 or AKT2. The

remaining 50 % was facilitated by instantaneous currents, which includes either or both, K^+ high-affinity transporters such as HAK / KUP / KT type K^+ / H^+ symporters (for historical reasons, these three abbreviations denote the same type of symporters; for details see e.g. Ashley *et al.* (2006) and Szczerba *et al.* (2009)) or non-selective cation channels. At apoplast concentrations below 3 - 5 mM, uptake of K^+ would have to occur through high-affinity uptake mechanisms. The K^+ concentrations tested in the present study covered the range 0.1 to 10 mM. Therefore, it is possible that different K^+ uptake mechanisms contributed to the growth and pH response of leaves depending on the K^+ concentration of bathing medium. When K^+ uptake was blocked through application of inhibitors (Cs^+, TEA) of K^+ inward-rectifying Shaker-type channels, or at least reduced significantly, growth was reduced by 50 %. A similar reduction in growth was observed in response to vanadate and CsCl-vanadate double treatments (applied at 10 mM bathing medium K^+; Fig. 3.17). The latter observation excludes the possibility that Cs^+ (K^+ channels) and vanadate (PM-H^+-ATPase) inhibited 'different' 50 % of growth and were additive. Instead, growth was reduced through some common mechanism. Membrane potential was not measured in response to the above treatments, but the most likely scenario is that inhibition of PM-H^+-ATPase through vanadate depolarised membrane potential to such an extent that uptake of K^+ through channels was thermodynamically not possible. This would explain why direct blockage of channels through Cs^+ caused the same growth reduction as blockage of PM-H^+-ATPase. Similarly, Tode & Lüthen (2001) concluded from experiments involving TEA that the acid-growth type response of maize coleoptiles required the activity of inward-rectifying K^+ channels. Linkage of K^+ transport, leaf growth and cell wall acidification was found in light-induced growth of tobacco leaves (Stiles *et al.*, 2003), yet K^+ uptake was required for H^+ efflux and growth without any noticeable accumulation of solutes (Stiles & Van Volkenburgh, 2004). This would exclude a primarily osmotic requirement for K^+.

4.2.2 High affinity potassium transporters and leaf growth

High affinity K^+ transporters, but not K^+ selective channels, are reduced in transport activity by ammonium (Kronzucker *et al.*, 2003; Rodriguez-Navarro & Rubio, 2006; Szczerba *et al.*, 2009; Hoopen *et al.*, 2010). Application of 20 mM NH_4^+ during LVDT experiments reduced growth by as much as Cs^+, TEA and vanadate treatments did. This shows that high affinity K^+ uptake systems were involved in K^+ uptake and

growth response of elongating barley leaf cells. The results also show that the three components, apoplast pH, high-affinity and channel-mediated K^+ uptake were related to each other in some way that prevented inhibition of each component from being additive.

Boscari *et al.* (2009) observed that HvHAK4 was expressed particularly in the elongation zone of barley leaves. It is not known whether HvHAK4 functions as K^+ / H^+ symporter as thought for other HAK family members (Britto & Kronzucker, 2008; Szczerba *et al.*, 2009). If it does, HvHAK4 may not only provide a major route for K^+ entry into growing barley leaf cells, but also present a key mechanism through which the pump activity of the PM-H^+-ATPase can be linked to osmotically-driven water uptake and apoplast acidification in growing leaf tissues. This needs to be studied further.

4.3 PM-H^+-ATPase expression and leaf elongation

Using four independent techniques (qPCR, ATPase assay and densitometry on SDS PAGE and Western blot) it was found that the expression, activity and protein level of PM-H^+-ATPase when related to the surface area of plasma membrane, was between 1.5 - 3.5 times higher in the elongation zone compared with the emerged blade (Table 4.1). The similarity in results for expression, protein level and activity may be a coincidence, but more likely reflects a true difference between growing and non-growing barley leaf tissues.

Table 4.1 Summary of data for PM-H^+-ATPase when related to surface area of plasma membrane. Ratio and standard deviation (SD) was calculated in two ways (a: averages of elongation zone (EZ) were divided by averages of emerged blade (EB) or i: average of ratio of paired EZ and EB). SDs in bracket are estimated SDs.

Experiment type	Ratio EZ : EB	SD
qPCR (Golf, a)	1.96	± (0.47)
qPCR (Golf, i)	1.99	± 0.28
qPCR (Jersey, a)	2.36	± (0.91)
qPCR (Jersey, i)	3.53	± 2.88
qPCR (Jersey protoplasts, a)	2.13	± (0.70)
qPCR (Jersey protoplasts, i)	2.35	± 0.49
Vanadate sensitive ATPase activity (Jersey, a)	2.22	± (0.55)
Coomassie stained SDS PAGE (Jersey, a)	1.50	± (0.35)
Western Blot (Jersey, a)	2.33	± (0.72)

Quantification of PM-H^+-ATPase protein level using Coomassie stained PAGE gels gave the lowest difference between elongation zone and emerged blade. This may result from individual bands, such as the band of the PM-H^+-ATPase, containing numerous different proteins. For example, Hynek *et al.* (2006) concluded from MS / MS analyses of the PM-H^+-ATPase band of plasma membrane vesicles prepared from barley aleurone layer that the band contained 22 different peptides. Together, the data suggest that the density at which functional PM-H^+-ATPase is localised in the plasma membrane, or at which PM-H^+-ATPase is expressed per unit plasma membrane surface area of cells is about twice as high in growing as in non-growing leaf regions. Also, expression and protein data suggest that the efficiency of translation of PM-H^+-ATPase mRNA is similar in the two leaf regions.

4.3.1 PM-H^+-ATPase density in plasma membrane and leaf growth

The higher plasma membrane density of PM-H^+-ATPase in the elongation zone will aid the energisation required for continuous solute uptake, in particular uptake of K^+, in growing leaf cells. It will also aid acidification of the apoplast as measured through pH microlelectrodes in the barley leaf elongation zone. Depending on the apoplast K^+ concentration, the pH in the elongation zone was by up to 1.0 pH unit lower (pH micro electrode measurements; Fig. 3.7) in the elongation zone compared with emerged blade. This corresponds to a 10-fold difference in apoplast H^+ concentration and suggests that there exist post-translational modifications which further increase the PM-H^+ATPase pump activity in growing barley leaf cells. Having said this, the wall space of growing cells is smaller (thinner walls) and this will aid apoplast acidification for a given pump activity. Apoplast acidification also depends on factors which are not related directly to the protein level and activity of PM-H^+-ATPase such as apoplast K^+ concentration (Claussen *et al.,* 1997;Tode & Lüthen, 2001), temperature (Stoddart & Lloyd, 1986; Pollock *et al.*, 1990) hormones (especially auxin, e.g.: Rayle & Cleland, 1970; Hager *et al.*, 1971; Rayle & Cleland, 1992; Claussen *et al.*, 1997; Tode & Lüthen, 2001; Hager, 2003; Grebe, 2005; Kutschera, 2006) and light (Van Volkenburgh & Cleland, 1980; Stahlberg & Van Volkenburgh, 1999).

4.3.2 qPCR data

Determination of cell size and cell number can involve comparably large errors, due to the variation in size between populations and types of cell and due to small difference in cell radius (protoplasts) causing large differences in calculated cell volumes. Despite these intrinsic uncertainties, the present calculations showed that the PM-H^+-ATPase expression per cell is very similar in growing and non-growing leaf tissue. Due to the lower surface area of the plasma membrane in growing cells (always assuming that there are no major invaginations of the plasma membrane, or that these would not differ between leaf regions), the density of PM-H^+-ATPase is higher than the density in non-growing cells. As growing cells reach their full size, plasma membrane surface area increases leading to a continuous 'dilution' of PM-H^+-ATPase molecules. In such a scenario, the amount of PM-H^+-ATPase per cell seems to be a fixed size, and cessation of growth seems to coincide with a continuous dilution of PM-H^+-ATPas activity, resulting in decreasing rates of apoplast acidification (see also Fig. 3.25, Fig. 3.26 and Fig. 3.27). qPCR analysis of mesophyll protoplasts isolated from the elongation zone and emerged blade of the barley cultivar Jersey further supported the reliability of the calculated cell numbers of qPCR samples. Total RNA content of Golf and Jersey tissues per cell was very similar to total RNA content per protoplast. PM-H^+-ATPase expression data obtained for protoplasts, when expressed per protoplast number or total plasma membrane surface were lower but not significantly different to the other qPCR data for Jersey where expression was related to the calculated cell number or total membrane surface (see Table 3.5 and Fig. 3.27). The lower expression values are in agreement with immuno localisation results on leaf cross-sections which showed that mesophyll cells have a comparatively (to other leaf tissues) lower PM-H^+-ATPase expression. For RNA extraction from leaf segments, all types of cells were homogenised and accordingly averaged. In contrast, protoplasts were islolated only from mesophyll.

qPCR expression analyses also showed that the Ct value of PM-H^+-ATPase expression was almost identical in growing and non-growing leaf regions using the same amount of total RNA (250 - 500 pg). Therefore, when expression data are related to unit of extracted RNA, PM-H^+-ATPase (Ha1 AY136627; GI:23306665) is an ideal reference gene for expression analysis when comparing growing and non-growing leaf regions, in agreement with Boscari *et al*. (2009) and Besse *et al.* (2011) (see Table 3.5 and Fig. 3.27). The same applies to the PM-H^+-ATPase isoforms AHA1 and AHA2 in *Arabidopsis* (Gaxiola *et al*., 2007).

4.3.4 Immunolocalisation of PM-H^+-ATPase

Immunohistological analyses provided results which are in agreement with previous studies on the tissue localisation of PM-H^+-ATPase protein (Villalba *et al.*, 1991; Bouche-Pillon *et al.*, 1994; Michelet & Boutry, 1995; Morsomme & Boutry, 2000; Palmgren, 2001; Gaxiola *et al.*, 2007). Most staining, and by implication, PM-H^+-ATPase protein, was observed in those leaf tissues which are characterised by high rates of solute exchange across the plasma membrane (guard cells) or high rates of solute loading / unloading associated with long-distance transport pathways (phloem; xylem parenchyma). Interestingly, but in agreement with previous studies, epidermis cells were not enriched in PM-H^+-ATPase (Villalba *et al*., 1991). This was observed in elongation zone and emerged blade and shows that there exists a cell-type-specific control of PM-H^+-ATPase protein level which is superimposed on any developmental gradient.

4.4 Leaf growth and changes in cell wall properties

The effect of chemical treatments (vanadate, CsCl, fusicoccin) on cell wall properties was followed with the LVDT system. Fusicoccin increased the elasticity without affecting the plasticity of walls. In contrast, CsCl decreased the plastic component yet did not alter the elastic component of cell wall. Vanadate did not modify either component. From these results it can be concluded that PM-H^+-ATPase activity, which is inhibited by vandate, is not required to maintain wall elasticity or plasticity. The fusicoccin treatment did not cause changes in the plastic component of the cell wall. Since plasticity is the relevant size for growth (irreversible expansion), and since plasticity is thought to change with apoplast pH through action of expansions (Cosgrove, 1996), fusicoccin probably did not decrease the apoplast pH (in agreement with the microelectrode measurements where fusicoccin failed to cause apoplast acidification) or it facilitated leaf elongation through a mechanism other than ‘acid growth’. The increased $\Delta\Delta v$ suggests that in the background of fusicoccin-related growth facilitated K^+ uptake may be found (both v_1 and v_2 were higher than in the control). The increased elasticity of the cell wall may be caused by a cell wall modifying protein or enzyme activated by increased H^+ transport acrosss the plasma membrane into the cell wall space as the experiments with the agarose gel system showed. If fusicoccin increased the H^+ excretion through plasma membrane and the H^+ returned into the cell through H^+ / K^+ symport, then micro pH measurements,

in-vitro gel records and cell wall property data would support each other. However, this would require that the change in H^+ concentration close to the site where proteins act in the wall was either so small or so inaccessible that it could not be measured with the microelectrodes.

4.5 'Acid growth' in barley leaves?

Auxin is one of the most important hormones in plants and its involvement in growth is unquestionable, at least in coleoptiles (Rayle & Cleland, 1970; Lüthen *et al.*, 1990; Rayle & Cleland, 1992; Kutschera, 1994) or roots (Christian *et al*., 2006; Kutschera, 2006).

Surprisingly, in the present study the artificial auxin NAA did not cause any effect on leaf growth or apoplast acidification as tested through the in-vitro gel system (Fig. 3.6) or LVDT measurements (Fig. 3.19). In a related study on the barley cultivar investigated here, the elongation zone was not exposed by peeling back the sheath of leaves one and two but, instead, a small window was cut into these sheaths, causing less physical damage to the plant. Even in this system, application of 5 and 10 μM indole acetic acid (IAA) to the apoplast of the elongation zone did not increase the growth rate of leaves (Touati *et al.*, unpublished). For some reason, the barley leaves tested here seem not to be sensitive to externally-applied auxin. A possible interpretation could be that the third leaf, when measured in this project was in the development stage of maximum growth, and the internal auxin concentration might have been so high that any auxin-dependent growth mechanisms was saturated and externally applied auxin could not cause any further increase in growth. The elongation zone of leaf one of wheat has been reported to contain IAA at 500 - 600 ng g^{-1} fresh weight (Vysotskaya *et al*., 2003) and this would mean that IAA oocurs naturally in the μM range.

4.6 Model of leaf growth in barley

Under different treatments the role of PM-H^+-ATPase and high or low affinity K^+ uptake system was tested in relation to elongation growth and apoplast acidification in leaf three of barley. The predicted effects of test reagents on growth and acidification are summarised in Fig. 4.1. The results partly support the classical 'acid growth' theory and partly the 'facilitated solute uptake' theory. PM-H^+-ATPase dependent H^+ excretion is essential for at least 50 % of leaf growth. However, the equilibrium pH is not necessarily reflecting changes in transmembrane H^+ pumping

because H^+ / K^+ symport might transport protons back into the cell as Fig. 4.1 shows. Treatments with different K^+ transport blockers (TEA, CsCl, NH_4^+) and their double treatments with sodium-orthovanadate, the PM-H^+-ATPase blocker, suggested that in the background of the 'acid growth' of barley leaves an active HAK type K^+ uptake system might play a key role in facilitating a H^+ / K^+ symport mechanism (Bañuelos *et al.*, 2002; Bucker *et al.*, 2006; Britto & Kronzucker, 2008; Szczerba *et al.*, 2009). Acidification of the cell wall or protonation of some enzymes in the cell wall might have additional important role in growth as cell wall property measurements showed. HvHAK4, a member of the family of K^+ transporters, is mainly present in barley shoots (Rubio *et al.*, 2000) and it has significantly higher expression in the leaf elongation zone (Boscari *et al*., 2009), further supporting the idea of a combined 'acid growth' and 'facilitated solute uptake'.

Based on qPCR, enzyme activity and Western blot result, PM-H^+-ATPase expression in the plasma membrane might be controlled by a simple mechanism. The enzyme density in the plasma membrane can be diluted by cell growth; its density in the plasma membrane changes with cell size. The total number of PM-H^+-ATPase molecules was constant at cellular level while the total membrane surface increasing more than two-fold during cell development (Fig. 3.25 and Fig. 3.26). Taking into consideration all of the present results (expression analysis and physiological measurements with pH, H^+ transport activity and K^+ uptake during the leaf development) and published information about expression of HvHAK4 (Rubio *et al.*, 2000; Boscari *et al.*, 2009) leads to the model shown on Fig. 4.2. The 50 % of leaf growth that was sensitive to inhibition of PM-H^+-ATPase requires high expression of HvHAK4 in the elongation zone (Boscari *et al.*, 2009) and a high plasma membrane density of PM-H^+-ATPase molecules.

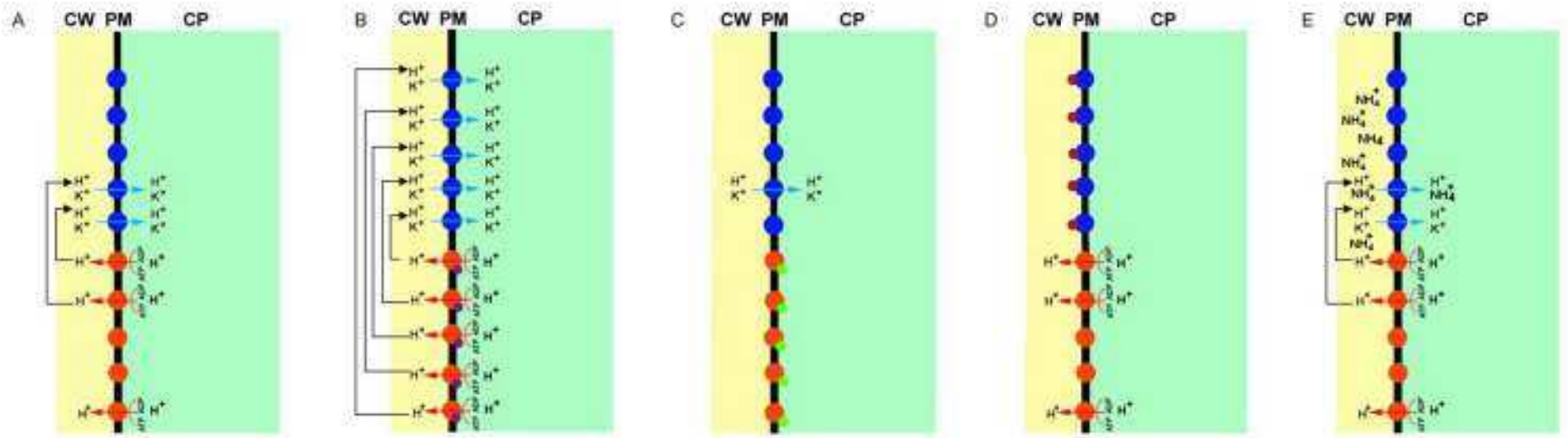

Figure 4.1 Supposed effect of the treatments on barley leaf cells

On the sketches cell wall (apoplast, CW) is labelled with yellow colour, cytoplasm (CP) is green and black lines refer to plasma membrane (PM). Orange balls symbolise PM-H^+-ATPase and blue balls are high affinity H^+ / K^+ symporters. Under control conditions PM-H^+-ATPases pump out the H^+ and K^+ are taken up into the cell through high affinity K^+ transporters (A). Fusicoccin (purple dots) permanently activate all the proton pumps and this massive H^+ efflux is short cut by K^+ transporter activity, causing higher turgor pressure in the cells and accelerates leaf growth (B). Vanadate (green dots) permanently blocks PM-H^+-ATPase and without H^+ transport K^+ uptake and growth are inhibited (C). Caesium ions blocks (deep red dots) K^+ transporters and reduce leaf growth (D) and ammonium ions (NH_4^+) reduce active K^+ accumulation through a competitive way and reduce growth (E).

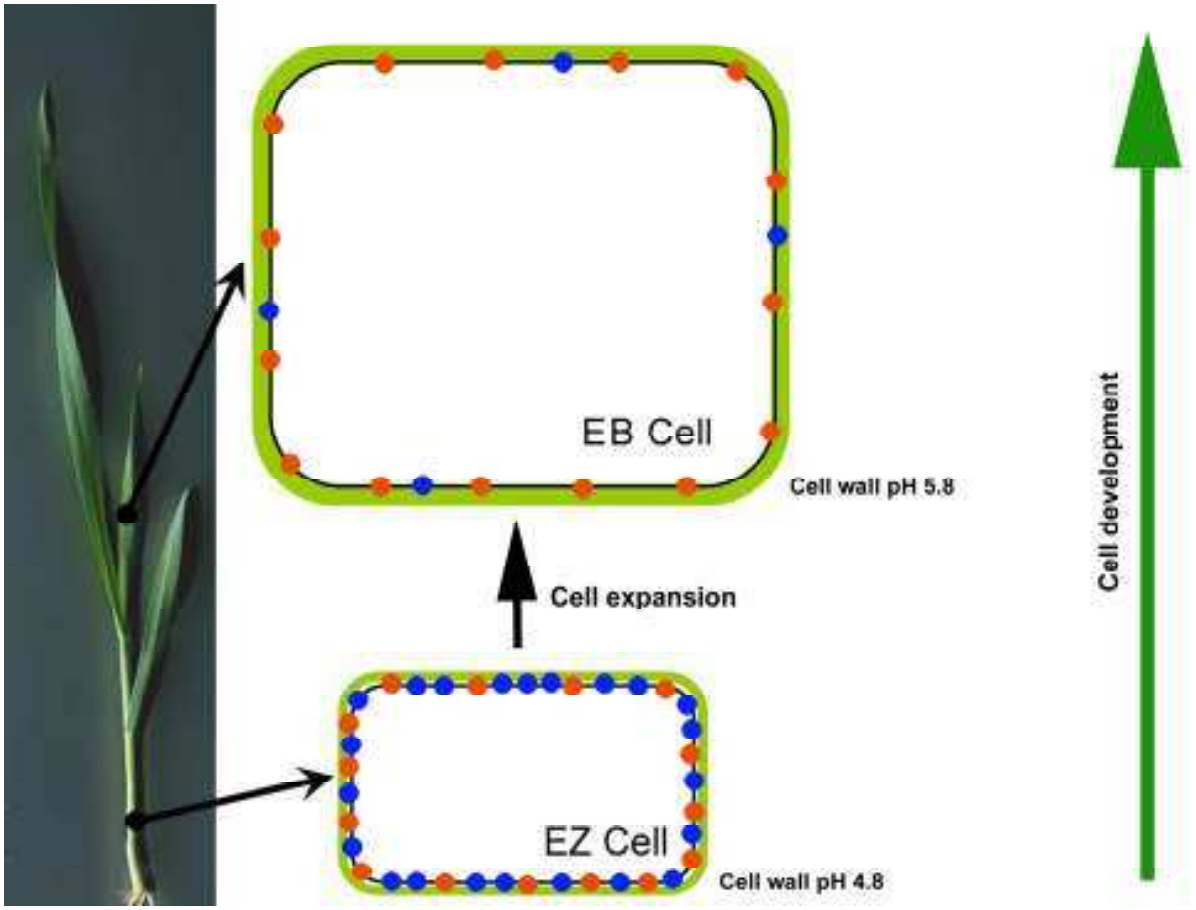

Figure 4.2 Model of leaf elongation in barley leaves

Cell size and membrane surface are increased 2 - 3 fold during cell development, as cells expand in the elongation zone (EZ) and finally reach full maturity in the emerged blade (EB). The number of PM-H^+-ATPase molecules (orange balls) per cell is constant where as HvHAK4 (blue balls) expression (and presumably protein level) per cell decreases significantly during cell development. Therefore, both the maximum proton transport and K^+ accumulation capacity are significantly higher in the elongation zone than in the emerged blade cell and can facilitate elongation growth through 'acid growth' and 'solute accumulation'. On the figure light green colour represents the cell wall and the black line the plasma membrane.

5 Conclusions and future work

5.1 Conclusions

(i) In this study the pH and H^+ transport activity were examined in the elongation zone and the non-growing emerged blade portion of leaf three of barley, using three independent approaches - an in-vitro gel system with bromochresol purple as pH indicator, confocal microscopy combined with pH sensitive fluoresceince probes and microelectrode technique. All techniques show a lower pH / higher proton efflux in the elongation zone compared with emerged blade and support the classical 'acid growth' theory for the elongation growth of plant organs.

(ii) Experiments with K^+ channel and transporter blockers, and with PM-H^+-ATPase activator and blocker point to new aspects of the acid growth theory when applied to barley leaves. LVDT measurements, analyses of cell wall property and microelectrode pH results suggest that a lower or higher H^+ transport activity is not linked directly to leaf growth, but linked through a H^+ / K^+ symport system which facilitates solute (especially K^+) uptake into growing cells. Changes in cell wall properties suggest that elongation of barley leaves can be described with a combination of the classical 'acid growth' and the 'facilitated solute uptake' theory.

(iii) In expression studies, both at the gene and protein level, a two fold higher PM-H^+-ATPase density per unit plasma membrane surface area is found in growing compared with non-growing leaf tissue. PM-H^+-ATPase seems an ideal reference gene in studies where growing and non-growing barley leaf tissues need to be compared. The copy number of the enzyme in the plasma membrane might be controlled by a simple mechanism of growth-dilution: the total amount of PM-H^+-ATPase is constant in the cells and the plasma membrane surface increases during cell and tissue development.

(iv) Immunohistological analyses show that PM-H^+-ATPase protein is present mainly in those leaf tissues which are characterised by high rates of solute exchange across the plasma membrane (guard cells) or high rates of solute loading / unloading associated with long-distance transport pathways (phloem; xylem parenchyma). This applies to both elongation zone and emerged blade and shows that there exists a cell-type-specific control of PM-H^+-ATPase protein level which is superimposed on any developmental gradient.

5.2 Future works

(i) Due to limited financial resources only some pH micro electrode measurements could be carried out. It would be interesting to further study the relation between apoplastic K^+ concentration and cell wall acidification applying 10 mM KCl treatment togheter with 5 μM fucicoccin and K^+ transporter blockers e.g. CsCl, TEA or NH_4^+.

(ii) Using inside-out plasma membrane vesicles and fluorimetric approach proton pumping activity could be monitored. Within this project preliminary experiments were carried out and 5(6)carboxyfluorescein seem a good candidate for these probes (better for this purpose than acridine orange that was used by many previous studies e.g. Yan *et al.* (1998); Yan *et al.* (2002); Zörb *et al.* (2005); Pitann *et al.* (2009b); Zhu *et al.* (2009); Wakeel *et al.* (2010). Due to time constraints, these experiments could not be finished. Results of these vesicular transport assays could further support PM-H^+-ATPase activity data.

(iii) Most of the present data point to HvHAK4 playing a key role in leaf cell elongation growth in barley. HvHAK4 is a putative K^+ / H^+ symporter, yet the precise function and characteristics of this transporter remain unknown. It would be good to carry out functionality tests of HvHAK4 and its regulation through test reagents which also impact on growth and PM-H^+-ATPase.

6 Literature

Amtmann A, Jelitto TC, Sanders D. 1999. K^+-selective inward-rectifying channels and apoplastic pH in barley roots. *Plant Physiol.* **120**: 331-338.

Arif I, Newman I. 1993. Proton efflux from oat coleoptile cells and exchange with wall calcium after IAA or fusicoccin treatment. *Planta* **189**: 377-383.

Ashley MK, Grant M, Grabov A. 2006. Plant responses to potassium deficiencies: A role for potassium transport proteins. *J. Exp. Bot.* **57**: 425-436.

Babcock DF. 1983. Examination of the intracellular ionic environment and of ionophore action by null point measurements employing the fluorescein chromophore. *J. Biol. Chem.* **258**: 6380-6389.

Bañuelos MA, Garciadeblas B, Cubero B, Rodríguez-Navarro A. 2002. Inventory and functional characterization of the HAK potassium transporters of rice. *Plant Physiol.* **130**: 784-795.

Besse M, Knipfer T, Miller AJ, Verdeil J-L, Jahn TP, Fricke W. 2011. Developmental pattern of aquaporin expression in barley (*Hordeum vulgare* L.) leaves. *J. Exp. Bot.* **62**: 4127-4142.

Boscari A, Clément M, Volkov V, Golldack D, Hybiak J, Miller AJ, Amtmann A, Fricke W. 2009. Potassium channels in barley: Cloning, functional characterization and expression analyses in relation to leaf growth and development. *Plant, Cell Environ.* **32**: 1761-1777.

Bouche-Pillon S, Fleurat-Lessard P, Fromont JC, Serrano R, Bonnemain JL. 1994. Immunolocalization of the plasma membrane H^+ -ATPase in minor veins of *Vicia faba* in relation to phloem loading. *Plant Physiol.* **105**: 691-697.

Boyer JS. 2001. Growth-induced water potentials originate from wall yielding during growth. *J. Exp. Bot.* **52**: 1483-1488.

Britto DT, Ebrahimi-Ardebili S, Hamam AM, Coskun D, Kronzucker HJ. 2010. ^{42}K analysis of sodium-induced potassium efflux in barley: Mechanism and relevance to salt tolerance. *New Phytol.* **186**: 373-384.

Britto DT, Kronzucker HJ. 2008. Cellular mechanisms of potassium transport in plants. *Physiol. Plant.* **133**: 637-650.

Brummer B, Felle H, Parish RW. 1984. Evidence that acid solutions induce plant cell elongation by acidifying the cytosol and stimulating the proton pump. *FEBS Letters* **174**: 223-227.

Bucker CA, de Souza SR, Fernandes MS. 2006. Effects of fusicoccin and vanadate on proton extrusion and potassium uptake by rice. *J. Plant Nutr.* **29**: 485-496.

Chazen O, Neumann PM. 1994. Hydraulic signals from the roots and rapid cell-wall hardening in growing maize (*Zea mays* L.) leaves are primary responses to polyethylene glycol-induced water deficits. *Plant Physiol.* **104**: 1385-1392.

Christian M, Steffens B, Schenck D, Burmester S, Böttger M, Lüthen H 2006. How does auxin enhance cell elongation? Roles of auxin-binding proteins and potassium channels in growth control. *Plant Biol.* 346-352.

Claussen M, Lüthen H, Blatt M, Bottger M. 1997. Auxin-induced growth and its linkage to potassium channels. *Planta* **201**: 227-234.

Clerc S, Barenholz Y. 1998. A quantitative model for using acridine orange as a transmembrane pH gradient probe. *Anal. Biochem.* **259**: 104-111.

Collins D, Walpole C, Ryan E, Winter D, Baird A, Stewart G. 2011. UT-B1 mediates transepithelial urea flux in the rat gastrointestinal tract. *J. Membr. Biol.* **239**: 123-130.

Conway EJ, O'Malley E. 1946. The nature of the cation exchanges during yeast fermentation, with formation of 0.02N-H ion. *Biochem. J.* **40**: 59-67.

Cosgrove DJ. 1993. Wall extensibility - its nature, measurement and relationship to plant-cell growth. *New Phytol.* **124**: 1-23.

Cosgrove DJ 1996. Plant cell enlargement and the action of expansins. BioEssays **18:** 533-540.

Cosgrove DJ. 1998. Cell wall loosening by expansins. *Plant Physiol.* **118**: 333-339.

Csiszár J, Erdei L, Pécsváradi A, Szabó M, Tari I. 2004. Növényélettan, növekedés- és fejlődésélettan (Plant physiology, growth and developing physiology). Szeged, JATEPress.

Darwin C. 1880. The power of movement in plants, chapter ix sensitiveness of plants to light: Its transmitted effects. London, John Murray.

Dennis PG, Hirsch PR, Smith SJ, Taylor RG, Valsami-Jones E, Miller AJ. 2009. Linking rhizoplane pH and bacterial density at the microhabitat scale. *J. Microbiol. Methods* **76**: 101-104

Döring O, Busch M, Lüthje S, Lüthen H, Hilgendorf F, Böttger M. 1996. Ionostats. *Protoplasma* **194**: 1-10.

Duby G, Boutry M. 2009. The plant plasma membrane proton pump ATPase: A highly regulated P-type ATPase with multiple physiological roles. *European J. Physiol.* **457**: 645-655.

DuPont FM. 1989. Effect of temperature on the plasma membrane and tonoplast ATPases of barley roots : Comparison of results obtained with acridine orange and quinacrine. *Plant Physiol.* **89**: 1401-1412.

Ehlert C, Plassard C, Cookson SJ, Tardieu F, Simonneau T. 2011. Do pH changes in the leaf apoplast contribute to rapid inhibition of leaf elongation rate by water stress? Comparison of stress responses induced by polyethylene glycol and down-regulation of root hydraulic conductivity. *Plant Cell Environ.* **34**: 1258-1266.

Epstein E, Rains DW, Elzam OE. 1963. Resolution of dual mechanisms of potassium absorption by barley roots. *PNAS* **49**: 684-692.

Felle HH. 2005. pH regulation in anoxic plants. *Annals Bot.* **96**: 519-532.

Felle HH. 2006. Apoplastic pH during low-oxygen stress in barley. *Annals Bot.* **98**: 1085-1093.

Felle HH, Herrmann A, Huckelhoven R, Kogel KH. 2005. Root-to-shoot signalling: Apoplastic alkalinization, a general stress response and defence factor in barley (*Hordeum vulgare*). *Protoplasma* **227**: 17-24.

Fleurat-Lessard P, Bouche-Pillon S, Leloup C, Bonnemain JL. 1997. Distribution and activity of the plasma membrane H^+-ATPase in *Mimosa pudica* L in relation to ionic fluxes and leaf movements. *Plant Physiol.* **113**: 747-754.

Frensch J. 1997. Primary responses of root and leaf elongation to water deficits in the atmosphere and soil solution. *J. Exp. Bot.* **48**: 985-999.

Fricke W. 2002a. Biophysical limitation of cell elongation in cereal leaves. *Annals Bot.* **90**: 157-167.

Fricke W. 2002b. Biophysical limitation of leaf cell elongation in source-reduced barley. *Planta* **215**: 327-338.

Fricke W. 2004. Rapid and tissue-specific accumulation of solutes in the growth zone of barley leaves in response to salinity. *Planta* **219**: 515.

Fricke W, Akhiyarova G, Veselov D, Kudoyarova G. 2004. Rapid and tissue-specific changes in ABA and in growth rate in response to salinity in barley leaves. *J. Exp. Bot.* **55**: 1115-1123.

Fricke W, Flowers TJ. 1998. Control of leaf cell elongation in barley. Generation rates of osmotic pressure and turgor, and growth-associated water potential gradients. *Planta* **206**: 53-65.

Fricke W, Leigh RA, Tomos AD. 1994. Concentrations of inorganic and organic solutes in extracts from invidual epidermal, mesophyll and bundle-sheath cells of barley leaves. *Planta* **192**: 310-316.

Fricke W, McDonald AJS, Mattson-Djos L. 1997. Why do leaves and leaf cells of N-limited barley elongate at reduced rates? *Planta* **202**: 522-530.

Fricke W, Peters WS. 2002. The biophysics of leaf growth in salt-stressed barley. A study at the cell level. *Plant Physiol.* **129**: 374-388.

Gaxiola RA, Palmgren MG, Schumacher K. 2007. Plant proton pumps. *FEBS Letters* **581**: 2204-2214.

Glass ADM, Siddiqi MY, Giles KI. 1981. Correlations between potassium uptake and hydrogen efflux in barley varieties : A potential screening method for the isolation of nutrient efficient lines. *Plant Physiol.* **68**: 457-459.

Graber ML, DiLillo DC, Friedman BL, Pastoriza-Munoz E. 1986. Characteristics of fluoroprobes for measuring intracellular pH. *Anal. Biochem.* **156**: 202-212.

Grebe M. 2005. Growth by auxin: When a weed needs acid. *Science* **310**: 60-61.

Green PB, Erickson RO, Buggy J. 1971. Metabolic and physical control of cell elongation rate: In vivo studies in nitella. *Plant Physiol.* **47**: 423-430.

Grignon C, Sentenac H. 1991. pH and ionic conditions in the apoplast. *Ann. Rev. Plant Physiol. Plant Mol. Biol.* **42**: 103-128.

Hachez C, Heinen RB, Draye X, Chaumont F. 2008. The expression pattern of plasma membrane aquaporins in maize leaf highlights their role in hydraulic regulation. *Plant Mol. Biol.* **68**: 337-353.

Hager A. 2003. Role of the plasma membrane H^+-ATPase in auxin-induced elongation growth: Historical and new aspects. *J. Plant Res.* **116**: 483-505.

Hager A, Debus G, Edel HG, Stransky H, Serrano R. 1991. Auxin induces exocytosis and the rapid synthesis of a high-turnover pool of plasma-membrane H^+-ATPase. *Planta* **185**: 527-537.

Hager A, Menzel H, Krauss A. 1971. Experiments and hypothesis concerning primary action of auxin in elongation growth. *Planta* **100**: 47-71.

Hatzig S, Hanstein S, Schubert S. 2010. Apoplast acidification is not a necessary determinant for the resistance of maize in the first phase of salt stress. *J. Plant Nut. Soil Sci.* **173**: 559-562.

Hohl M, Hong YN, Schopfer P. 1991. Acid- and enzyme-mediated solubilization of cell-wall β-1.3,β-1.4-D-glucan in maize coleoptiles : Implications for auxin-mediated growth. *Plant Physiol.* **95**: 1012-1018.

Hoopen FT, Cuin TA, Pedas P, Hegelund JN, Shabala S, Schjoerring JK, Jahn TP. 2010. Competition between uptake of ammonium and potassium in barley and *Arabidopsis* roots: Molecular mechanisms and physiological consequences. *J. Exp. Bot.* **61**: 2303-2315.

Hruz T, Wyss M, Docquier M, Pfaffl M, Masanetz S, Borghi L, Verbrugghe P, Kalaydjieva L, Bleuler S, Laule O, Descombes P, Gruissem W, Zimmermann P. 2011. Refgenes: Identification of reliable and condition specific reference genes for RT-qPCR data normalization. *BMC Genomics* **12**: 156.

Hsiao TC, Frensch J, Rojas-Lara BA. 1998. The pressure-jump technique shows maize leaf growth to be enhanced by increases in turgor only when water status is not too high. *Plant, Cell Environ.* **21**: 33-42.

Hsiao TC, Xu LK. 2000. Sensitivity of growth of roots versus leaves to water stress: Biophysical analysis and relation to water transport. *J. Exp. Bot.* **51**: 1595-1616.

Hynek R, Svensson B, Jensen ONr, Barkholt V, Finnie C. 2006. Enrichment and identification of integral membrane proteins from barley aleurone layers by reversed-phase chromatography, SDS-PAGE, and LC-MS/MS. *J. Proteome Res.* **5**: 3105-3113.

Johansson F, Sommarin M, Larsson C. 1993. Fusicoccin activates the plasma-membrane H^+-ATPase by a mechanism involving the c-terminal inhibitory domain. *Plant Cell* **5**: 321-327.

Katsumi M. 2007. Studies on plant growth substances in japan before 1945. *Plant Biotech.* **24**: 155-163.

Kavanagh CA. 2010. Changes in cell ultrastructure during leaf development in barley (*Hordeum vulgare* L.) and in response to salinity*. MSc Thesis*, University College Dublin, Dublin.

Keller CP, Van Volkenburgh E. 1998. Evidence that auxin-induced growth of tobacco leaf tissues does not involve cell wall acidification. *Plant Physiol.* **118**: 557-564.

Kim S, Dale BE. 2004. Global potential bioethanol production from wasted crops and crop residues. *Biomass and Bioenergy* **26**: 361-375.

Kjellbom P, Larsson C. 1984. Preparation and polypeptide composition of chlorophyll-free plasma-membranes from leaves of light-grown spinach and barley. *Physiol. Plant.* **62**: 501-509.

Knipfer T, Fricke W. 2011. Water uptake by seminal and adventitious roots in relation to whole-plant water flow in barley (*Hordeum vulgare* L.). *J. Exp. Bot.* **62**: 717-733.

Kronzucker HJ, Szczerba MW, Britto DT. 2003. Cytosolic potassium homeostasis revisited: ^{42}K-tracer analysis in *Hordeum vulgare* L. Reveals set-point variations in K^+. *Planta* **217**: 540-546.

Kruger N 2002. The Bradford method for protein quantitation. *The protein protocols handbook*, **15:** (4) 15-21.

Kutschera U. 1994. Tansley review no. 66. The current status of the acid-growth hypothesis. *New Phytol.* **126**: 549-569.

Kutschera U. 2006. Acid growth and plant development. *Science* **311**: 952-954.

Kutschera U, Bergfeld R, Schopfer P. 1987. Cooperation of epidermis and inner tissues in auxin-mediated growth of maize coleoptiles. *Planta* **170**: 168-180.

Kutschera U, Schopfer P. 1985a. Evidence against the acid-growth theory of auxin action. *Planta* **163**: 483-493.

Kutschera U, Schopfer P. 1985b. Evidence for the acid-growth theory of fusicoccin action. *Planta* **163**: 494-499.

Laemmli UK. 1970. Cleavage of structural proteins during the assembly of the head of bacteriophage T4. *Nature* **227**: 680-685.

Larkin PJ. 1976. Purification and viability determinations of plant protoplasts. *Planta* **128**: 213-216.

Lenaeus MJ, Vamvouka M, Focia PJ, Gross A. 2005. Structural basis of TEA blockade in a model potassium channel. *Nature Struct. Mol. Biol.* **12**: 454-459.

Li L, Li S-M, Sun J-H, Zhou L-L, Bao X-G, Zhang H-G, Zhang F-S. 2007. Diversity enhances agricultural productivity via rhizosphere phosphorus facilitation on phosphorus-deficient soils. *PNAS* **104**: 11192-11196.

Lockhart JA. 1965. An analysis of irreversible plant cell elongation. *J Theor. Biol.* **8**: 264-275.

Lüthen H, Bigdon M, Böttger M. 1990. Reexamination of the acid growth theory of auxin action. *Plant Physiol.* **93**: 931-939.

Lüthen H, Böttger M. 1988. Kinetics of proton secretion and growth in maize roots - action of various plant-growth effectors. *Plant Sci.* **54**: 37-43.

Maathuis FJM, Filatov V, Herzyk P, C. Krijger G, B. Axelsen K, Chen S, Green BJ, Li Y, Madagan KL, Sánchez-Fernández R, Forde BG, Palmgren MG, Rea PA, Williams LE, Sanders D, Amtmann A. 2003. Transcriptome analysis of root transporters reveals participation of multiple gene families in the response to cation stress. *Plant J.* **35**: 675-692.

Malnic G, Geibel JP. 2000. Cell pH and H^+ secretion by S3 segment of mammalian kidney: Role of H+-ATPase and Cl^-. .*J. Membr. Biol.* **178**: 115-125.

Manente S, Pieri SD, Iero A, Rigo C, Bragadin M. 2008. A comparison between the responses of neutral red and acridine orange: Acridine orange should be preferential and alternative to neutral red as a dye for the monitoring of contaminants by means of biological sensors. *Anal. Biochem.* **383**: 316-319.

Marré E. 1979. Fusicoccin - tool in plant physiology. *Ann. Rev. Plant Physiol. Plant Mol. Biol.* **30**: 273-288.

Martre P, Bogeat-Triboulot M-B, Durand J-L. 1999. Measurement of a growth-induced water potential gradient in tall fescue leaves. *New Phytol.* **142**: 435-439.

McQueen-Mason S, Durachko DM, Cosgrove DJ. 1992. Two endogenous proteins that induce cell wall extension in plants. *Plant Cell* **4**: 1425-1433.

McQueen-Mason SJ. 1995. Expansins and cell wall expansion. *J. Exp. Bot.* **46**: 1639-1650.

Michelet B, Boutry M. 1995. The plasma membrane H^+-ATPase: A highly regulated enzyme with multiple physiological functions. *Plant Physiol.* **108**: 1-6.

Miller AJ, Smith SJ. 1992. The mechanism of nitrate transport across the tonoplast of barley root cells. *Planta* **187**: 554-557.

Mito N, Wimmers LE, Bennett AB. 1996. Sugar regulates mrna abundance of h^+-atpase gene family members in tomato. *Plant Physiol.* **112**: 1229-1236.

Moloney MM, Elliott MC, Cleland RE. 1981. Acid growth effects in maize roots - evidence for a link between auxin-economy and proton extrusion in the control of root-growth. *Planta* **152**: 285-291.

Moran N. 2007. Osmoregulation of leaf motor cells. *FEBS Letters* **581**: 2337-2347.

Morsomme P, Boutry M. 2000. The plant plasma membrane H^+-ATPase: Structure, function and regulation. *BBA – Biomembr.* **1465**: 1-16.

Morth JP, Pedersen BP, Buch-Pedersen MJ, Andersen JP, Vilsen B, Palmgren MG, Nissen P. 2011. A structural overview of the plasma membrane Na^+,K^+-ATPase and H^+-ATPase ion pumps. *Nature Rev. Mol. Cell. Biol.* **12**: 60-70.

Neumann PM. 1993. Rapid and reversible modifications of extension capacity of cell walls in elongating maize leaf tissues responding to root addition and removal of NaCl. *Plant, Cell Environ.* **16**: 1107-1114.

Neves-Piestun BG, Bernstein N. 2001. Salinity-induced inhibition of leaf elongation in maize is not mediated by changes in cell wall acidification capacity. *Plant Physiol.* **125**: 1419-1428.

O'Neal ME, Landis DA, Isaacs R. 2002. An inexpensive, accurate method for measuring leaf area and defoliation through digital image analysis. *J. Econ. Entom.* **95**: 1190-1194.

Oecking C, Eckerskorn C, Weiler EW. 1994. The fusicoccin receptor of plants is a member of the 14-3-3-superfamily of eukaryotic regulatory proteins. *FEBS Letters* **352**: 163-166.

Olivari C, Meanti C, De Michelis MI, Rasi-Caldogno F. 1998. Fusicoccin binding to its plasma membrane receptor and the activation of the plasma membrane H^+-ATPase. IV. Fusicoccin induces the association between the plasma membrane H^+-ATPase and the fusicoccin receptor. *Plant Physiol.* **116**: 529-537.

Paál Á. 1918. Über phototropsche Reizleitungen. *Jehrb. wiss. Bot.* **58**: 406-458.

Palmgren MG. 1991. Acridine-orange as a probe for measuring pH gradients across membranes - mechanism and limitations. *Anal. Biochem.* **192**: 316-321.

Palmgren MG. 2001. Plant plasma membrane H^+-ATPases: Powerhouses for nutrient uptake. *Ann. Rev. Plant Physiol. Plant Mol. Biol.* **52**: 817-845.

Palmgren MG, Sommarin M, Serrano R, Larsson C. 1991. Identification of an autoinhibitory domain in the C-terminal region of the plant plasma membrane H^+-ATPase. *J. Biol. Chem.* **266**: 20470-20475.

Pedersen BP, Buch-Pedersen MJ, Morth JP, Palmgren MG, Nissen P. 2007. Crystal structure of the plasma membrane proton pump. *Nature* **450**: 1111-1119.

Perrot-Rechenmann C. 2010. Cellular responses to auxin: Division versus expansion. *Cold Spring Harbor Persp. Biol.* **2**: a001446; 1-15.

Peters WS. 2004. Growth rate gradients and extracellular pH in roots: How to control an explosion. *New Phytol.* **162**: 571-574.

Peters WS, Felle HH. 1999. The correlation of profiles of surface pH and elongation growth in maize roots. *Plant Physiol.* **121**: 905-912.

Peters WS, Luthen H, Bottger M, Felle H. 1998. The temporal correlation of changes in apoplast pH and growth rate in maize coleoptile segments. *Austr. J. Plant Physiol.* **25**: 21-25.

Peters WS, Richter U, Felle HH. 1992. Auxin-induced H^+-pump stimulation does not depend on the presence of epidermal-cells in corn coleoptiles. *Planta* **186**: 313-316.

Pfaffl MW. 2001. A new mathematical model for relative quantification in real-time RT-PCR. *Nucl. Acids Res.* **29**: e45.

Philippar K, Büchsenschütz K, Edwards D, Löffler J, Lüthen H, Kranz E, Edwards K, Hedrich R. 2006. The auxin-induced k^+ channel gene *ZMK1* in maize functions in coleoptile growth and is required for embryo development. *Plant Mol. Biol.* **61**: 757-768.

Philippar K, Fuchs I, Lüthen H, Hoth S, Bauer CS, Haga K, Thiel G, Ljung K, Sandberg G, Böttger M, Becker D, Hedrich R. 1999. Auxin-induced K^+ channel expression represents an essential step in coleoptile growth and gravitropism. *PNAS* **96**: 12186-12191.

Philippar K, Ivashikina N, Ache P, Christian M, Lüthen H, Palme K, Hedrich R. 2004. Auxin activates KAT1 and KAT2, two K^+-channel genes expressed in seedlings of *Arabidopsis thaliana*. *Plant J.* **37**: 815-827.

Pitann B, Kranz T, Muhling KH. 2009a. The apoplastic pH and its significance in adaptation to salinity in maize (*Zea mays* L.): Comparison of fluorescence microscopy and ph-sensitive microelectrodes. *Plant Sci.* **176**: 497-504.

Pitann B, Schubert S, Muhling KH. 2009b. Decline in leaf growth under salt stress is due to an inhibition of H+-pumping activity and increase in apoplastic pH of maize leaves. *J. Plant Nutr. Soil Sci.* **172**: 535-543.

Pollock CJ, Tomos AD, Thomas A, Smith CJ, Lloyd EJ, Stoddart JL. 1990. Extension growth in a barley mutant with reduced sensitivity to low-temperature. *New Phytol.* **115**: 617-623.

Pope AJ, Leigh RA. 1988. Dissipation of ph gradients in tonoplast vesicles and liposomes by mixtures of acridine orange and anions: Implications for the use of acridine orange as a pH probe. *Plant Physiol.* **86**: 1315-1322.

Pritchard J. 1994. The control of cell expansion in roots. *New Phytol.* **127**: 3-26.

Rayle DL. 1973. Auxin-induced hydrogen-ion secretion in avena coleoptiles and its implications. *Planta* **114**: 63-73.

Rayle DL, Cleland R. 1970. Enhancement of wall loosening and elongation by acid solutions. *Plant Physiol.* **46**: 250-253.

Rayle DL, Cleland RE. 1992. The acid growth theory of auxin-induced cell elongation is alive and well. *Plant Physiol.* **99**: 1271-1274.

Reidy B, McQueen-Mason S, Nösberger J, Fleming A. 2001. Differential expression of α- and β-expansin genes in the elongating leaf of festuca pratensis. *Plant Mol. Biol.* **46**: 491-504.

Richardson A, Wojciechowski T, Franke R, Schreiber L, Kerstiens G, Jarvis M, Fricke W. 2007. Cuticular permeance in relation to wax and cutin development along the growing barley (*Hordeum vulgare*) leaf. *Planta* **225**: 1471-1481.

Rodriguez-Navarro A, Rubio F. 2006. High-affinity potassium and sodium transport systems in plants. *J. Exp. Bot.* **57**: 1149-1160.

Rubio F, Santa-María GE, Rodríguez-Navarro A. 2000. Cloning of *Arabidopsis* and barley cDNAs encoding HAK potassium transporters in root and shoot cells. *Physiol. Plant.* **109**: 34-43.

Sabirzhanova IB, Sabirzhanov BE, Chemeris AV, Veselov DS, Kudoyarova GR. 2005. Fast changes in expression of expansin gene and leaf extensibility in osmotically stressed maize plants. *Plant Physiol. Biochem.* **43**: 419-422.

Sakurai N, Masuda Y. 1978. Auxin-induced changes in barley coleoptile cell-wall composition. *Plant Cell Physiol.* **19**: 1217-1223.

Santi S, Cesco S, Varanini Z, Pinton R. 2005. Two plasma membrane H^+-ATPase genes are differentially expressed in iron-deficient cucumber plants. *Plant Physiol. Biochem.* **43**: 287-292.

Sarkadi B, Price EM, Boucher RC, Germann UA, Scarborough GA. 1992. Expression of the human multidrug resistance cdna in insect cells generates a high-activity drug-stimulated membrane ATPase. *J. Biol. Chem.* **267**: 4854-4858.

Schopfer P. 1989. pH-dependence of extension growth in *Avena*-coleopiles and its implications for the mechanism of auxin action. *Plant Physiol.* **90**: 202-207.

Schulte D, Close TJ, Graner A, Langridge P, Matsumoto T, Muehlbauer G, Sato K, Schulman AH, Waugh R, Wise RP, Stein N. 2009. The international barley sequencing consortium - At the threshold of efficient access to the barley genome. *Plant Physiol.* **149**: 142-147.

Senn ME, Rubio F, Bañuelos MA, Rodríguez-Navarro A. 2001. Comparative functional features of plant potassium hvhak1 and hvhak2 transporters. *J. Biol. Chem.* **276**: 44563-44569.

Shen H, He LF, Sasaki T, Yamamoto Y, Zheng SJ, Ligaba A, Yan XL, Ahn SJ, Yamaguchi M, Sasakawa H, Matsumoto H. 2005. Citrate secretion coupled with the modulation of soybean root tip under aluminum stress. Up-regulation of transcription, translation, and threonine-oriented phosphorylation of plasma membrane H^+-ATPase. *Plant Physiol.* **138**: 287-296.

Slayman CL. 1965. Electrical properties of *Neurospora crassa*. *J. General Physiol.* **49**: 69-92.

Spalding EP, Hirsch RE, Lewis DR, Qi Z, Sussman MR, Lewis BD. 1999. Potassium uptake supporting plant growth in the absence of AKT1 channel activity: Inhibition by ammonium and stimulation by sodium. *J. Gen. Physiol.* **113**: 909-918.

Speth C, Jaspert N, Marcon C, Oecking C. 2010. Regulation of the plant plasma membrane H^+-ATPase by its c-terminal domain: What do we know for sure? *European J. Cell Biol.* **89**: 145-151.

Stahlberg R, Van Volkenburgh E. 1999. The effect of light on membrane potential, apoplastic pH and cell expansion in leaves of *Pisum sativum* L. var. Argenteum. - role of the plasma-membrane H^+-ATPase and photosynthesis. *Planta* **208**: 188-195.

Steudle E. 2000. Water uptake by roots: Effects of water deficit. *J. Exp. Bot.* **51**: 1531-1542.

Stiles K, McClintick A, Volkenburgh E. 2003. A developmental gradient in the mechanism of K^+ uptake during light-stimulated leaf growth in *Nicotiana tabacum* L. *Planta* **217**: 587-596.

Stiles KA, Van Volkenburgh E 2004. Role of K^+ in leaf growth: K^+ uptake is required for light-stimulated H^+ efflux but not solute accumulation. *Plant, Cell Environ***. 27:** 315-325.

Stoddart JL, Lloyd EJ. 1986. Modification by gibberellin of the growth-temperature relationship in mutant and normal genotypes of several cereals. *Planta* **167**: 364-368.

Szczerba MW, Britto DT, Kronzucker HJ. 2006. Rapid, futile K^+ cycling and pool-size dynamics define low-affinity potassium transport in barley. *Plant Physiol.* **141**: 1494-1507.

Szczerba MW, Britto DT, Kronzucker HJ. 2009. K^+ transport in plants: Physiology and molecular biology. *J. Plant Physiol.* **166**: 447-466.

Sze H, Li X, Palmgren MG. 1999. Energization of plant cell membranes by H+-pumping ATPases: Regulation and biosynthesis. *Plant Cell* **11**: 677-690.

Tang AC, Boyer JS. 2008. Xylem tension affects growth-induced water potential and daily elongation of maize leaves. *J. Exp. Bot.* **59**: 753-764.

Tang C, Drevon JJ, Jaillard B, Souche G, Hinsinger P. 2004. Proton release of two genotypes of bean (*Phaseolus vulgaris* L.) as affected by N nutrition and P deficiency. *Plant Soil* **260**: 59-68.

Taylor G, Davies WJ. 1985. The control of leaf growth of betula and acer by photoenvironment. *New Phytol.* **101**: 259-268.

Tode K, Lüthen H. 2001. Fusicoccin- and IAA-induced elongation growth share the same pattern of K^+ dependence. *J. Exp. Bot.* **52**: 251-255.

Ullrich CI, Novacky AJ. 1990. Extracellular and intracellular ph and membrane-potential changes induced by K^+, Cl^-, $H_2PO_4^-$, and NO_3^- uptake and fusicoccin in root hairs of limnobium-stoloniferum. *Plant Physiol.* **94**: 1561-1567.

Van Volkenburgh E, Boyer JS. 1985. Inhibitory effects of water deficit on maize leaf elongation. *Plant Physiol.* **77**: 190-194.

Van Volkenburgh E, Cleland RE. 1980. Proton excretion and cell expansion in bean *Phaseolus vulgaris* leaves. *Planta* **148**: 273-278.

Vera-Estrella R, Barkla BJ, Higgins VJ, Blumwald E. 1994. Plant defense response to fungal pathogens (activation of host-plasma membrane H^+-ATPase by elicitor-induced enzyme dephosphorylation). *Plant Physiol.* **104**: 209-215.

Vesper MJ, Evans ML. 1979. Nonhormonal induction of H^+ efflux from plant tissues and its correlation with growth. *PNAS* **76**: 6366-6370.

Villalba JM, Lützelschwab M, Serrano R. 1991. Immunocytolocalization of plasma-membrane H^+-ATPase in maize coleoptiles and enclosed leaves. *Planta* **185**: 458-461.

Vogelstein B, Kinzler KW. 1999. Digital PCR. *PNAS* **96**: 9236-9241.

Volkov V, Boscari A, Clément M, Miller AJ, Amtmann A, Fricke W. 2009. Electrophysiological characterization of pathways for K^+ uptake into growing and non-growing leaf cells of barley. *Plant, Cell Environ.* **32**: 1778-1790.

Volkov V, Hachez C, Moshelion M, Draye X, Chaumont F, Fricke W. 2007. Water permeability differs between growing and non-growing barley leaf tissues. .*J. Exp. Bot.* **58**: 377-390.

Vysotskaya LB, Arkhipova TN, Timergalina LN, Veselov SY, Dedov AV, Kudoyarova GR. 2003. Effect of partial root excision on shoot water relations. *J. Plant Physiol.* **160**: 1011-1015.

Wakeel A, Hanstein S, Pitann B, Schubert S. 2010. Hydrolytic and pumping activity of H+-ATPase from leaves of sugar beet (*Beta vulgaris* L.) as affected by salt stress. *J. Plant Physiol.* **167**: 725-731.

Wei WX, Alexandersson E, Golldack D, Miller AJ, Kjellborn PO, Fricke W. 2007. HvPIP1;6, a barley (*Hordeum vulgare* L.) plasma membrane water channel particularly expressed in growing compared with non-growing leaf tissues. *Plant Cell Physiol.* **48**: 1132-1147.

Wieczorek H, Putzenlechner M, Zeiske W, Klein U. 1991. A vacuolar-type proton pump energizes K^+ / H^+ antiport in an animal plasma-membrane. *J. Biol. Chem.* **266**: 15340-15347.

Würtele M, Jelich-Ottmann C, Wittinghofer A, Oecking C. 2003. Structural view of a fungal toxin acting on a 14-3-3 regulatory complex. *EMBO J.* **22**: 987-994.

Yan F, Feuerle R, Schaffer S, Fortmeier H, Schubert S. 1998. Adaptation of active proton pumping and plasmalemma ATPase activity of corn roots to low root medium pH. *Plant Physiol.* **117**: 311-319.

Yan F, Zhu Y, Muller C, Zorb C, Schubert S. 2002. Adaptation of H^+-pumping and plasma membrane H^+ ATPase activity in proteoid roots of white lupin under phosphate deficiency. *Plant Physiol.* **129**: 50-63.

Zhu Y, Tingjun DI, Guohua XU, Xi C, Houqing Z, Feng YAN, Qirong S. 2009. Adaptation of plasma membrane H^+-ATPase of rice roots to low pH as related to ammonium nutrition. *Plant, Cell Environ.* **32**: 1428-1440.

Zoccarato F, Cavallini L, Alexandre A. 1999. The pH-sensitive dye acridine orange as a tool to monitorexocytosis/endocytosis in synaptosomes. *J. Neurochem.* **72**: 625-633.

Zörb C, Stracke B, Tramnitz B, Denter D, Sümer A, Mühling KH, Yan F, Schubert S. 2005. Does H^+ pumping by plasmalemma ATPase limit leaf growth of maize *Zea mays* during the first phase of salt stress? *J. Plant Nutr. Soil Sci.* **168**: 550-557.

7 Appendix

7.1 Processing of qPCR data

(i) Total cell volume was considered to equal the total water content of plant tissue (neglecting any water in intercellular space). The water content was calculated from the fresh weight of the samples:

$$m_w = m_{FW} \cdot w_{\%} \text{ [g]}$$

$$V_{cell} = m_w \cdot 10^{12} \text{ [µm}^3\text{]}$$

where: m_w: amount of water in the tissue (g); m_{FW}: fresh weight of tissue (g) and $w_{\%}$: percentage water content of the tissue, $100 \cdot \left(\frac{m_{FW} - m_{DW}}{m_{FW}} \right)$; m_{DW}, dry weight); V_{cell}: total cell volume (µm^3).

(ii) From water content, from the proportion of leaf volume occupied by epidermis (0.26) and mesophyll (0.646) and from the cell sizes (99,372 µm^3 for epidermis cells in elongation zone; 461,552 µm^3 for epidermis cells in emerged blade; 6,620 µm^3 for mesophyll cells in elongation zone and 14,830 for mesophyll cells in emerged leaf blade) the number of epidermal cells, mesophyll cells and total number of the cells were calculated:

Elongation zone: $N_{Epcell} = \frac{V_{cell} \cdot 0.260}{99{,}372}$; $N_{Mcell} = \frac{V_{cell} \cdot 0.646}{6{,}620}$ [piece]

Emerged Blade: $N_{Epcell} = \frac{V_{cell} \cdot 0.296}{461{,}552}$; $N_{Mcell} = \frac{V_{cell} \cdot 0.653}{14{,}830}$ [piece]

Total cell number: $N_{cell} = N_{Epcell} + N_{Mcell}$ [piece]

where: N_{Epcell}: number of epidermal cells; N_{Mcell}: number of mesophyll cells and N_{cell}: total cell number.

(iii) Plasma membrane surface was calculated as:

Elongation zone: $A = N_{Epcell} \cdot 19{,}704 + N_{Mcell} \cdot 1{,}632$ [µm^2]

Emerge blade: $A = N_{Epcell} \cdot 50{,}004 + N_{Mcell} \cdot 2{,}855$ [µm^2]

where: A: plasma membrane surface of the sample (µm^2).

(iv) Calculation of the PM-H$^+$-ATPase copy number in the sample was carried out with the help of calibration curve using PM-H$^+$-ATPase DNA standard. This calibration curve was different for each qPCR measurement. An example of this calculation may be found in Fig. 7.1.

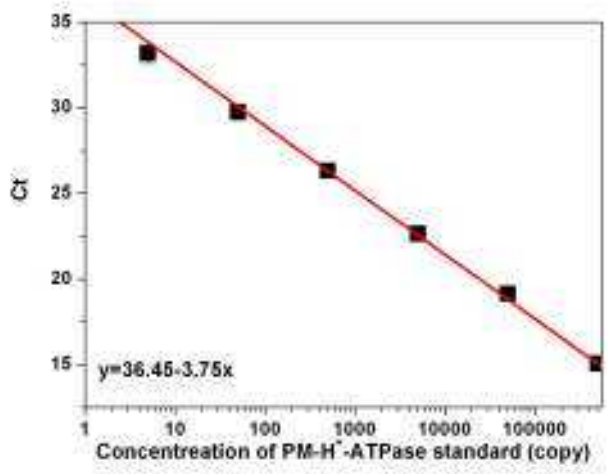

Figure 7.1 Typical calibration curve for converting Ct values into transcript copy number

For calibration three replicates were used and r^2 of the fitted line was always higher than 0.98.

From the calibration curve Ct values were converted into copy number of PM-H$^+$-ATPase transcript. For example, using the above calibration curve resulted in the following:

$$N_{PM-H^+-ATPase} = 10^{\frac{36.45-\overline{Ct}}{3.75}} \text{ [copy]}$$

where: $N_{PM-H^+-ATPase}$: copy number of PM-H$^+$-ATPase in the PCR sample (typically 250 pg); $\overline{Ct}$: average Ct values of 3 technical replicates.

(v) From the copy number of PCR reaction the total copy number in 1 μg RNA could easily be calculated through multiplying the results with respective dilution factors; these were typically 4,000 using 250 pg template in each reaction:

$$N_{copy1\mu g} = N_{PM-H^+-ATPase} \cdot 4{,}000 \text{ [copy]}$$

where: $N_{copy1\mu g}$ is the PM-H$^+$-ATPase copy number in 1 μg RNA

(vi) The copy number of transcript in 1 μg RNA could then be multiplied by the total RNA content of the leaf sample used for extraction of RNA:

$$N_{totalcopy} = N_{copy1\mu g} \cdot m_{RNA} \text{ [copy]}$$

where: $N_{totalcopy}$: the total PM-H^+-ATPase mRNA copy in the sample; m_{RNA} is amount of total RNA (μg) in the sample.

(vii) Finally, this total copy number of PM-H^+-ATPase transcripts could then be realted to the total number of cells or the total plasma membrane surface area in the leaf sample:

$$c_{copy \cdot cell^{-1}} = \frac{N_{totalcopy}}{N_{cell}} \text{ [copy cell}^{-1}\text{]}$$

$$c_{copy \cdot A^{-1}} = \frac{N_{totalcopy}}{A} \cdot 10^6 \text{ [copy mm}^{-2}\text{]}$$

where: $c_{copy \cdot cell^{-1}}$: PM-H^+-ATPase copy number in a single cell; $c_{copy \cdot A^{-1}}$: PM-H^+-ATPase copy number in 1 mm^2 plasma membrane.

Example for these calculations can be found on Table 7.1 for Golf and Table 7.2 for Jersey barley cultivar.

Table 7.1 Example for qPCR calculation of Golf cultivar. S1 - 3 label different batches

	Elongation zone			Emerged blade		
	S1	**S2**	**S3**	**S1**	**S2**	**S3**
Fresh weight (mg)	56.6	57.7	50.0	53.5	50.7	48.7
Water content (mg)	52.1	51.3	46.0	46.4	44.0	42.3
Number of epidermis cells (x 10^4)	13.6	13.4	12.0	2.98	2.82	2.71
Number of mesophyll cells (x 10^6)	5.08	5.00	4.49	2.04	1.94	1.86
Total number of cells (x 10^6)	5.22	5.14	4.61	2.07	1.97	1.87
Total membrane surface of epidermis cells (mm^2 x 10^3)	2.69	2.64	2.37	1.49	1.41	1.36
Total membrane surface of mesophyll cells (mm^2 x 10^3)	8.30	8.17	7.33	5.84	5.53	5.31
Total membrane surface of the sample (mm^2 x 10^3)	10.9	10.8	9.70	7.32	6.94	6.67
Total RNA in the sample (µg)	123	106	105	61.3	51.9	40.9
PM-H^+-ATPase copy in 1 µg RNA (x 10^6)	14.8	11.5	13.7	9.91	6.63	14.1
PM-H^+-ATPase copy in the sample (x 10^9)	1.83	1.21	1.43	0.607	0.344	0.577
PM-H^+-ATPase copy in a cell	350	236	312	293	175	306
PM-H^+-ATPase copy per mm^2 plasma membrane (x 10^4)	166	112	148	83.0	49.6	86.6

Table 7.2 Example for qPCR calculation of Jersey cultivar. S1 - 3 label different batches

	Elongation zone			Emerged blade		
	S1	**S2**	**S3**	**S1**	**S2**	**S3**
Fresh weight (mg)	69.2	57.6	58.7	77.1	74.9	62.2
Water content (mg)	64.9	54.0	55.1	68.5	66.5	55.2
Number of epidermis cells (x 10^4)	17.0	14.1	14.4	4.39	4.27	3.54
Number of mesophyll cells (x 10^6)	6.33	5.27	5.37	3.01	2.93	2.43
Total number of cells (x 10^6)	6.50	5.41	5.52	3.06	2.97	2.47
Total membrane surface of epidermis cells (mm^2 x 10^3)	3.35	2.79	2.84	2.20	2.13	1.77
Total membrane surface of mesophyll cells (mm^2 x 10^3)	10.3	8.60	8.77	8.61	8.36	6.94
Total membrane surface of the sample (mm^2 x 10^3)	13.7	11.4	11.6	10.8	10.5	8.71
Total RNA in the sample (µg)	161	119	121	24.7	108	26.8
PM-H^+-ATPase copy in 1 µg RNA (x 10^6)	5.90	4.76	4.45	4.52	4.13	5.56
PM-H^+-ATPase copy in the sample (x 10^9)	9.49	5.65	5.34	1.11	4.47	1.49
PM-H^+-ATPase copy in a cell	146	104	97	36	150	60
PM-H^+-ATPase copy per mm^2 plasma membrane (x 10^4)	6.94	4.97	4.60	1.03	4.26	1.71

Table 7.3 Example for qPCR calculation of Jersey protoplasts. S1 - 3 label different batches

	Elongation zone			Emerged blade		
	S1	**S2**	**S3**	**S1**	**S2**	**S3**
Protoplast No (x 10^6)	5.13	5.05	5.51	5.57	3.84	7.85
Surface (mm^2 x 10^{10})	8.37	8.24	9.00	1.59	1.10	2.24
Total RNA(□g)	26.5	28.2	37.9	31.6	29.2	65.3
PM-H^+-ATPase copy in 1 µg RNA (x 10^6)	5.34	3.95	7.02	3.09	2.06	5.60
PM-H^+-ATPase copy in the sample (x 10^7)	14.1	11.1	26.6	9.75	6.00	36.6
PM-H^+-ATPase copy in a cell	27.6	22.0	48.3	17.5	15.6	46.6
PM-H^+-ATPase copy in 1 mm^2 plasma membrane (x 10^4)	1.69	1.35	2.96	0.613	0.548	1.63

7.2 List of chemicals

$(NH_4)_2HPO_4$	M&B
5(6)carboxyfluorescein	Sigma
Acetic acid	Reanal, BDH
Acridine orange	BDH
Acylamide (C_3H_5NO)	Sigma-Aldrich
Agarose	Bioline
Ammonium molibdate	M&B
APS (ammonium persulfate; $(NH_4)_2S_2O_8$)	Sigma-Aldrich
APTES (3-aminopropyltriethoxysilane)	Sigma-Aldrich
Ascorbic acid	Szkarabeusz
ATP (adenosine 5′-triphosphate disodium salt hydrate)	Sigma
Bis acrylamide (N,N′-methylenebis(acrylamide), $C_7H_{10}N_2O_2$)	Sigma
BIS-TRIS propane ($CH_2[CH_2NHC(CH_2OH)_3]_2$)	Sigma
Boric acid	BDH
Brij^{TM}58	Sigma
Bromocresol purple	DIFCO
Bromophenol blue ($C_{19}H_{10}Br_4O_5S$)	Reanal
BSA (bovine serum albumin fraction V)	Sigma-Aldrich
$Ca(NO_3)_2x4H_2O$	Reanal, BDH
$CaCl_2$	Reanal, BDH
$CaSO_4$	BDH
Cellulase	Worthington
Coomassie brilliant blue R-250 ($C_{45}H_{44}N_3NaO_7S_2$)	Reanal
CsCl	Gibco BLR
$CuSO_4x5H_2O$	BDH
Dextran T-500	Sigma-Aldrich
Driselase	Sigma
DTT (dithiothreitol, $C_4H_{10}O_2S_2$)	Sigma, Fluka
EDTA	Reanal, BDH
Entellan®	Merck
Ethanol	Merck
Ethidium bromide	Sigma
Fe^{III}NaEDTA	BDH
Formalin	BDH

Fusicoccin	Sigma
Glycerol	Reanal, Fluka
Glycine	Reanal
H_2SO_4	Molar
H_3BO_3	BDH
HCl	BDH
HEPES ($C_8H_{18}N_2O_4S$)	Sigma
Hydrogen Ionophore II Cocktail A	Fluka
K_2HPO_4	Reanal, BDH
KCl	Reanal, BDH
KH_2PO_4	Reanal, BDH
KNO_3	Reanal, BDH
KOH	Reanal, BDH
MES (2-[N-morpholino]ethanesulfonic acid, $C_6H_{13}NO_4S$)	Sigma
Methanol	Reanal, BDH
$MgSO_4x7H_2O$	Reanal, BDH
$MnSO_4xH_2O$	BDH
MOPS (3-[N-morpholino]propanesulfonic acid, $C_7H_{15}NO_4S$)	Sigma
$Na_2HPO_4x2H_2O$	BDH
$Na_2MoO_4x2H_2O$	BDH
Na_3VO_4	Sigma
NAA (1-naphthaleneacetic acid, $C_{12}H_{10}O_2$)	Sigma
Na-ascorbate	Fluka
NaCl	BDH
$NaH_2PO_4x2H_2O$	BDH
NaN_3	Sigma
NaOH	BDH
Neo-clear®	Merck
$NH_4H_2PO_4$	M&B
Nitrocellulose	Sigma
Non soluble PVP (polyvinylpyrrolidone)	Serva
Paraffin wax	BDH
Pectolyase	Sigma
PEG-3350	Sigma
Phtalate buffer	Sigma

PMSF (phenylmethylsulfonyl fluoride, $C_7H_7FO_2S$)	Sigma
Potassium antimony (III) oxid tartrate	BDH
Potassium hydrogen phthalate ($KHC_8H_4O_4$)	Sigma-Aldrich
PVC (high molecular weight polyvinyl chloride)	Fluka
PVP K30 (polyvinylpyrrolidone)	Sigma
SDS (Sodium dodecyl sulfate, $CH_3(CH_2)_{11}OSO_3Na$)	Sigma
Sorbitol	Sigma
Sucrose ($C_{12}H_{22}O_{11}$)	Reanal, Sigma
TAPS (N-tris[Hydroxymethyl]methyl-3-amino-propanesulfonic acis)	Sigma
TEMED (*N*,*N*,*N*′,*N*′-tetramethylethylenediamine, $C_6H_{16}N_2$)	Fluka
THF (tetrahydrofuran, C_4H_8O)	Sigma-Aldrich
Toluidine blue	Sigma
TRIS (tris(hydroxymethyl)aminomethane, $NH_2C(CH_2OH)_3$)	Reanal, IBI
Triton®X-100	Reanal, Sigma
Tween®20	Sigma
$ZnCl_2$	BDH
β-mercapto ethanol ($HSCH_2CH_2OH$)	Sigma
α-Naphthaleneacetic acid (NAA)	Sigma

Apoplast acidification in growing barley (*Hordeum vulgare* L.) leaves

Tamás Visnovitz (‘Okleveles Biológus’; MSc)

The thesis is submitted to University College Dublin in fulfilment of the requirements for the degree of Doctor of Philosophy

School of Biology and Environmental Science

Head of School: Prof. Thomas Bolger

Principal Supervisor: Dr Wieland Fricke

Members of the Doctoral Studies Panel: Dr Paul McCabe & Prof. Bruce Osborne

August 2011

Contents

Contents ii

List of figures v

List of tables viii

Abstract x

Statement of Original Authorship xi

Collaborations xii

Acknowledgements xiii

1 General Introduction - 1 -

1.1 Plant growth - 1 -

1.1.1 Plant cell expansion - 1 -

1.1.1.1 Cell wall - 1 -

1.1.1.2 Solutes - 3 -

1.1.1.3 Water - 4 -

1.1.2 pH conditions in the apoplast - 4 -

1.1.3 'Acid growth' theory - 5 -

1.1.3.1 'Acid growth' and effect of auxin and fusiccoccin on growth - 5 -

1.1.3.2 Experimental systems using coleoptiles - 6 -

1.1.3.3 Acid growth of coleoptiles - 6 -

1.1.3.4 Acid growth of dicotyledonous leaves - 8 -

1.1.3.5 Acid growth of roots - 9 -

1.1.4 Potassium uptake and 'acid growth' - 10 -

1.2 Plasma membrane H^+-ATPase - 11 -

1.2.1 Isoforms of PM-H^+-ATPase - 12 -

1.2.2 Structure of PM-H^+-ATPase - 14 -

1.2.3 Catalytic cycle of P-type ATPase and H^+ transport mechanism - 15 -

1.2.4 Control of PM-H^+-ATPase - 15 -

1.2.5 Fusicoccin-dependent PM-H^+-ATPase activation - 17 -

1.3 Barley - 18 -

1.3.1 The two weeks old barley seedlings and their advantage - 18 -

1.3.1.1 Morphology of developing barley leaves - 19 -

1.3.1.2 Anatomy of developing barley leaf - 20 -

1.3.2 Growth and potassium uptake of barley - 21 -

1.4 Technical approaches - 22 -

1.5 Objectives of the present study - 23 -

2 Materials and Methods - 24 -

2.1 Plant material - 24 -

2.1.1 Plant growth for study of leaves - 24 -

2.1.2 Plant growth for study of coleoptiles - 25 -

2.2 Apoplast pH measurements - 25 -

2.2.1 In-vitro gel system - 26 -

2.2.2 Microelectrode measurements - 27 -

2.3 Confocal microscopy - 29 -

2.3 LVDT measurements - 30 -

2.3.1 Leaf growth measurements - 30 -

2.3.2 Analysis of cell wall properties - 31 -

2.4 Expression analyses - 32 -
2.4.1 Plant harvest - 32 -
2.4.2 RNA extraction and cDNA synthesis - 33 -
2.4.3 PCR - 34 -
2.4.4 qPCR - 36 -
2.4.5 Analysis of qPCR data - 37 -

2.5 Cell size and tissue ratio measurements - 38 -
2.5.1 Mesophyll and epidermis cell size - 38 -
2.5.2 Tissue ratio calculation in elongation zone and emerged blade - 38 -
2.5.3 Cell size and plasma membrane surface estimation for qPCR analysis - 38 -

2.6 Plasma membrane isolation - 39 -
2.6.1 Plant harvest - 39 -
2.6.2 Preparation of microsomal fraction - 39 -
2.6.3 Purification of plasma membrane vesicles - 40 -

2.7 Determination of the total protein content of plasma membrane vesicles - 41 -
2.7.1 Bradford method - 41 -
2.7.2 Densitometric analysis of Laemmli gels - 41 -

2.8 Polyacrylamide gel electrophoresis (PAGE) - 42 -
2.8.1 Gradient polyacrylamide gel electrophoresis (PAGE) - 42 -
2.8.1.1 Solubilisation of membrane protein - 42 -
2.8.1.2 Gradient PAGE gel system - 43 -
2.8.2 Linear (12 %) PAGE - 45 -

2.9 ATPase assay - 45 -

2.10 Approach for light microscopy - 46 -
2.10.1 Fixation of leaf tissue - 46 -
2.10.2 Dehydration and embedding - 46 -
2.10.3 Staining with toluidine blue - 47 -

2.11 Immunological methods for PM-H$^+$-ATPase detection - 48 -
2.11.1 Qualitative Western blot analysis - 48 -
2.11.2 Quantitative Western blot analysis - 49 -
2.11.3 Immunostaining of paraffin-embedded sections - 50 -

2.11.4 Densitometric analysis of Western blots - 51 -

2.12 Protoplast experiments - 51 -
2.12.1 Protoplast isolation - 51 -
2.12.2 Purification of protoplasts - 52 -
2.12.3 Calculation of size and surface of the protoplast - 52 -

2.13 Statistical analysis - 52 -

3 Results - 53 -

3.1 Apoplastic pH measurements - 53 -
3.1.1 In-vitro agarose gel system - 53 -
3.1.2 Microelectrode measurements - 57 -
3.1.1 Confocal microscopy - 60 -

3.2 LVDT analyses of growth responses to treatments - 65 -
3.2.1 Leaf elongation under different treatments - 65 -
3.2.2 Cell wall changes in response to treatments - 69 -

3.3 Expression analysis of PM-H$^+$-ATPase using qPCR - 70 -
3.3.1 Quality control of the standard required for absolute qPCR - 71 -
3.3.2 Calculation of cell number and membrane surface - 72 -
3.3.3 Gene expression data based on absolute qPCR method - 74 -

3.4 PM-H$^+$-ATPase activity and expression at protein level - 77 -
3.4.1 Optimization of membrane isolation and ATPase assay - 78 -
3.4.1.1 Plasma membrane isolation - 78 -
3.4.1.2 Determination of total protein content in plasma membrane vesicles - 79 -

3.4.1.3 ATPase assay - 79 -
3.4.2 Quality of plasma membrane fractions - 81 -
3.4.3 Quantitative analysis of PM-H^+-ATPase protein - 82 -
3.4.4 Activity of PM-H^+-ATPase - 83 -
3.4.5 Immunolocalisation of PM-H^+-ATPase - 83 -

4 Discussion - 85 -

4.1 Growth-associated apoplast acidification - 85 -
4.1.1 Apoplast pH difference between growing and non-growing leaf tissue - 85 -
4.1.2 Reliability of pH values measured in elongation zone and emerged blade - 85 -
4.1.3 Relation between apoplast acidification and leaf growth - 86 -

4.2 K^+ and apoplast acidification - 87 -
4.2.1 Potassium uptake and leaf growth - 87 -
4.2.2 High affinity potassium transporters and leaf growth - 88 -

4.3 PM-H^+-ATPase expression and leaf elongation - 89 -
4.3.1 PM-H^+-ATPase density in plasma membrane and leaf growth - 90 -
4.3.2 qPCR data - 91 -
4.3.4 Immunolocalisation of PM-H^+-ATPase - 92 -

4.4 Leaf growth and changes in cell wall properties - 92 -

4.5 'Acid growth' in barley leaves? - 93 -

4.6 Model of leaf growth in barley - 93 -

5 Conclusions and future work - 97 -

5.1 Conclusions - 97 -

5.2 Future works - 98 -

6 Literature - 99 -

7 Appendix - 109 -

7.1 Processing of qPCR data - 109 -

7.2 List of chemicals - 115 -

List of figures

Figure 1.1 Model how expansins might interact with other wall components ..... - 3 -
Figure 1.2 Fusicoccin and auxin effect on maize coleoptiles..... - 7 -
Figure 1.3 Root elongation growth rate (REGR) and apoplast pH changes ..... - 9 -
Figure 1.4 Trajectory of a root element ..... - 10 -
Figure 1.5 Potassium transport dependency of abraded maize coleoptiles ..... - 11 -
Figure 1.6 Structure of AHA2 without auto-inhibitory domain..... - 14 -
Figure 1.7 Catalytic cycle and H^+ transport of PM-H^+-ATPase..... - 15 -
Figure 1.8 Auto-inhibition of PM-H^+-ATPase ..... - 17 -
Figure 1.9 14-3-3 protein-fusicoccin-PM-H^+-ATPase complex ..... - 18 -
Figure 1.10 Two-week old barley seedling ..... - 20 -
Figure 1.11 Toluidine blue stained cross section of barley leaves from different developmental stage ..... - 21 -
Figure 2.1 Leaf pieces in pH sensitive agarose gel medium ..... - 27 -
Figure 2.2 Measurement of cell wall properties..... - 32 -
Figure 2.3 Thermal profile of the two step PCR reactions..... - 35 -
Figure 2.4 Thermal profile of qPCR reactions ..... - 36 -
Figure 2.5 Five purification steps during plasma membrane isolation. ..... - 41 -
Figure 2.6 Typical gel for the measurement of protein content of plasma membrane samples..... - 42 -
Figure 2.7 Coomassie Brilliant Blue R250 stained gradient PAGE gels which were loaded with plasma membrane protein solubilised in two different ways ..... - 43 -
Figure 3.1 Leaf growth and apoplast acidification as analysed through the agarose gel system ..... - 54 -
Figure 3.2 Time course of growth and acidification of in-vitro gel experiments .... - 55 -
Figure 3.3 Leaf growth and acidification in agarose gel under cold treatment..... - 55 -
Figure 3.4 Average rate of leaf elongation (A) and medium acidification (B) in leaves exposed to fusicoccin, vanadate and caesium treatments as tested through the agarose gel system ..... - 56 -
Figure 3.5 Effect of auxin on leaf growth and medium acidification using the in-vitro gel system ..... - 57 -
Figure 3.6 Growth effect of auxin when applied in liquid medium..... - 57 -
Figure 3.7 Microelectrode analyses of apoplast pH in the elongation zone and emerged blade-portion of leaf three of barley..... - 58 -

Figure 3.8 Growth rate of leaf three in response to K^+-treatments during micro pH measurements. ..... - 59 -
Figure 3.9 Microelectrode pH analyses in the leaf elongation zone of barley in response to sodium orthovanadate and fusicoccin treatments..... - 60 -
Figure 3.10 Growth rate of leaf three of barley in response to vanadate and fusicoccin treatments as analysed through different approaches..... - 60 -
Figure 3.11 Confocal microscopic analysis of apoplastic pH using acridine orange fluoresce pH sensitive fluorescence dye ..... - 62 -
Figure 3.12 Confocal microscopic analysis of apoplastic pH using 5(6)carboxyfluorescein fluoresce pH sensitive fluorescence dye..... - 63 -
Figure 3.13 Carboxyfluorescein and acridine orange accumulation pattern in elongation zone and emerged blade ..... - 64 -
Figure 3.14 Effect of pH sensitive dyes on leaf growth rate ..... - 64 -
Figure 3.15 pH sensitivity of fluorochromes ..... - 65 -
Figure 3.16 Testing the responsiveness of the LVDT setup to treatments which were expected to increase (37 ℃) or stop growth (1 M Na Cl)..... - 66 -
Figure 3.17 The effect of test reagents in the apoplastic bathing medium on leaf growth as measured with the LVDT setup..... - 67 -
Figure 3.18 Potassium dependency of the leaf growth response to fusicoccin (5 µM) and vanadate (500 µM) ..... - 68 -
Figure 3.19 Auxin effect on leaf elongation growth..... - 68 -
Figure 3.20 Cell wall changes under different treatments ..... - 69 -
Figure 3.21 Growth rate before and in response to an additional applied force ... - 70 -
Figure 3.22 reference genes for qPCR experiments ..... - 71 -
Figure 3.23 Digital PCR pattern of external standard DNA ..... - 72 -
Figure 3.24 Representative cross sections used for determination of the contribution of different tissues and air space to total leaf volume..... - 73 -
Figure 3.25 Expression of PM-H^+-ATPase using absolute qPCR..... - 75 -
Figure 3.26 PM-H^+-ATPase expression using absolute qPCR and relating expression data to total plasma membrane surface area..... - 76 -
Figure 3.27 Comparison of molecular biological data using leaf tissues or mesophyll protoplasts..... - 77 -
Figure 3.28 Impact on the quality of PAGE separation of washing steps during plasma membrane isolation ..... - 78 -

Figure 3.29 Protein measurement in plasma membrane vesicles using two different methods ..... - 79 -
Figure 3.30 Typical ATPase assay ..... - 80 -
Figure 3.31 Kinetics of P_i detection assay ..... - 80 -
Figure 3.32 Coomassie stained SDS polyacrylamide gel and Western blot of plasma membrane proteins from different leaf regions ..... - 81 -
Figure 3.33 PM-H^+-ATPase ratio in total membrane protein ..... - 82 -
Figure 3.34 ATPase activity of inside-out plasma membrane vesicles ..... - 83 -
Figure 3.35 PM-H^+-ATPase immunolocalisation on leaf cross and longitudinal sections ..... - 84 -
Figure 4.1 Supposed effect of the treatments on barley leaf cells ..... - 95 -
Figure 4.2 Model of leaf elongation in barley leaves ..... - 96 -
Figure 7.1 Typical calibration curve for converting Ct values into transcript copy number ..... - 110 -

List of tables

Table 1.1 Localisation of specific PM-H^+-ATPase isoforms in plant body - 13 -

Table 2.1 Composition of the ½ strength Hoagland solution for barley seedlings - 25 -

Table 2.2 Composition of the pH sensor for microelectrodes - 28 -

Table 2.3 Composition of the buffer solutions used for calibrating pH microelectrodes - 29 -

Table 2.4 DNase treatment and reverse transcription - 34 -

Table 2.5 Components of PCR reactions - 35 -

Table 2.6 PCR primers - 35 -

Table 2.7 Composition of the stock solution (5x concentrated) of TRIS base boric acid EDTA buffer (TBA) - 35 -

Table 2.8 Components of qPCR reaction - 36 -

Table 2.9 Composition of the homogenisation buffer used for membrane isolation - 39 -

Table 2.10 Composition of the phase buffer used for membrane isolation - 40 -

Table 2.11 Composition of the resuspension buffer used for membrane isolation - 40 -

Table 2.12 Composition of Bradford reagent - 41 -

Table 2.13 Composition of Laemmli buffer used for PAGE - 43 -

Table 2.14 Components of the gradient PAGE system - 44 -

Table 2.15 Components of the solutions for Coomassie Brilliant Blue gel staining - 44 -

Table 2.16 ATPase reaction buffer and colour development reagent - 46 -

Table 2.17 Fixation and embedding of leaf samples for immunohistochemistry - 47 -

Table 2.18 Staining embedded leaf sections with toluidine blue - 47 -

Table 2.19 Composition of blotting buffer used for Western analyses - 48 -

Table 2.20 Composition of TRIS buffer saline buffer (TBS) - 49 -

Table 2.21 Composition of Tween®20 TRIS buffer saline buffer (TTBS) - 49 -

Table 2.22 Protocol for immunostaining of embedded leaf sections - 50 -

Table 2.23 Composition of phosphate buffer saline (PBS; pH 7.4) - 50 -

Table 2.24 Composition of protoplast isolation buffer - 51 -

Table 2.25 Enzyme concentrations in protoplast isolation buffer - 51 -

Table 3.1 Water content of two different regions of leaf three in two cultivars of barley - 72 -

Table 3.2 The contribution of different tissues to total leaf volume in the elongation zone (EZ) and emerged blade (EB) of leaf three of barley. - 73 -

Table 3.3 Cell size calculation based on the present and literature data. - 74 -

Table 3.4 Ct values of PM-H^+-ATPase expression together with RNA content per cell in the elongation zone (EZ) and emerged blade (EB) of leaf three of barley. - 75 -

Table 3.5 RNA content and PM-H^+-ATPase expression in the elongation zone (EZ) and emerged blade (EB) of leaf three of barley (Golf, Jersey). - 76 -

Table 4.1 Summary of data for PM-H^+-ATPase when related to surface area of plasma membrane. - 89 -

Table 7.1 Example for qPCR calculation of Golf cultivar. -112-

Table 7.2 Example for qPCR calculation of Jersey cultivar. -113-

Table 7.3 Example for qPCR calculation of Jersey protoplasts. -114-

Abstract

Apoplast acidification associated with growth is well-documented in roots, coleoptiles and internodes but not in leaves. In the present project on barley (*Hordeum vulgare* L.) advantage was taken of the high cuticle permeability in the elongation zone of leaves to measure apoplast pH and growth in response to application of test reagents. The role of the plasma membrane H^+-ATPase (PM-H^+-ATPase) and K^+ in this process was of particular interest. An in vitro gel system with bromocresol purple as pH indicator, pH microelectrodes and pH-sensitive fluorescence dye combined with confocal microscopy were used to monitor apoplast pH. Growth was measured in parallel or in separate experiments using a linear variable differential transformer (LVDT). Test reagents which blocked (vanadate) or stimulated (fusicoccin) PM-H^+-ATPase, or which reduced (NH_4^+, Cs^+, tetraethylammonium) K^+ uptake were applied. Plasma membranes were isolated from growing and mature leaf tissue and used to determine the activity (ATPase assay) and abundance (Western blotting) of PM-H^+-ATPase protein. Protein localisation was studied by immunohistochemistry and expression of mRNA quantified using real time PCR (qPCR). Apoplast pH was by up to 1.0 pH unit lower in growing compared to non-growing leaf tissue. Depending on the K^+ concentration in the bathing medium used during electrophysiological analyses, apoplast pH in the elongation zone ranged from pH 4.8 (0.1 mM K^+) to pH 5.8 (10 mM K^+). In the emerged blade, apoplast pH remained at about pH 5.8 irrespective of the K^+ concentration in the bathing medium Growth was more responsive to test reagents than to changes in apoplast pH. Expression of PM-H^+-ATPase was comparable between growing and non-growing leaf regions when expression was related to per unit extracted RNA or cell number. However, when expression was related to per unit surface area of plasma membrane, expression of PM-H^+-ATPase was about twice as high in growing compared to non-growing leaf tissue. The same applied to the protein level and activity of PM-H^+-ATPase. Immunohistochemical analyses showed that PM-H^+-ATPase was present in all living leaf tissues, particular in those (guard cells, phloem, and xylem parenchyma) associated with high rates of trans-membrane solute transport. It is concluded that leaf cell expansion in barley depends on the activity of the PM-H^+-ATPase and K^+ transport processes. The higher surface density of PM-H^+-ATPase activity in growing barley leaf tissue aids apoplast acidification and growth. A H^+ / K^+ co-transport system may play a key role in linking growth with apoplast pH, H^+ pump activity and K^+-uptake.

Statement of Original Authorship

I hereby certify that the submitted work is my own work, was completed while registered as candidate for the degree of Doctor of Philosophy, and I have not obtained a degree elsewhere on the basis of the research presented in this submitted work.

…….

Tamás Visnovitz

Collaborations

(i) pH measurements using pH microelectrodes were carried out under the supervision of Dr Anthony J. Miller at the Department of Plant Pathology and Microbiology of Rothamsted Research (Harpenden, Hertfordshire AL5 2JQ, UK). Towards the end of this project, Dr Miller moved to the John Innes Centre (Norwich Research Park, Colney, Norwich, NR4 7UH, UK), which is similar to Rothamsted Research a BBSRC (Biotechnology and Biological Sciences Research Council) funded institute.

(ii) Plasma membrane isolation, SDS PAGE, ATPase hydrolysis assays and part of the Western blot analysis was carried out in the laboratory of Dr Éva Sárvári and Dr Ilona Rácz with the help of Ádám Solti at the Department of Plant Physiology and Molecular Plant Biology, Institute of Biology, Faculty of Science, Eötvös Loránd University (Pázmány Péter sétány 1/C, Budapest, Hungary, H1117).

Acknowledgements

- First of all I want to thank my supervisor **Dr Wieland Fricke** for his expert guidance and advice in all aspect during the three years. He not just guided my steps in science, he gave the opportunity to plan my research workflow, experiments and test my own ideas.
- I would like to thank the help to everybody who worked with me in our research group **Matthieu Besse**, **Thorsten Knipfer**, **Mostefa Touati**, **Ehsan Bijanzadeh** and **Shimi Suku** who helped me a lot and we could spend great time in the lab together.
- Many thanks for the technical assistance and help to **Brendan**, **Eugen**, **Francis**, **Gwyneth**, **Eileen** (UCD), **Sue** (Rothamsted), **Györgyi** and **Zsuzsa** (ELTE). **Damian Egan** and **Eric Callaghan** helped me especially a lot, and special thanks to Eric for his critical reading of the thesis.
- I would like to thank **Prof. Jeremy C. Simpson** for access to the confocal microscopy unit and **Dr Gavin Stewart** and **Caragh Walpole** for their help with Western blotting at UCD.
- I never will forget the days in Rothamsted, thanks a million for **Dr Tony Miller** for his help in all aspect and I hope I will have the chance to work together in the future.
- At Eötvös University I had extremely big help from **Dr Éva Sárvári**, **Dr Ilona Rácz**, **Dr Szabolcs Rudnóy** and from **Prof. Zoltán Szigeti**. Without the guides of **Ádám Solti** the protein part of the work would not have been successful. **Dr György Csikós** helped a lot in immune histochemistry.
- Enormous thanks for my wife **Kriszti**. Without her help I would not able to finish this research and thesis. She was always with me when I was despondent and felt that I never will finish.
- Thank to all of my friends at UCD, Rothamsted and ELTE whose are not mentioned by name.
- Particular thanks to **IRCSET** (Irish Research Council for Science, Engineering and Technology) which made this PhD project possible through awarding me an EMBARK post-graduate fellowship.
- …és végül de nem utolsó sorban köszönöm a támogatást szüleimnek akik támogattak mindenben és elviselték, hogy Írországban éltem és doktoráltam.

1 General Introduction

1.1 Plant growth

Plant growth can be defined as an irreversible increase in the size of cells, tissues, organs or whole plants (Csiszár *et al.*, 2004). Cell expansion is generally considered to be caused by wall loosening and driven by turgor pressure (Christian et al., 2006). The term 'cell growth' mainly refers to the increase in size of proliferating cells in the cell cycle (meristematic cells), with increase in the total nucleic acid and protein content without vacuolization of the protoplast. In contrast, the term 'cell expansion' refers to the manifold increase in size of newly produced cells that is associated with the formation of a large central vacuole and finally leads to cell differentiation (Perrot-Rechenmann, 2010). While plants need to produce new cells to grow, it is cell expansion which leads to the physical increase in plant size and biomass.

1.1.1 Plant cell expansion

The enlargement of cells reflects increase in water content of cells. Irreversibility of this process is guaranteed by the plastic properties of the cell wall. From the biophysical view, plant cells need a wall which gives in to turgor pressure (mechanical driving force) and solutes which drive water uptake through osmosis. Therefore, cell expansion may be limited by the mechanical (yielding and extensibility) properties of the cell wall and the rate at which water and solutes are taken up or produced (solutes) by cells internally (Fricke & Flowers, 1998; Fricke & Peters, 2002).

1.1.1.1 Cell wall

It is a popular theory that expansion of leaf and root cells is controlled by cell wall properties. Based on the work of Green *et al*. (1971) on giant algae cells (*Nitella* sp.) and Lockhart's (1965) theoretical considerations, a growth model was developed which relates the growth rate (GR) to extensibility properties (m), yield threshold of cell wall where no cell expansion occurs (Y) and cell turgor (P):

$$GR = m \cdot (P-Y)$$

The impact of the mechanical properties of the cell wall for plant growth was found in many studies both in roots and shoots (Cosgrove, 1993; Pritchard, 1994; Cosgrove,

1998; Hsiao & Xu, 2000). The implication of these studies is that the rate of cell expansion, and therefore plant growth, may be regulated by altering the mechanical properties of the wall, making it 'softer' (more growth) or 'harder' (less growth). One way to alter wall properties is through changes in wall (apoplast) pH.

Acidification can affect growth through cell wall loosening (Rayle & Cleland, 1970) and different theories have been proposed to explain this phenomenon. One hypothesis suggested that H^+ directly affects non-covalent bonds between β-glucan within the cell wall, causing wall loosening (Hohl *et al.*, 1991). Another hypothesis suggested that due to H^+ excretion Ca^{2+} ions are displaced in the cell wall and that this leads to a more flexible cell wall (Arif & Newman, 1993). A breakthrough in our understanding of pH-related wall loosening came in 1992 when two proteins were extracted from cucumber hypocotyls which were capable of inducing extension in isolated, heat-inactivated cell walls of several plant species. These 'wall loosening' proteins were termed 'expansins'. The pH optimum of these proteins was pH3.5 - 4.5 (McQueen-Mason *et al.*, 1992) and this may explain at least in part why apoplast acidification increases the growth rate of plant organs.

Expansins are specifically expressed in growing tissues of monocotyledons and dicotyledonous plants. They are highly conserved in size and amino acid sequence (Cosgrove, 1996). However, studies on fescue suggest that another group of wall proteins, xyloglucan endotransglycosylases, may be more involved in regulation of cell expansion than expansins (Reidy *et al.*, 2001).

Expansins do not induce wall extension through simple polymer hydrolysis. They mainly disrupt hydrogen bonding not just in-vivo, in a paper sheet as well and reengineering the cell wall structure facilitating plant growth (McQueen-Mason, 1995). Promoting cell wall relaxation is necessary for expansion of plant cells (Cosgrove, 1993). An overview of expansin action is given in Fig. 1.1.

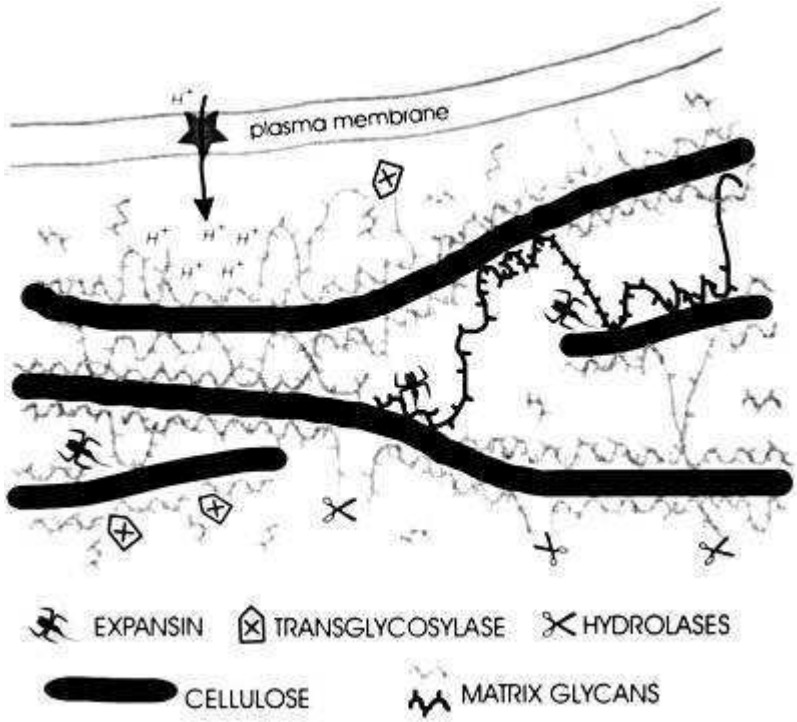

Figure 1.1 Model how expansins might interact with other wall components

Expansins might cause a transient release of short segments of matrix hemicelluloses glycans attached to cellulose microfibrils. Wall hydrolyses cut matrix glucans into shorter segments leading to weakening but not to creep of the cell wall. Transglycosylases are recombining glycans into shorter or longer pieces. PM-H^+-ATPases may lower the wall pH and control enzymes by their pH optima. Reprint from Cosgrove (1998) based on open access policy of www.plantphysiology.org with copyright American Society of Plant Biologists.

1.1.1.2 Solutes

Based on the original growth model described above (Lockhart, 1965; Green *et al.*, 1971), turgor pressure and solute uptake should have significant impact on cell expansion and growth. The availability of solutes seems to co-limit growth especially under water (Frensch, 1997; Hsiao *et al.*, 1998) and salt stress (Fricke & Peters, 2002).

Osmolality and turgor pressure change little along the elongation zone of cereal leaves (Fricke *et al.*, 1997; Fricke & Flowers, 1998; Martre *et al.*, 1999; Fricke, 2002a) and roots (Pritchard, 1994). The implication of a constant turgor pressure in expanding cells might be that cells instantly deposit solutes to maintain osmolality as the osmotic force driving water uptake while they expand and cell contents become diluted (Fricke, 2002a).

1.1.1.3 Water

In barley, it has been suggested that the rate of tissue-water transport might limit cell expansion in leaves (Fricke, 2002b). Similar conclusions have been made for soybean hypocotyls and maize leaves by the work of Boyer and colleagues who coined the term ‘growth-induced water potentials’ (Boyer, 2001; Tang & Boyer 2008). The mere existance of significant gradients in water potential between growing tissue and water source suggests that the conductance of the pathway between the two is limiting water transport. In a multi-layered tissue e.g. in roots, the radial hydraulic conductance can be one to three orders of magnitude larger under transpirating than under non-transpirating conditions (Steudle, 2000). Recent studies showed that in barley roots water uptake occurred along a pathway which involved crossing of membranes. It was not clear whether osmotic forces were sufficient to support water uptake (Knipfer & Fricke, 2011). Aquaporins have an essential role in the water transport at cellular level (Hachez *et al.* 2008). Aquaporins also may play essential role in elongation growth of barley leaves (Besse *at al.*, 2011).

1.1.2 pH conditions in the apoplast

The present analyses did not, or did little distinguish between cell wall space and apoplast. The latter also comprises intercellular spaces and middle lamellae. Therefore, and for simplicity, it is referred to ‘apoplast’ throughout the present work. The apoplast of higher plants occupies typically 5 % or less of the total tissue volume. This applies in particular to living tissues. The apoplast determines ionic conditions around the cells; it affects transport solutes into and out of cells, provides a diffusion barrier in speciliased cases (e.g. Casparian bands) and defines mechanical and osmotic conditions – conditions which may be or may not be compatible with cell expansion. The latter applies in particular to the pH of the apoplast. Using different methods (pH indicators in agar, microelectrodes and fluorescence probes) a huge variety in apoplast pH has been reported for roots of different plant species. Values ranged from pH 4.0 to pH 7.0 with most values being in the region pH 5.0 to pH 6.5 (Grignon & Sentenac, 1991). Dicotyledonous plants have generally a higher (less acidic) pH than monocotyledonous plants have, and apoplast pH is lower in gymno- compared to angiosperms (Grignon & Sentenac, 1991).

In fully developed barley leaves an apoplast pH of pH 5.0 was measured using microelectrodes (Felle, 2006). The pH varied in dependence of oxygen availability

(anoxia) (Felle, 2005; Felle *et al.*, 2005; Felle, 2006). Similar pH values have been reported for maize leaves using microelectrodes and fluorescence probes (Pitann *et al.*, 2009a; Ehlert *et al.*, 2011).

1.1.3 'Acid growth' theory

'Acid growth' originally was discovered by Bonner in 1934 when he described that the growth rate of *Avena* coleoptiles in pH 4.1 buffer was significantly higher than in pH 7.2 buffer (Kutschera, 1994). Later this effect was re-discovered and characterised in more detail by Rayle & Cleland (1970) and Hager *et al.*, (1971). Although in the literature 'acid growth' is mainly mentioned in relation to growth effects caused by the phytohormone auxin and the fungal toxin fusicoccin, which permanently activates PM-H^+-ATPase, linked plant growth, acid growth is a more general phenomenon and can be induced by other factors (Vesper & Evans, 1979). In 'acid growth', acid related cell 'wall-loosening' may constitute the initial event (Rayle & Cleland, 1970; Cosgrove, 1993). During the past decades, the 'acid growth' theory, or parts of the underlying mechanistic model, has been questioned repeatedly (Kutschera & Schopfer, 1985a; Kutschera, 1994; Grebe, 2005), However, with some limitation it is 'alive and well' (Lüthen *et al.*, 1990; Hager *et al.*, 1991; Rayle & Cleland, 1992; Kutschera, 2006). An alternative theory for 'acid growth' is the 'facilitated solute uptake' theory. This theory states that it is not the secreted H^+ which are causing directly the increased growth rate through alteration of wall properties, but that a proton-coupled transport mechanism across the plasma membrane is stimulated (Brummer *et al.*, 1984).

1.1.3.1 'Acid growth' and effect of auxin and fusiccoccin on growth

Almost at the same time, Darwin and Sachs proposed the theory that growth and development of plants is controlled by hormones (Darwin, 1880; Kutschera 1994). Using *Avena sativa* coleoptiles, Darwin, in 1880, showed that coleoptiles were bending towards the light source and once the tip of the coleoptiles was covered or cut, the coleoptiles were unable to produce this bending effect. In 1909, Fitting showed that coleoptile bending was a result of the non-homogeneous distribution of some factor, possibly a hormone (Katsumi, 2007). With gelatine cubes and glass pieces Boysen-Jensen (1913) proofed that this factor was transported from the tip to basal end of the coleoptile (Csiszár *et al.*, 2004). Paál (1918) could induce coleoptile bending without light, changing the orientation of coleotile tips (Paál, 1918; Csiszár *et*

al., 2004). Finally, in 1937, Went discovered the hormone (auxin) and showed that if the hormone was in gelatine cubes the tip was not necessary for coleoptile bending (Kutschera 1994). Heyn in 1940 proposed that auxin (in its physiological form indol acetic acid - IAA) promotes growth by enhancing cell wall extensibility. In 1934 and 1970 the 'acid growth' theory was born to explain auxin related plant growth (Kutschera, 1994). Fusicoccin, a phytotoxin of the fungus *Fusicoccum amygdale*, was discovered as 'super-auxin' a few years latter (Marré, 1979) and is still used today in many plant growth studies.

1.1.3.2 Experimental systems using coleoptiles

Coleoptiles of monocotyledon plants have widely been used as a model system to study plant growth. Coleptiles can be obtained on plants which need to grow for only a few days, are well characterised in terms of their phototropic or gravitropic response, show defined regions of growth and auxin production, are simple in anatomy and are easy to handle and cut. The main disadvantage, however, of coleoptiles is that their cuticle provides a permeance barrier to applied test reagents and diffusion barrier for protons and that this causes difficulties for applying treatments and measuring apoplastic pH (changes). In different laboratories this problem has been solved in different ways by peeling off part of the outer epidermis (Rayle, 1973), abrasion of coleoptiles with wet emery cloth prior to cutting (Kutschera & Schopfer, 1985a), abrasion with distilled water and SiC powder (Lüthen et al., 1990) or using dry polishing cloth for abrasion of coleoptiles before excision of segments (Schopfer, 1989). None of these methods were free from artefacts; however the results have been informative.

In most experiments, the incubation medium in which pH measurements were conducted was slightly buffered to prevent pH changes as a result of changes in CO_2 content of the atmosphere e.g. Rayle (1973); Stahlberg & Van Volkenburgh (1999) and Felle (2006). At the same time, the buffer capacity of the medium may affect pH measurements. Probably the best system for pH measurement was the method of ionostat (Döring *et al.*, 1996), because the incubation medium was not buffered and changes in H^+ efflux were measured rather than pH.

1.1.3.3 Acid growth of coleoptiles

Using maize coleoptiles, which were SiC-abraded in water and analysed using a computer controlled pH stat, both auxin and fusicoccin treatments affected growth in

a way which supported the ‘acid growth’ theory (Fig. 1.2). Neutral and alkaline solutions partly inhibited auxin- and fusicoccin-induced growth, whereas fusicoccin-induced growth under constant pH conditions. Fusicoccin and auxin did not show any additive effect (Lüthen *et al.*, 1990). Cell wall pH and growth rate were in close temporal correlation indicating co-regulation of apoplast solute composition (Peters *et al.*, 1998).

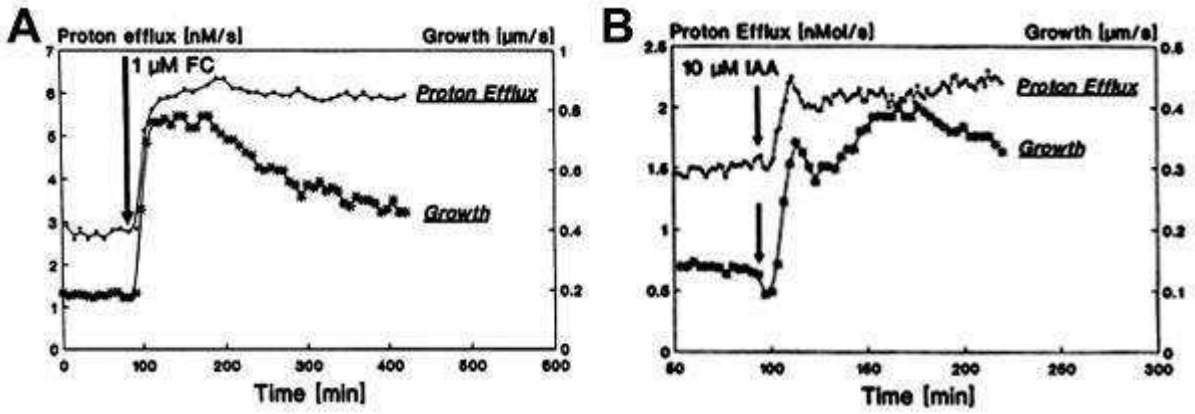

Figure 1.2 Fusicoccin and auxin effect on maize coleoptiles

Typical trace of fusicoccin (A) and auxin (IAA) effect (B). Dots represent the proton secretion while asterisks the coleoptiles growth rate. Experiments were carried out using SiC abraded maize coleoptile segments and a pH stat to maintain pH. Reprint from Lüthen *et al*. (1990) based on open access policy of www.plantphysiology.org with copyright American Society of Plant Biologists.

Other studies suggested that fusicoccin, but not auxin, caused ‘acid growth’. Using the wet emery cloth abrading technique and buffered incubation medium, fusicoccin-induced growth was totally inhibited by alkaline solutions (Kutschera & Schopfer, 1985b) while auxin-induced growth was not affected (Kutschera & Schopfer, 1985a). The difference between these and the above-mentioned results might have been caused by the experimental set ups. The abrading technique was different and the solution was buffered in case of Kutschera & Schopfer (1985ab), while Lüthen *at al*. (1990) could use unbuffered solutions. Difference in cation composition might have impacted too, with 10 mM KCl and 1 mM Ca^{2+} used by Lüthen *et al.* 1990), while Kutschera & Schopfer (1985ab) used Ca^{2+} in the incubation medium and K^{+} at minimal concentrations (discussed in Lüthen *et al*., 1990).

It is possible that extension growth of multi-tissue organs such as roots, coleoptiles and leaves is limited mechanically by the extension of one component tissue. This idea, which dates back to the 19th century (Kutschera, 1994), is proposed in particular for the epidermis of round, compact organs (containing little intercellular

air space) such as hypocotyls and coleoptiles. Therfore the wall of the epidermis may be important for growth, and it is possible that ‘acid growth’ may occur in all tissues of an organ or only in the epidermis or in all tissue but the epidermis. This could explain discrepancies in results obtained between researchers and for different organs and species. Peeling off just part of the epidermis of coleoptiles might cause immediately changes in growth conditions but also experimental artefacts (Kutschera, 1994). It was assumed that fusicoccin may interact with proton pumps of inner coleoptile tissues whereas auxin affects H^+ secretion of epidermal cells. Peeling off the epidermis caused 80 % less proton excretion of coleoptiles compared when coleoptiles were abraded with wet emery cloth (Kutschera *et al.*, 1987). These results are supported by immunolocalisation results. Fusicoccin sensitive plasma membrane H^+-ATPase (PM-H^+-ATPase) proton pumps were found mainly in mesophyll cells rather than in the epidermis (Villalba *et al.*, 1991); other authors, using electrophysiology, showed that auxin-induced H^+ pump activity did not depend on the presence of epidermal cells in maize coleoptiles (Peters *et al.*, 1992).

1.1.3.4 Acid growth of dicotyledonous leaves

The ‘acid growth’ theory has been tested much less in detail on dicotyledonous compared to monocotyledonous plants (coleoptiles) and the results in the literature are in part confusing. The validity of the acid growth theory appears to depend on the species tested. Light-induced leaf expansion of bean (*Phaseolus vulgaris*) and silver birch (*Betula pendula*) clearly showed an ‘acid growth’ type response. Apoplast pH decreased within 5 - 15 min of illumination, parallel to an increase in growth. Exogenous acidic buffer induced loosening of the cell wall and stimulated leaf growth whereas buffer at neutral pH inhibited growth. Fusicoccin stimulated both leaf growth and apoplast acidification (Van Volkenburgh & Cleland, 1980; Taylor & Davies, 1985; Cosgrove, 1996). In contrast, leaf expansion of sycamore (*Acer pseudoplatanus*) and tobacco (*Nicotiana tabacum*) could not be explained through ‘acid growth’. Apoplast acidification was not related to auxin-induced growth, yet fusicoccin-related ‘acid growth’ was present in tobacco leaves and independently of any auxin effect (Taylor & Davies, 1985; Keller & Van Volkenburgh, 1998). Growth related acidification in dicotyledonous leaves seems controlled by light and follows a partially independent pathway from photosynthesis as experiments with pea (*Pisum sativum*) leaves showed (Stahlberg & Van Volkenburgh, 1999). In tobacco leaves, some mechanistic link between light-stimulated leaf growth, H^+ excretion and K^+ uptake (Stiles *et al.*,

2003; Stiles & Van Volkenburgh, 2004) was observed. The role of K^+ could be to provide electrical counterbalance of H^+ rather than to provide an osmolyte for uptake (Stiles & Van Volkenburgh, 2004).

1.1.3.5 Acid growth of roots

Early results suggested auxin linked 'acid growth' in roots (Moloney *et al.*, 1981). However, more recent data showed that auxin increased growth of shoot and coleoptiles yet equally rapidly inhibited root growth (Christian *et al.*, 2006). Positive 'acid (pH 4.0) growth' has been not recorded in root elongation and at pH 3.5 organ elongation is reduced (Kutschera, 2006). In contrast with these results correlation was found between cell wall acidity and root elongation. Fusicoccin-induced H^+ efflux and growth rate of maize roots rather than auxin that reduced both H^+ efflux and root elongation (Lüthen & Böttger, 1988).

Using pH microelectrodes in the elongation zone of 4 day old maize primary roots a lower pH was recorded than in the non-growing zone when the pH was higher than pH 5.0 of the incubation medium (Fig. 1.3 and Fig. 1.4). Relative elemental growth rate and surface acidity were eliminated by auxin and cyanide treatments, respectively (Fig. 1.3) (Peters & Felle, 1999; Peters, 2004).

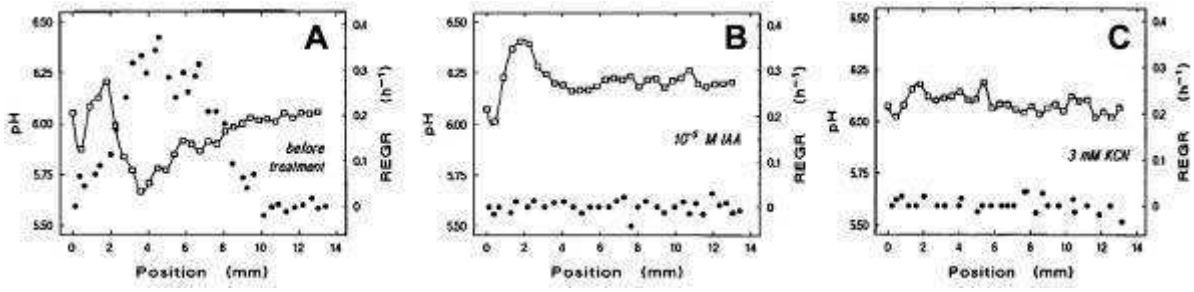

Figure 1.3 Root elongation growth rate (REGR) and apoplast pH changes

Profile of surface pH (□) and REGR (•) along the apical 12 mm of a growing maize root measured in pH 6.75 medium (A) and after 10 µM IAA treatment (B) or 3 mM KCN treatment (C). Position 0 refers to the tip of the root cap. Reprint from Peters & Felle (1999) based on open access policy of www.plantphysiology.org with copyright American Society of Plant Biologists.

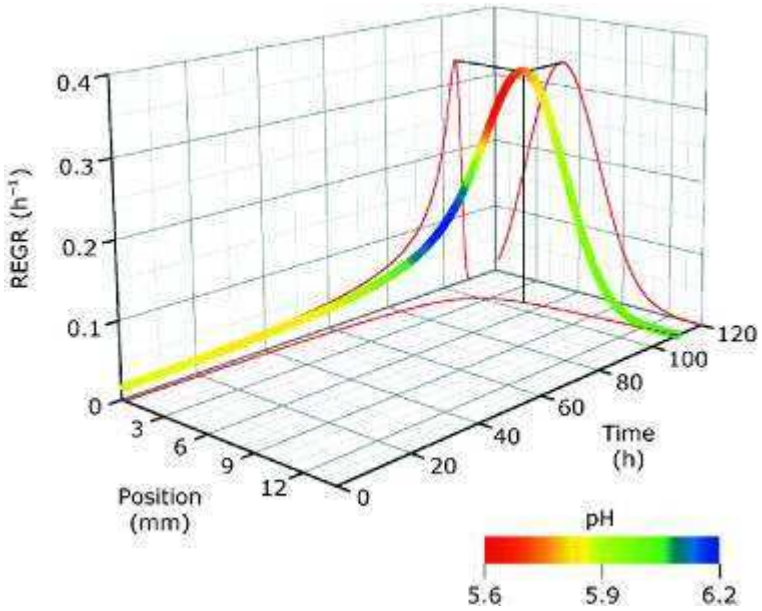

Figure 1.4 Trajectory of a root element

The figure shows the relation of the parameter time, position on the root, relative elemental growth rate (REGR) and surface pH (colour-coded) in growing maize root. The element considered is located at 0.2 mm above root apex at 0 time point. Reprint from Peters (2004) with the permission of the publisher (Licence No: 2693010825600, 'John Wiley and Sons')

Amtmann *et al.*, (1999) using different experimental systems had similar results on barley roots. They found that H^+ excretion could have crucial role in activation of inward K^+ channels. Changes in cytosolic pH and K^+ might be significant factors which contribute to the root growth response to changes in K^+ supply.

1.1.4 Potassium uptake and 'acid growth'

Potassium is the main inorganic solute used by most plant cells to generate osmotic pressure. Its cytosolic concentration is tightly regulated. Therefore, one would expect that changes in the PM-H^+-ATPase pump activity affect growth not only through changes in wall properties, but also through changes in K^+ uptake. Recent data show that 'acid growth' and K^+ uptake are related processes. Auxin and fusicoccin-induced growth was not present in absence of K^+ (Claussen *et al.*, 1997; Tode & Lüthen, 2001).

Claussen *et al.* in 1997 observed for abraded maize coleoptiles that auxin-induced growth and K^+ uptake were related processes. For auxin-induced growth the K^+ concentration in the medium was essential. In absence of K^+ an effect of auxin on growth was not observed, whereas when K^+ was added to the medium, auxin-related growth was immediately measured. The K^+ channel blocker triethylammonium (TEA)

also suppressed the growth response to auxin, and when the blocker was removed, growth recovered as shown in Fig. 1.5 (Claussen *et al.*, 1997). In a related study, a similar K^+-dependency was observed for fusicoccin-induced growth (Tode & Lüthen, 2001).

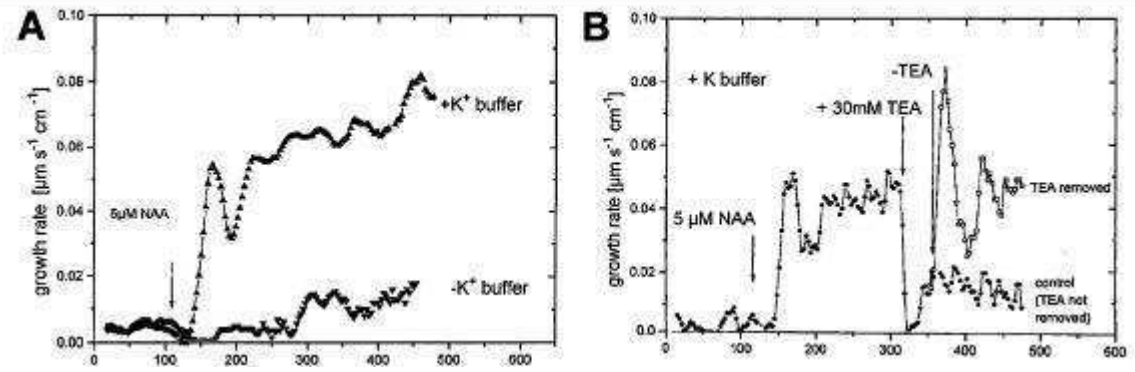

Figure 1.5 Potassium transport dependency of abraded maize coleoptiles

Potassium dependency of growth of coleoptiles was tested using a medium which contained 10 mM K^+ or no added K^+ (A). TEA, a K^+ channel blocker, inhibited auxin-induced growth; the blockage was completely reversible (B). When TEA was removed and replaced by incubation medium containing 10 mM K^+ and NAA, the growth rate recovered at the level before TEA treatment. Reprint from Claussen *et al.* (1997) with the permission of the publisher (Licence No: 2693030934022, 'Springer')

ZMK1 and ZMK2 K^+ channels genes from maize were tested from the viewpoint of coleoptile growth. ZMK1 seemed to be growth related, acidification immediately increased channel activity and auxin increased its expression but acidic pH did not changed the expression pattern (Philippar *et al.,* 1999). Over- expression of ZMK1 leads to K^+ independent growth (Philippar *et al.*, 2006). Similar results have been obtained for the *Arabidopsis* K^+ channel AtKAT1 in growing hypocotyl and flower stalk (Philippar *et al.*, 2004).

1.2 Plasma membrane H^+-ATPase

Plasma membrane H^+-ATPase (PM-H^+-ATPase) was first discovered in 1946 when acid dependent glucose transport was described during the fermentation of the yeast *Saccharomyces cerevisiae* (Conway & O'Malley, 1946). Cyanide and sodium azide caused plasma membrane potential decreases in *Neurospora crassa* within seconds, which also suggested an ATP-dependent H^+ pump activity (Slayman, 1965). The enzyme from fungi *Schizosaccharomyces pombe* and *S. cerevisiae* was isolated and shown to be a proton-pumping ATPase creating -150 to -300 mV plasma membrane potential in plants and fungi (Morth *et al.*, 2011).

PM-H^+-ATPase is a single polypeptide with a molecular mass of ~ 100kDa (Michelet & Boutry, 1995). ATPase activity is usually between 1 - 2 μmol P_i min^{-1} mg^{-1} in purified plasma membrane (Morsomme & Boutry, 2000). The enzyme is essential for living plant cells as it constitutes, to the best of our current knowledge, the primary ion pump which generates the electrochemical potential across the plasma membrane. This electrochemical gradient is responsible for ionotropic signalling, secondary transport, nutrient uptake, pH homeostasis, salt tolerance, stomatal and leaf movements and cell growth (Palmgren, 2001; Moran, 2007; Duby & Boutry, 2009). The PM-H^+-ATPase protein is a member of the family of P-type ATPases. Other members of this family include the Na^+,K^+-ATPase, the principal ion pump in animals and humans (Morth *et al.*, 2011).

1.2.1 Isoforms of PM-H^+-ATPase

Using the model plant *Arabidopsis thaliana* twelve PM-H^+-ATPase isoforms were identified from the genome (AHA1-12). The AHA12 isoforms carries two large deletions and is possibly a pseudogene (Palmgren, 2001). AHA1 and AHA2 are virtually expressed in all tissues and organs and function as housekeeping gene (Gaxiola *et al.*, 2007) while other PM-H^+-ATPase isoforms show some tissue specificity of expression (Morsomme & Boutry, 2000; Palmgren, 2001; Gaxiola *et al.*, 2007). Tissue-specific localization of PM-H^+-ATPase is summarised in Table 1.1, based on information provided in (Palmgren, 2001).

There is only one isoform of PM-H^+-ATPase known in full detail for barley (*Hordeum vulgare*) based on nucleotide and protein data bases (NCBI, http://www.ncbi.nlm.nih.gov/ and UniProt http://www.uniprot.org/). However, MS / MS results suggest that there exist at least two different PM-H^+-ATPase isoforms in barley (Hynek *et al.*, 2006).

Table 1.1 Localisation of specific PM-H^+-ATPase isoforms in plant body (Palmgren, 2001)

Tissue	PM-ATPase protein	Plant
Seedlings:		
Cotyledon	PMA1, PMA2, PMA4	*N. plumbaginifolia*
Primary root	PMA1, PMA4	*N. plumbaginifolia*
Root:		
Cortex parenchyma	PMA2, PMA3, PMA4	*N. plumbaginifolia*
Extension zone	PMA4	*N. plumbaginifolia*
Lateral root initials	PMA2, PMA4	*N. plumbaginifolia*
Lateral roots	PMA4, PMA9	*N. plumbaginifolia*
Root hair and epidermis	PMA1, PMA3, PMA4 MHA2	*N. plumbaginifolia* *Zea mays*
Root cap	PMA2, PMA4	*N. plumbaginifolia*
Stele (central cylinder)	PMA2, PMA3, PMA4	*N. plumbaginifolia*
Stem:		
Axillary buds	PMA2, PMA4, PMA9	*N. plumbaginifolia*
Cortex parenchyma	PMA1, PMA2, PMA4	*N. plumbaginifolia*
Pith	PMA4	*N. plumbaginifolia*
Vascular tissue	PMA2, PMA3, PMA4, PMA9	*N. plumbaginifolia*
	MHA2	*Zea mays*
	AHA3	*A. thaliana*
Leaf:		
Guard cells	PMA2, PMA4	*N. plumbaginifolia*
	VHA1, VHA2	*Vicia faba*
	MHA2	*Zea mays*
Mesophyll	PMA2, PMA4	*N. plumbaginifolia*
	VHA1, VHA2	*Vicia faba*
Trichomes (long)	PMA4	*N. plumbaginifolia*
Trichomes (short)	PMA6	*N. plumbaginifolia*
Vascular tissue	PMA2, PMA3, PMA4	*N. plumbaginifolia*
	MHA2	*Zea mays*
	AHA3	*A. thaliana*
Flower:		
Carpel	PMA2	*N. plumbaginifolia*
Ovules	PMA1, PMA2, PMA3, PMA4, PMA6, PMA9	*N. plumbaginifolia*
	AHA3, AHA10	*A. thaliana*
Nectaries	PMA2	*N. plumbaginifolia*
Stamen; pollen	PMA1, PMA2, PMA3, PMA4, PMA6, PMA6	*N. plumbaginifolia*
	AHA3, AHA9	*A. thaliana*
Style	PMA1, PMA3, PMA4	*N. plumbaginifolia*
Vascular tissue	PMA1, PMA2, PMA3, PMA4, PMA6	*N. plumbaginifolia*
	AHA3	*A. thaliana*

1.2.2 Structure of PM-H$^+$-ATPase

The crystal structure of AHA2, a PM-H$^+$-ATPase from *Ababidopsis thaliana*, has recently been described (Fig. 1.6). The protein contains a transmembrane domain with ten helices (M1-10) and three cytosolic domains: a nucleotide-binding domain (N), a phosphorylation domain (P) and an actuator domain (A). ATP is bound with the adenosine part at the N domain and its triphosphate group protruded towards the P domain. ATPase binding site was determined using 5'-(β,γ-methlene)-triphosphate (AMPPCP) a non-hydrolysable analogue of ATP (Pedersen *et al.*, 2007).

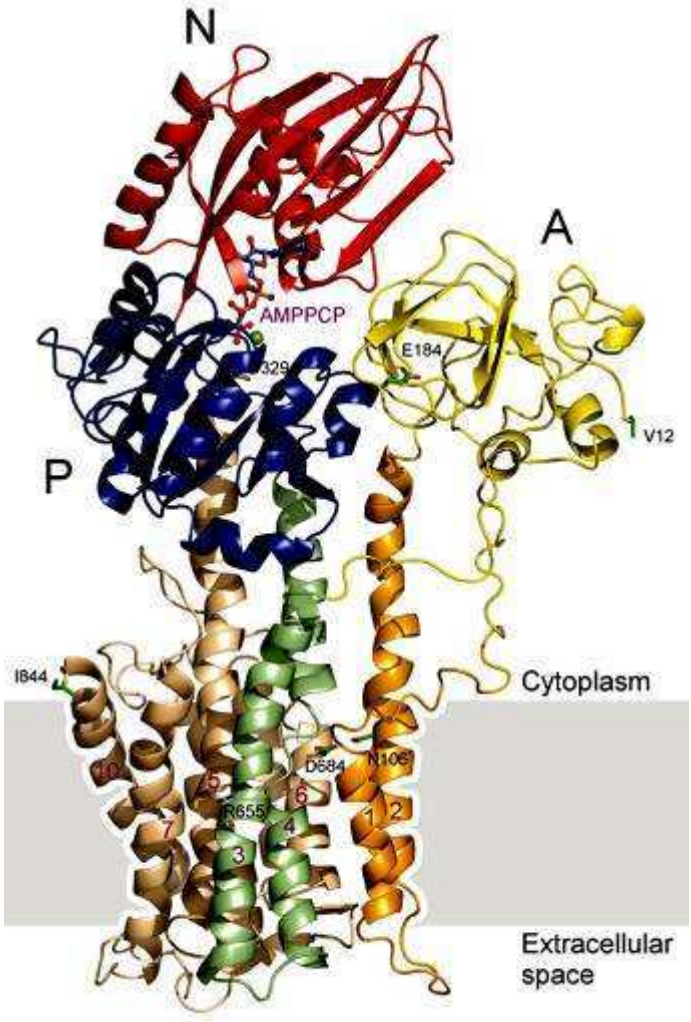

Figure 1.6 Structure of AHA2 without auto-inhibitory domain

AHA2 contains ten transmembrane helices (orange, green and brown); a nucleotide binding domain (N), red; a phosphorylation domain (P), blue; and an actuator domain (A); yellow. AMPPCP is shown as ball-and stick representation. The grey box represents the location of the plasma membrane; reprinted from Pedersen *et al.* (2007) with the permission of the publisher (Licence No: 2693040963163, 'Nature Publishing Group').

1.2.3 Catalytic cycle of P-type ATPase and H^+ transport mechanism

PM-H^+-ATPase undergoes conformational changes during each catalytic cycle. The enzyme has two distinct conformational states termed E1 and E2. The two conformation states differ in reactivity at the nucleotide binding site, which can be phosphorylated by ATP in the E1 form or by free P_i in the E2 form. E1 is the form that binds ATP and H^+. The catalytic cycle is shown in details in Fig 1.7 (Morsomme & Boutry, 2000; Pedersen *et al.*, 2007).

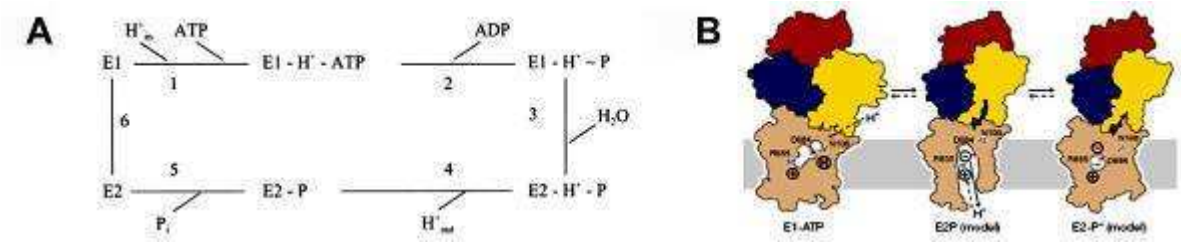

Figure 1.7 Catalytic cycle and H^+ transport of PM-H^+-ATPase

Originally the catalytic cycle was proposed for Ca^{2+} ATPase (subfigure A) E1 form binding ATP and H^+ (1), then a high energy intermediate is formed while ADP is released (2). Conformation of the enzyme is changing from E1 to E2 (3). Proton release to cell exterior (4), finally P_i is released (5) and conformation of the enzyme returning to form E1 (Morsomme & Boutry, 2000). The E1 form binds H^+ and ATP better than the E2 binds these substances, as subfigure B shows; reprinted from Pedersen et al. (2007) with the permission of the publisher (Licence No: 2693040963163, 'Nature Publishing Group').

1.2.4 Control of PM-H^+-ATPase

Activity of PM-H^+-ATPase is modulated by several physiological signals (such as temperature and salt stress). In comparison, there exists little evidence of a regulation of PM-H^+-ATPase activity through changes at the transcriptional or protein level. Moderate PM-H^+-ATPase expression changes have been describe for high aluminium treatment, (Shen *et al.*, 2005), iron deficiency (Santi *et al.*, 2005), in presence of high sugar concentration (Mito *et al.*, 1996) and high salt treatment (Maathuis *et al.*, 2003) .

Higher (compared to the 'average' tissue) PM-H^+-ATPase protein concentrations have been found in guard cells, root epidermis, phloem xylem parenchymas (Bouche-Pillon *et al.*, 1994; Michelet & Boutry, 1995; Morsomme & Boutry, 2000; Palmgren, 2001; Gaxiola *et al.*, 2007) and motor organs of seismonastic plants (Fleurat-Lessard *et al.*, 1997; Moran, 2007).

Regulated exocytosis of vesicles that contains PM-H^+-ATPase molecules constitutes an alternative regulation pathway (Hager *et al.*, 1991), yet post-

translational modification of the enzyme seem the most common control mechanism for causing changes in PM-H^+-ATPase activity (Gaxiola *et al.*, 2007).

Phosphorylation / dephosphorylation are further mechanisms through which PM-H^+-ATPase can be regulated. Elicitor-induced dephosphorylation in tomato plants (*Lycopersicon esculentum*) resulted in an increase in PM-H^+-ATPase activity (Vera-Estrella *et al.*, 1994) while subsequent phosphorylation of the enzyme reduced its activity; although Ca^{2+}-dependent phosphorylation caused decreased H^+ pumping activity. Phosphorylation also activates PM-H^+-ATPase activity through the fusicoccin (and 14-3-3 protein) activation pathway (Morsomme & Boutry, 2000).

The C-terminal auto-inhibitor regulation domain (R) could be mainly responsible for rapid activity changes of PM-H^+-ATPase. Removal of the R domain from the enzyme by trypsin digestion activated PM-H^+-ATPase (Palmgren *et al.*, 1991). Structural information of molecular mechanism of the auto-inhibition is not available yet. In AHA2 neutralisation of the auto-inhibitory R domain by binding of 14-3-3 protein results in pump activation. Before the activation process, the penultimate Thr947 needs to be phosphorylated by a protein kinase which is induced by environmental factors such as light, nutrient status and pathogens. This phosphorylation can lead to the binding of 14-3-3 protein on the R domain complex. The Thr947 is not freely accessible to protein kinase activity, structural modification is necessary by ligand binding or kinase docking. Phosphorylation of Ser931 inhibits PM-H^+-ATPase and destroys the 14-3-3 protein binding site (Sze *et al.*, 1999; Morth *et al.*, 2011). It seems that phosphorylation of most residues within the C-terminal domain impacts on 14-3-3 binding. The enzyme regulation is controlled by distinct protein kinases and phosphatases allowing gradual increase and decrease of the activity of PM-H^+-ATPase (Speth *et al.*, 2010). More details are provided in Fig. 1.8.

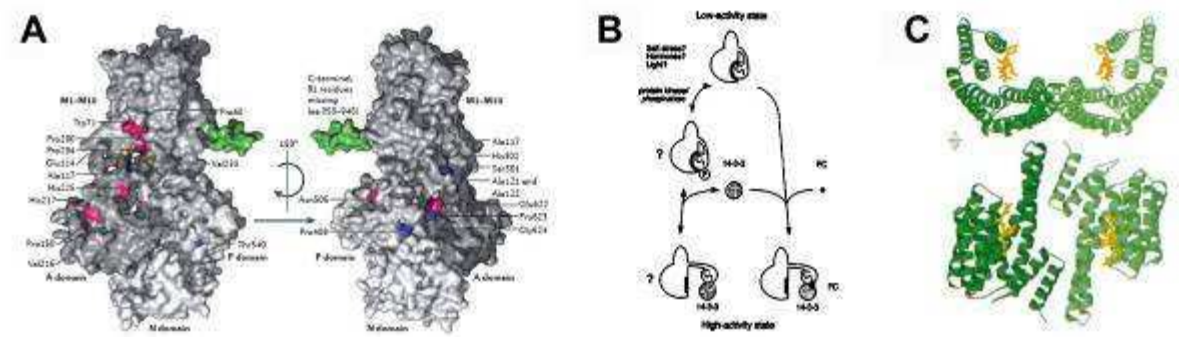

Figure 1.8 Auto-inhibition of PM-H$^+$-ATPase

On subfigure A residues are highlighted on the PM-H$^+$-ATPase (AHA2) that interact with the regulatory domain. Blue: present in yeast; red: present in plant; yellow: present in plant Ca^{2+}-ATPase.; green: 13 residue carboxy-terminal extension. Plant and fungal sites do not overlap, and it is likely that their pumps are inhibited by different mechanisms (Morth *et al.*, 2011). B: schematic summary of protein kinase/phosphatise-dependent and fusicoccin-dependent activation pathway of PM-H$^+$-ATPase. Subfigure C shows the ribbon plot of different orientation of dimeric tobacco 14-3-3c protein (green) bound to the C-terminal end (yellow) of PMA2 (tobacco PM-H$^+$-ATPase) (Würtele *et al.*, 2003). Figures are reprint from Morth *et al.* (2011) with the permission of the publisher, Licence No: 2693050346303, 'Nature Publishing Group' (A); Sze *et al.* (1999) based on open access policy of www.plantcell.org with copyright American Society of Plant Biologists (B) and Würtele *et al.* (2003) with the permission of the publisher, Licence No: 2693070537163, 'Nature Publishing Group' (C).

1.2.5 Fusicoccin-dependent PM-H$^+$-ATPase activation

Fusicoccin (a diterpene glycoside) is a phytotoxin, produced by the fungus *Fusicoccum amygdali*. The fungus is host specific, but isolated fusicoccin causes higher H^+ efflux in any higher plant tested so far (Marré, 1979). Recent structural studies show that fusicoccin is increasing H^+ pump activity by stabilising the interaction between 14-3-3 protein and auto-inhibitor R domain of PM-H$^+$-ATPase. Fusicoccin effective due binding its plasma membrane receptor (Olivari *et al.*, 1998) that is on the C-terminal of the R-domain of the PM-H$^+$-ATPase (Johansson *et al.*, 1993). This results in permanent binding of 14-3-3 protein to the regulation domain (Oecking *et al.*, 1994) and activates PM-H$^+$-ATPase permanently as shown in Fig. 1.8.

The toxin causes no major conformation changes; it fills a cavity between 14-3-3 protein and PM-H$^+$-ATPase (Fig. 1.9) and increases the stability of the complex about 90-fold (Würtele *et al.*, 2003).

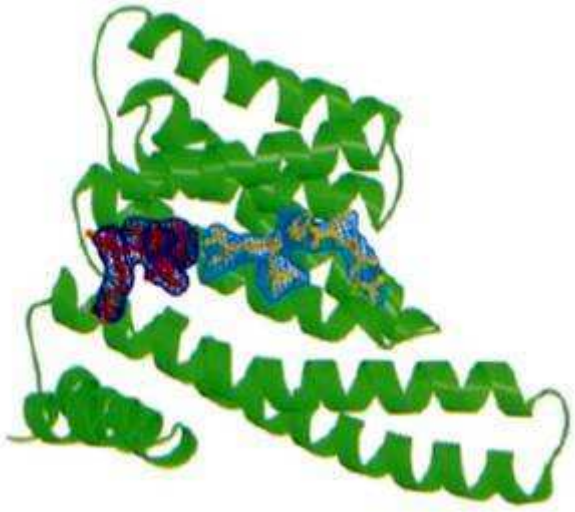

Figure 1.9 14-3-3 protein-fusicoccin-PM-H$^+$-ATPase complex

Ribbon diagram of a 14-3-3 protein monomer (green) with PM-H$^+$-ATPase peptide (yellow) and fusicoccin (orange). Blue represent the Van der Waals space of fusicoccin and PM-H$^+$-ATPase peptide (reprint from Würtele *et al.* (2003) with the permission of the publisher, Licence No: 2693070537163, 'Nature Publishing Group')

1.3 Barley

Barley (*Hordeum vulgare*) was domesticated 10,000 years ago and ranks fourth among cereals after maize (*Zea mays*), rice (*Oryza sativa*) and wheat (*Triticum aestivium*) in terms of global production. About two-thirds of the annual global barley production is used for animal feeding and the remaining third covers the needs of malting, brewing (beer) and distilling (whiskey) industries (Schulte *et al.*, 2009). The average annual production of barley in the world is about $1.24 \cdot 10^{11}$ kg and 62 % of this is harvested in Europe. The highest yield per hectar occurs in Ireland with 5.7 Mg ha^{-1} (Kim & Dale, 2004). In Ireland and Scotland brewing and distilling has a particularly big economic impact, not least because of the whiskey industry.

1.3.1 The two weeks old barley seedlings and their advantage

Barley seedlings at a developmental stage of two weeks old (between 14 - 17 days) present ideal research objects for leaf growth studies. At this stage leaf three is the main growing leaf and shows maximum or near-maximum growth rate (2 - 3 mm h^{-1}). Older leaves, which cause self-shading and reduce the potential biomass increase have not developed yet and younger seedlings are not yet fully dependent on the external medium for supply of mineral nutrients but still receive a considerable portion through seed reserves. The base 40 mm of leaf three that contains the leaf

elongation zone is enclosed by the sheath of the older leaves one and two (Fricke & Flowers, 1998; Fricke, 2002a). There are small quantities of cuticle waxes deposited on the epidermal surface along the base 20 - 30 mm of the elongation zone. This means that the permeance of the cuticle is much higher in the elongation zone compared to the emerged blade, which makes external application of test reagents to measurements of proton extrusion from the leaf apoplast comparatively easy without having to mechanically remove the cuticle (Richardson *et al.*, 2007).

1.3.1.1 Morphology of developing barley leaves

Barley leaves consist of two parts, the basal sheath and the leaf blade, separated by ligule and auricle. The sheath at the leaf base mechanically supports the blade which is the photosynthetic and transpirating active part of the leaf. The sheath also encloses the basal apical meristem, and any younger leaves emerge from within sheaths of older leaves. Leaves develop from the main meristem, which is located at the base. As a consequence, oldest tissues are at the leaf tip and youngest ones near the leaf base. The elongation zone of leaf three stretches to about 40 mm from the point of leaf insertion (‘leaf base’), with highest relative elemental growth rates between 10 - 30 mm (Fricke & Peters, 2002). In the elongation zone cells are elongating manyfold in size. Above the elongation zone is a zone which can be referred to as ‘non-elongation zone’. This zone extends to the point of emergence of the developing leaf from the sheath of leaf two and contains cells which are not elongating any more but can show some lateral expansion. The fully emerged leaf blade contains fully-differentiated cells, which are not dividing or expanding any more. Details are provided in Fig. 1.10.

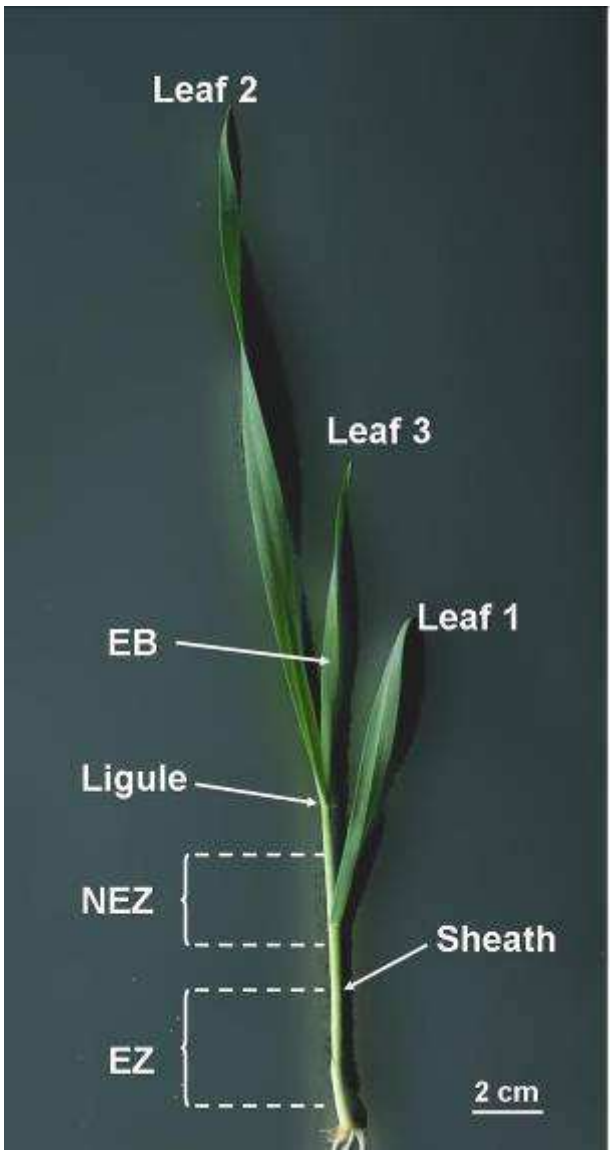

Figure 1.10 Two-week old barley seedling

The two-weeks old barley seedling has three leaves. Leaf one is the oldest leaf and leaf three is the youngest and main developing leaf. EZ: elongation zone; NEZ: non-elongation zone; EB: emerged leaf blade

1.3.1.2 Anatomy of developing barley leaf

Anatomical changes during leaf development can be visualised on cross sections of different parts of the leaf (Fig. 1.11). Cell size is increased manyfold in mature compared to immature tissue, although it is difficult to see this on cross sections, particularly in the epidermis, where elongation growth contributes most to cell enlargment. The most conspicuous difference between the different developmental stages is the specialisation of mesophyll cells for photosynthesis (chloroplast development), xylem (conductance of water and dissolved solutes) and increased intercellular spaces.

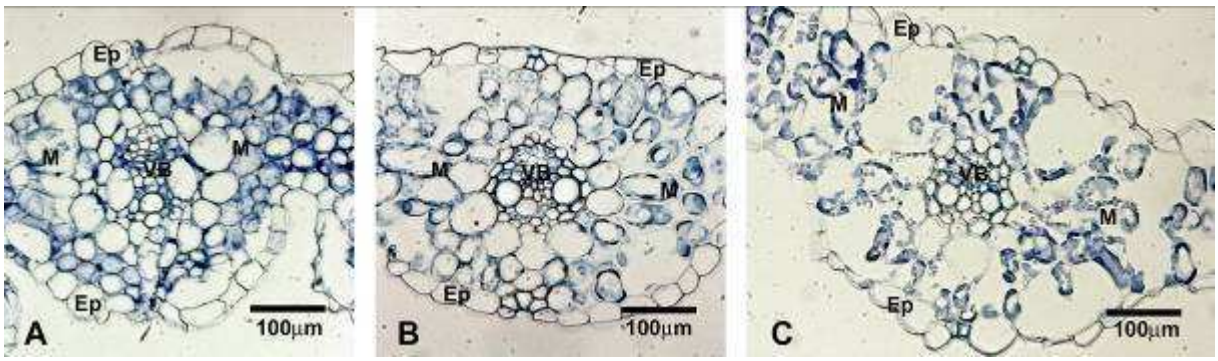

Figure 1.11 Toluidine blue stained cross section of barley leaves from different developmental stage

Cross sections from elongation zone (A) non-elongation zone (B) and fully emerged blade (C) of leaf three. Ep: epidermis; M: mesophyll cells; VB: vascular bundle.

1.3.2 Growth and potassium uptake of barley

The classical dual K^+ uptake mechanism has first been described for roots of barley (Epstein *et al.*, 1963). Further studies proofed the relevance of high affinity K^+ transporters for K^+ uptake; also H^+ / K^+ co-transport has a high significance in K^+ uptake of roots (Glass *et al*., 1981; Amtmann *et al*., 1999). For barley, four HAK genes have been described (HvHAK1-4). HvHAK1 was mainly expressed in roots, HvHAK3 in both shoots and roots while HvHAK4 was mainly expressed in shoots (Rubio *et al.*, 2000). HvHAK4 had significantly higher expression in the elongation zone of leaves compare with parts of barley seedlings (Boscari *et al.*, 2009). HvHAK1 is very similar to AtHAK5 and seems to be a high affinity K^+ transporters in contrast with HvHAK2, which facilitates K^+ uptake in a range of low or medium affinity (K_M of about 5 mM comparing with K_M of about10 µM for HvHAK1 (Rubio *et al.*, 2000; Senn *et al.*, 2001; Ashley *et al.*, 2006).

In previous studies on K^+ transport in barley it was concluded that apoplast K^+ must exceed 3 - 5 mM to allow growing leaf cells to take up K^+ through channels (Boscari *et al.*, 2009; Volkov *et al.*, 2009). Calculations showed that at 10 mM apoplast K^+, about 50 % of K^+ uptake was facilitated by time-dependent inward-rectifying currents typical of Shaker K^+ channels such as AKT1 or AKT2. The remaining 50 % was facilitated by instantaneous currents, which includes either or both, K^+ high-affinity transporters such as HAK / KUP / KT type K^+ / H^+ symporters or non-selective cation channels.

Potassium channels and transporters might study using different blockers of these proteins. Tetraethylammonia (TEA) inhibits K^+ transport through channels reversibly as K^+ analogue at the dehydration transition step (Lenaeus *et al.*, 2005).

Cs^+ ions as huge K^+ analogue block both channels and transporters (Rodriguez-Navarro & Rubio, 2006; Szczerba *et al.*, 2009) and NH_4^+ ions with competitive manner inhibit high affinity K^+ transporters (Spalding *et al.*, 1999; Kronzucker *et al.*, 2003; Rodriguez-Navarro & Rubio, 2006; Szczerba *et al.*, 2006; Britto & Kronzucker, 2008; Szczerba *et al.*, 2009; Britto *et al.*, 2010; Hoopen *et al.*, 2010)

1.4 Technical approaches

(i) Cell wall acidification was measured using three independent methods (pH sensitive fluorescence probe, micro pH electrode technique and in-vitro agarose gel system with bromocresol purple pH indicator. During these experiments leaf elongation was measured with a ruler (micro pH measurements) or image analysis tools (in-vitro gel experiments).

(ii) A linear variable differential transformer (LVDT) was used to determine the growth rate continuously and at micrometer resolution. This made it possible to record any rapid and short term response of leaf growth to application of test reagents to the apoplast of the leaf elongation zone.

(iii) Expression of PM-H^+-ATPase was determined by absolute qPCR technique and the PM-H^+-ATPase enzyme ratio in total purified plasma membrane protein was measured using Western blot analysis and densitometry on Coomassie Brilliant Blue stained SDS polyacrylamide gels. Activity of the enzyme was determined as vanadate sensitive ATPase hydrolysis activity of inside-out plasma membrane vesicles.

(iv) PM-H^+-ATPase tissue specific distribution was studied using immunolocalisation on paraffin embedded section and a commercially-available antibody of PM-H^+-ATPase isoforms.

1.5 Objectives of the present study

The aim of this project was to test whether apoplast pH differs between growing and non-growing leaf tissue of barley, how this acidification relates to growth and to which degree apoplast acidification relies on the activity, transcription and occurrence of PM-H^+-ATPase. The developing leaf three of barley was studied. Apoplastic pH and leaf elongation was measured together in the same experiments or in separate experiments. Differences in pH and leaf growth were followed using three independent techniques. Treatments affecting PM-H^+-ATPase activity (increase or decrease) or blockers of different type of K^+ transport (channel, transporter) were used to determine the physiological background of leaf elongation. Expression and activity of PM-H^+-ATPase was measured to test whether any higher acidity in the apoplast of the elongation zone originated from a higher expression of the enzyme or any other control mechanism, in particular post-translational modification. Finally tissue specific distribution of PM-H^+-ATPase was determined at different leaf developmental stages on cross sections.

2 Materials and Methods

2.1 Plant material

2.1.1 Plant growth for study of leaves

Barley seeds (*Hordeum vulgare* L. cv. Golf; and *Hordeum vulgare* L. cv. Jersey) were imbibed overnight in water, germinated in dark on approx. 0.5 mM $CaSO_4$ for 3 days and exposed to light for a further 3 days while remaining on $CaSO_4$ solution. On day seven, four seedlings were transferred into 1 l borosilicate glass beakers wrapped in tin foil (containing 0.8 - 0.9 l nutrient solution) on aerated ½ strength Hoagland solution (Table 2.1) and grown for a further 7 - 11 days at 70 - 80 % relative humidity and 300 – 350 µmol m^{-2} s^{-1} photosynthetically active radiation at third-leaf level, during a 16 h / 8 h, 21 ℃ / 15 ℃ day / night cycle in a growth chamber (I MAGO F3000, Snijders Scientific). Nutrient solution was not replaced during plant growth. These were the growth conditions at University College Dublin, where most experiments were carried out. Some experiments, including plant growth, were also carried out at Rothamsted Research (UK) and Eötvös University (Hungary). Plants were analysed when they were 14 - 18 d old.

At Rothamsted Research (pH microelectrode measurements) the growth temperature was different (constantly 20 ℃ during day / night). At Eötvös University (plasma membrane isolation) plants were grown under a 14 h / 10 h day / night period (150 µmol m^{-2} s^{-1}) with 20 / 18 ℃ day / night temperature. These alterations in growth conditions were due to local availability of growth facilities and the seedlings achieved the leaf three development stage about 2 - 3 d later at Eötvös University and 1 - 2 earlier at Rothamsted Research compared with Dublin.

The barley Golf cultivar was used for most experiments. Towards the end of the study, the availability of Golf seeds became limited due to vast demand by the laboratory in general, no further commercial (breeder) availability of this cultivar and due to limited availability of growth space at UCD to grow plants to the seeding stage. Therefore, experiments which were carried out towards the end of the study, in particular plasma membrane isolation, were performed on the barley cultivar Jersey. Both, Golf and Jersey are spring barleys.

Table 2.1 Composition of the ½ strength Hoagland solution for barley seedlings

Macronutrients (1 l each)	**Stock** (mM)	**Amount for 1 l stock** (g)	**Final concentration** (mM)	**Dilution**
(1) $NH_4H_2PO_4$	100	11.5g	0.5	200x
+ $(NH_4)_2HPO_4$	100	13.2	0.5	200x
(2) KNO_3	400	40.4	2.0	200x
(3) $MgSO_4x7H_2O$	100	24.7	0.5	200x
+ NaCl	100	5.84	0.5	200x
(4) $Ca(NO_3)2x4H_2O$	400	94,4	2.0	200x

Micronutrients (0.5 l each)	**Stock** (mM)	**Amount for 0.5l stock** (g)	**Final concentration** (µM)	**Dilution**
(a) H_3BO_3	25	0.775	6.25	4000x
(b) $CuSO_4x5H_2O$	0.5	0.0625	0.125	4000x
(c) $MnSO_4xH_2O$	2	0.169	0.5	4000x
(d) $Na_2MoO_4x2H_2O$	0.76	0.092	0.19	4000x
(e) $ZnCl_2$ (or $ZnSO_4$)	2	0.136	0.5	4000x
(f) Fe^{III}NaEDTA	36	6.606	27	1333x

2.1.2 Plant growth for study of coleoptiles

To grow coleoptiles for auxin sensitivity test Golf barley seeds were imbibed overnight in water and were germinated in the dark for 5 d in the growth chamber under the same temperature settings (16 h at 21 °C, 8 h at 15 °C) as described for seedlings. The apical 10 mm of the coleoptile tip was used and the first leaf developing inside the coleoptiles was removed (compare Sakurai & Masuda, 1978).

2.2 Apoplast pH measurements

Cell wall pH was measured through three independent approaches: an in-vitro gel system, electrophysiology and confocal microscopy. The in-vitro gel system involved incubating leaf segments in agarose which contained the pH indicator bromocresol purple. The advantage of this system was that it was easy to use. This made it possible to test many treatments and to directly relate changes in wall acidity to changes in growth rate. The pH microelectrode technique was used to obtain precise values of apoplast pH in growing and non-growing leaf regions. This technique, which was carried out at Rothamsted Research, required the most experimental effort and was used to a limited extent, due to limited funding for travel. Therefore only selected treatments were tested. Finally, intact plants were studied using

confocal microscopy, by loading plants with pH fluorescence probes added to the root medium. Epidermal peels were also studied as control material.

2.2.1 In-vitro gel system

The base 70 mm of leaf three was placed into a Petri dish which had been filled with agarose medium containing the pH indicator bromocresol purple (Tang *et al.*, 2004; Li *et al.*, 2007). The younger fourth leaf was removed from inside leaf three prior to experiments.

The agarose medium contained 10 mM, 1 mM $CaCl_2$, 0.5 % agarose (gelling temperature 38.3 °C) and 90 mg l^{-1} bromocresol purple. Any additional test reagents were added to the medium while it was fluid and the pH was adjusted to 7.0 using 3 mM KOH. The amount of K^+ added through this pH adjustment was negligible compared to the amount of K^+ added through 10 mM K^+. Leaf pieces were placed into the medium when it was almost semi rigid and had a temperature of between 28 - 32 °C. Petri dishes were incubated under the same conditions under which the plants had grown, except for cold-treatments, where dishes were incubated in the dark in a cold room (5 °C). At regular time intervals (every hour for the first 10 h of incubation), Petri dishes were photographed with a Canon EOS 350D digital camera. Two replicate pictures were made every hour. Final pictures were made after 24 h. Digital photographs were used to assess acidification of the medium and measure elongation growth of leaf pieces. ImageJ 1.41o software (http://rsbweb.nih.gov/ij) was used to measure the length of leaf pieces. Values were calibrated with the aid of graph paper which had been fixed to Petri dishes prior to the start of experiment. Due to the alkaline pH of the graph paper, the paper served as sort of an internal pH control as well since it gave the colour (bluish) of bromocresol purple in non-acidified medium. Acidic areas, which showed up as yellow in the purple-stained medium (see Fig. 2.1), were selected on pictures using the magic wand of Adobe® Photoshop® 7.0.1 (tolerance factor 10) and measured using Scion Image for Windows 4.0.3.2 (http://www.scioncorp.com, O'Neal *et al.*, 2002).

Preparation of leaf pieces and transfer to agarose medium resulted in an immediate, non-specific acidification of the medium, most likely as a result of unpeeling leaf three from the sheaths of leaves one and two. This non-specific acidification levelled off within 4 - 5 h. Preliminary experiments showed that the acid area value obtained after 1 h of incubation reflected the size of the exposed leaf surface of the individual plants therefore it was used as the reference point for the

start of experiment (A_1). Any areas measured at further time points 't' (A_t) were related to this reference point according to 'A_t / A_1'. Areas were expressed in mm^2.

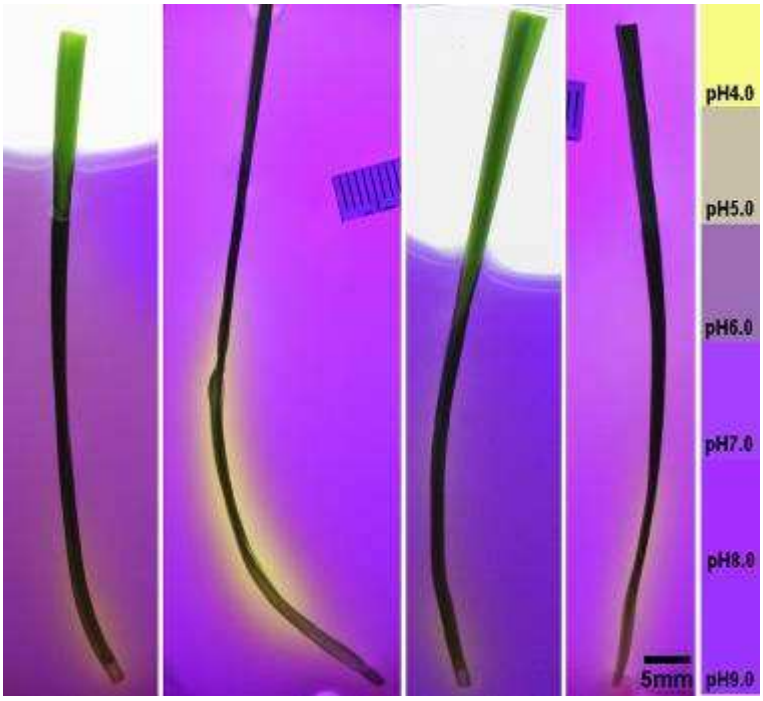

Figure 2.1 Leaf pieces in pH sensitive agarose gel medium

Agarose gels contained the pH indicator bromocresol purple pH. This pH indicator shows yellowish colour at acidic, purple at neutral and blueish colour at alkaline pH (see right column). Basal leaf segments were 70 mm long at the beginning of the experiments, and their tip end was sticking out from the medium. Graph paper was used as an internal alkaline control and to calibrate length of leaf segments to measure growth during the incubation period.

2.2.2 Microelectrode measurements

Apoplastic pH was measured with the aid of pH-sensitive microelectrodes. The elongation zone and emerged, mature portion of the developing leaf three of barley were analysed. The older leaves one and two were peeled back to expose the abaxial surface of the basal elongation zone of leaf three. The elongation zone was covered with wet tissue paper which had been soaked for the previous 24 h in distilled water. The latter was done to guarantee pH neutrality (which is not the case for tissue paper which is used 'fresh'). During experiments, the tissue paper was soaked in bath solutions, as specified in results, to alter the apoplastic environment of the leaf elongation zone. Due to the absence of a major permeability barrier (cuticle) in the elongation zone (Richardson *et al.*, 2007), apoplastic pH could be measured directly by bringing the microelectrode in close contact with the epidermal surface. Measurements were carried out at 20 - 30 mm from the base. In the fully-

cutinised emerged-blade portion of the developing leaf three, apoplastic pH was measured by inserting the microelectrode through stomatal pores (compare Fricke *et al*., 1994; Felle 2005;). Double-barrelled pH sensitive microelectrodes were prepared as described in Miller & Smith (1992) using the same setup and microelectrode cocktail as described in Dennis *et al.* (2009). The only difference was that in the present study a pH 5.0 rather than pH 3.0 calibration buffer was used and that an additional pH 8.5 calibration buffer was included. Calibration was performed before and after readings. The composition of the pH sensitive cocktail and calibration buffers is given in Table 2.2 and Table 2.3. Microelectrode outputs were analysed with Origin® 6.1 (OriginLab Corporation) software.

Analysis of one leaf region of one plant typically lasted between 2 - 6 hours, and between 1 - 6 pH recordings were taken for each leaf region under room temperature and humidity in the dark. To avoid too long exposure of plants on the microelectrode rig, recordings for elongation zone and emerged blade were obtained from different plants. Elongation growth of leaf three of plants mounted on the rig was measured by measuring the length of leaf three at the beginning and end of experiments using a ruler. Preparation of plants reduced leaf elongation growth by about 50-60 % compared to elongation growth of undisturbed plants in the growth chamber.

Table 2.2 Composition of the pH sensor for microelectrodes

Component of pH sensor	Amount of the component
Hydrogen Ionophore II Cocktail A	35 mg
High molecular weight PVC	16 mg
Nitrocellulose	6 mg
Tetrahydrofuran (THF)	Dissolve the other components

Table 2.3 Composition of the buffer solutions used for calibrating pH microelectrodes

pH	Composition of buffer
4.0	20 mM $KHC_8H_4O_4$ (potassium hydrogen phthalate) 120 mM KCl 10 mM $NaH_2PO_4x2H_2O$ Adjust pH using 1 N NaOH
5.0 and 6.0	20 mM MES (2-[N-Morpholino]ethanesulfonic acid) 120 mM KCl 10 mM $NaH_2PO_4x2H_2O$ Adjust pH using 1 N NaOH
7.0	20 mM MOPS (3-[N-Morpholino]propanesulfonic acid) 120 mM KCl 10 mM $NaH_2PO_4x2H_2O$ Adjust pH using 1 N NaOH
8.5	20 mM TAPS (N-tris[Hydroxymethyl]methyl-3-amino-propanesulfonic acis) 120mM KCl 10 mM $NaH_2PO_4x2H_2O$ Adjust pH using 1 N NaOH

2.3 Confocal microscopy

The pH sensitive fluorochromes 5(6)carboxyfluorescein (10 μM) and acridine orange (2.5 μM) were used. In contrast to carboxyfluorescein, acridine orange can be taken up into cells and has been widely used to monitor pH inside animal (Wieczorek *et al.*, 1991; Zoccarato *et al.*, 1999; Malnic & Geibel, 2000) and plant cells (Pope & Leigh, 1988; DuPont, 1989). Carboxyfluorescein is a large double-negative charged anion that can permeate the plasma membrane only in its non-fluorescing diacetate form (Babcock, 1983; Graber *et al.*, 1986). By using its anionic form, its presence in the apoplast and absence in the symplast was guaranteed. The application of acridine orange has some limitations (Palmgren, 1991) but with adequate controls these limitations can be overcome (Clerc & Barenholz, 1998; Manente *et al.*, 2008). The fluorescence intensity of carboxyfluorescein between pH 4.5 and 6.5 can be used to reflect changes in pH conditions in this pH range (Babcock, 1983; Graber *et al.*, 1986).

Dyes were added to the root medium of intact plants in the growth chamber. Plants were allowed to take up dyes into the apoplastic space of both roots and leaves and analysed after an incubation period of 24 h (carboxyfluorescein) and 48 - 72 h (acridine orange). Detached leaves, epidermal peels or leaves still attached to the remainder of the plant were examined with an Olympus FV1000 confocal microscope. Dyes were excited at 488 nm and fluorescence was detected between

500 - 550 nm (carboxyfluorescein) and 516 - 536 nm (acridine orange). To test how effective the uptake of dye into the leaf apoplast had been during the incubation period and how pH sensitive the approach was, epidermal strips were peeled from first leaves of incubated barley plants or from the elongation zone and emerged blade of leaf three. The strips were placed into buffers of specified pH for 30 min, before being examined under the confocal microscope. Calibration of fluorochromes was carried out with a Leica DMIL fluorescence microscope. The microscope's excitation filter was cut between 450 - 490 nm and the suppression filter at 515 nm. For pH calibration, 50 mM phthalate buffer (pH 4.0), 100 mM MES / KOH (pH 5.5, pH 6.5) and 100 mM TRIS-HCl (pH 7.5) was used. Digital images were analysed with ImageJ 1.41o software (http://rsbweb.nih.gov/ij) and Adobe® Photoshop® 7.0.1.

The pH dependence of fluorescence of 5(6)carboxyfluorescein and acridine orange were examined by recording fluorescence spectra at different pH using a FluoraMax-2® (Instruments S.A.) (pH 5.0; pH 5.5; pH 6.0 – 50 mM MES-KOH; pH 6.5 – 50 mM MES-BisTRIS and pH 7.0; pH 7.5 – 50 mM HEPES-HCl).

2.3 LVDT measurements

A linear variable differential transformer (LVDT) was used to measure changes in leaf length continuously and at micrometer resolution in response to treatments (compare Fricke, 2004; Fricke *et al.*, 2004). The setup could also be used to determine changes in cell wall properties.

2.3.1 Leaf growth measurements

Plants were prepared in the same way as for electrophysiological analyses to be able to relate the results from both types of experiments to each other. Leaves one and two were peeled back and the exposed elongation zone of leaf three was wrapped in washed (24 h in distilled water) tissue paper which was soaked in the respective test solution. The wet tissue paper guaranteed a humid microclimate and prevented the elongation zone from drying out; it also allowed application of test reagents to the apoplast of elongating tissue. The base 40 - 50 mm of leaf three was wrapped to provide sufficient mechanical support to allow the leaf to remain in an upright position. Above 50 mm from the leaf base, the cuticle is sufficiently developed preventing the leaf tissue from drying out (Richardson *et al.*, 2007). Roots were left in the same medium in which the particular plant had grown. The tip of leaf three was attached to fishing line and connected through cellotape to a LVDT (DFG 5.0; RS

Components, Corby, UK). A counterweight of 2 g was applied. The LVDT signal was digitalised with a Burster 92101 data logger module with ICP 100 software. Changes in voltage output were recorded on PC using Pfloek 1.09 software (LS Pflanzenökologie, Universität Bayreuth, Germany). The system was calibrated by replacing the plant with a micrometer screw. The rate of growth was calculated from LVDT outputs using Origin® 6.1 software (OriginLab Corporation) and Microsoft® Excel. Although leaf elongation rate was comparable between replicate plants and batches, values for treatments were expressed as percentage of the control to further minimise any plant-to-plant variation. The control value was the elongation rate of a particular plant attached to the LVDT before a treatment was applied. Typically, control plants had the elongation zone of leaf three wrapped with tissue paper soaked in either 1 or 0.1 mM KCl. It took up to 1 h for elongation rate to reach a steady level following attachment of plants to the LVDT. Application of vanadate and CsCl treatments required a similar period of stabilisation (about 1 h), while application of fusicoccin and ammonium treatments required leaf elongation rate to stabilise for up to 2 - 3 h. LVDT experiments were carried out at room temperature and humidity under ambient laboratory light.

To assess how much plant preparation affected the elongation rate of leaf three, intact plants which did not have leaves one and two peeled back, were attached to the LVDT. In addition, leaf elongation rate was determined for undisturbed plants in the growth chamber by measuring twice daily the increment in leaf length with a ruler.

2.3.2 Analysis of cell wall properties

Cell wall elasticity and plasticity was measured with the same LVDT system as described above by applying an additional 3 g counterweight for 10 min following the approach taken by Neumann (1993) (see also Chazen & Neumann (1994) and Sabrizhanova *et al.* (2005)). Plants were prepared and chemical treatments applied in the same way as for growth analyses. When the growth rate had stabilised (control, treatment), the additional 3 g counterweight was applied to the LVDT for 10 min and then removed; 30 - 40 min later, when growth rate had stabilised again, the experiment was repeated, and the average of these two measurements was used for calculations of wall properties. Elasticity and plasticity of walls and growth rate with and without the applied force (additional 3 g counterweight) was calculated from LVDT traces as detailed in Fig. 2.2.

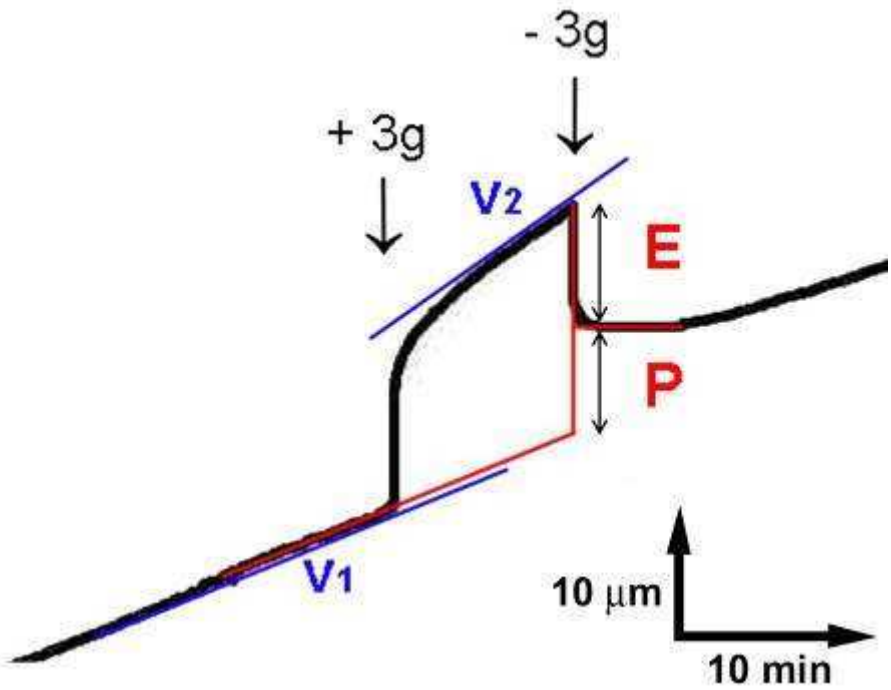

Figure 2.2 Measurement of cell wall properties

LVDT traces show the change in leaf length with time. LVDT traces before and after application of an additional 3 g counterweight (0.03 N of applied force), growth rates were calculated from the slope of the lines fitted to the stabilised part of traces (v_1 and v_2). The applied force caused an extension, part of which was reversible (elasticity, E) of wall) and part of which was irreversible (plasticity, P of wall).

2.4 Expression analyses

The aim of expression analyses was to test whether any elevated proton efflux in the leaf elongation zone was due to higher PM-H^+-ATPase expression.

2.4.1 Plant harvest

Plants were harvested 2 - 6 h into the photoperiod. Samples from the elongation zone were about 1 cm long and were cut from the mid-portion of the elongation zone (between 20 - 30 mm from the leaf base). Samples of the emerged blade were 1 - 2 cm long and taken from the mid-portion of the part of leaf three that had emerged from the sheath of leaf two. The leaf segments were weighed on a digital balance (Mettler Toledo, Sweden), immediately frozen in liquid nitrogen and stored at -80 ℃ until they were used for RNA extraction.

2.4.2 RNA extraction and cDNA synthesis

For RNA extraction, corresponding leaf segments from 3 - 4 plants were pooled; their combined fresh weight was between 0.04 - 0.07 g (Besse *et al.*, 2011) Total RNA was extracted using a QUIAGEN RNeasy kit following the manufacturer's instructions. RNA was eluted into 50 µl RNase free water. The concentration and quality of RNA was determined with Nanodrop® (ThermoFisher Scientific Inc., Waltham, USA).

After DNase treatment, following the manufacturer's instructions (Deoxyribonuclease I, Amplification Grade; Invitrogen Corporation, Carlsbad, California, USA), 1 µg RNA was used for cDNA synthesis. cDNA synthesis was performed as recommended by the manufacturer (SuperScriptTM II Reverse Transcriptase; Invitrogen Corporation, Carlsbad, California, USA) using anchor $oligo_dT_{16}$ primer. The final volume of cDNA was 20 µl. Details of the procedure and reagents used are provided in Table 2.4.

In some experiments, RNA was also extracted from protoplasts. RNA extraction from a protoplast suspension was carried out in a way similar to the one described above, with minor modifications. RNeasy lysis buffer (300 - 1000 µl) was added to 300 - 1000 µl protoplast suspension (~ 0.5 – 7 million protoplasts) or to 1 ml cell-free protoplast isolation medium. The latter was used as background control to reflect RNA released from broken cells or protoplasts into the isolation medium and was prepared by centrifuging the protoplast suspension at 30 g for 1 min and taking the supernatant and centrifuging it again at 12,000 g for 5 min. The final volume of RNA extract for protoplasts or isolation medium was 30 µl rather than 50 µl as obtained for leaf extracts.

Table 2.4 DNase treatment and reverse transcription

DNase treatment		Total volume
	1 µg (8 µl) RNA 1 µl 10x DNaseI Reaction buffer 1 µl (1 U) DNaseI Ampl. Grade enzyme	10 µl
	Incubation 15 min 25 ℃ 1 ml EDTA (25 µM)	11 µl
	Incubation 10 min 65 ℃	
Reverse transcription		
	11 µl sample from DNase treatment 1 µl anchor oligo-dT primer (100 µM) 1 µl $_d$NTP (10 mM)	13 µl
	Incubation 5 min 65 ℃ 4 µl 5x First-Strand Buffer 2 µl DTT (0.1 M)	19 µl
	Incubation 2 min 42 ℃ 1 µl SuperSript™ RT Enzyme (200U)	20 µl
	Incubation 50 min 42 ℃ then 70 ℃ 15 min	

2.4.3 PCR

Before cDNA samples were used for qPCR analysis, which required expensive reagents, the quality of cDNA, suitability of designed primers and optimum PCR conditions was tested through conventional PCR (G-Storm 482 thermocycler, Gene Technology). A GoTaq® Flexi DNA Polymerase (Promega Corporation, Madison, USA) kit was used in 25 µl total volume with 1 µl 200x diluted cDNA as template. A precise protocol of the PCR reaction is given in Table 2.5. Primers are listed in Table 2.6. The PCR was run in amplification two steps; after initial step (95 ℃; 30 s) through 35 cycle step one (95 ℃, 30 s) and step two (60 ℃, 60 s) were repeated and then a final step (72 ℃, 120 s) was used as Fig. 2.3 shows.

PCR products were separated on 1 % agarose gels in 0.5 strength TRIS base boric acid EDTA (TBA, see Table 2.7) buffer containing 1 µg ml^{-1} ethidium bromide and viewed under UV light (Image Master® VDS, Pharmacia Biotech, USA).

Table 2.5 Components of PCR reactions

Component	Volume	Final concentration
5x Green GoTaq® Flexi Buffer	5 µl	1x
MgCl Solution (25 mM)	2 µl	2 µM
dNTP (10 mM)	0.5 µl	0.2 µM each nucleotide
Forward primer (10 mM)	0.5 µl	0.2 µM
Reverse primer (10 mM)	0.5 µl	0.2 µM
GoTaq® DNA Polymerase (5 U / ml)	0.125 µl	0.625 U
Template cDNA (200x diluted)	1 µl	5000x diluted
Nuclease-Fee Water	15.375 µl	N/A
Total volume	25 µl	

Table 2.6 PCR primers

Primer name	Primer sequence
Anchor oligo$_d$T$_{16}$	5'NVTTTTTTTTTTTTTT3'
ATPase forward	5'ACATCGACACCATCAACCAA3'
ATPase reverse	5'ACAACTAGGGGCTGGTCAGA3'

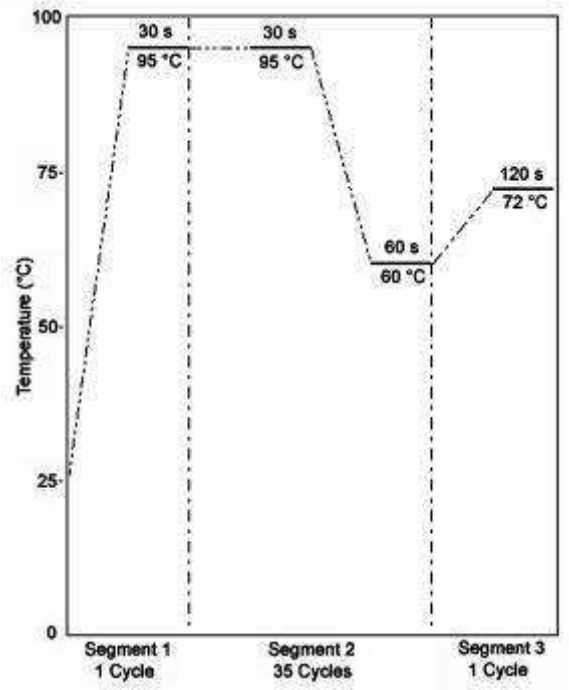

Figure 2.3 Thermal profile of the two step PCR reactions

Two step PCR protocol was used when quality of cDNA or primers were tested. This protocol was as similar as possible to the protocol used for qPCR analyses.

Table 2.7 Composition of the stock solution (5x concentrated) of TRIS base boric acid EDTA buffer (TBA)

Component	***Amount for 1 l***
TRIS base	53 g
Boric acid	27.5 g
EDTA (0.5 M, pH 8.0)	20 ml

2.4.4 qPCR

qPCR expression analysis was carried out on a real time thermal cycler STRATAGENE Mx3000P (Agilent Technologies, Inc., Santa Clara, USA), using a SYBRgreen master mix and following the supplier's instructions (SYBR®*Premix Ex Taq*™, Takara Bio Inc, Otsu, Japan) (see Table 2.8). The reaction mix was loaded onto 96-well plates (96 Multiply PCR plate natural, SARSTEDT AG & Co., Nümbrecht, Germany). Three technical and biological (independent batches of plants) replicates were run together with external standards (purified PM-H^+-ATPase PCR product; see below) on the same plate. Samples were maintained for 10 s at 95 ℃ as initial step, then 5 s at 95 ℃ and 30 s a t 60 ℃ through 45 cycles. After amplification, melting curves were recorded (95 ℃ 1 min then temperature gradient from 55 ℃ to 95 ℃ in 81 steps) to check product s ize and homogeneity, see also Fig. 2.4.

Table 2.8 Components of qPCR reaction

Component	Final Volume	Final concentration
SYBR®*Premix Ex Taq™*	6.25 µl	1x
Forward primer (10 mM)	0.25 µl	0.2 µM
Reverse primer (10 mM)	0.25 µl	0.2 µM
Rox Dye II	0.25 µl	N/A
Template cDNA (200x diluted)	1 µl	2500x diluted
Nuclease-Free Water	4.5 µl	N/A
Total volume	12.5 µl	

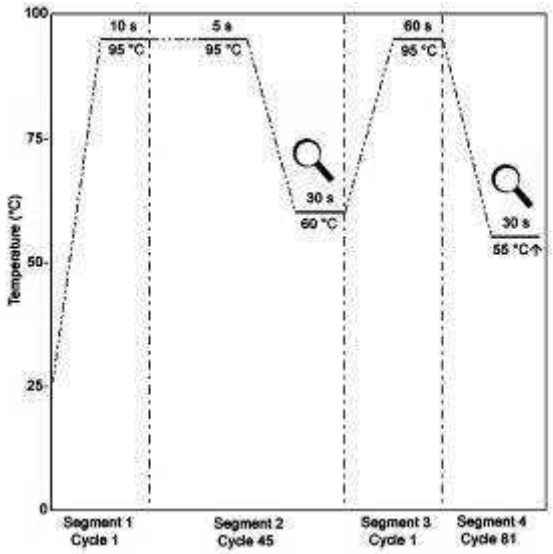

Figure 2.4 Thermal profile of qPCR reactions

Magnifying glass symbols indicate detection sites of SYBR Green fluorescence

To quantify the number of mRNA transcripts of the target gene (PM-H^+-ATPase), cDNA samples which contained known copy numbers of PM-H^+-ATPase cDNA molecules were required. This external standard was obtained by purifying PM-H^+-ATPase PCR product and a pCR®8/GW/TOPO construct that contained the ATPase PCR product as insert. Initially, the plasmids were used as an alternative external standard in addition to purified PM-H^+-ATPase. However, preliminary experiments showed that purification of plasmids from *E. coli* cells did not yield sufficiently pure product to use it as external standards.

To obtain purified ATPase PCR product, PCR was performed in 50 µl volume as described above using colourless reaction buffer. After the quality of PCR product was checked by running the samples on an agarose gel, the PCR product was cleaned with a NucleaSpin®Extract II PCR clean-up / Gel extraction kit (Macherey-Nagel GmbH & Co. KG, Germany) following the manufacturer's instructions. The purified DNA was eluted from the NucleaSpin®Extract II Column with nuclease free water. The DNA content was measured with Nanodrop® (ThermoFisher Scientific Inc., Waltham, USA) and the concentration / copy number of cDNA molecules was calculated from the expected molecular weight of the cDNA product for PM-H^+-ATPase (100,587 g mol^{-1}). From this purified stock, dilutions of 0.5, 5, 50, $5 \cdot 10^2$, $5 \cdot 10^3$, $5 \cdot 10^4$ and $5 \cdot 10^5$ copy μl^{-1} were prepared.

2.4.5 Analysis of qPCR data

An absolute quantification method was used to compare the PM-H^+-ATPase expression between elongation zone and fully developed emerged blade. This approach was chosen in favour of the conventional Δ-Ct approach (Pfaffl, 2001) because the generally most suitable reference gene of expression e.g. ubiquitin, gave more than one PCR product due to the existence of poly-ubiquitins. Using the Genevestigator (http://genevestigator.com) online application this problem (Hruz *et al.*, 2011) could not be solved.

To further relate the copy number of transcripts to a biologically relevant size, qPCR results were expressed per cell or per mm^2 plasma membrane surface. The total number of cells and plasma membrane surface contained in the plant material which was used for extraction was calculated based on the water content of leaf tissue, protoplast number and stereological electron and light microscopic analyses as detailed in section 2.5.

2.5 Cell size and tissue ratio measurements

Cell size and tissue ratio in different leaf regions (elongation zone and emerged leaf blade) were determined and data combined with published data to calculate the total number of cells which were contained in samples used for qPCR analysis.

2.5.1 Mesophyll and epidermis cell size

The diameter of mesophyll cells was measured on living protoplasts with the help of Scion Image for Windows 4.0.3.2 (http://www.scioncorp.com) software. The data were then combined with data obtained by Volkov *et al*. (2007, 2009) for the same barley cultivar (Golf) and data obtained by Kavanagh (2010) through stereological electron-microscopic analyses. Epidermal cell size was calculated based on stereological results of Kavanagh (2010) and a light-microscopic study of Fricke & Flowers (1998) on the same barley cultivar (Golf) studied.

2.5.2 Tissue ratio calculation in elongation zone and emerged blade

The percentage of cross-sectional leaf volume occupied by leaf tissues (epidermis; mesophyll including vascular parenchymateous bundle sheath; vascular bundles except parenchymateous bundle sheath) and intercellular air space was determined on paraffin-embedded toluidine blue-stained cross sections (few micrometers thick) with the help of Adobe® Photoshop® 7.0.1 and Scion Image for Windows 4.0.3.2 software. By assuming that intercellular air spaces did not contain any significant amount of liquid, but that almost all liquid was contained within tissues, it was possible to calculated the total water content (and approximate) volume of each tissue used for RNA extraction since the water content of leaf samples had been determined.

2.5.3 Cell size and plasma membrane surface estimation for qPCR analysis

Mesophyll cells volume and surface were calculated as they were spheres using the equation of $(\pi/6)d^3$ for volume and πd^2 for surface. Epidermis cells were treated as long rods. In the total cell volume different cell types were present as their corrected tissue share. Corrected tissue share was calculated as dividing the tissue share by (1-share of air space) because air space did not contains any living plant cell. The

whole calculation and data can find in the Results at section 3.3.2 and in the Appendix.

2.6 Plasma membrane isolation

Plasma membranes were isolated from barley seedlings following the approach developed by Kjellbom & Larsson (1984) and Yan *et al.*, (1998). All steps were performed under cold conditions. For each plasma membrane isolation between 1.5 – 6 g of plant material was required (elongation zone; emerged blade). Between 200 - 400 barley seedlings had to be grown and harvested in each experiment.

2.6.1 Plant harvest

Plant tissues, elongation zone (basal 40 mm without the lower 1 - 2 mm, containing meristematic zone) and emerged blade (leaf blade without the lower and upper 1 cm) of barley (cv Jersey) leaf three were harvested into 50 ml ice cold homogenisation buffer (all components are listed in Table 2.9). The tissues were gently vacuum infiltrated (3 times using a laboratory water jet vacuum pump) and used immediately for plasma membrane isolation.

Table 2.9 Composition of the homogenisation buffer used for membrane isolation

Component	***Final concentration***
Sucrose	500 mM
EDTA	2 mM (from 200 mM stock)
Glycerol	10 % (v/v)
BSA	0.5 % (w/v)
DTT	2 mM
PMSF	1 mM (prepared freshly from 12 mg ml^{-1} EtOH stock)
β-mercaptoethanol	5 mM
Non-soluble PVP	1 % (w/v)
Na-ascorbate	0.1 % (w/v) prepared freshly
HEPES-KOH	50 mM set to pH 7.8

2.6.2 Preparation of microsomal fraction

Tissues were homogenised in the homogenisation buffer with a razor blender (3 times 25 sec). The homogenate was filtered through four layers of gauze and one layer of Miracloths (Fisher Scientific). The filtrate was centrifuged at 11,500 g for 10 min at 4 ℃ (Sigma 3K15 and 3K10 bench top centrifu ge, fixed angle rotor). The supernatant was collected and centrifuged at 30,000 rpm (~82,000 g) in a

Beckman L7-65 ultracentrifuge for 40 min with a SW40Ti swinging bucket rotor. The resulting microsomal pellet was resuspended in phase buffer (Table 2.10).

Table 2.10 Composition of the phase buffer used for membrane isolation

Component	***Final concentration***
Sucrose	330 mM
KCl	3 mM
KH_2PO_4	5 mM
K_2HPO_4	5 mM
KOH	To adjust buffer to pH 7.8

2.6.3 Purification of plasma membrane vesicles

The microsomal fraction was further fractioned by a two-phase aqueous dextran T-500 and PEG-3350 system. From the polymers, 20 % (w/w) (dextran) and 40 % (w/w) (PEG) stock solutions were made in phase buffer. The final concentration of both polymers was 6.1 % (w/w) in the start tube, taking into account dilution through addition of phase buffer and resuspended microsomal fraction. The final weight of the tube was 12 g. The tube was mixed by inversion 30 times and the phase separation was carried out by centrifugation at 1,500 g at 4 °C (Sigma 3K15 and 3K10 bench top centrifuge with swinging bucket rotor) for 25 min. The upper phase was transferred into a new tube and completed to 12 g with fresh lower phase (prepared separately with the help of extraction funnel). The separation was done as before but for 15 min, and this purification step was repeated 3 - 4 times until the upper phase became clear and did not show any green colour (which would have been indicative of contamination with chloroplast membranes) (Fig. 2.5). The final upper phase was diluted 3 - 4x with phase buffer and ultracentrifuged (35,000 rpm, 1 h). The pellet was resuspended in resuspension buffer (Table 2.11) and washed by ultracentrifugation (35,000 rpm, 1 h) two times in resuspension solution. The final purified pellet was resuspended in 50 - 150 µl resuspension buffer and divided into aliquots, frozen in liquid nitrogen and stored at -80 ℃.

Table 2.11 Composition of the resuspension buffer used for membrane isolation

Component	***Final concentration***
Sucrose	330 mM
KCl	3 mM
KOH	To set pH 7.8

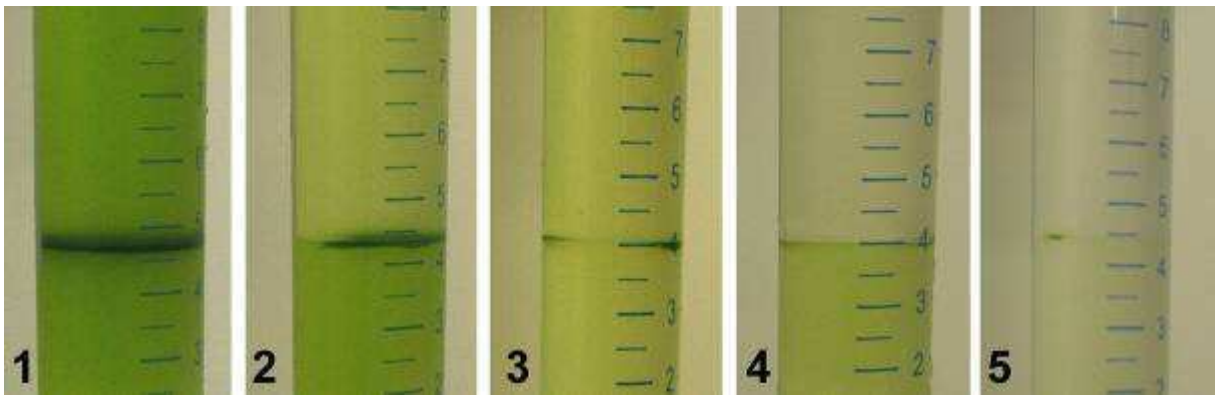

Figure 2.5 Five purification steps during plasma membrane isolation.

The upper phase becomes less and less green (indicative of thylakoid contamination). After the 5th step the upper phase is clear, no green colour is seen.

2.7 Determination of the total protein content of plasma membrane vesicles

2.7.1 Bradford method

The protein content of plasma membrane preparation was estimated using the method of Bradford (Kruger, 2002). The reagent was prepared and filtered through Whatman no. 1 filter paper. It was stored at room temperature in an amber bottle and used within weeks. The composition of the reagent is given in Table 2.12. The assays were carried out in duplicates in 1.1 ml final volume. For the calibration curve 0, 1, 2, 4, 6 and 8 μg bovine serum albumin (BSA) was used as standards. Absorbance was measured at 595 nm between 5 to 15 min following addition of Bradford reagent to samples (PerkinElmer Lambda25 UV/VIS Spectrophotometer)

Table 2.12 Composition of Bradford reagent

Component	***Amount of the component***
Coomassie Brilliant Blue G250	100 mg dissolved in 50 ml 95 % ethanol
Phosphoric acid 85 %	100 ml
Distilled water	Made up to 1 l

2.7.2 Densitometric analysis of Laemmli gels

The final values of protein concentration (used for ATPase assay, densitometry on polyacrylamide gels and Western blot analysis) were calculated from Laemmli gels (Sárvári et al, unpublished) using the modified protein solubilisation described below. Known volume of membrane vesicle sample (determined based on protein measurement using Bradford method, usually between 5 - 30 μl) were run on a gradient SDS polyacrylamid gel together with protein standards (Sigma). The amount

of total membrane protein was calculating by densitometry by Phoretix 4.01 software (Phoretix International). A typical gel photo is shown in Fig. 2.6.

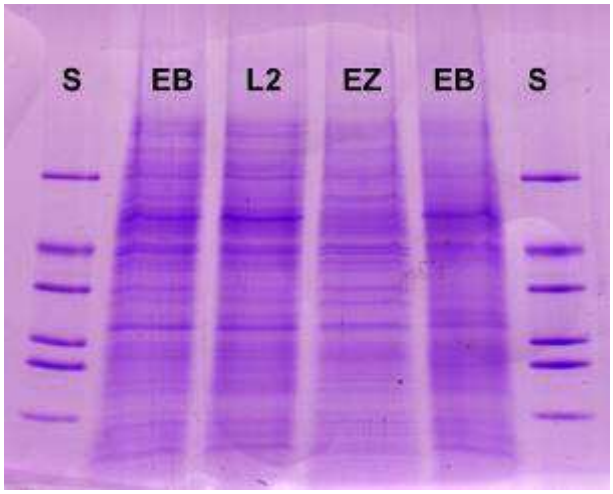

Figure 2.6 Typical gel for the measurement of protein content of plasma membrane samples

Coomassie Brilliant Blue R250 stained SDS gels were used to determine the total membrane protein content of different samples through a densitometric approach. EB – emerged leaf blade of leaf three; EZ – elongation zone of leaf three; L2 – mature blade of leaf two; S – Sigma protein standard, with a total protein content of 17.5 μg (2.5 μg each band) and proteins of molecular weights 66 (uppermost band), 45, 36, 29, 24, 20.1 and 14.2 kDa (lowermost band).

2.8 Polyacrylamide gel electrophoresis (PAGE)

Qualitative and quantitative analyses were carried out on isolated plasma membrane vesicles using polyacrylamide gel electrophoresis (PAGE).

2.8.1 Gradient polyacrylamide gel electrophoresis (PAGE)

A gradient polyacrylamide gel electrophoresis was performed based on (Laemmli, 1970), with some modification in the solubilisation of membrane protein, to check the quality of isolated plasma membrane fraction and quantify its (total) protein content.

2.8.1.1 Solubilisation of membrane protein

To optimise the solubilisation of plasma membrane protein, the approach taken by Kjellbom & Larsson (1984) was followed. TritonX®-100 detergent was added to the Laemmli buffer. Equal volumes of 0.1 % TritonX®-100 and plasma membrane suspension were mixed and vortexed. The mixture was then combined with an equal volume of Laemmli buffer (Table 2.13), incubated at room temperature for 30 min

and heated (90 °C) three times for 10 s each followed by vortexing. Non-solubilised protein was removed by centrifugation (5 min at 10,000 g) and the supernatant used for PAGE. With this modified solubilisation procedure, almost all protein was solubilised and no pellet was observed after centrifugation. In addition, gel bands stained with Coomassie Brilliant Blue R250 were much sharper and distinct (Fig. 2.7).

Table 2.13 Composition of Laemmli buffer used for PAGE

Component	***Concentration in the agent***	***Final concentration***
TRIS-HCl pH 6.8	2.3 % (w/v)	0.76 % (w/v)
SDS	7.15 % (w/v)	2.38 % (w/v)
Glycerol	30 % (v/v)	10 % (v/v)
DTT	5.5 % (w/v)	1.83 % (w/v)
Bromophenol blue	0,003 % (w/v)	0.001 % (w/v)

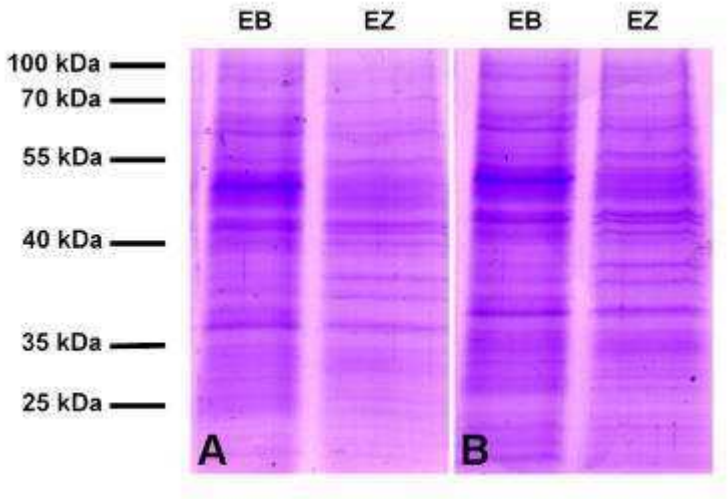

Figure 2.7 Coomassie Brilliant Blue R250 stained gradient PAGE gels which were loaded with plasma membrane protein solubilised in two different ways

Plasma membrane protein was solubilised using the conventional Laemmli solubilisation method (A) or a modification involving TritonX®-100 (B). The bands are sharper and more distinct using the modified solubilisation method. Samples were derived from the elongation zone (EZ) and emerged blade (EB) of leaf three of barley.

2.8.1.2 Gradient PAGE gel system

Solubilised proteins were separated on 7 cm long 10 - 18 % gradient gels in a MiniProtean (BioRad Laboratories, Inc.) gel running system based on Laemmli (1970) under 20 mA / gel at 4 °C until the bromphenol blue front exited the gel (after about 2 h). The components of the gel are listed in Table 2.14. The acrylamide / bis-acrylamide ratio was 30:0.8.

Table 2.14 Components of the gradient PAGE system

Stacking gel

Component	*Concentration in the gel*
Acrylamide	5 % (w/v)
TRIS-HCl, pH 6.8	125 mM
SDS	0.1 % (w/v)
TEMED	0.01 % (v/v)
APS (ammonium persulfate)	0.1 % (v/v)

Separation gel

Component	*Concentration in the gel*
Acrylamide	10 - 18 % (w/v) linear gradient
TRIS-HCl, pH 6.8	375 mM
SDS	0.1 % (w/v)
TEMED	0.013 - 0.017 % (v/v) gradient
APS	0.04 % (v/v)

Gel running buffer

Component	*Concentration in the buffer*
TRIS, pH 8.3	25 mM
Glycine	192 mM
SDS	0.1 % (w/v)

The polyacrylamide gel was stained overnight with Coomassie Brilliant Blue R-250 and washed 3 - 4 times with washing solution (Table 2.15) on a horizontal swinging table (BIOSAN Multi MR-12). After the final washing step the gel was placed into distilled water for 20 min and then scanned with an UMAX Aster-1220S gel scanner. Each gel was stored for longer-term use in 7 % acetic acid solution.

Table 2.15 Components of the solutions for Coomassie Brilliant Blue gel staining

Coomassie brilliant blue stain

Component	*Concentration*
Coomassie brilliant blue R-250	1 % (w/v)
Methanol	41.67 % (v/v)
Acetic acid	16.66 % (v/v)
Distilled water	41.67 % (v/v)

Washing buffer

Component	*Concentration*
Methanol	30 % (v/v)
Acetic acid	10 % (v/v)
Distilled water	60 % (v/v)

2.8.2 Linear (12 %) PAGE

For Western blotting at UCD, Dublin, linear (12 %) polyacrylamide gels were used for protein separation. Purified and solubilised plasma membrane samples were run on the polyacrylamide gels using a Hoefer^{TM} SE260 gel running system (Hoefer Inc, USA) at 240 V and 80 mA for 1.5 h using the same gel running buffer as described before (Table 2.14). For gel electrophoresis a 12 % separation and 4 % stacking gel were prepared following the instructions of the manufacturer (ProtoGel® 30 % Kit, National Diagnostics, U.S.A.). Each well was loaded with 5 µg total membrane protein. Gels were not stained, but separated proteins were blotted to nitrocellulose membrane to quantify PM-H^+-ATPase content of the samples by Western blot analysis.

2.9 ATPase assay

The ATPase assay was designed based on the method described by Sarkadi *et al*. (1992) and Pitann *et al.* (2009b). The ATP-dependent release of inorganic phosphate was followed. Precisely 3 µg total membrane protein was incubated in 100 µl reaction buffer (Table 2.16) at 28 ℃ for 60 min in a BIOSAN TS-100 Thermo Shaker. The reaction was stopped through addition of 50 µl 10 % (w/v) phosphate free SDS. For colour development, 400 µl colour developing reagent (Table 2.16), 1 ml ultra-pure water and 200 µl 1 % freshly made ascorbic acid solution were added in succession to each reaction tube. Colour development occurred at 37 ℃ and was completed within 20 - 30 min. Within 1 min following the end of colour development, the absorbance of samples was read at 880 nm using a PerkinElmer Lambda25 UV/VIS Spectrophotometer. Appropriate standards (0, 10, 20, 40, 60 nmol P_i per sample of K_2HPO_4) were always run in parallel to samples and used to convert absorbance readings into nmol P_i generated.

Table 2.16 ATPase reaction buffer and colour development reagent

ATPase reaction buffer

Component	*Concentration*
MES-KOH, pH 6.5	10 mM
$MgSO_4$	5 mM
Sodium ATP	5 mM
KCl	50 mM
KNO_3	50 mM
Brij58	0.02 % (w/v)
NaN_3	10m M

Colour developing reagent for ATPase reaction

Component	*Concentration*
H_2SO_4	2.5 M
Ammonium molybdate	1 % (v/w)
Potassium antimony (III) oxid tartrate	0.014 % (v/w)

2.10 Approach for light microscopy

2.10.1 Fixation of leaf tissue

Leaf pieces (1 cm in length) from the elongation zone and emerged blade were fixed in 4 % formalin (overnight, 4 ℃). To facilitate th e penetration of the fixative, samples were vacuum infiltrated (3 times for 10 sec) using a Millipore WP6122050 vacuum pump (Millipore, USA).

2.10.2 Dehydration and embedding

Dehydration of leaf tissue was achieved through an ethanol series, and tissues were cleared with Neo-clear® and embedded into paraffin wax. Details of the protocol are given in Table 2.17. Sections of 5 µm thickness were cut using a MicroTec® 4060 rotary microtome (MicroTec Laborgeräte GmbH, Germany). Sections were mounted on slides and dried at 37 ℃ (overnight) and staine d. For immunostaining, samples were mounted on APTES (3-aminopropyltriethoxysilane) coated slides, prepared based on the instruction of the supplier (Sigma-Aldrich), to prevent tissue damage during the overnight staining procedure. Slides were washed in absolute ethanol before coating and were immersed into 2 % APTES (dissolved in absolute ethanol) for 5 s, briefly rinsed in ethanol, washed in running tap water (5 min), rinsed in distilled water and dried overnight at 55 - 60 ℃.

Table 2.17 Fixation and embedding of leaf samples for immunohistochemistry

Fixation		
	Solution	***Duration***
	4 % Formalin	Overnight, 4 ℃
Dehydration		
	Solution	***Duration***
	30 % Ethanol	1 h
	50 % Ethanol	1 h
	70 % Ethanol	1 h
	90 % Ethanol	1 h
	96 % Ethanol	1 h
	Absolute Ethanol	2x 1 h
Clearing		
	50 - 50 % Ethanol Neo-clear®	Overnight, 4 ℃
	Neo-clear®	2x1 h
Infiltration		
	Neo-clear®-wax	30 min
	50 - 50 % Nea-clear®-wax	1 h, 65 ℃
	100 % wax	2x 1 h, 65 ℃

2.10.3 Staining with toluidine blue

Paraffin-embedded sections were rehydrated, stained with 1 % (w/v) aqueous toluidine blue, washed, dehydrated, cleared and mounted in Entellan® mountant (Table 2.18). Sections were examined with a Leica DMIL and Olympus BX60 microscope.

Table 2.18 Staining embedded leaf sections with toluidine blue

Rehydration		
	Solutions	***Duration***
	Neo-Clear® A	10 min
	Neo-Clear® B	10 min
	Absolute ethanol	5 min
	96 % ethanol	5 min
	70 % ethanol	2 min
	Running water	5 min
Staining		
	1 % aqueous toluidine blue	10 min
	Running water	5 min
Dehydration		
	70 % ethanol	Dip twice
	96 % ethanol	Dip four times
	Absolute ethanol 1	5 min
	Absolute ethanol 2	5 min
	Neo-clear® C	5 min
	Neo-clear® D	5 min
Mounting		
	Entellan®	Mount under cover slip

2.11 Immunological methods for PM-H$^+$-ATPase detection

2.11.1 Qualitative Western blot analysis

At Eötvös University the PM-H$^+$-ATPase content of the isolated membrane vesicles and identity and molecular weight of PM-H$^+$-ATPase protein was determined using Western blotting. Gradient SDS polyacrylamide gels were run as described above. Separated proteins were transferred onto nitrocellulose membrane (Hybound^{TM}-C Extra, Amesham-Pharmacia, USA) using the Mini Transfer Blot (BioRad Laboratories, Inc.) system. The composition of blotting buffer is given in Table 2.19. Protein transfer was carried out in an ice-cold buffer tank (4 ℃) at 90 V constant voltage (I < 0.4 A) for 2 - 3 h.

Table 2.19 Composition of blotting buffer used for Western analyses

Component	***Concentration***
TRIS-HCl, pH 8.3	25 mM
Glycine	192 mM
Methanol	10 % (v/v)
SDS	0.01 % (w/v)

The blotted and washed nitrocellulose membrane was blocked with 3 % (w/v) gelatine in TRIS buffer saline (TBS) for 1h (composition is given in Table 2.20). As primary antibody, plant PM-H$^+$-ATPase specific polyclonal rabbit IgG (Agrisera, Uppsala, Sweden) was used at 1,000x dilution in TBS buffer containing 1 % gelatine (overnight; room temperature). Non-bound antibody was removed by washing the membrane in Tween®20 TRIS buffer saline (TTBS) (Table 2.21), twice for 20 min, followed by two washes for 20 min each in TBS. Horseradish peroxidase (HRP)-labelled anti rabbit IgG produced in goat (BioRad Laboratories, Inc.) was used as secondary antibody. It was used at 3,000x dilution in TBS buffer (2 h). The membrane was washed in the same way as described for primary antibody and was then developed in developing solution (0.06 % (w/v) HRP Colour Development Reagent^{TM} (BioRad Laboratories, Inc.)). The colour development reagent contained 4-Cl-1-naftol as active component and was dissolved in -20 ℃ methanol and 0.015 % H_2O_2 in TBS. The bands were digitalized (HP Scanjet) before the membrane had dried out.

Table 2.20 Composition of TRIS buffer saline buffer (TBS)

Component	*Concentration*
TRIS-HCl, pH 7.5	20 mM
NaCl	150 mM

Table 2.21 Composition of Tween®20 TRIS buffer saline buffer (TTBS)

Component	*Concentration*
TRIS-HCl, pH 7.5	20 mM
NaCl	150 mM
Tween®20	0.005 % (w/v)

2.11.2 Quantitative Western blot analysis

Plasma membranes could only be isolated at Eötvös University, yet the more sensitive Western blot system was available at UCD, Dublin. Therefore, Western analyses of plasma membrane fractions were carried out not only at Eötvös University but also at UCD using plasma membrane vesicle samples which had been brought back (flight back from Hungary) on dry ice. The Western analyses system at UCD was the same one as described by Collins *et al*. (2011).

The separated proteins were blotted onto nitrocellulose membrane (Whatman® PROTRAN BA 85) using a Hoefer™ TE22 blotting system, at 40 V and 120 mA overnight at room temperature. The gel running buffer contained 20 % (v/v) methanol. Blotted nitrocellulose membranes were stained with Ponceau S stain (Sigma) and washed with washing buffer (0.2 % Tween®20 containing gel running buffer). Thereafter, membranes were blocked with 5 % skimmed milk powder in washing buffer for 1 h, at 30 rpm on a horizontal shaker. Primary antibody ($PM\text{-}H^+$-ATPase specific polyclonal rabbit IgG antibody; Agrisera, Sweden) was applied overnight at 2,500x dilution in washing buffer containing 5 % milk powder, at 30 rpm shaking. Non-bound primary antibody was removed through washing three times (10 min each; 70 rpm) in washing buffer. Peroxidase-labelled anti rabbit IgG produced in goat (Invitrogen Corporation, Carlsbad, California USA) was applied as secondary antibody at 10,000 x dilution in washing buffer containing 5 % milk powder (2 h; 70 rpm). After three final washes (10 min each) in washing buffer, bound secondary antibody was visualised through an EZ-ECL Chemiluminescence Detection Kit for HRP (Biologica Industries, Israel) and LAS-4000 Luminescence Image Analyser (Fujifilm, USA).

2.11.3 Immunostaining of paraffin-embedded sections

PM-H^+-ATPase tissue specific localisation was determined on paraffin-embedded samples using immunohistochemistry. The same PM-H^+-ATPase specific primary antibody was used as for Western blotting. Anti rabbit IgG alkaline phosphatase-labelled antibody, produced in goat (Sigma), was applied as secondary antibody as detailed in Table 2.22. Colour development was carried out with SIGMAFAST™ Fast Red TR / Naphthol AS-MX Tablets (Sigma) following the instructions of the manufacturer. Colour development was stopped with 7 % acetic acid. After a 5 min washing in running tap water, samples were mounted in 80 % glycerol in phosphate buffered saline (PBS, its composition is given in Table 2.23) under a cover slip.

Table 2.22 Protocol for immunostaining of embedded leaf sections

	Solutions	***Duration***
Rehydration		
	Neo-Clear® A	10 min
	Neo-Clear® B	10 min
	Absolute ethanol	5 min
	96 % ethanol	5 min
	70 % ethanol	2 min
	Running water	5 min
Blocking		
	5 % (v/v) goat serum in PBS	10 min
Staining		
	Primary antibody (100x diluted) in 2.5 % (v/v) goat serum in PBS	Overnight, 4 ℃
	Washing with PBS	3x 5 min
	Secondary antibody (30x diluted) in 2.5 % (v/v) goat serum in PBS	2 h
	Washing with PBS	4x 5 min
Colour development		
	SIGMAFAST™ Fast Red	2 - 10 min
	5 % (v/v) acetic acid	1 - 5 min
	Running water	5 min
Mounting		
	80 % glycerol in PBS	Mount under cover slip

Table 2.23 Composition of phosphate buffer saline (PBS; pH 7.4)

Component	**Concentration (mM)**	**Concentration (g / l)**
NaCl	137	8.00
KCl	2.7	0.20
$Na_2HPO_4x2H_2O$	8.1	1.44
KH_2PO_4	1.76	0.24

2.11.4 Densitometric analysis of Western blots

Densitometric analysis of Coomassie-stained polyacrylamide gels and Western blots was carried out with a Photetix 1D Advanced 4.01 system (Phoretix International, Newcastle, UK). Raw data were processed using Microsoft® Office Excel 2003 (Microsoft Corporation, USA) and Origin®6.1 (OrigiLab Corporation, USA) statistical software.

2.12 Protoplast experiments

2.12.1 Protoplast isolation

Protoplasts were isolated according to Volkov *et al.* (2007), with some modifications.

Osmolality of the isolation buffer, incubation time and shaking frequency were optimised. Cell walls and middle lamellae from tissue of the elongation zone were digested in 500 mOsm kg^{-1} isolation buffer with 90 rpm shaking frequency over a period of 2 - 3 hours in the dark, while pieces of the emerged blade were incubated in isolation buffer of 600 mOsm kg-1 osmolalility, over a 1 h period and at 160 rpm shaking frequency in the dark.

Cell wall digestive enzymes (Table 2.24) were dissolved in isolation medium (components are in Table 2.25) overnight, at 4 ℃, without any shaking or vortexing. Prior to use, enzyme solutions were centrifuged (5 min, 10,000 g, mini Spin plus, Eppendorf AG, Hamburg, Germany) and the supernatant was used for cell wall digestion.

Table 2.24 Composition of protoplast isolation buffer

Component	***Concentration***
Murashige and Skoog salt	4 g l^{-1}
MES	10 mM
Sorbitol	500 - 600 mOsm kg^{-1}
PVP K30	0.025 % (w/v)
BSA	0.1 % (w/v)
KOH	Used to adjust to pH 5.7

Table 2.25 Enzyme concentrations in protoplast isolation buffer

Enzyme	***Concentration***
Cellulase	1 % (w/v)
Driselase	0.5 % (w/v)
Pectolyase	0.05 % (w/v)

2.12.2 Purification of protoplasts

After enzymatic digestion of the cell wall, protoplast were passed through a 100 μm mesh and washed with 4 - 5 volume isolation buffer. Protoplasts were collected by centrifugation (30 g, 2 min; Eppendorf 5810 R, swinging bucket rotor) and resuspended in 0.3 – 1 ml volume using isolation buffer. Viability of protoplasts was tested using 0.001 % (w/v) fluorescein diacate (Larkin, 1976), which was prepared from a 0.1 % (w/v) acetone stock. Protoplasts were viewed with a Leica DMIL fluorescence microscope equipped with an excitation filter (450 - 490 nm) and suppression filter (515 nm).

Protoplasts were counted with a Neubauer ultra plane counting chamber (Hausser Scientific) under a Leica DMIL microscope. These data were used to relate expression values obtained through qPCR experiments to protoplast number.

2.12.3 Calculation of size and surface of the protoplast

The diameter of protoplasts was measured on micrographs taken with a Leica DMIL microscope with the help of Scion Image for Windows 4.0.3.2 software. From the diameter (d), the protoplast volume, $((\pi/6)d^3)$ and surface (πd^2) could be calculated,due to the almost perfectly spherical shape of protoplasts.

2.13 Statistical analysis

Statistical analysis was carried out with Origin® 6.1 (OriginLab Corporation) software, using paired and independent Student's t test and one-way ANOVA.

3 Results

3.1 Apoplastic pH measurements

Apoplast pH was measured through three independent approaches: in-vitro gel system, electrophysiology and confocal microscopy. The in-vitro gel system involved incubating leaf segments in agarose containing a pH indicator that made it possible to directly relate changes in apoplast acidity to changes in growth. With pH microelectrodes precise values of apoplast pH in growing and non-growing leaf regions could be obtained. Finally, confocal microscopy involved loading plants with pH fluorescence probes and had the advantage that intact plants could be studied.

3.1.1 In-vitro agarose gel system

The base 70 mm of leaf three was placed in agarose gel medium containing the pH indicator bromocresol purple. Growth was monitored parallel to acidification of the medium. The basic assumption underlying this experiment was that any changes in the extent of acidity of the medium adjacent to leaf tissue reflected similar changes in the net H^+ production rate (due to PM-H^+-ATPase activity) in the tissue's apoplast. 'Extent' of acidity can refer to either or both, changes in pH and changes in the area of medium which was acidic. Gel images of a typical set of experiments, involving application of fusicoccin and vanadate, are shown in Fig. 3.1 A-C.

There was a non-specific acidification of medium with a maximum acidification at the first hour following the placement of unpeeled leaf segments into the agarose. This acidification, which most likely reflected changes in apoplast pH caused by the unpeeling and which was not restricted to the base 40 mm (leaf elongation zone), disappeared within 4 - 5 h and then reappeared in a growth-dependent manner (Fig. 3.2 A and B). Growth dependency of acidification was also tested by applying an initial (0 - 24 h) cold treatment. There was no acidification of medium and no growth either during the cold treatment (Fig. 3.3). As soon as the cold treatment finished, growth resumed parallel to the acidification of medium (Fig. 3.3).

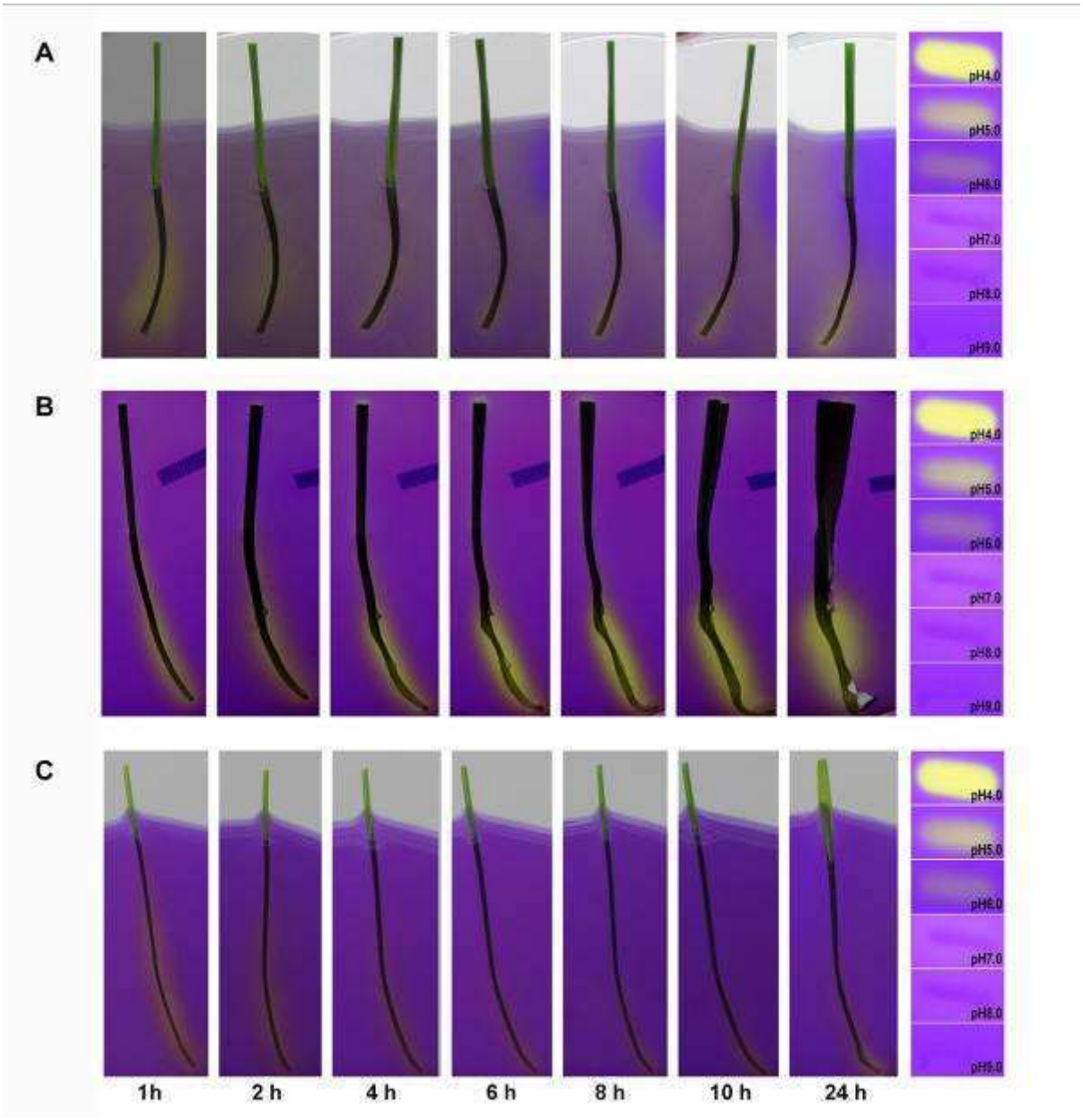

Figure 3.1 Leaf growth and apoplast acidification as analysed through the agarose gel system

Typical images of an experiment involving control leaves (A) and leaves which were placed in agarose containing 5 µM fusicoccin (B) and 500 µM vanadate (C). Scale bar is 1 cm long.

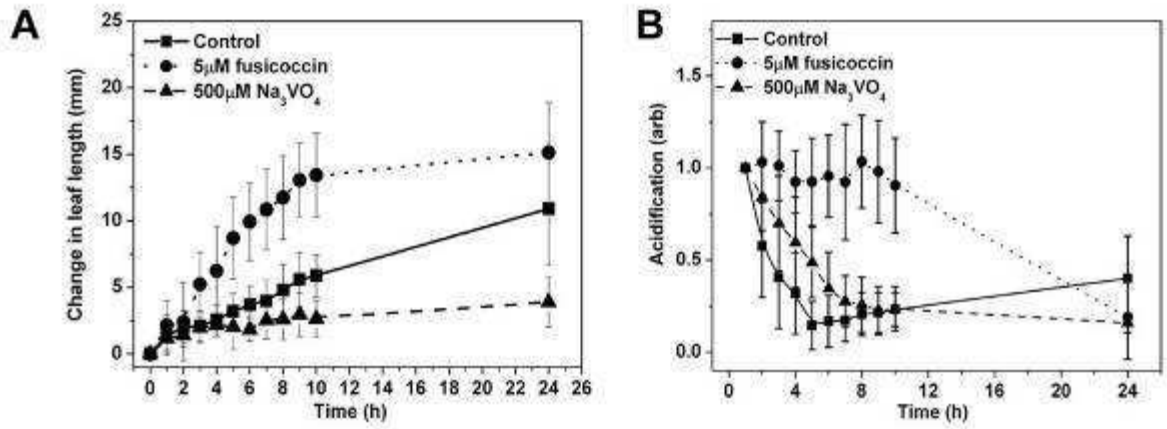

Figure 3.2 Time course of growth and acidification of in-vitro gel experiments

Typical time course of changes in leaf length (A) and medium acidification (B) in response to treatments are shown. Values are averages and standard deviations (error bars) of 27 (control) and 10 (treatments) plants.

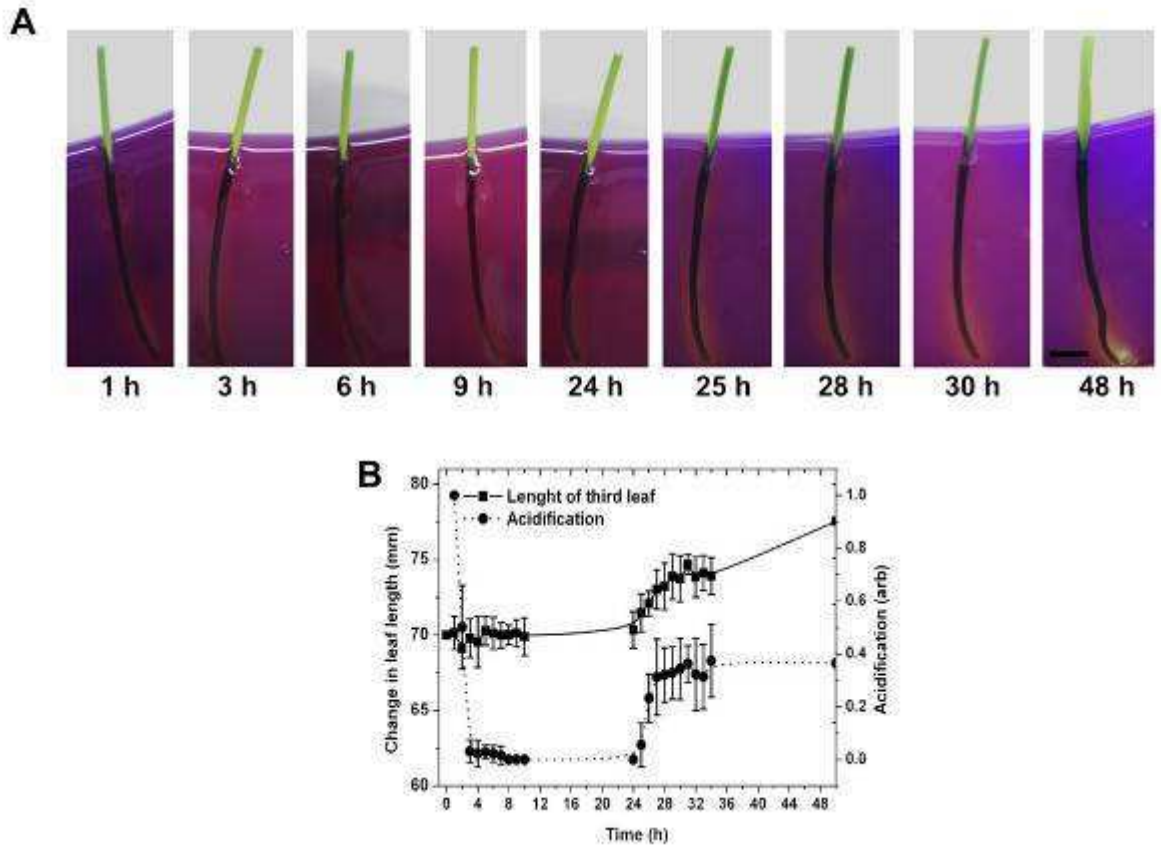

Figure 3.3 Leaf growth and acidification in agarose gel under cold treatment

Typical images of an experiment involving cold treated leaves 0–24 h and under control condition 24 - 48 h (A). Scale bar represents 1 cm. Response of medium acidification and change in leaf length (growth) to cold treatment and subsequent incubation in the growth chamber (B); values are averages and standard deviations (error bars) of 10 plants.

A range of treatments was tested for their effect on medium acidification and leaf growth (Fig. 3.4). Fusicoccin increased significantly leaf elongation rate and medium acidity. Vanadate caused the opposite effect, as did caesium, which inhibits K^+ channels (Szczerba *et al.*, 2009; Volkov *et al.*, 2009).

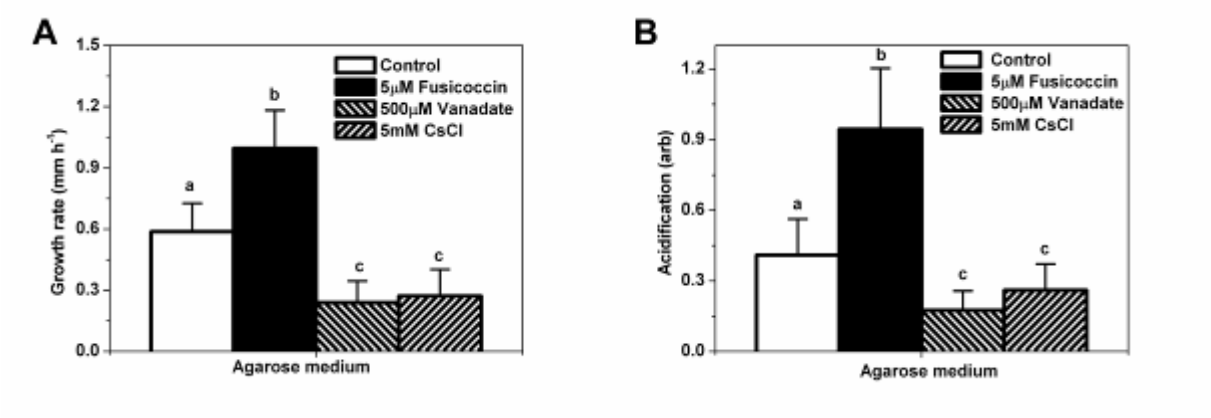

Figure 3.4 Average rate of leaf elongation (A) and medium acidification (B) in leaves exposed to fusicoccin, vanadate and caesium treatments as tested through the agarose gel system

All media contained 10 mM KCl and test reagents were applied at 5 μM (fusicoccin), 500 μM (vandate) or 5 mM (CsCl). Values are averages and standard deviations of 20 (control), 9 (fusicoccin), 7 (vanadate) and 14 (CsCl) plants. Different letters show a statistically significant difference at $p < 0.05$ (Student's t-test and ANOVA).

Although auxin-induced growth is often related to cell wall acidification and referred to as 'acid growth', no such stimulation of either growth or acidification was observed in the present study. Using in-vitro gel system and applying the artificial auxin, α-Naphthaleneacetic acid (NAA), growth did not change and acidification was similar to control. If anything, acidification of NAA treated plants continuously decreased whereas control plants started to slightly decrease after 5 h (Fig. 3.5).

Auxin-induced growth was not detected either when the experiment was carried out in liquid medium (10 mM KCl and 1 mM $CaCl_2$ without agarose and bromocresol purple) to check whether the absence of any auxin effect was due to conditions associated with the agarose gel. To check whether it was possible to induce any auxin-specific effects, coleoptiles were tested since these represent the classical 'acid growth' system. A significant increase in growth was measured (Fig. 3.6).

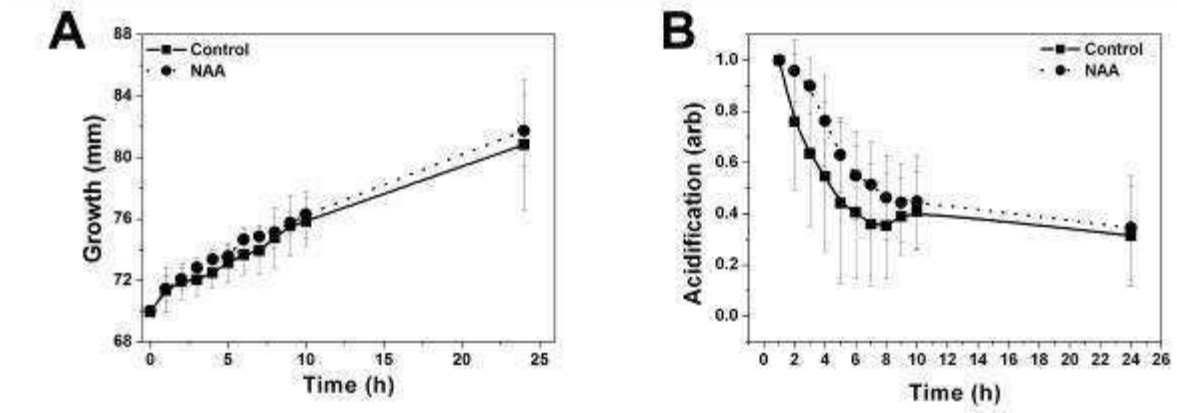

Figure 3.5 Effect of auxin on leaf growth and medium acidification using the in-vitro gel system

Difference in growth (A) was not found between 5 μM NAA treated and control plants. Medium acidification was similar in auxin-treated and non-treated (control) leaves (B). Traces are average of 10 - 27 plants, error bars represent standard errors.

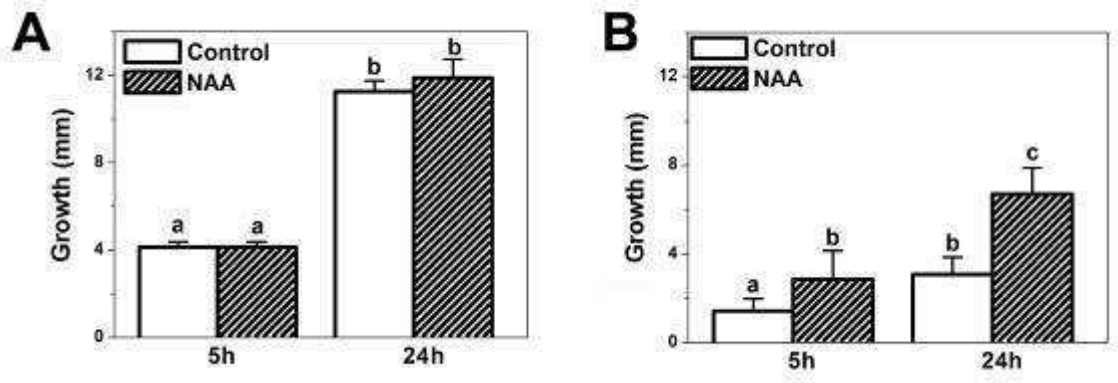

Figure 3.6 Growth effect of auxin when applied in liquid medium

NAA (5 μM) effect on growth was tested in liquid medium on leaf (A) and coleoptile pieces (B). Measurements were carried out at 5 h and 24 h of incubation. Values are averages and standard deviations (error bars) of 4 leaf pieces and 40 coleoptile segments. Different letters show a statistically significant difference at $p < 0.05$ using Student's t-test and ANOVA.

3.1.2 Microelectrode measurements

Microelectrode measurements of apoplastic pH in the growing leaf three showed that the pH in the elongation zone was by up to one pH unit lower than the pH in the emerged blade (Fig. 3.7 A). Apoplastic pH in the elongation zone depended on the K^+ concentration in the bathing medium which was in direct contact with the leaf surface during measurements. At the lowest K^+ concentration tested (0.1 mM), apoplast pH was 4.8. Apoplast pH increased with the K^+ concentration of the medium. At 10 mM K^+, apoplast pH in the elongation zone was 5.8 and

indistinguishable from the value in the emerged blade. In contrast to apoplast pH in the elongation zone, apoplast pH of the emerged blade did not change with bathing medium K^+. When the pH of the bathing medium was adjusted to pH 7.0 using KOH (final K concentration of 0.3 - 0.5 mM) apoplastic pH in the elongation zone was between 4.8 and 5.2. This proved that the lower apoplastic pH measured in the elongation zone was independent from the pH of the bulk (bathing) solution which was in direct contact with the apoplast, when the solution did not contain any buffer component. When the pH of the bathing solution was adjusted to pH 7.0 using 100 mM TRIS-HCl, including 0.1 mM KCl, the pH of the apoplast was 6.1 - 6.2 in both elongation zone and emerged blade (Fig. 3.7 B). Although this pH was lower by almost one pH unit than the pH of the bathing medium, this experiment showed that apoplast pH of the emerged blade was responsive to changes in the composition of the bathing medium and that the two were in direct contact. Bathing medium must have bypassed the cuticle and entered leaves through stomata. Growth of leaves on the microelectrode stage was not affected by K^+ treatments, despite the K^+-dependency of apoplast pH (Fig. 3.8).

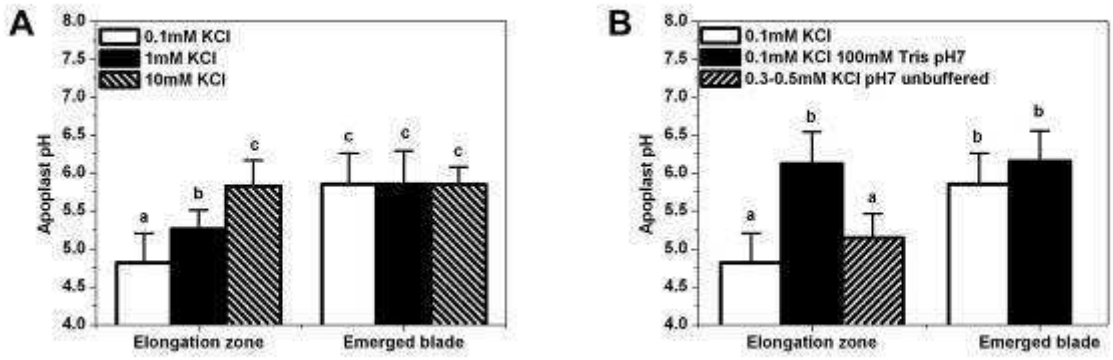

Figure 3.7 Microelectrode analyses of apoplast pH in the elongation zone and emerged blade-portion of leaf three of barley.

Apoplast pH was measured in dependence of the K^+ concentration (added as KCl) of the electrode bathing medium which was in direct contact with the leaf tissue analysed (A). Apoplast pH measured when buffered solutions were applied as bathing medium (B). Values are averages ±SD of 7 - 15 measurements obtained on 3 - 6 plants of each treatment. Different letters show a statistically significant difference at $p < 0.05$ (Student's t-test and ANOVA).

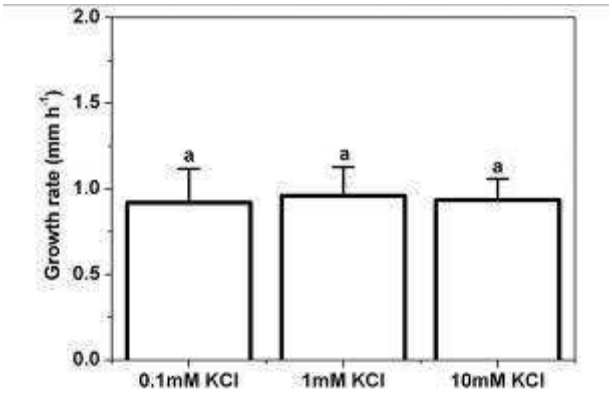

Figure 3.8 Growth rate of leaf three in response to K^+-treatments during micro pH measurements.

Values are averages ±SD of 7 - 15 measurements obtained on 3 - 6 plants of each treatment. Different letters show a statistically significant difference at $p < 0.05$ (ANOVA).

Vanadate (Na_3VO_4) and fusicoccin were added to the bathing medium to test whether the lower pH in the apoplast of the elongation zone was dependent on the activity of the PM-H^+-ATPase. Vanadate, which inhibits the PM-H^+-ATPase, was tested at a concentration of 500 µM in presence of 0.1 mM KCl. Apoplast pH in the elongation zone increased from pH 4.8 to pH 5.8, precisely the pH value observed in the emerged blade (Fig. 3.9). Fusicoccin, which stimulates the PM-H^+-ATPase (Marré, 1979; Würtele *et al*., 2003), was tested at a concentration of 5 µM in presence of 1 mM KCl. Apoplast pH was 5.2 and identical to the pH measured in absence of fusiccocin at 1 mM KCl in the bathing medium (Fig. 3.9). The rate of leaf elongation decreased in response to vanadate and increased in response to fusicoccin treatments (Fig. 3.10). This was observed for all experimental setups (Fig. 3.10).

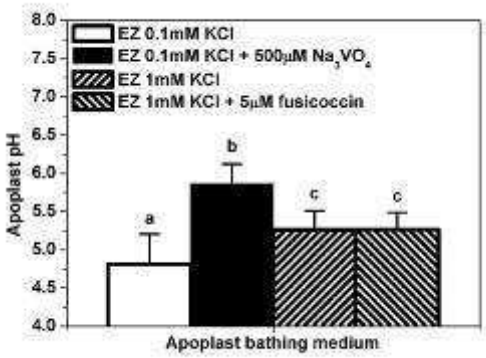

Figure 3.9 Microelectrode pH analyses in the leaf elongation zone of barley in response to sodium orthovanadate and fusicoccin treatments

The KCl concentration in the bathing medium was as indicated. Values are averages and standard deviations (error bars) of 12 (controls of 0.1 mM and 1 mM KCl), 4 (500 µM vanadate) and 4 (5 µM fusicoccin) datasets of between 3 - 6 different plants each. Different letters show a statistically significant difference at $p < 0.05$ (Student's t-test and ANOVA).

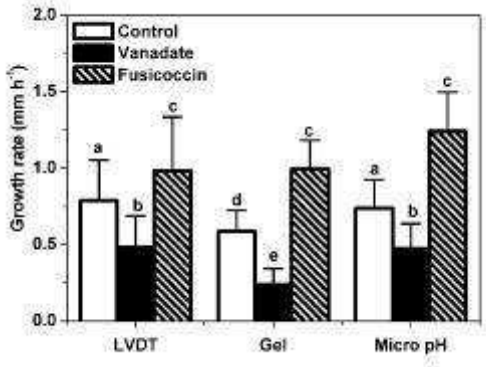

Figure 3.10 Growth rate of leaf three of barley in response to vanadate and fusicoccin treatments as analysed through different approaches

Values are averages and standard deviations (error bars) of 13 - 60 (control), 3 - 8 (vanadate) and 3 - 10 (fusicoccin) replicates. Different letters show a statistically significant difference at $p < 0.05$ (Student's t-test and ANOVA).

3.1.1 Confocal microscopy

Acridine orange and 5(6)carboxyfluorescein are pH sensitive fluorescence dyes. They were used to test whether the apoplastic pH was lower in the elongation zone compared with emerged blade in intact barley plants. First, the system had to be calibrated. This was achieved by peeling epidermal strips from plants which had been grown for 24 h in the presence of 5(6)carboxyfluorescein and 48 h in presence

of acridine orange in the root medium to allow sufficient uptake of dye into leaf tissue. Exposure of epidermal strips to solutions of different pH showed (i) that dye had been taken up into the leaf apoplast and (ii) that the fluorescence intensity of dye in the apoplast changed in the physiological pH range, in the same manner as observed for dye in free solution (Fig. 3.11 A, B for acridine orange and Fig. 3.12 A, B for carboxyfluorescein). Fluorescence decreased with pH. Optical sections from the epidermis of intact third leaves showed that the fluorescence intensity, and by implication pH, were considerably lower in the apoplast of the elongation zone than in the apoplast of the emerged blade (Fig. 3.11 C-F for acridine orange and Fig. 3.12 C-F for carboxyfluorescein).

It is possible that the difference in fluorescence intensity between leaf regions resulted not from differences in apoplast pH but from differences in the concentration of dye accumulated during the uptake period. This was tested by peeling epidermis strips from the elongation zone and emerged blade (leaf three) of dye-loaded plants and incubating the peels in pH 7.5 buffer solution. Peels were examined after a 30 min incubation period using a Leica epifluorescence microscope. The fluorescence intensity and by implication carboxyfluorescein and acridine orange concentration was similar in the epidermis of the two leaf regions; if anything, it was higher in the elongation zone (Fig. 3.13). This experiment showed that the lower apoplast pH in the epidermis of the elongation zone of intact, dye-loaded plants, was not the result of a lower fluorochrome concentration but reflected most likely a true difference in apoplast pH between the two leaf regions. Uptake of dyes through roots and accumulation in leaf tissue did not cause changes in leaf growth (Fig. 3.14 A, B).

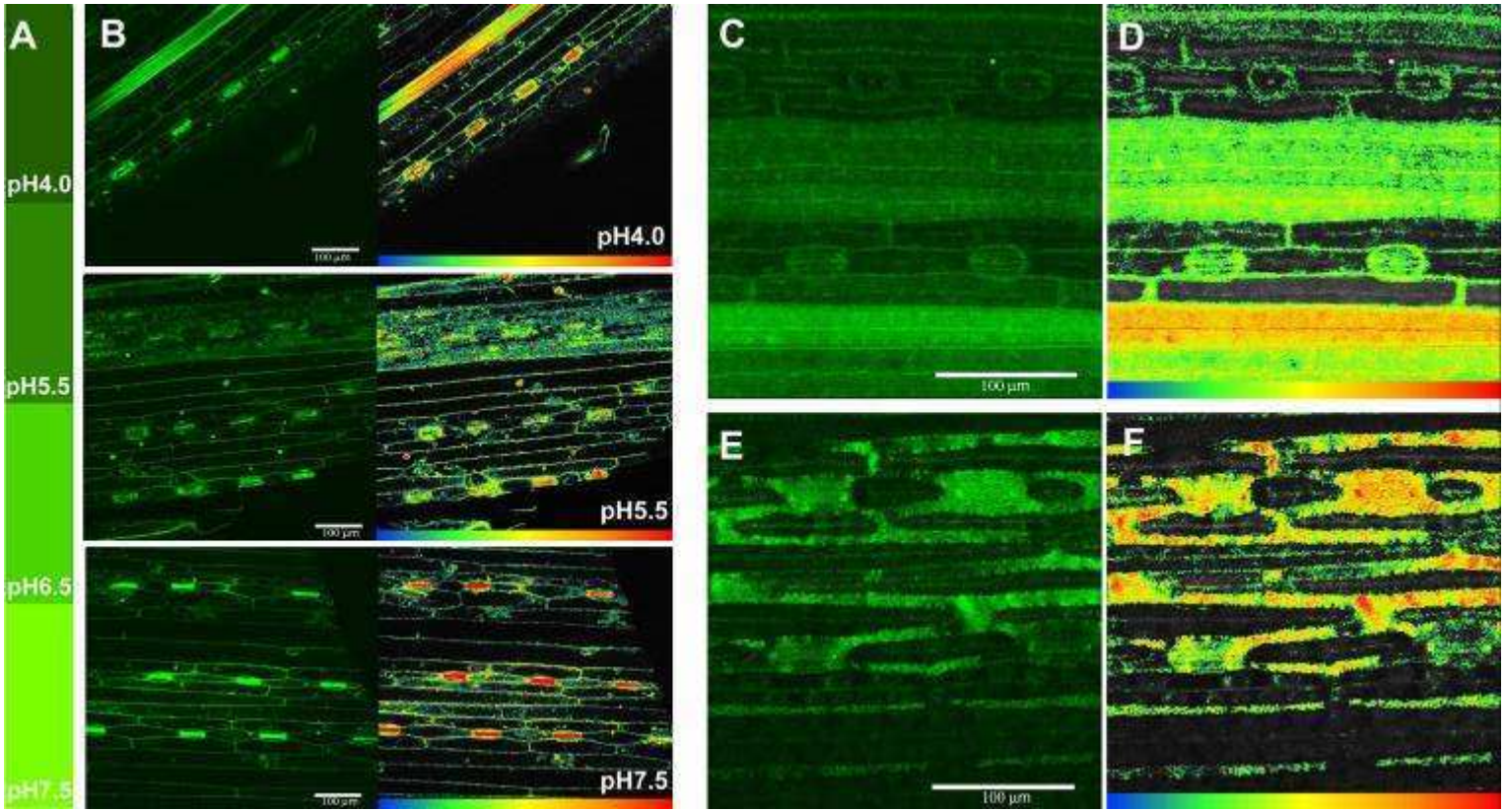

Figure 3.11 Confocal microscopic analysis of apoplastic pH using acridine orange fluoresce pH sensitive fluorescence dye

The pH sensitivity of fluorescence of dye as tested on sample droplets which contained 2.5 µM acridine orange and were buffered at the pH indicated (A). Confocal images of epidermal peels of the mature leaf one; following incubation of peels for 30 min in the solutions as shown in (B). Typical confocal images (C, E) and their heat map (D, F). Elongation (C, D) and emerged (E, F) region of leaf three of intact plants. Images containing scale bars show the original fluorescence image, while corresponding images without scale bars represent heat maps of images.

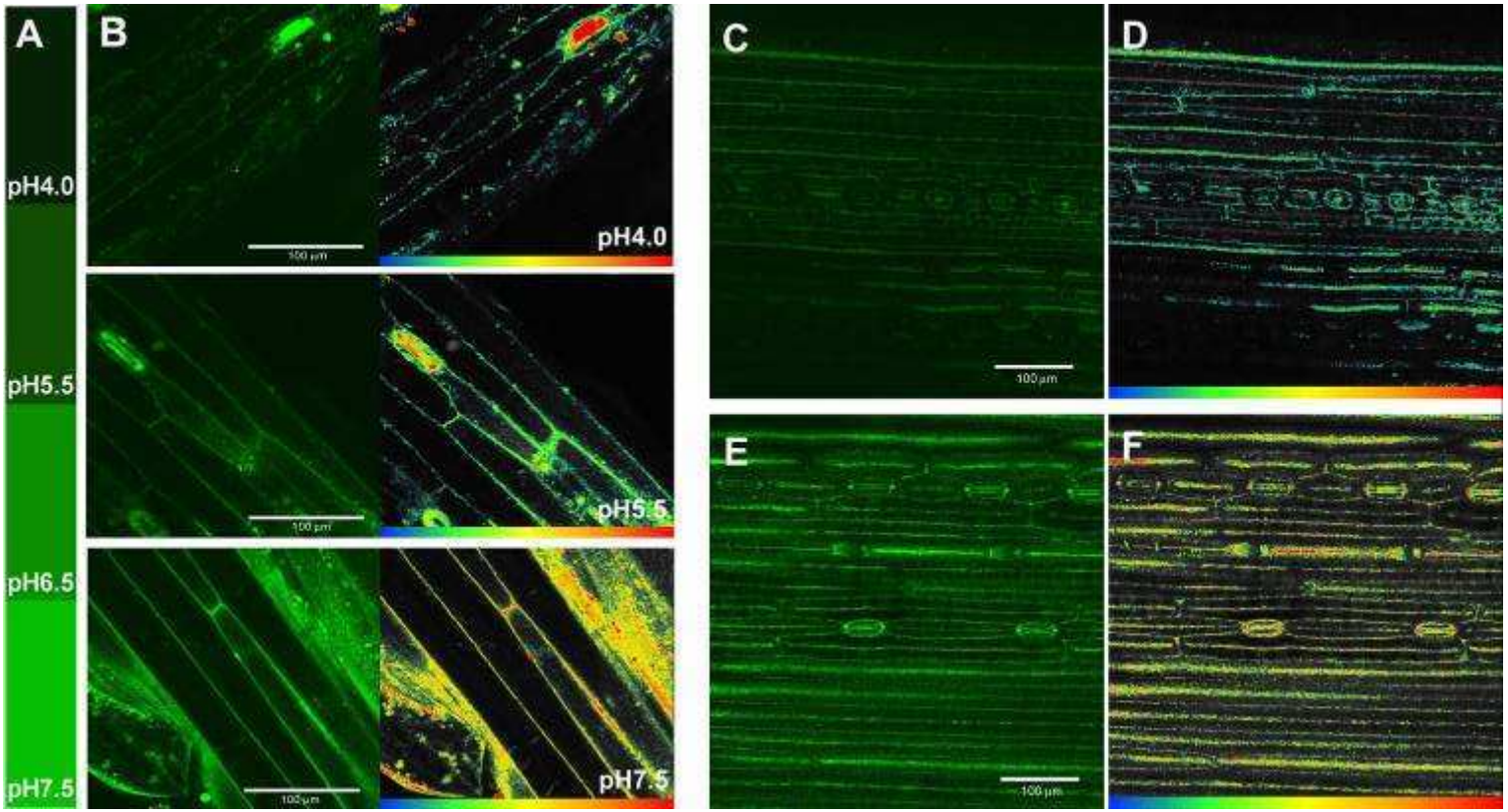

Figure 3.12 Confocal microscopic analysis of apoplastic pH using 5(6)carboxyfluorescein fluoresce pH sensitive fluorescence dye

The pH sensitivity of fluorescence of dye as tested on sample droplets which contained 10 µM carboxyfluorescein and were buffered at the pH indicated (A). Confocal images of epidermal peels of the mature leaf one; following incubation of peels for 30 min in the solutions as shown in (B). Typical confocal images (C, E) and their heat map (D, F). Elongation (C, D) and emerged (E, F) region of leaf three of intact plants. Images containing scale bars show the original fluorescence image, while corresponding images without scale bars represent heat maps of images.

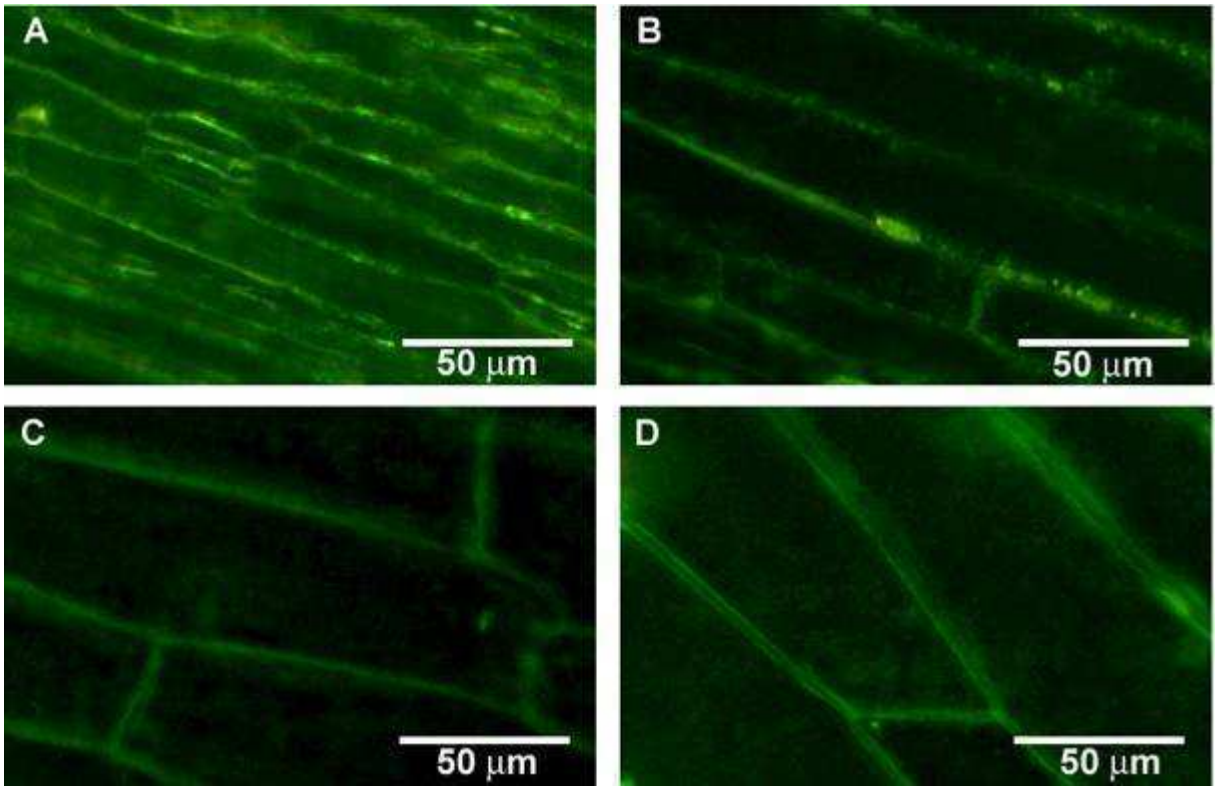

Figure 3.13 Carboxyfluorescein and acridine orange accumulation pattern in elongation zone and emerged blade

The distribution of the pH sensitive probes (5(6)carboxyfluorecein, A, C and acridine orange, B, D) appears to be similar in the elongation zone (A, C) and emerged leaf blade (B, D). The dye was taken up through the roots of intact plants and the epidermal strips of leaf three were incubated (30 min) in pH 7.5 buffer prior to be viewed under the microscope (Leica DMIL; 450 - 490 nm excitation filter and 515 nm suppression filter).

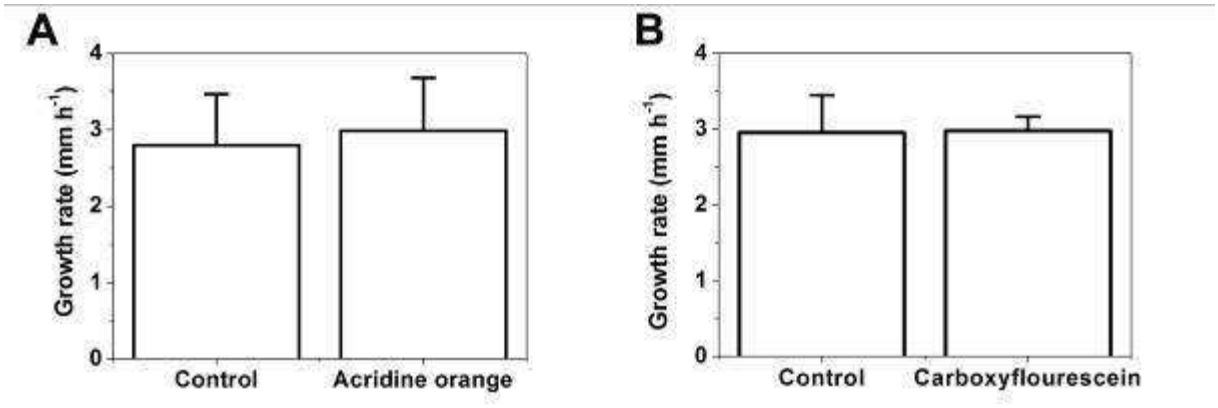

Figure 3.14 Effect of pH sensitive dyes on leaf growth rate

Growth, as measured with the LVDT on intact plants (unpeeled leaf three) did not change after 48 h incubation of plants in nutrient solution containing 2.5 μM acridine orange (A); the same was observed for plants after 24 h incubation in nutrient solution containing 10 μM carboxyfluorescein. Values are averages of 3 replicates, and error bars represent standard errors.

The pH sensitivity of fluorochrome 5(6)carboxyfluorescein and acridine orange was determined by fluorescence spectroscopy. Both fluorescein probes showed pH-sensitivity in the physiological pH range and had single peak spectra. Carboxyfluorescein showed a larger pH sensitivity in the pH range of interest compared with acridine orange (Fig. 3.15).

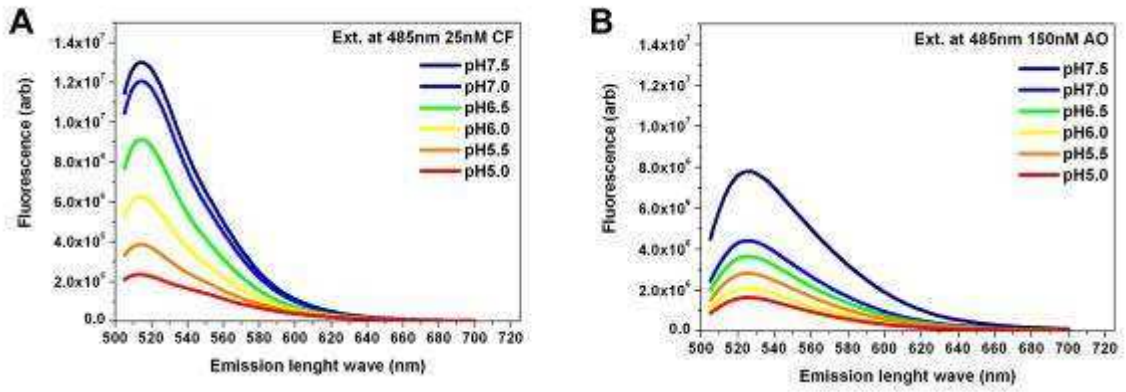

Figure 3.15 pH sensitivity of fluorochromes

Fluorescence spectra and pH sensitivity of 5(6)carboxyfluorescein (A) and acridine orange (B) was recorded. Both fluorochromes had pH sensitivity although carboxyfluorescein gave more explicit signal and better pH fidelity in the physiological pH range.

3.2 LVDT analyses of growth responses to treatments

3.2.1 Leaf elongation under different treatments

The basic assumption underlying LVDT experiments was that the wet tissue paper which was soaked in test solution and in direct contact with the surface of the elongation zone of leaf three allowed the test solution to diffuse into the apoplast. The responsiveness of setup to treatments was tested through two types of experiment, one designed to increase (37 ℃) and on e designed to reduce growth (1 M NaCl). Elongation growth of grass leaves responds little to changes in ambient temperature but to the temperature close to the basal meristem (Stoddart & Lloyd, 1986). Therefore, parts of a potato which had been heated to 37 ℃ in an incubator were placed round the leaf elongation zone without any direct contact between the potato and the barley seedling. Growth started to increase within minutes (Fig. 3.16 A, B). With time, the potato cooled down and leaf elongation rate decreased. When finally 1 M NaCl was added to impose a severe osmotic stress, growth stopped instantly and remained zero or close to zero (Fig. 3.16 A, B).

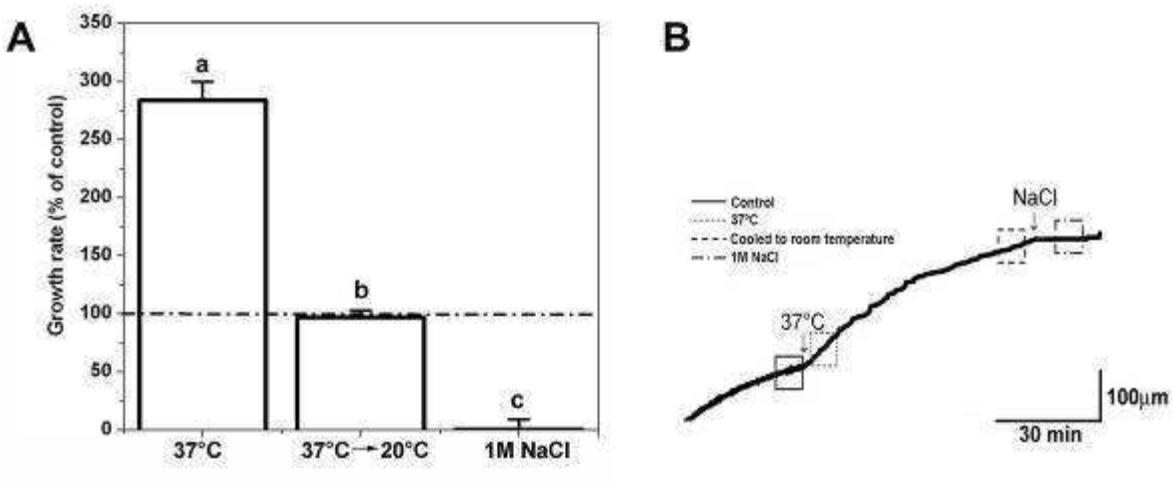

Figure 3.16 Testing the responsiveness of the LVDT setup to treatments which were expected to increase (37 ℃) or stop growth (1 M NaCl)

Average values (three plants) and standard deviations (error bars) (A) and a typical trace (B) are shown. The apoplastic bathing medium always contained 1 mM KCl. Different letters show a statistically significant difference at $p < 0.001$ (Student's t-test).

Having tested the responsiveness of the LVDT setup, treatments were applied. In presence of 1 mM KCl in the test solution fusicoccin (5 µM) increased leaf elongation rate to 160 % the rate observed in control plants. Vanadate, CsCl and CsCl–vanadate double treatments caused a 50 % decrease in growth rate (Fig. 3.17). The same was observed for the K^+ channel blocker tetraethylammonium (TEA) and ammonium, which blocks high-affinity K^+ transporters (NH_4^+; HAK-type transporters (Kronzucker *et al.*, 2003; Rodriguez-Navarro & Rubio, 2006; Szczerba *et al.*, 2006).

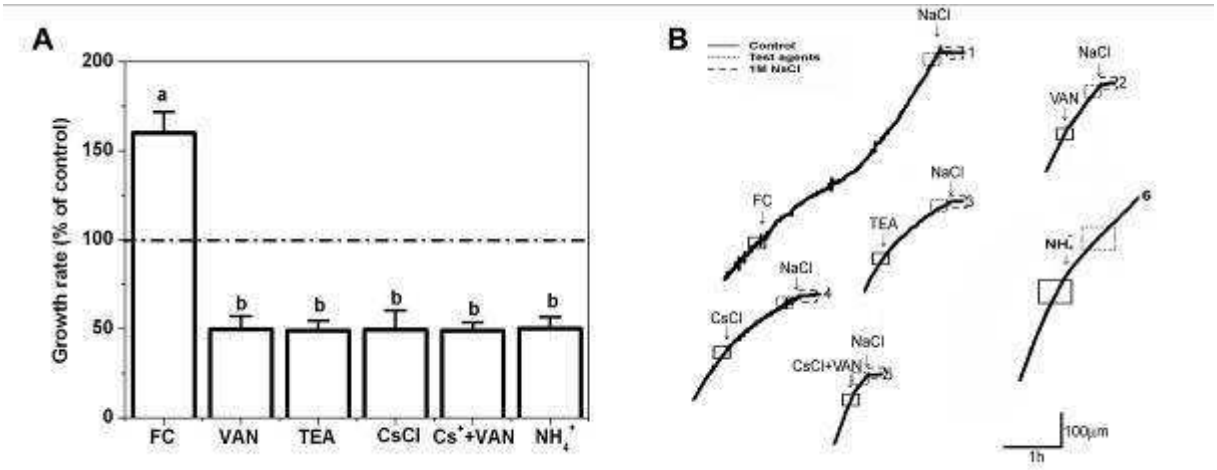

Figure 3.17 The effect of test reagents in the apoplastic bathing medium on leaf growth as measured with the LVDT setup

Average values and standard deviations of experiments (A) involving application of test reagents are shown (fusicoccin (5 µM, n = 3 plants), vanadate (VAN, 500 µM, 6 plants), tetraethylammonium chloride (TEA, 50 mM, 6 plants), CsCl (40 mM, 4 plants), CsCl+VAN double-treatment (40 mM / 500 µM, 3 plants), and $(NH_4)_2SO_4$ (20 mM, 3 plants)). Media always contained 1 mM KCl. Typical traces of experiments (B). Growth rates are expressed as percent of the respective KCl control, which contained only KCl but no test reagents in the apoplastic bathing medium. Different letters show a statistically significant difference at $p < 0.05$ (Student's t-test and ANOVA).

The effect of fusicoccin on elongation growth was dependent on the K^+ concentration in the bathing medium which was in direct contact with the leaf elongation zone (Fig. 3.18). The higher the K^+ concentration was, the larger was the stimulation of growth. In contrast, the inhibitory effect of vanadate on leaf elongation growth did not depend on the K^+ concentration in the bathing medium (Fig. 3.18). This experiment showed that changes in the K^+ concentration *per se* did not affect growth but required a functional PM-H^+-ATPase to affect growth.

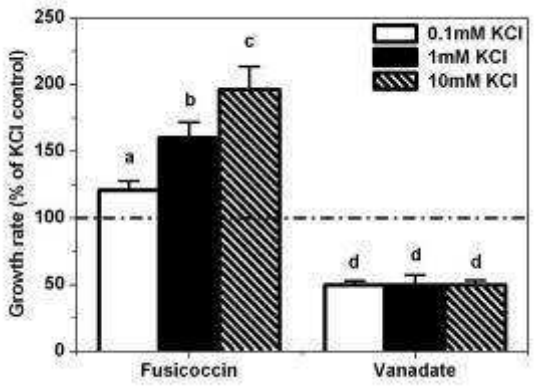

Figure 3.18 Potassium dependency of the leaf growth response to fusicoccin (5 µM) and vanadate (500 µM)

Values are averages and standard deviations (error bars) of 3 - 6 plants, and the K^+ concentration of apoplastic bathing medium was as indicated. Growth rates are expressed as percent of the respective KCl control, which contained only KCl and no test reagents in the apoplastic bathing medium. Different letters show a statistically significant difference at $p < 0.05$ (Student's t-test and ANOVA).

Short term (1 - 4 h) auxin-induced leaf growth was measured with the same LVDT set up. Treatments (5 µM NAA with 1 mM KCl) did not caused any significant increase in growth rate, moreover the leaf elongation rate slightly (but not significantly) decreased rather than increased (Fig. 3.19). These results suggested that leaf elongation can not be further increased by auxin treatments.

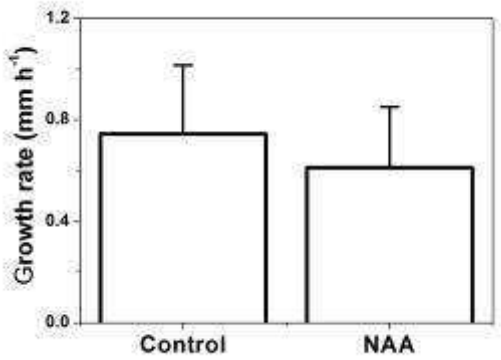

Figure 3.19 Auxin effect on leaf elongation growth

Elongation growth was monitored using the LVDT system. Growth in control (1 mM KCl) and NAA treated plants (1 mM KCl and 5 µM NAA) did not significantly differ from each other. Values are averages and standard deviations (error bars) of 3 replicates. The difference in growth between control and NAA treatment is statistically not significant (Student's t-test).

3.2.2 Cell wall changes in response to treatments

Changes in cell wall properties were tested for 500 µM vanadate, 40 mM CsCl and 5 µM fusicoccin treatments by applying an additional 3 g counterweight on the LVDT system. Control plants had 1 mM KCl in the apoplast bathing medium of the elongation zone. The elastic growth component significantly changed only in response to the fusicoccin treatment, whereas plasticity was affected significantly in response to CsCl (Fig. 3.20 A). Additional stress (0.03 N) on the cell wall did not change the relative growth rate compared with control (1 mM KCl, $\Delta\Delta v$), except in fusicoccin-treated leaves. Fusicoccin treatment caused a 50 % increase in $\Delta\Delta v$ compared with all other treatments and the control (Fig. 3.20 B).

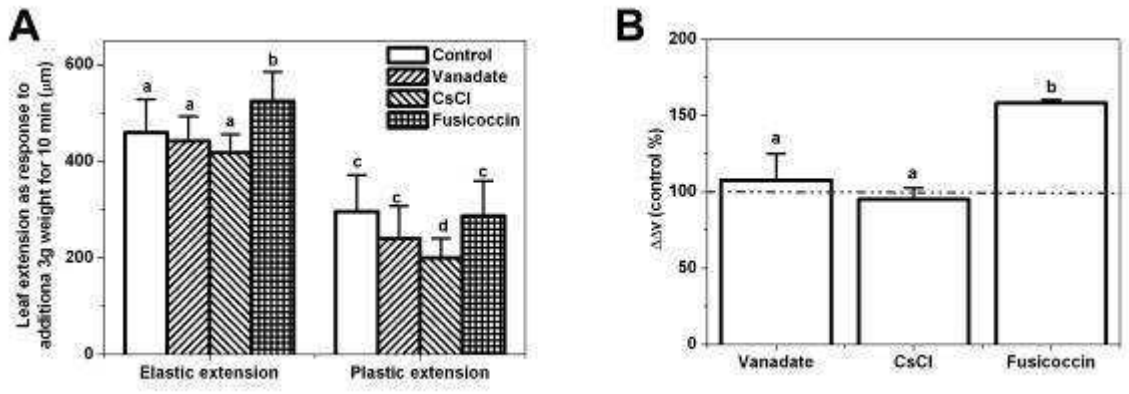

Figure 3.20 Cell wall changes under different treatments

Elastic and plastic growth (A) and 0.03 N stress caused growth rate (B) was measured on 3 independent plants in two replicates each. $\Delta\Delta v$ means the difference between $\Delta v_{control}$ and $\Delta v_{treatment}$ where Δv is the difference in growth rate before and under the applied additional stress (v_2-v_1 on Fig. 3.2). Different letters show statistically different values at $p < 0.05$ level with Student's t-test and ANOVA.

Growth rate before (v_1) and under (v_2) applied 0.03 N force was in agreement with previous effect of test reagents on growth (compare Fig. 3.17 and Fig. 3.21). The fusicoccin treatment caused a large increase in growth, although the increase was statistically not significant.

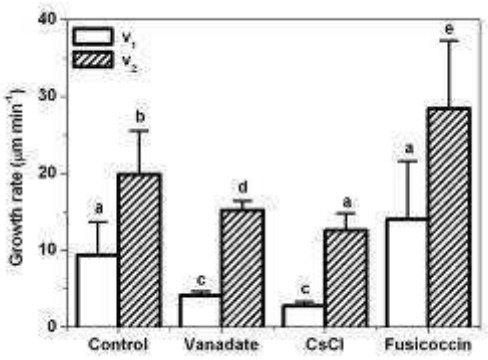

Figure 3.21 Growth rate before and in response to an additional applied force (0.03 N)

Growth rate before (v_1) and under (v_2) applied force (3 g) using different treatments as vanadate (500 μM), CsCl (40 mM) or fusicoccin (5 μM). Bath medium of control plants contained 1 mM KCl. Values are averages of 3 - 3 replicates. Different letters shows statistically different values at $p < 0.05$ level with Student's t-test and ANOVA.

3.3 Expression analysis of PM-H$^+$-ATPase using qPCR

PM-H$^+$-ATPase expression was analysed using qPCR. Altogether five reference genes (GADPH, cyclophilin, ubiquitin, HSP70 and PM-H$^+$-ATPase) were tested in the experimental system. Only ubiquitin and the two PM-H$^+$-ATPase (Ha1 and ATPase) primer pairs showed similar expression in the elongation zone and emerged blade (Fig. 3.22 A). Other, commonly used reference genes such as actin, tubulin, EF1, LHC were not suited because growing and non-growing leaf regions had to be compared (see Besse *et al*., 2011; Volkov *et al*., 2009). Ubiquitin could not be used as reference gene because the PCR product was not homogenous but produced more than one band as agarose gel analysis showed (Fig. 3.22 B). Applying Genevestigator bioinformatics application (www.genevestigator.com) could not solve the problem. Therefore, it was decided to carry out absolute qPCR quantification to determine PM-H$^+$-ATPase expression levels in the leaf elongation zone and emerged blade.

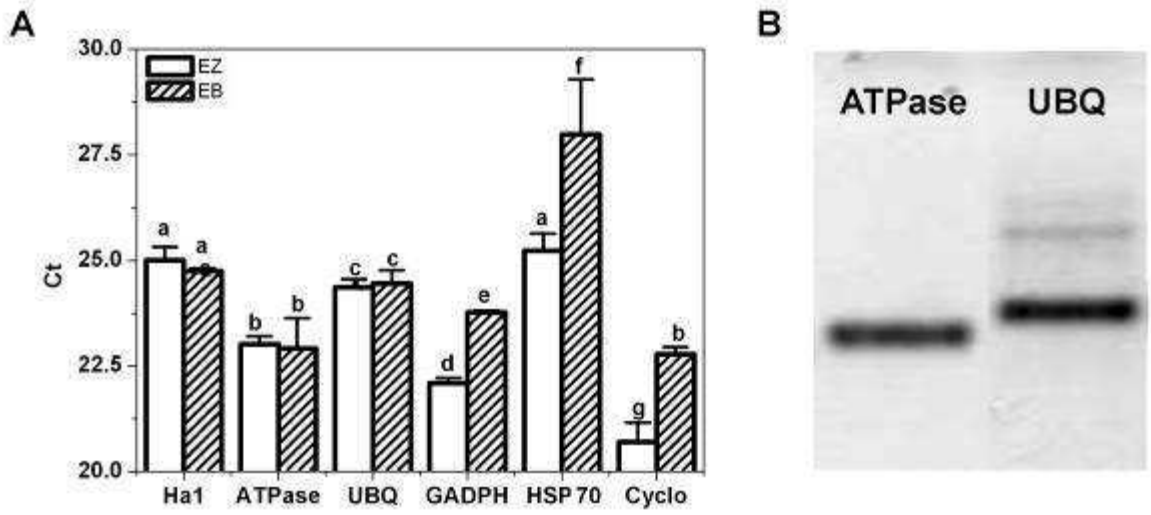

Figure 3.22 reference genes for qPCR experiments

500 pg total RNA-equivalent cDNA was used in each reaction well to check the qPCR profile of candidate reference genes. Expression, as shown as Ct-value, of the two PM-H^+-ATPase PCR primer pair (Ha1 and ATPase) and ubiquitin (UBQ) was similar between the two leaf regions, effectively qualifying them as reference genes of expression. In contrast, expression of glyceraldehyde-3-phosphate dehydrogenase (GADPH), heat shock protein 70 kDa (HSP70) and cyclophylin (Cyclo) differed significantly between leaf regions (A). Values are averages of 3 replicates and error bars represent SD. Different letters show significantly different values at $p < 0.05$ level using Student's t-test and ANOVA. Agarose gel picture of PM-H^+-ATPase (ATPase) and ubiquitin (UBQ) show that that ubiquitin shows more than one PCR product (B).

3.3.1 Quality control of the standard required for absolute qPCR

Quality of reference DNA (purified PM-H^+-ATPase PCR fragments) was validated using end point detection digital PCR technique (Vogelstein & Kinzler, 1999). The concentration of fragments was calculated as 0.5 copy μl^{-1} based on Nanodrop® measurements. From 40 PCR reactions 21 were PCR positive and 19 negative (Fig. 3.23). This suggested a concentration of 0.525 DNA copy μl^{-1} in the external standard and was just 2.5 % higher compared with the calculated copy concentration (0.5 copy μl^{-1}).

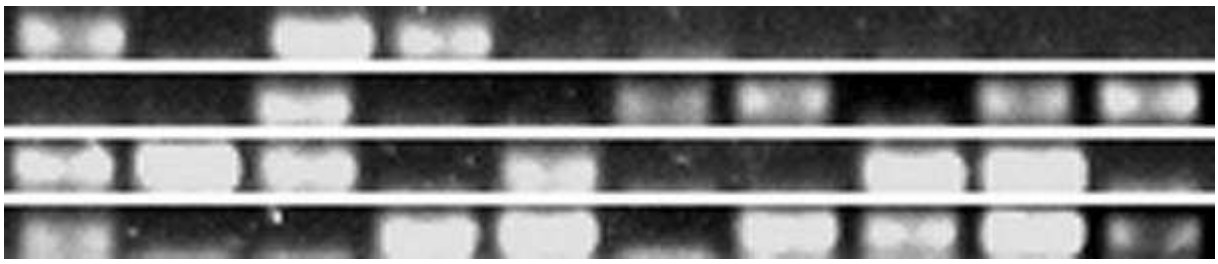

Figure 3.23 Digital PCR pattern of external standard DNA

Using digital PCR technique the concentration of the external standard for PM-H^+-ATPase expression was verified. The PCR positive / negative ratio was 21 / 19, which suggests a concentration of 0.525 copy of ATPase DNA in 1 µl of standard compared with the calculated 0.5. Therefore, the reliability of the standard was higher than 95%.

3.3.2 Calculation of cell number and membrane surface

Total cell volume of the leaf regions was calculated for the two barley cultivars using the water content of the plant material, cell dimensions and contribution of each tissue to total leaf symplast volume (Table 3.1). The water content differed significantly between the two leaf regions but not between the two cultivars.

Table 3.1 Water content of two different regions of leaf three in two cultivars of barley

Cultivar	Leaf part	No replicates	Water content (%)	SD
Golf	Elongation zone	3	92.06	1.57
	Emerge blade	3	86.78	2.25
Jersey	Elongation zone	7	93.78	3.12
	Emerge blade	7	87.78	1.07

The tissue volume ratio was measured on cross sections using light microscopy (Table 3..2 and Fig. 3.24) and average cell size was estimated from the present protoplast measurements and data published for Golf (Fricke & Flowers, 1998; Volkov *et al.*, 2007; Volkov *et al.*, 2009, Kavanagh, 2010) (Table 3.3). Mesophyll and epidermis cell size and surface area was calculated separately and the total number of cells and surface area was calculated from data on the contribution of each tissue to total leaf symplastic volume (not considering intercellular air space). Mesophyll cell size differed between growing and mature, emerged tissues around 2.2-fold and epidermis cells differed 4.6-fold, in each case being larger in emerged tissue. The surface was about 2.6-fold and 1.9-fold higher in the emerged blade for epidermis and mesophyll, respectively.

Table 3.2 The contribution of different tissues to total leaf volume in the elongation zone (EZ) and emerged blade (EB) of leaf three of barley. Values are given as % of the total leaf volume and are either not corrected or corrected for intercellular air space, effectively giving a contribution to total leaf symplastic volume.

	EZ		EB	
Epidermis (%)	24.85	± 1.54	23.37	± 2.94
Mesophyll (%)	61.75	± 1.93	51.61	± 4.36
Vascular bundle (%)	8.99	± 1.97	4.01	± 0.93
Intercellular air space (%)	4.40	± 1.32	21.01	± 4.29
Epidermis corrected (%)	26.00	± 1.28	29.59	± 3.72
Mesophyll corrected (%)	64.60	± 1.96	65.34	± 5.52
Vascular bundle corrected (%)	9.41	± 1.80	5.08	± 1.18

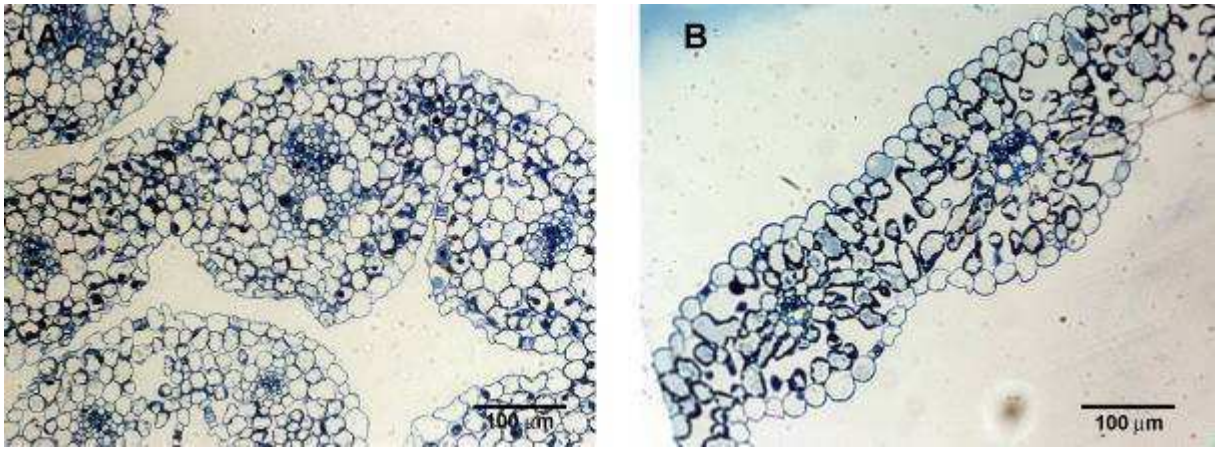

Figure 3.24 Representative cross sections used for determination of the contribution of different tissues and air space to total leaf volume

Toluidine blue stained cross sections were used to calculate the percentage of different tissues to total leaf and symplastic volume in the elongation zone (A) and emerged blade (B) of leaf three of barley.

Table 3.3 Cell size calculation based on the present and literature data. Values shown in bold were used for to relate ATPase expression and activity data to cell volume and surface area

	EZ		EB	
Cell volume	Average	SD	Average	SD
Epidermis cell size (Fricke & Flowers, 1998)	99.4		461	
Epidermis cell size average (pl)	**99.4**		**461**	
Mesophyll cell size (my protoplast results)	3.7		9.4	
Mesophyll cell size (Volkov *et al*., 2007)	8.9		24.4	
Mesophyll cell size (Volkov *et al*., 2009)	11.8		17.4	
Mesophyll cell size (Kavanagh, 2010)	2.08		8.11	
Mesophyll cell size average (pl)	**6.62**	± 4.52	**14.83**	± 7.59
Cell surface				
Surface of epidermis cell (Fricke & Flowers, 1998)	27100		65200	
Surface of epidermis cell (Kavanagh, 2010)	12308		34809	
Surface of epidermis cell average (μm^2)	**19,707**	± 10,459	**50,004**	±21,490
Mesophyll cell size (my protoplast results)	1,157		2,154	
Mesophyll cell size (Volkov *et al*., 2007)	2,077		4,068	
Mesophyll cell size (Volkov *et al*., 2009)	2,506		3,247	
Mesophyll cell size (Kavanagh, 2010)	788		1,952	
Surface of mesophyll cell (μm^2)	**1,632**	± 796	**2,855**	± 988

3.3.3 Gene expression data based on absolute qPCR method

Using the absolute qPCR method, together with cell size and tissue volume contributions it was found that PM-H^+-ATPase had a constant expression pattern in both elongation zone and emerged leaf blade; it was deemed to be a perfect reference gene in both Golf and Jersey cultivars (Fig. 3.25 and Table 3.4). The total RNA content was similar in the elongating zone and emerge leaf blade. This applied to both Golf and Jersey cultivars (Table 3.4).

Results expessed per plasma membrane surface unit were significant, being around 2 times higher PM-H^+-ATPase protein concentration as might be presumed in elongation zone compare with emerge blade in both barley cultivars. Absolute expression was 3 times higher in Golf compare to Jersey cultivar (Fig. 3.26). The calculation here presumed that protein translation from mRNA was linear and had equal probability in elongation zone and emerge blade. More details of the calculation can be found in the Appendix.

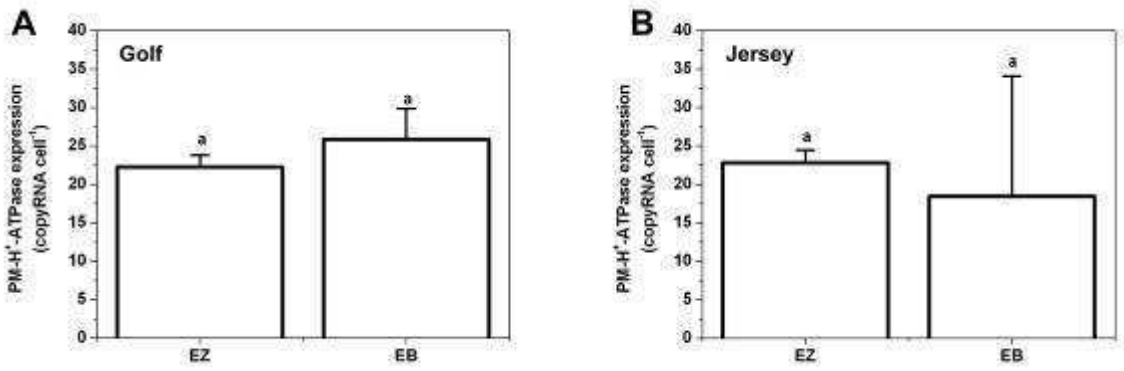

Figure 3.25 Expression of PM-H$^+$-ATPase using absolute qPCR

Using absolute qPCR, the total number of mRNA transcripts was determined for each cDNA sample. The amount of cDNA obtained from a given amount of leaf region (elongation zone, EZ; emerged blade, EB) was known, as was the number of cells for each region. This made it possible to express qPCR data as mRNA copy number per cell. Results are shown for the barley cultivars Golf (A) and Jersey (B) and represent averages and standard deviation (error bars) of three independent experiments (batches of plants). PM-H$^+$-ATPase expression (copyRNA cell^{-1}) did not differ significantly between elongation zone (EZ) and emerged blade (EB) in either Golf or Jersey (Student's t-test).

Table 3.4 Ct values of PM-H$^+$-ATPase expression together with RNA content per cell in the elongation zone (EZ) and emerged blade (EB) of leaf three of barley. Two barley cultivars were studied, Golf and Jersey, and three independent experiments were carried out.

	Ct	SD	RNA content (pg cell^{-1})	SD
EZ (Golf)	23.8	0.2	22.3	1.5
EB (Golf)	24.2	0.5	25.9	4.0
EZ (Jersey)	22.7	0.2	22.8	1.7
EB (Jersey)	22.8	0.2	18.5	15.6

Since the determination of cell number in a given leaf region involved large errors, an additional control experiment was conducted in which RNA was extracted from protoplast suspension of the Jersey cultivar. The number of protoplasts could easily be calculated. RNA yield of 300 - 1000 µl protoplast suspension (about 0.5 - 7 million cells) was 250 - 2,000 ng µl^{-1} and the 'background' protoplast medium which was taken as supernatant folowed gentle centrifugation of protoplasts, yielded virtually no extractable RNA (less than 1 - 10 ng µl^{-1}, which was below the measuring range of the Nanodrop® equipment). Results for protoplasts were expressed in copy number of PM-H$^+$-ATPase transcript protoplast^{-1} and in copy number of PM-H$^+$-ATPase transcript mm^{-2} protoplast plasma membrane surface area. These figures

were in the same range as results obtained for the Jersey cultivar when calculated cell number was used as reference system (see Fig. 2.25).

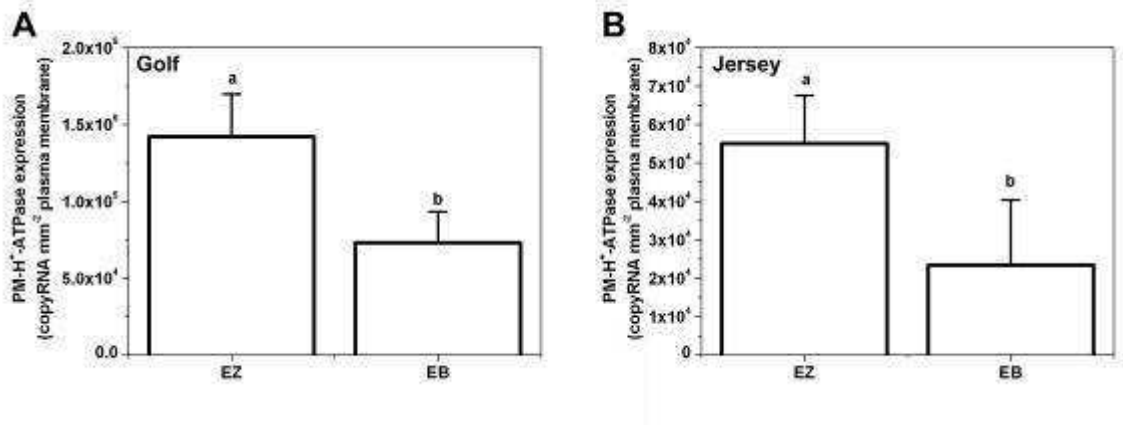

Figure 3.26 PM-H$^+$-ATPase expression using absolute qPCR and relating expression data to total plasma membrane surface area

PM-H$^+$-ATPase gene shows significantly (around 2 times) higher expression in the elongation zone (EZ) compared with emerged leaf blade (EB). Values for the Golf barley cultivar (A) were 3 fold higher than values for the Jersey barley cultivar (B). Results are averages and standard deviations (error bars) of three 3 independent experiments. Different letters shows statistically different values between leaf regions (student's t-test, $p < 0.05$).

Table 3.5 RNA content and PM-H$^+$-ATPase expression in the elongation zone (EZ) and emerged blade (EB) of leaf three of barley (Golf, Jersey). Different reference systems were used. Results are averages and SD of 3 - 6 independent experiments. Protoplasts were isolated only from the Jersey barley cultivar. PM, plasma membrane; protopl., protoplast.

	RNA (pg cell^{-1})		ATPase copy cell^{-1}		ATPase copy mm^{-2} PM (x 10^3)	
EZ (Golf)	22.3	± 1.5	300	± 60	142	± 28
EB (Golf)	25.9	± 4.0	260	± 70	73	± 20
EZ (Jersey)	22.8	± 1.7	120	± 30	55	± 12
EB (Jersey	18.5	± 15.6	80	± 60	23	± 17
EZ protopl.	18.7	± 17.5	50	± 30	38	± 23
EB protopl.	20.7	± 19.2	50	± 40	12	± 7

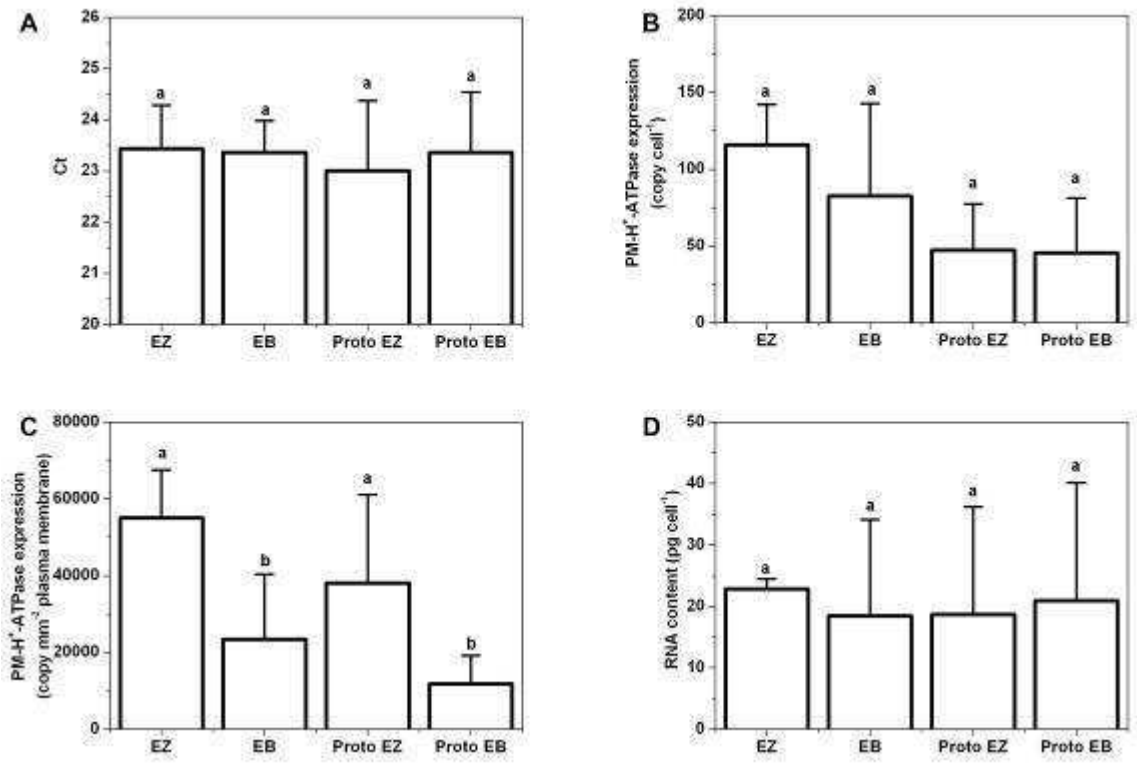

Figure 3.27 Comparison of molecular biological data using leaf tissues or mesophyll protoplasts

Ct values (A), PM-H^+-ATPase copy in a cell (B), per mm^2 plasma membrane (C) and total RNA content in a cell (D) was compared between experiments where RNA was isolated from whole leaf segments of the elongation zone (EZ) and emerged blade (EB) and from isolated mesophyll protoplasts of the elongation zone (Proto EZ) and emerged blade (Proto EB). Values are averages of 3 - 6 batches of plants. Different letters show statistically significant differences at $p < 0.05$ using Student's t-test and ANOVA. All experiments were conducted on the barley cultivar Jersey

3.4 PM-H^+-ATPase activity and expression at protein level

Data from qPCR experiments showed that the copy number of PM-H^+-ATPase transcripts per unit plasma membrane surface area was significantly higher in growing compared with non-growing leaf tissue. This could partially explain the lower apoplast pH in elongating tissue. To test to which degree changes in the activity of the PM-H^+-ATPase protein also contributed to the lower pH, plasma membrane fractions were isolated from growing and non-growing part of barley leaves and used to determine the activity of PM-H^+-ATPase. Due to the lack of availability of Golf seeds towards the end of this project, these experiments were carried out on the spring barley cultivar Jersey.

3.4.1 Optimization of membrane isolation and ATPase assay

Membrane isolation and ATPase assay had to be optimized. The original method had been described for a large amount of plant tissue (125 g) (Kjellbom & Larsson, 1984) however previous studies showed that with the method plasma membrane fraction might be purified from lower amout of plant material (Wei *et al.*, 2007). The P_i determination assay had been designed originally for animal membranes (Sarkadi *et al.*, 1992), with animal cells notably lacking any vacuolar ATPases.

3.4.1.1 Plasma membrane isolation

It was impossible to harvest more than 6 g leaf material from the elongation zone and emerged blade portion of leaf three, given the growth constraints (growth chamber, laboratory space) since this required already between 200 - 400 barley seedlings. Preliminary experiments were carried out to find the minimum amount of leaf tissue which was required for a two-phase separation system with 12 g final separation weight. These experiments showed that below 1 g initial leaf tissue virtually no membrane fraction could be obtained and above 10 g the plasma membrane fraction could not be separated from chloroplast membranes using 5 - 6 purification steps.

One washing step of the membrane fraction as recommended by Pitann *et al.* (2009b) was not enough to fully eliminate the rest of the polymers (dextran and PEG) from the purified membrane fraction. In the presence of one or both of these polymers PAGE could not be carried out properly and protein bands appeared blurred on the gel (Fig. 3.28).

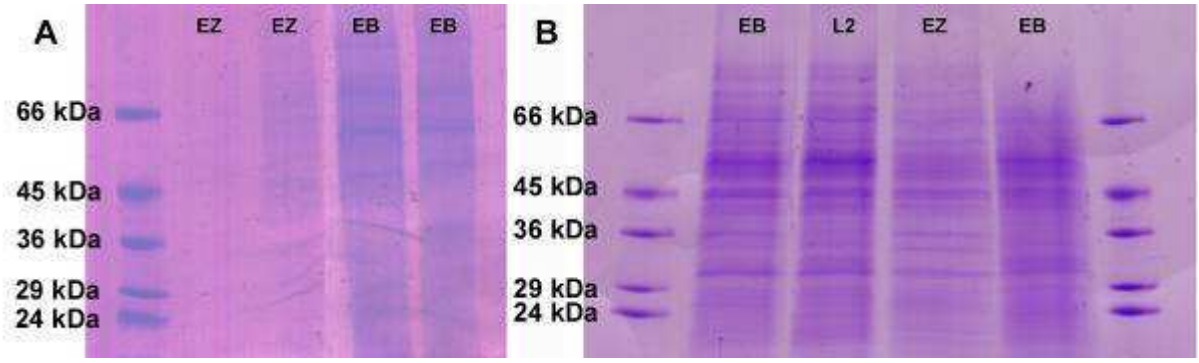

Figure 3.28 Impact on the quality of PAGE separation of washing steps during plasma membrane isolation

Residues of the polymers in plasma membrane fractions caused proteins to appear blurred on the polyacrylamide gel. One washing step was not enough to completely eliminate the polymers (A) while applying two steps (B) the blurring effect was not found on Coomassie stained gels. EZ – elongation zone, EB – emerged leaf blade and L2 – leaf blade of second leaf.

3.4.1.2 Determination of total protein content in plasma membrane vesicles

In studies where plasma membranes have been isolated, protein concentration has typically been quantified with the Bradford method or a modification of it (Yan *et al.*, 1998; Yan *et al.*, 2002; Zörb *et al.*, 2005; Pitann *et al.*, 2009b; Zhu *et al.*, 2009; Hatzig *et al.*, 2010; Wakeel *et al.*, 2010). Using this approach, it was found in the present study that protein concentration was grossly underestimated, compared to quantification of proteins through densitometry by Phoretix 4.01 software (Phoretix International) on Coomassie stained PAGE gels and calibration with protein standards (Sigma) of known protein content. (Fig. 3.29).

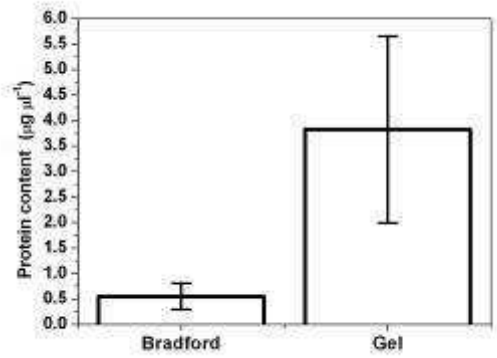

Figure 3.29 Protein measurement in plasma membrane vesicles using two different methods

The protein concentration of the plasma membrane vesicles was significantly lower when determined with the Bradford method than when determined through densitometry of samples run on PAGE gels. The difference in protein concentration between the two methods was statistically significant at $p < 0.05$ (Student's t-test).

3.4.1.3 ATPase assay

Optimization of ATPase assay was carried out to find the optimal reaction volume, detection method and membrane protein amount for the assay. Preliminary experiments showed that colour development was more reproducible in 1750 µl compared with 200 µl (microtiter plate). The optical density of the samples had to be measured within a minute of completion of colour development, together with the calibration curve. If this was not considered, the absorbance changed rapidly (Fig. 3.31). When 3 µg total membrane protein were used and the assay was run for 60 min at 28 °C reproducible and easy to measure amoun t of released (from ATP) amount of P_i could be measured A typical ATPase assay is shown in Fig. 3. 30.

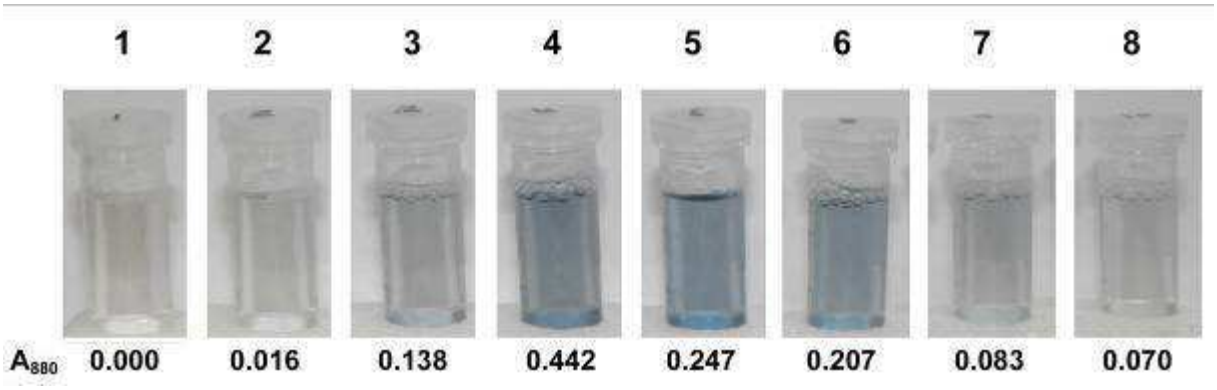

Figure 3.30 Typical ATPase assay

The concentration of P_i was determined by a blue colour reaction (detecting the absorbance at 880 nm) using calibration curve standards (1 - 4; with 0, 10, 30 and 60 nmol P_i per reaction. Without blocking bacterial and vacuolar type of ATPases (5) slightly more P_i could be measured compared with a reaction where these ATPase were blocked with 10 mM NaN_3 and 100 mM KNO_3 (6); 500 µM vanadate (7) blocked ATPase activity almost to the same extent as when total protein was denatured using SDS (8). Values below the tubes show the absorbance at 880 nm.

To determine the optimal detection time of the colour development reaction kinetics was recorded (Fig. 3.31). Between 20 - 30 min the absorbance was between 0.1 - 0.6 (arbitrary units) and could be measured with high reproducibility. In addition, the calibration curve was linear in this time range.

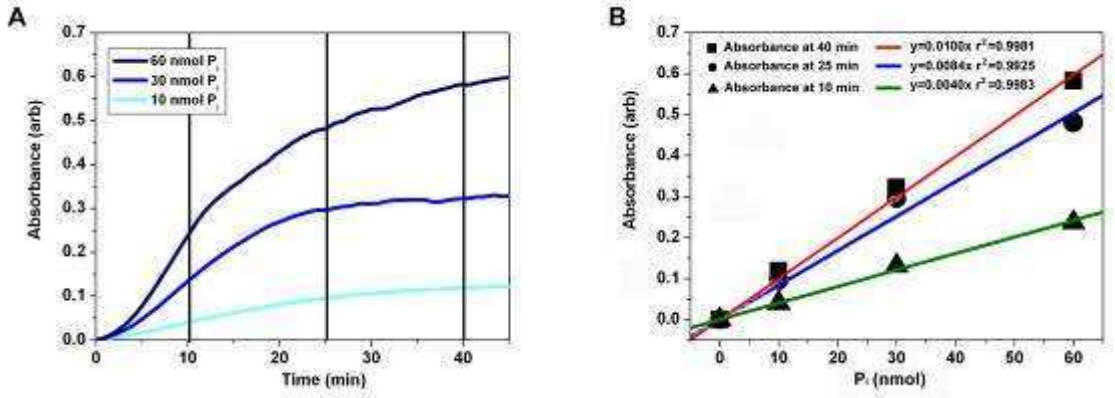

Figure 3.31 Kinetics of P_i detection assay

Kinetics of the P_i detection assay was recorded at 10, 30 and 60 nmol P_i concentration (A) and calibration curve at the time point 10, 25 and 40 min (B). Before 20 min the absorbance values were too low to be use reliably for measurements and the absorbance changed quickly. Between 20 to 30 min the reaction was slower and the values ideal for measurements whereas past 40 min of colour development absorbance values became too high and higher P_i concentrations resulted in errors.

3.4.2 Quality of plasma membrane fractions

The quality of plasma membrane fractions was checked on SDS PAGE gradient gels stained with Coomassie Brilliant Blue and on Western blots. Based on SDS gels the plasma membrane protein pattern of the emerged leaf blade (leaf three) and fully expanded blade (leaf two) was comparable whereas the elongation zone of leaf three and microsomal fraction (no plasma membrane purification) of emerged blade of leaf three differ from the other two (Figure 3.32 A). Western blot analysis confirmed the presence of PM-H^+-ATPase in the isolates (Figure 3.32 B), although based on these Western blots quantitative analysis of PM-H^+-ATPase density in the plasma membrane of different leaf regions could not be achieved. Subsequently, a more sensitive Western blot system (at UCD) was used to compare PM-H^+-ATPase content of plasma membranes between elongation zone and emerged blade.

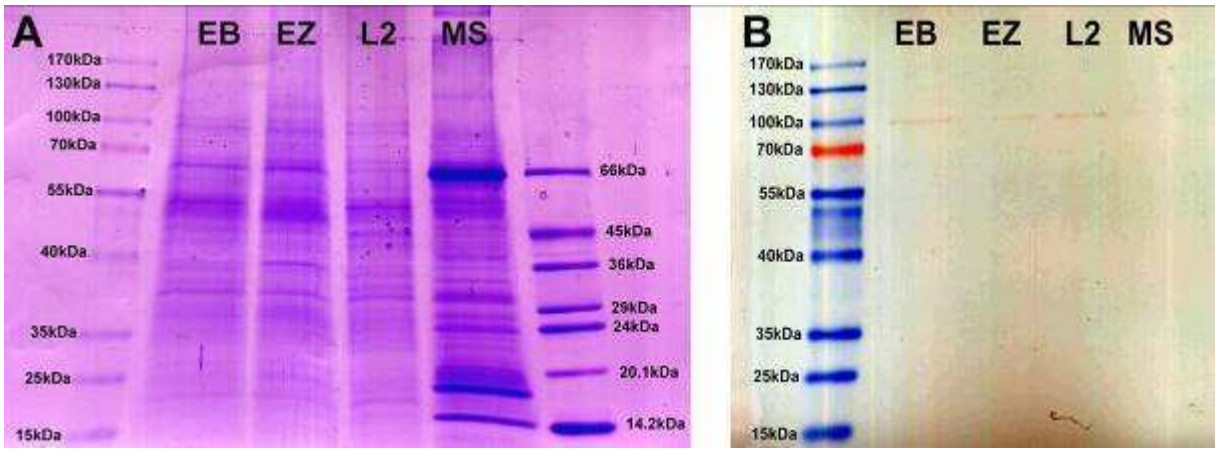

Figure 3.32 Coomassie stained SDS polyacrylamide gel and Western blot of plasma membrane proteins from different leaf regions

Gradient SDS polyacrylamide gel stained Coomassie Brilliant Blue R250 (A) shows the difference or similarity in membrane protein pattern of emerged leaf blade three (EB), elongation zone of leaf three (EZ), fully expanded leaf blade from leaf two (L2) and microsomal fraction from emerged leaf blade two (MS). Western blot (B) analysis demonstrated the presence of PM-H^+-ATPase in the isolates and also that the commercially available antibody recognised barley PM-H^+-ATPase (expected molecular weight of about 105 kDa). The band intensity was too weak to allow densitometric analyses of bands. This had to be done subsequently using a more sensitive detection system for the secondary antibody employed

3.4.3 Quantitative analysis of PM-H$^+$-ATPase protein

Sensitivity of the Western blot detection system at Eötvös University, where plasma membrane isolations and ATPase enzyme assays were carried out, was not enough to perform quantitative analysis on blots. Using the same samples in Dublin (having transported the samples on dry ice from Budapest) on thinner gels and chemiluminescence detection the proportion of PM-H$^+$-ATPase in total membrane protein was measured using a densitometric approach. The same amount of total membrane protein (5 μg) from the elongation zone contained 2.33 times higher concentration of PM-H$^+$-ATPase protein than non-growing leaf blade (Fig. 3.33 A). Densitometry of Coomassie stained gradient gels supported Western blot data. A higher PM-H$^+$-ATPase protein expression was measured in the elongation zone (Fig. 3.33 B) although the difference using the PM-H$^+$-ATPase band on SDS gels (identified based on molecular weight and Western blots) was lower with the ratio between the two leaf regions being 1.5 fold compared with 2.33-fold above.

The higher sensitivity of the second Western blot approach made it possible to detect a second band on the blot, at around 70 kDa. This might represents a fragment of the PM-H$^+$-ATPase enzyme (Fig. 3.33 C)

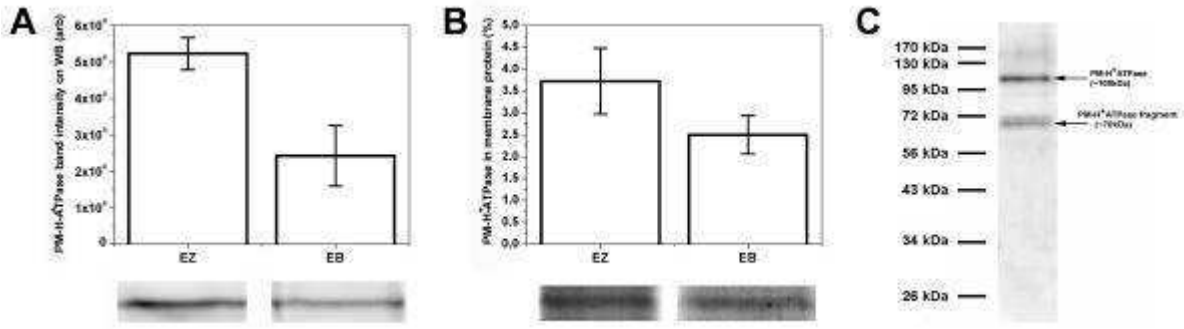

Figure 3.33 PM-H$^+$-ATPase ratio in total membrane protein

PM-H$^+$-ATPase protein, expressed on the basis of total plasma membrane protein applied onto gels (and entered into Western blots) was significantly higher in the elongation zone (EZ) compare with emerged blade (EB) (A); the same applied to densitometric analyses of Coomassie Brilliant Blue stained polyacrylamide gels (B). Results are significant using Student's t-test ($p < 0.05$). Using higher sensitivity on Western blots a second band was found which respresents most likely a 70 kDa fragment of the PM-H$^+$-ATPase (C).

3.4.4 Activity of PM-H^+-ATPase

Vandate-sensitive ATPase activity of membrane fractions was measured using inside-out plasma membrane vesicles and an ATP hydrolysis assay. Results were expressed in nmolP_i h^{-1} μg^{-1} total membrane protein at 28 °C. As Fig. 3.34 shows plasma membrane vesicles of the elongation zone had more than 2 times higher vanadate-sensitive ATPase activity compared with vesicles prepared from the emerged blade. Vacuolar and prokaryotic types of ATPases were blocked using high azide and nitrate concentration in the reaction mixture, and data were validated with vanadate sensitivity. The resulting enzyme activity represented PM-H^+-ATPase activity and this was two fold higher in the plasma membrane of the elongation zone compare with membranes prepared from the emerged leaf blade.

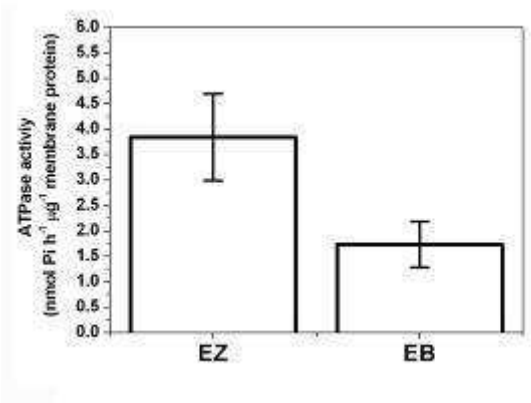

Figure 3.34 ATPase activity of inside-out plasma membrane vesicles

Vanadate-sensitive ATP hydrolysis activity of inside-out plasma membrane vesicles of the elongation zone (EZ) was more than two times higher than activity in the emerged blade of leaf three of barley (EB). Results are averages of four independent batches of membranes and 9 - 10 replicate activity determinations. Differences were statistically significant ($p < 0.05$) using Student's t-test.

3.4.5 Immunolocalisation of PM-H^+-ATPase

Paraffin-embedded sections were used to localise the tissue-specific distribution of PM-H^+-ATPase protein. Alkaline phosphatase-labelled secondary antibody with fast red detection was used. Reddish colour showed the location of PM-H^+-ATPase protein. There was no difference in PM-H^+-ATPase distribution between the elongation zone (Fig. 3.35 A) and emerged blade (Fig. 3.35 B). Higher expression of PM-H^+-ATPase was found in guard cells (Fig. 3.35 E), phloem, and xylem parenchyma. PM-H^+-ATPase was detected virtually on the plasma membrane of every living cell. Longitudinal sections of the elongation zone (Fig. 3.35 D) provided

further detail. Guard cells were easily identifiable. Dead parts of xylem tubes were free from red colour, whereas phloem and xylem parenchyma cells contained large amount of PM-H^+-ATPase. Negative control (Fig. 3.35 C), where primary PM-H^+-ATPase specific antibody was not applied, verified the selectivity of the assay as immunospecific staining was not present.

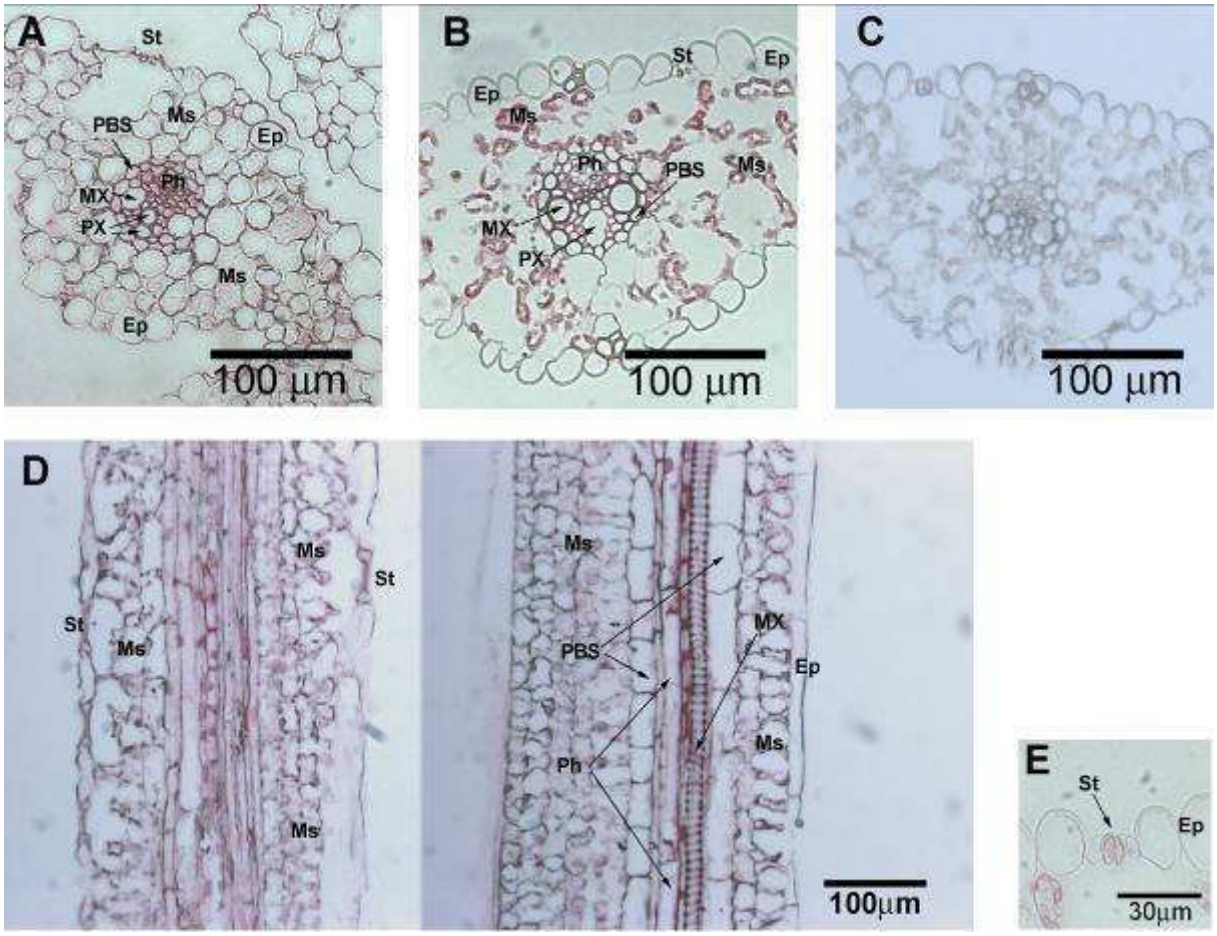

Figure 3.35 PM-H^+-ATPase immunolocalisation on leaf cross and longitudinal sections

PM-H^+-ATPase expression was detectable on all plasma membranes, both in the elongation zone (A) and emerged blade (B). Higher expression was present in guard cells (E), phloem and xylem and phloem subsidiary cells. Differences between elongation zone and emerged blade were not visible. Negative control (primary antibody was not applied) was free from immunolabelling (C). Longitudinal sections of elongation zones (D) were supporting observations from cross sections, stomata guard cells and vascular elements and subsidiary cells being heavily stained. Ep: epidermis; St: stomata; MX: metaxylem; PX: protoxylem; Ph: phloem; Ms: mesophyll cells; PBD: parenchymateous bundle sheath.

4 Discussion

4.1 Growth-associated apoplast acidification

Using different methods to measure or visualise apoplastic pH or H^+ transport activity into the intercellular space, a lower pH was recorded in the elongation zone compared with emerged blade of barley leaves. This observation is in agreement with the 'acid growth theory' which would predict a more acid apoplast pH in growing tissue.

4.1.1 Apoplast pH difference between growing and non-growing leaf tissue

Three independent approaches were used to analyse apoplast pH. Microelectrode pH measurements provided the most quantitative data. Also, similar to confocal analyses and contrary to the in-vitro gel system, microelectrode analyses measured pH in the actual wall or apoplast space. These measurements showed that the pH in the apoplast was by up to 1 pH unit lower and, therefore, the H^+ concentration up to 10-fold higher in elongating tissue. There do not exist any directly comparable studies on other grass leaves, although slightly different approaches have been taken for some species. When pH was measured in droplets placed on the exposed elongation zone of maize leaves a lower apoplastic pH compared with the emerged blade or elongation zone under non-growing conditions was measured; the absolute pH values in these droplets were significantly higher than the ones measured here, and the pH reading was not stable but drifted during recordings (Van Volkenburgh & Boyer, 1985; Neves-Piestun & Bernstein, 2001). Using 0.5 g of growing maize leaf segments in 2 ml unbuffered bathing medium, Neves-Piestun & Bernstein (2001) measured a pH of 4.8, a value which is very similar to the value recorded here for barley leaves.

4.1.2 Reliability of pH values measured in elongation zone and emerged blade

Microelectrode measurements revealed that apoplast pH in the leaf elongation zone depended on the bathing medium concentration of K^+. At the lowest K^+ concentration tested (0.1 mM) apoplast pH was 4.8, yet at 10 mM K^+, apoplast pH increased to 5.8

and was identical to the value in emerged tissue (Fig. 3.7). Since the emerged leaf contains at its surface a major permeance barrier (cuticle) to externally applied solution, this could mean that the difference in pH observed between leaf regions was an artefact and reflected differences in the access of bath solution between leaf regions. If, by chance, the K^+ concentration in the apoplast of the emerged blade of intact plants had been 10 mM, or at least higher than 1 mM, and if none of the external bathing solution had reached the apoplast, one would have predicted an apoplast pH of 5.8 based on measurements for elongating tissue at 10 mM K^+. Felle (2006) measured an apoplastic K^+ concentration of 2.6 mM in mature barley leaves. Also, if the apoplast K^+ concentration in the leaf elongation zone *in-planta* was close to 10 mM, one would not expect to find a difference in apoplast pH between the two leaf regions in intact, undisturbed plants. Recently, Ehlert *et al*. (2011) reported apoplast pH between 4.1 and 5.9 with average mean of 5.1 for elongating maize leaf tissue as analysed through pH microelectrodes.

Felle (2006) inserted pH microelectrodes through stomatal pores of mature barley leaves and measured a pH of 4.88. This pH is significantly lower than the pH reported here (pH 5.8) for emerged blade tissue. Possibly, the difference in results is due to use of 2 mM MES / TRIS buffer (pH 5.0) in the bathing medium in the study by Felle (2006). Also, measurements by Felle (2006) were carried out under illumination, stimulating PM-H^+-ATPase pump activity (Stahlberg & Van Volkenburgh, 1999), whereas the present measurements were carried out in the dark. In a natural setting, the mature blade is exposed to full, ambient light whereas the elongation zone receives less light, and this light is green-filtered due to subtending sheaths. Therefore, it is possible that the difference in apoplast pH between leaf regions in field-grown and -analysed plants is considerably smaller than the difference measured here with the microelectrode setup in a darkened laboratory environment or through confocal analyses on intact leaves. Vanadate experiments on detached leaves clearly showed that the lower apoplast pH in the barley leaf elongation zone depended on the activity of the PM-H^+-ATPase.

4.1.3 Relation between apoplast acidification and leaf growth

Acidification of the apoplast in the elongation zone of barley leaves generally coincided with growth, but there were notable exceptions. A positive relation was best visualised by cold treatment in the in-vitro gel system (Fig. 3.3). In the same system vanadate and fusicoccin treatments caused parallel changes in the growth

rate of leaves and acidification of medium adjacent to leaf apoplast (Fig. 3.1). Also, vanadate treatment in the microelectrode setup reduced growth and increased apoplast pH in the elongation zone to a value usually observed for mature tissue. However, when fusicoccin was applied in the pH microelectrode setup, growth increased while apoplast pH remained unchanged (Fig. 3.9 and 3.10). Also, changing the apoplast K^+ concentration from 0.1 to 1 or 10 mM significantly increased apoplast pH in the elongation zone, yet growth did not change (Fig. 3.7 and 3.8). Irrespective of the underlying mechanisms, these data show that there does not exist a simple, single relation of how apoplast pH relates to growth in the leaf elongation zone. The seemingly contradictory fusicoccin data obtained through the microelectrode and in-vitro gel setup could be explained through differences in what these two setups measured. The in-vitro gel system measured bulk effects on pH further away from the leaf surface and showed an increase in the acidified area and corresponding net production rate of H^+, and H^+ was titrated by the pH indicator bromocresol purple. In contrast, the microelectrode setup provided a point measurement of pH closer to the cell surface, irrespective of the rate at which H^+ diffused into surrounding bathing medium or was consumed through transport processes involving K^+. Thus, while fusicoccin will have stimulated H^+ pumping in both setups and led to increased diffusion, apoplast pH may not have changed in either setup.

4.2 K^+ and apoplast acidification

Potassium uptake coupled to H^+ uptake (symport) has been discussed as an alternative explanation for some of the effects associated with the 'acid growth' theory. For example, K^+ uptake and apoplast acidification were linked to growth in roots (Glass *et al.*, 1981; Ullrich & Novacky, 1990; Amtmann *et al.*, 1999) and coleoptiles (Claussen *et al.*, 1997; Tode & Lüthen, 2001; Christian *et al.*, 2006). The present data also suggest that K^+ transport and apoplast acidification are linked with each other in some way during elongation of barley leaf cells.

4.2.1 Potassium uptake and leaf growth

A previous patch-clamp study on K^+ transport in barley concluded that apoplast K^+ must exceed 3 - 5 mM to allow growing leaf cells to take up K^+ through channels (Boscari *et al*., 2009; Volkov *et al*., 2009). Calculations showed that at 10 mM apoplast K^+, about 50 % of K^+ uptake was facilitated by time-dependent inward-rectifying currents typical of Shaker K^+ channels such as AKT1 or AKT2. The

remaining 50 % was facilitated by instantaneous currents, which includes either or both, K^+ high-affinity transporters such as HAK / KUP / KT type K^+ / H^+ symporters (for historical reasons, these three abbreviations denote the same type of symporters; for details see e.g. Ashley *et al.* (2006) and Szczerba *et al.* (2009)) or non-selective cation channels. At apoplast concentrations below 3 - 5 mM, uptake of K^+ would have to occur through high-affinity uptake mechanisms. The K^+ concentrations tested in the present study covered the range 0.1 to 10 mM. Therefore, it is possible that different K^+ uptake mechanisms contributed to the growth and pH response of leaves depending on the K^+ concentration of bathing medium. When K^+ uptake was blocked through application of inhibitors (Cs^+, TEA) of K^+ inward-rectifying Shaker-type channels, or at least reduced significantly, growth was reduced by 50 %. A similar reduction in growth was observed in response to vanadate and CsCl-vanadate double treatments (applied at 10 mM bathing medium K^+; Fig. 3.17). The latter observation excludes the possibility that Cs^+ (K^+ channels) and vanadate (PM-H^+-ATPase) inhibited 'different' 50 % of growth and were additive. Instead, growth was reduced through some common mechanism. Membrane potential was not measured in response to the above treatments, but the most likely scenario is that inhibition of PM-H^+-ATPase through vanadate depolarised membrane potential to such an extent that uptake of K^+ through channels was thermodynamically not possible. This would explain why direct blockage of channels through Cs^+ caused the same growth reduction as blockage of PM-H^+-ATPase. Similarly, Tode & Lüthen (2001) concluded from experiments involving TEA that the acid-growth type response of maize coleoptiles required the activity of inward-rectifying K^+ channels. Linkage of K^+ transport, leaf growth and cell wall acidification was found in light-induced growth of tobacco leaves (Stiles *et al.*, 2003), yet K^+ uptake was required for H^+ efflux and growth without any noticeable accumulation of solutes (Stiles & Van Volkenburgh, 2004). This would exclude a primarily osmotic requirement for K^+.

4.2.2 High affinity potassium transporters and leaf growth

High affinity K^+ transporters, but not K^+ selective channels, are reduced in transport activity by ammonium (Kronzucker *et al.*, 2003; Rodriguez-Navarro & Rubio, 2006; Szczerba *et al.*, 2009; Hoopen *et al.*, 2010). Application of 20 mM NH_4^+ during LVDT experiments reduced growth by as much as Cs^+, TEA and vanadate treatments did. This shows that high affinity K^+ uptake systems were involved in K^+ uptake and

growth response of elongating barley leaf cells. The results also show that the three components, apoplast pH, high-affinity and channel-mediated K^+ uptake were related to each other in some way that prevented inhibition of each component from being additive.

Boscari *et al.* (2009) observed that HvHAK4 was expressed particularly in the elongation zone of barley leaves. It is not known whether HvHAK4 functions as K^+ / H^+ symporter as thought for other HAK family members (Britto & Kronzucker, 2008; Szczerba *et al.*, 2009). If it does, HvHAK4 may not only provide a major route for K^+ entry into growing barley leaf cells, but also present a key mechanism through which the pump activity of the PM-H^+-ATPase can be linked to osmotically-driven water uptake and apoplast acidification in growing leaf tissues. This needs to be studied further.

4.3 PM-H^+-ATPase expression and leaf elongation

Using four independent techniques (qPCR, ATPase assay and densitometry on SDS PAGE and Western blot) it was found that the expression, activity and protein level of PM-H^+-ATPase when related to the surface area of plasma membrane, was between 1.5 - 3.5 times higher in the elongation zone compared with the emerged blade (Table 4.1). The similarity in results for expression, protein level and activity may be a coincidence, but more likely reflects a true difference between growing and non-growing barley leaf tissues.

Table 4.1 Summary of data for PM-H^+-ATPase when related to surface area of plasma membrane. Ratio and standard deviation (SD) was calculated in two ways (a: averages of elongation zone (EZ) were divided by averages of emerged blade (EB) or i: average of ratio of paired EZ and EB). SDs in bracket are estimated SDs.

Experiment type	Ratio EZ : EB	SD
qPCR (Golf, a)	1.96	± (0.47)
qPCR (Golf, i)	1.99	± 0.28
qPCR (Jersey, a)	2.36	± (0.91)
qPCR (Jersey, i)	3.53	± 2.88
qPCR (Jersey protoplasts, a)	2.13	± (0.70)
qPCR (Jersey protoplasts, i)	2.35	± 0.49
Vanadate sensitive ATPase activity (Jersey, a)	2.22	± (0.55)
Coomassie stained SDS PAGE (Jersey, a)	1.50	± (0.35)
Western Blot (Jersey, a)	2.33	± (0.72)

Quantification of PM-H^+-ATPase protein level using Coomassie stained PAGE gels gave the lowest difference between elongation zone and emerged blade. This may result from individual bands, such as the band of the PM-H^+-ATPase, containing numerous different proteins. For example, Hynek *et al.* (2006) concluded from MS / MS analyses of the PM-H^+-ATPase band of plasma membrane vesicles prepared from barley aleurone layer that the band contained 22 different peptides. Together, the data suggest that the density at which functional PM-H^+-ATPase is localised in the plasma membrane, or at which PM-H^+-ATPase is expressed per unit plasma membrane surface area of cells is about twice as high in growing as in non-growing leaf regions. Also, expression and protein data suggest that the efficiency of translation of PM-H^+-ATPase mRNA is similar in the two leaf regions.

4.3.1 PM-H^+-ATPase density in plasma membrane and leaf growth

The higher plasma membrane density of PM-H^+-ATPase in the elongation zone will aid the energisation required for continuous solute uptake, in particular uptake of K^+, in growing leaf cells. It will also aid acidification of the apoplast as measured through pH microlelectrodes in the barley leaf elongation zone. Depending on the apoplast K^+ concentration, the pH in the elongation zone was by up to 1.0 pH unit lower (pH micro electrode measurements; Fig. 3.7) in the elongation zone compared with emerged blade. This corresponds to a 10-fold difference in apoplast H^+ concentration and suggests that there exist post-translational modifications which further increase the PM-H^+ATPase pump activity in growing barley leaf cells. Having said this, the wall space of growing cells is smaller (thinner walls) and this will aid apoplast acidification for a given pump activity. Apoplast acidification also depends on factors which are not related directly to the protein level and activity of PM-H^+-ATPase such as apoplast K^+ concentration (Claussen *et al.,* 1997;Tode & Lüthen, 2001), temperature (Stoddart & Lloyd, 1986; Pollock *et al.*, 1990) hormones (especially auxin, e.g.: Rayle & Cleland, 1970; Hager *et al.*, 1971; Rayle & Cleland, 1992; Claussen *et al.*, 1997; Tode & Lüthen, 2001; Hager, 2003; Grebe, 2005; Kutschera, 2006) and light (Van Volkenburgh & Cleland, 1980; Stahlberg & Van Volkenburgh, 1999).

4.3.2 qPCR data

Determination of cell size and cell number can involve comparably large errors, due to the variation in size between populations and types of cell and due to small difference in cell radius (protoplasts) causing large differences in calculated cell volumes. Despite these intrinsic uncertainties, the present calculations showed that the PM-H^+-ATPase expression per cell is very similar in growing and non-growing leaf tissue. Due to the lower surface area of the plasma membrane in growing cells (always assuming that there are no major invaginations of the plasma membrane, or that these would not differ between leaf regions), the density of PM-H^+-ATPase is higher than the density in non-growing cells. As growing cells reach their full size, plasma membrane surface area increases leading to a continuous 'dilution' of PM-H^+-ATPase molecules. In such a scenario, the amount of PM-H^+-ATPase per cell seems to be a fixed size, and cessation of growth seems to coincide with a continuous dilution of PM-H^+-ATPas activity, resulting in decreasing rates of apoplast acidification (see also Fig. 3.25, Fig. 3.26 and Fig. 3.27). qPCR analysis of mesophyll protoplasts isolated from the elongation zone and emerged blade of the barley cultivar Jersey further supported the reliability of the calculated cell numbers of qPCR samples. Total RNA content of Golf and Jersey tissues per cell was very similar to total RNA content per protoplast. PM-H^+-ATPase expression data obtained for protoplasts, when expressed per protoplast number or total plasma membrane surface were lower but not significantly different to the other qPCR data for Jersey where expression was related to the calculated cell number or total membrane surface (see Table 3.5 and Fig. 3.27). The lower expression values are in agreement with immuno localisation results on leaf cross-sections which showed that mesophyll cells have a comparatively (to other leaf tissues) lower PM-H^+-ATPase expression. For RNA extraction from leaf segments, all types of cells were homogenised and accordingly averaged. In contrast, protoplasts were islolated only from mesophyll.

qPCR expression analyses also showed that the Ct value of PM-H^+-ATPase expression was almost identical in growing and non-growing leaf regions using the same amount of total RNA (250 - 500 pg). Therefore, when expression data are related to unit of extracted RNA, PM-H^+-ATPase (Ha1 AY136627; GI:23306665) is an ideal reference gene for expression analysis when comparing growing and non-growing leaf regions, in agreement with Boscari *et al*. (2009) and Besse *et al.* (2011) (see Table 3.5 and Fig. 3.27). The same applies to the PM-H^+-ATPase isoforms AHA1 and AHA2 in *Arabidopsis* (Gaxiola *et al*., 2007).

4.3.4 Immunolocalisation of PM-H^+-ATPase

Immunohistological analyses provided results which are in agreement with previous studies on the tissue localisation of PM-H^+-ATPase protein (Villalba *et al.*, 1991; Bouche-Pillon *et al.*, 1994; Michelet & Boutry, 1995; Morsomme & Boutry, 2000; Palmgren, 2001; Gaxiola *et al.*, 2007). Most staining, and by implication, PM-H^+-ATPase protein, was observed in those leaf tissues which are characterised by high rates of solute exchange across the plasma membrane (guard cells) or high rates of solute loading / unloading associated with long-distance transport pathways (phloem; xylem parenchyma). Interestingly, but in agreement with previous studies, epidermis cells were not enriched in PM-H^+-ATPase (Villalba *et al*., 1991). This was observed in elongation zone and emerged blade and shows that there exists a cell-type-specific control of PM-H^+-ATPase protein level which is superimposed on any developmental gradient.

4.4 Leaf growth and changes in cell wall properties

The effect of chemical treatments (vanadate, CsCl, fusicoccin) on cell wall properties was followed with the LVDT system. Fusicoccin increased the elasticity without affecting the plasticity of walls. In contrast, CsCl decreased the plastic component yet did not alter the elastic component of cell wall. Vanadate did not modify either component. From these results it can be concluded that PM-H^+-ATPase activity, which is inhibited by vandate, is not required to maintain wall elasticity or plasticity. The fusicoccin treatment did not cause changes in the plastic component of the cell wall. Since plasticity is the relevant size for growth (irreversible expansion), and since plasticity is thought to change with apoplast pH through action of expansions (Cosgrove, 1996), fusicoccin probably did not decrease the apoplast pH (in agreement with the microelectrode measurements where fusicoccin failed to cause apoplast acidification) or it facilitated leaf elongation through a mechanism other than ‘acid growth’. The increased $\Delta\Delta v$ suggests that in the background of fusicoccin-related growth facilitated K^+ uptake may be found (both v_1 and v_2 were higher than in the control). The increased elasticity of the cell wall may be caused by a cell wall modifying protein or enzyme activated by increased H^+ transport acrosss the plasma membrane into the cell wall space as the experiments with the agarose gel system showed. If fusicoccin increased the H^+ excretion through plasma membrane and the H^+ returned into the cell through H^+ / K^+ symport, then micro pH measurements,

in-vitro gel records and cell wall property data would support each other. However, this would require that the change in H^+ concentration close to the site where proteins act in the wall was either so small or so inaccessible that it could not be measured with the microelectrodes.

4.5 'Acid growth' in barley leaves?

Auxin is one of the most important hormones in plants and its involvement in growth is unquestionable, at least in coleoptiles (Rayle & Cleland, 1970; Lüthen *et al.*, 1990; Rayle & Cleland, 1992; Kutschera, 1994) or roots (Christian *et al*., 2006; Kutschera, 2006).

Surprisingly, in the present study the artificial auxin NAA did not cause any effect on leaf growth or apoplast acidification as tested through the in-vitro gel system (Fig. 3.6) or LVDT measurements (Fig. 3.19). In a related study on the barley cultivar investigated here, the elongation zone was not exposed by peeling back the sheath of leaves one and two but, instead, a small window was cut into these sheaths, causing less physical damage to the plant. Even in this system, application of 5 and 10 μM indole acetic acid (IAA) to the apoplast of the elongation zone did not increase the growth rate of leaves (Touati *et al.*, unpublished). For some reason, the barley leaves tested here seem not to be sensitive to externally-applied auxin. A possible interpretation could be that the third leaf, when measured in this project was in the development stage of maximum growth, and the internal auxin concentration might have been so high that any auxin-dependent growth mechanisms was saturated and externally applied auxin could not cause any further increase in growth. The elongation zone of leaf one of wheat has been reported to contain IAA at 500 - 600 ng g^{-1} fresh weight (Vysotskaya *et al*., 2003) and this would mean that IAA oocurs naturally in the μM range.

4.6 Model of leaf growth in barley

Under different treatments the role of PM-H^+-ATPase and high or low affinity K^+ uptake system was tested in relation to elongation growth and apoplast acidification in leaf three of barley. The predicted effects of test reagents on growth and acidification are summarised in Fig. 4.1. The results partly support the classical 'acid growth' theory and partly the 'facilitated solute uptake' theory. PM-H^+-ATPase dependent H^+ excretion is essential for at least 50 % of leaf growth. However, the equilibrium pH is not necessarily reflecting changes in transmembrane H^+ pumping

because H^+ / K^+ symport might transport protons back into the cell as Fig. 4.1 shows. Treatments with different K^+ transport blockers (TEA, CsCl, NH_4^+) and their double treatments with sodium-orthovanadate, the PM-H^+-ATPase blocker, suggested that in the background of the 'acid growth' of barley leaves an active HAK type K^+ uptake system might play a key role in facilitating a H^+ / K^+ symport mechanism (Bañuelos *et al.*, 2002; Bucker *et al.*, 2006; Britto & Kronzucker, 2008; Szczerba *et al.*, 2009). Acidification of the cell wall or protonation of some enzymes in the cell wall might have additional important role in growth as cell wall property measurements showed. HvHAK4, a member of the family of K^+ transporters, is mainly present in barley shoots (Rubio *et al.*, 2000) and it has significantly higher expression in the leaf elongation zone (Boscari *et al*., 2009), further supporting the idea of a combined 'acid growth' and 'facilitated solute uptake'.

Based on qPCR, enzyme activity and Western blot result, PM-H^+-ATPase expression in the plasma membrane might be controlled by a simple mechanism. The enzyme density in the plasma membrane can be diluted by cell growth; its density in the plasma membrane changes with cell size. The total number of PM-H^+-ATPase molecules was constant at cellular level while the total membrane surface increasing more than two-fold during cell development (Fig. 3.25 and Fig. 3.26). Taking into consideration all of the present results (expression analysis and physiological measurements with pH, H^+ transport activity and K^+ uptake during the leaf development) and published information about expression of HvHAK4 (Rubio *et al.*, 2000; Boscari *et al.*, 2009) leads to the model shown on Fig. 4.2. The 50 % of leaf growth that was sensitive to inhibition of PM-H^+-ATPase requires high expression of HvHAK4 in the elongation zone (Boscari *et al.*, 2009) and a high plasma membrane density of PM-H^+-ATPase molecules.

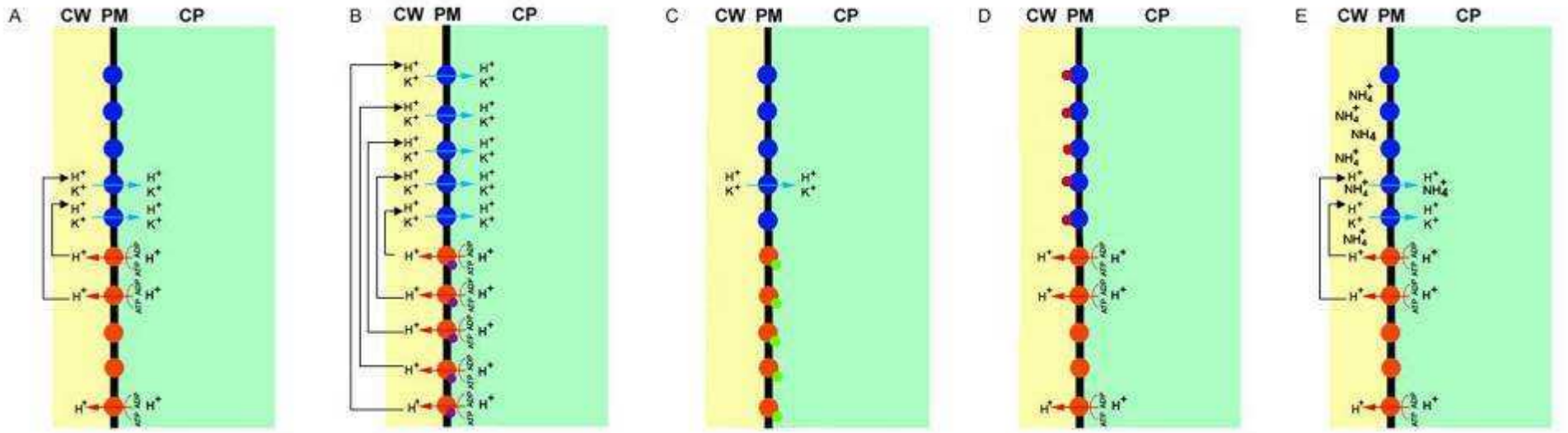

Figure 4.1 Supposed effect of the treatments on barley leaf cells

On the sketches cell wall (apoplast, CW) is labelled with yellow colour, cytoplasm (CP) is green and black lines refer to plasma membrane (PM). Orange balls symbolise PM-H^+-ATPase and blue balls are high affinity H^+ / K^+ symporters. Under control conditions PM-H^+-ATPases pump out the H^+ and K^+ are taken up into the cell through high affinity K^+ transporters (A). Fusicoccin (purple dots) permanently activate all the proton pumps and this massive H^+ efflux is short cut by K^+ transporter activity, causing higher turgor pressure in the cells and accelerates leaf growth (B). Vanadate (green dots) permanently blocks PM-H^+-ATPase and without H^+ transport K^+ uptake and growth are inhibited (C). Caesium ions blocks (deep red dots) K^+ transporters and reduce leaf growth (D) and ammonium ions (NH_4^+) reduce active K^+ accumulation through a competitive way and reduce growth (E).

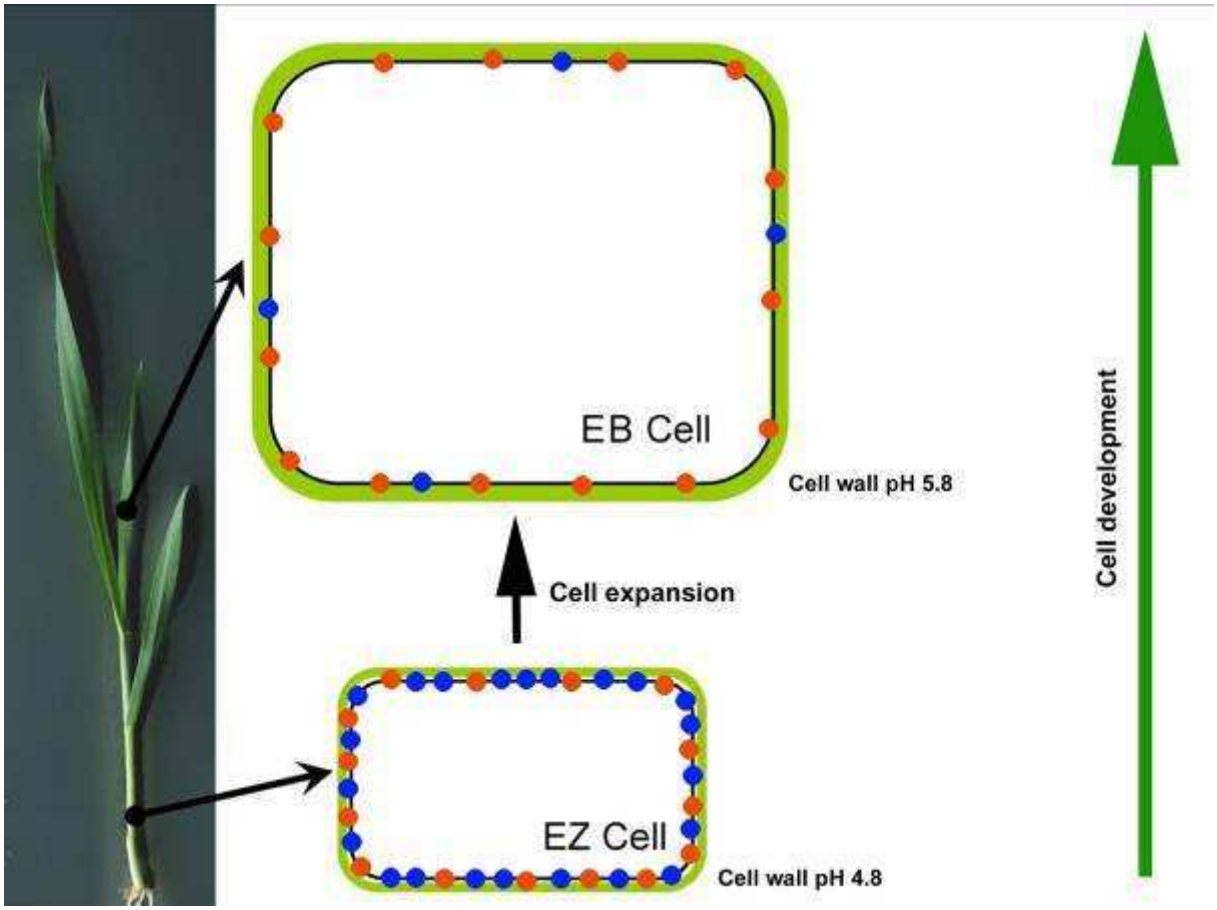

Figure 4.2 Model of leaf elongation in barley leaves

Cell size and membrane surface are increased 2 - 3 fold during cell development, as cells expand in the elongation zone (EZ) and finally reach full maturity in the emerged blade (EB). The number of PM-H^+-ATPase molecules (orange balls) per cell is constant where as HvHAK4 (blue balls) expression (and presumably protein level) per cell decreases significantly during cell development. Therefore, both the maximum proton transport and K^+ accumulation capacity are significantly higher in the elongation zone than in the emerged blade cell and can facilitate elongation growth through ‘acid growth’ and ‘solute accumulation’. On the figure light green colour represents the cell wall and the black line the plasma membrane.

5 Conclusions and future work

5.1 Conclusions

(i) In this study the pH and H^+ transport activity were examined in the elongation zone and the non-growing emerged blade portion of leaf three of barley, using three independent approaches - an in-vitro gel system with bromochresol purple as pH indicator, confocal microscopy combined with pH sensitive fluoresceince probes and microelectrode technique. All techniques show a lower pH / higher proton efflux in the elongation zone compared with emerged blade and support the classical 'acid growth' theory for the elongation growth of plant organs.

(ii) Experiments with K^+ channel and transporter blockers, and with PM-H^+-ATPase activator and blocker point to new aspects of the acid growth theory when applied to barley leaves. LVDT measurements, analyses of cell wall property and microelectrode pH results suggest that a lower or higher H^+ transport activity is not linked directly to leaf growth, but linked through a H^+ / K^+ symport system which facilitates solute (especially K^+) uptake into growing cells. Changes in cell wall properties suggest that elongation of barley leaves can be described with a combination of the classical 'acid growth' and the 'facilitated solute uptake' theory.

(iii) In expression studies, both at the gene and protein level, a two fold higher PM-H^+-ATPase density per unit plasma membrane surface area is found in growing compared with non-growing leaf tissue. PM-H^+-ATPase seems an ideal reference gene in studies where growing and non-growing barley leaf tissues need to be compared. The copy number of the enzyme in the plasma membrane might be controlled by a simple mechanism of growth-dilution: the total amount of PM-H^+-ATPase is constant in the cells and the plasma membrane surface increases during cell and tissue development.

(iv) Immunohistological analyses show that PM-H^+-ATPase protein is present mainly in those leaf tissues which are characterised by high rates of solute exchange across the plasma membrane (guard cells) or high rates of solute loading / unloading associated with long-distance transport pathways (phloem; xylem parenchyma). This applies to both elongation zone and emerged blade and shows that there exists a cell-type-specific control of PM-H^+-ATPase protein level which is superimposed on any developmental gradient.

5.2 Future works

(i) Due to limited financial resources only some pH micro electrode measurements could be carried out. It would be interesting to further study the relation between apoplastic K^+ concentration and cell wall acidification applying 10 mM KCl treatment togheter with 5 μM fucicoccin and K^+ transporter blockers e.g. CsCl, TEA or NH_4^+.

(ii) Using inside-out plasma membrane vesicles and fluorimetric approach proton pumping activity could be monitored. Within this project preliminary experiments were carried out and 5(6)carboxyfluorescein seem a good candidate for these probes (better for this purpose than acridine orange that was used by many previous studies e.g. Yan *et al.* (1998); Yan *et al.* (2002); Zörb *et al.* (2005); Pitann *et al.* (2009b); Zhu *et al.* (2009); Wakeel *et al.* (2010). Due to time constraints, these experiments could not be finished. Results of these vesicular transport assays could further support PM-H^+-ATPase activity data.

(iii) Most of the present data point to HvHAK4 playing a key role in leaf cell elongation growth in barley. HvHAK4 is a putative K^+ / H^+ symporter, yet the precise function and characteristics of this transporter remain unknown. It would be good to carry out functionality tests of HvHAK4 and its regulation through test reagents which also impact on growth and PM-H^+-ATPase.

6 Literature

Amtmann A, Jelitto TC, Sanders D. 1999. K^+-selective inward-rectifying channels and apoplastic pH in barley roots. *Plant Physiol.* **120**: 331-338.

Arif I, Newman I. 1993. Proton efflux from oat coleoptile cells and exchange with wall calcium after IAA or fusicoccin treatment. *Planta* **189**: 377-383.

Ashley MK, Grant M, Grabov A. 2006. Plant responses to potassium deficiencies: A role for potassium transport proteins. *J. Exp. Bot.* **57**: 425-436.

Babcock DF. 1983. Examination of the intracellular ionic environment and of ionophore action by null point measurements employing the fluorescein chromophore. *J. Biol. Chem.* **258**: 6380-6389.

Bañuelos MA, Garciadeblas B, Cubero B, Rodríguez-Navarro A. 2002. Inventory and functional characterization of the HAK potassium transporters of rice. *Plant Physiol.* **130**: 784-795.

Besse M, Knipfer T, Miller AJ, Verdeil J-L, Jahn TP, Fricke W. 2011. Developmental pattern of aquaporin expression in barley (*Hordeum vulgare* L.) leaves. *J. Exp. Bot.* **62**: 4127-4142.

Boscari A, Clément M, Volkov V, Golldack D, Hybiak J, Miller AJ, Amtmann A, Fricke W. 2009. Potassium channels in barley: Cloning, functional characterization and expression analyses in relation to leaf growth and development. *Plant, Cell Environ.* **32**: 1761-1777.

Bouche-Pillon S, Fleurat-Lessard P, Fromont JC, Serrano R, Bonnemain JL. 1994. Immunolocalization of the plasma membrane H^+ -ATPase in minor veins of *Vicia faba* in relation to phloem loading. *Plant Physiol.* **105**: 691-697.

Boyer JS. 2001. Growth-induced water potentials originate from wall yielding during growth. *J. Exp. Bot.* **52**: 1483-1488.

Britto DT, Ebrahimi-Ardebili S, Hamam AM, Coskun D, Kronzucker HJ. 2010. ^{42}K analysis of sodium-induced potassium efflux in barley: Mechanism and relevance to salt tolerance. *New Phytol.* **186**: 373-384.

Britto DT, Kronzucker HJ. 2008. Cellular mechanisms of potassium transport in plants. *Physiol. Plant.* **133**: 637-650.

Brummer B, Felle H, Parish RW. 1984. Evidence that acid solutions induce plant cell elongation by acidifying the cytosol and stimulating the proton pump. *FEBS Letters* **174**: 223-227.

Bucker CA, de Souza SR, Fernandes MS. 2006. Effects of fusicoccin and vanadate on proton extrusion and potassium uptake by rice. *J. Plant Nutr.* **29**: 485-496.

Chazen O, Neumann PM. 1994. Hydraulic signals from the roots and rapid cell-wall hardening in growing maize (*Zea mays* L.) leaves are primary responses to polyethylene glycol-induced water deficits. *Plant Physiol.* **104**: 1385-1392.

Christian M, Steffens B, Schenck D, Burmester S, Böttger M, Lüthen H 2006. How does auxin enhance cell elongation? Roles of auxin-binding proteins and potassium channels in growth control. *Plant Biol.* 346-352.

Claussen M, Lüthen H, Blatt M, Bottger M. 1997. Auxin-induced growth and its linkage to potassium channels. *Planta* **201**: 227-234.

Clerc S, Barenholz Y. 1998. A quantitative model for using acridine orange as a transmembrane pH gradient probe. *Anal. Biochem.* **259**: 104-111.

Collins D, Walpole C, Ryan E, Winter D, Baird A, Stewart G. 2011. UT-B1 mediates transepithelial urea flux in the rat gastrointestinal tract. *J. Membr. Biol.* **239**: 123-130.

Conway EJ, O'Malley E. 1946. The nature of the cation exchanges during yeast fermentation, with formation of 0.02N-H ion. *Biochem. J.* **40**: 59-67.

Cosgrove DJ. 1993. Wall extensibility - its nature, measurement and relationship to plant-cell growth. *New Phytol.* **124**: 1-23.

Cosgrove DJ 1996. Plant cell enlargement and the action of expansins. BioEssays **18:** 533-540.

Cosgrove DJ. 1998. Cell wall loosening by expansins. *Plant Physiol.* **118**: 333-339.

Csiszár J, Erdei L, Pécsváradi A, Szabó M, Tari I. 2004. Növényélettan, növekedés- és fejlődésélettan (Plant physiology, growth and developing physiology). Szeged, JATEPress.

Darwin C. 1880. The power of movement in plants, chapter ix sensitiveness of plants to light: Its transmitted effects. London, John Murray.

Dennis PG, Hirsch PR, Smith SJ, Taylor RG, Valsami-Jones E, Miller AJ. 2009. Linking rhizoplane pH and bacterial density at the microhabitat scale. *J. Microbiol. Methods* **76**: 101-104

Döring O, Busch M, Lüthje S, Lüthen H, Hilgendorf F, Böttger M. 1996. Ionostats. *Protoplasma* **194**: 1-10.

Duby G, Boutry M. 2009. The plant plasma membrane proton pump ATPase: A highly regulated P-type ATPase with multiple physiological roles. *European J. Physiol.* **457**: 645-655.

DuPont FM. 1989. Effect of temperature on the plasma membrane and tonoplast ATPases of barley roots : Comparison of results obtained with acridine orange and quinacrine. *Plant Physiol.* **89**: 1401-1412.

Ehlert C, Plassard C, Cookson SJ, Tardieu F, Simonneau T. 2011. Do pH changes in the leaf apoplast contribute to rapid inhibition of leaf elongation rate by water stress? Comparison of stress responses induced by polyethylene glycol and down-regulation of root hydraulic conductivity. *Plant Cell Environ.* **34**: 1258-1266.

Epstein E, Rains DW, Elzam OE. 1963. Resolution of dual mechanisms of potassium absorption by barley roots. *PNAS* **49**: 684-692.

Felle HH. 2005. pH regulation in anoxic plants. *Annals Bot.* **96**: 519-532.

Felle HH. 2006. Apoplastic pH during low-oxygen stress in barley. *Annals Bot.* **98**: 1085-1093.

Felle HH, Herrmann A, Huckelhoven R, Kogel KH. 2005. Root-to-shoot signalling: Apoplastic alkalinization, a general stress response and defence factor in barley (*Hordeum vulgare*). *Protoplasma* **227**: 17-24.

Fleurat-Lessard P, Bouche-Pillon S, Leloup C, Bonnemain JL. 1997. Distribution and activity of the plasma membrane H^+-ATPase in *Mimosa pudica* L in relation to ionic fluxes and leaf movements. *Plant Physiol.* **113**: 747-754.

Frensch J. 1997. Primary responses of root and leaf elongation to water deficits in the atmosphere and soil solution. *J. Exp. Bot.* **48**: 985-999.

Fricke W. 2002a. Biophysical limitation of cell elongation in cereal leaves. *Annals Bot.* **90**: 157-167.

Fricke W. 2002b. Biophysical limitation of leaf cell elongation in source-reduced barley. *Planta* **215**: 327-338.

Fricke W. 2004. Rapid and tissue-specific accumulation of solutes in the growth zone of barley leaves in response to salinity. *Planta* **219**: 515.

Fricke W, Akhiyarova G, Veselov D, Kudoyarova G. 2004. Rapid and tissue-specific changes in ABA and in growth rate in response to salinity in barley leaves. *J. Exp. Bot.* **55**: 1115-1123.

Fricke W, Flowers TJ. 1998. Control of leaf cell elongation in barley. Generation rates of osmotic pressure and turgor, and growth-associated water potential gradients. *Planta* **206**: 53-65.

Fricke W, Leigh RA, Tomos AD. 1994. Concentrations of inorganic and organic solutes in extracts from invidual epidermal, mesophyll and bundle-sheath cells of barley leaves. *Planta* **192**: 310-316.

Fricke W, McDonald AJS, Mattson-Djos L. 1997. Why do leaves and leaf cells of N-limited barley elongate at reduced rates? *Planta* **202**: 522-530.

Fricke W, Peters WS. 2002. The biophysics of leaf growth in salt-stressed barley. A study at the cell level. *Plant Physiol.* **129**: 374-388.

Gaxiola RA, Palmgren MG, Schumacher K. 2007. Plant proton pumps. *FEBS Letters* **581**: 2204-2214.

Glass ADM, Siddiqi MY, Giles KI. 1981. Correlations between potassium uptake and hydrogen efflux in barley varieties : A potential screening method for the isolation of nutrient efficient lines. *Plant Physiol.* **68**: 457-459.

Graber ML, DiLillo DC, Friedman BL, Pastoriza-Munoz E. 1986. Characteristics of fluoroprobes for measuring intracellular pH. *Anal. Biochem.* **156**: 202-212.

Grebe M. 2005. Growth by auxin: When a weed needs acid. *Science* **310**: 60-61.

Green PB, Erickson RO, Buggy J. 1971. Metabolic and physical control of cell elongation rate: In vivo studies in nitella. *Plant Physiol.* **47**: 423-430.

Grignon C, Sentenac H. 1991. pH and ionic conditions in the apoplast. *Ann. Rev. Plant Physiol. Plant Mol. Biol.* **42**: 103-128.

Hachez C, Heinen RB, Draye X, Chaumont F. 2008. The expression pattern of plasma membrane aquaporins in maize leaf highlights their role in hydraulic regulation. *Plant Mol. Biol.* **68**: 337-353.

Hager A. 2003. Role of the plasma membrane H^+-ATPase in auxin-induced elongation growth: Historical and new aspects. *J. Plant Res.* **116**: 483-505.

Hager A, Debus G, Edel HG, Stransky H, Serrano R. 1991. Auxin induces exocytosis and the rapid synthesis of a high-turnover pool of plasma-membrane H^+-ATPase. *Planta* **185**: 527-537.

Hager A, Menzel H, Krauss A. 1971. Experiments and hypothesis concerning primary action of auxin in elongation growth. *Planta* **100**: 47-71.

Hatzig S, Hanstein S, Schubert S. 2010. Apoplast acidification is not a necessary determinant for the resistance of maize in the first phase of salt stress. *J. Plant Nut. Soil Sci.* **173**: 559-562.

Hohl M, Hong YN, Schopfer P. 1991. Acid- and enzyme-mediated solubilization of cell-wall β-1.3,β-1.4-D-glucan in maize coleoptiles : Implications for auxin-mediated growth. *Plant Physiol.* **95**: 1012-1018.

Hoopen FT, Cuin TA, Pedas P, Hegelund JN, Shabala S, Schjoerring JK, Jahn TP. 2010. Competition between uptake of ammonium and potassium in barley and *Arabidopsis* roots: Molecular mechanisms and physiological consequences. *J. Exp. Bot.* **61**: 2303-2315.

Hruz T, Wyss M, Docquier M, Pfaffl M, Masanetz S, Borghi L, Verbrugghe P, Kalaydjieva L, Bleuler S, Laule O, Descombes P, Gruissem W, Zimmermann P. 2011. Refgenes: Identification of reliable and condition specific reference genes for RT-qPCR data normalization. *BMC Genomics* **12**: 156.

Hsiao TC, Frensch J, Rojas-Lara BA. 1998. The pressure-jump technique shows maize leaf growth to be enhanced by increases in turgor only when water status is not too high. *Plant, Cell Environ.* **21**: 33-42.

Hsiao TC, Xu LK. 2000. Sensitivity of growth of roots versus leaves to water stress: Biophysical analysis and relation to water transport. *J. Exp. Bot.* **51**: 1595-1616.

Hynek R, Svensson B, Jensen ONr, Barkholt V, Finnie C. 2006. Enrichment and identification of integral membrane proteins from barley aleurone layers by reversed-phase chromatography, SDS-PAGE, and LC-MS/MS. *J. Proteome Res.* **5**: 3105-3113.

Johansson F, Sommarin M, Larsson C. 1993. Fusicoccin activates the plasma-membrane H^+-ATPase by a mechanism involving the c-terminal inhibitory domain. *Plant Cell* **5**: 321-327.

Katsumi M. 2007. Studies on plant growth substances in japan before 1945. *Plant Biotech.* **24**: 155-163.

Kavanagh CA. 2010. Changes in cell ultrastructure during leaf development in barley (*Hordeum vulgare* L.) and in response to salinity*. MSc Thesis*, University College Dublin, Dublin.

Keller CP, Van Volkenburgh E. 1998. Evidence that auxin-induced growth of tobacco leaf tissues does not involve cell wall acidification. *Plant Physiol.* **118**: 557-564.

Kim S, Dale BE. 2004. Global potential bioethanol production from wasted crops and crop residues. *Biomass and Bioenergy* **26**: 361-375.

Kjellbom P, Larsson C. 1984. Preparation and polypeptide composition of chlorophyll-free plasma-membranes from leaves of light-grown spinach and barley. *Physiol. Plant.* **62**: 501-509.

Knipfer T, Fricke W. 2011. Water uptake by seminal and adventitious roots in relation to whole-plant water flow in barley (*Hordeum vulgare* L.). *J. Exp. Bot.* **62**: 717-733.

Kronzucker HJ, Szczerba MW, Britto DT. 2003. Cytosolic potassium homeostasis revisited: ^{42}K-tracer analysis in *Hordeum vulgare* L. Reveals set-point variations in K^+. *Planta* **217**: 540-546.

Kruger N 2002. The Bradford method for protein quantitation. *The protein protocols handbook*, **15:** (4) 15-21.

Kutschera U. 1994. Tansley review no. 66. The current status of the acid-growth hypothesis. *New Phytol.* **126**: 549-569.

Kutschera U. 2006. Acid growth and plant development. *Science* **311**: 952-954.

Kutschera U, Bergfeld R, Schopfer P. 1987. Cooperation of epidermis and inner tissues in auxin-mediated growth of maize coleoptiles. *Planta* **170**: 168-180.

Kutschera U, Schopfer P. 1985a. Evidence against the acid-growth theory of auxin action. *Planta* **163**: 483-493.

Kutschera U, Schopfer P. 1985b. Evidence for the acid-growth theory of fusicoccin action. *Planta* **163**: 494-499.

Laemmli UK. 1970. Cleavage of structural proteins during the assembly of the head of bacteriophage T4. *Nature* **227**: 680-685.

Larkin PJ. 1976. Purification and viability determinations of plant protoplasts. *Planta* **128**: 213-216.

Lenaeus MJ, Vamvouka M, Focia PJ, Gross A. 2005. Structural basis of TEA blockade in a model potassium channel. *Nature Struct. Mol. Biol.* **12**: 454-459.

Li L, Li S-M, Sun J-H, Zhou L-L, Bao X-G, Zhang H-G, Zhang F-S. 2007. Diversity enhances agricultural productivity via rhizosphere phosphorus facilitation on phosphorus-deficient soils. *PNAS* **104**: 11192-11196.

Lockhart JA. 1965. An analysis of irreversible plant cell elongation. *J Theor. Biol.* **8**: 264-275.

Lüthen H, Bigdon M, Böttger M. 1990. Reexamination of the acid growth theory of auxin action. *Plant Physiol.* **93**: 931-939.

Lüthen H, Böttger M. 1988. Kinetics of proton secretion and growth in maize roots - action of various plant-growth effectors. *Plant Sci.* **54**: 37-43.

Maathuis FJM, Filatov V, Herzyk P, C. Krijger G, B. Axelsen K, Chen S, Green BJ, Li Y, Madagan KL, Sánchez-Fernández R, Forde BG, Palmgren MG, Rea PA, Williams LE, Sanders D, Amtmann A. 2003. Transcriptome analysis of root transporters reveals participation of multiple gene families in the response to cation stress. *Plant J.* **35**: 675-692.

Malnic G, Geibel JP. 2000. Cell pH and H^+ secretion by S3 segment of mammalian kidney: Role of H+-ATPase and Cl^-. .*J. Membr. Biol.* **178**: 115-125.

Manente S, Pieri SD, Iero A, Rigo C, Bragadin M. 2008. A comparison between the responses of neutral red and acridine orange: Acridine orange should be preferential and alternative to neutral red as a dye for the monitoring of contaminants by means of biological sensors. *Anal. Biochem.* **383**: 316-319.

Marré E. 1979. Fusicoccin - tool in plant physiology. *Ann. Rev. Plant Physiol. Plant Mol. Biol.* **30**: 273-288.

Martre P, Bogeat-Triboulot M-B, Durand J-L. 1999. Measurement of a growth-induced water potential gradient in tall fescue leaves. *New Phytol.* **142**: 435-439.

McQueen-Mason S, Durachko DM, Cosgrove DJ. 1992. Two endogenous proteins that induce cell wall extension in plants. *Plant Cell* **4**: 1425-1433.

McQueen-Mason SJ. 1995. Expansins and cell wall expansion. *J. Exp. Bot.* **46**: 1639-1650.

Michelet B, Boutry M. 1995. The plasma membrane H^+-ATPase: A highly regulated enzyme with multiple physiological functions. *Plant Physiol.* **108**: 1-6.

Miller AJ, Smith SJ. 1992. The mechanism of nitrate transport across the tonoplast of barley root cells. *Planta* **187**: 554-557.

Mito N, Wimmers LE, Bennett AB. 1996. Sugar regulates mrna abundance of h^+-atpase gene family members in tomato. *Plant Physiol.* **112**: 1229-1236.

Moloney MM, Elliott MC, Cleland RE. 1981. Acid growth effects in maize roots - evidence for a link between auxin-economy and proton extrusion in the control of root-growth. *Planta* **152**: 285-291.

Moran N. 2007. Osmoregulation of leaf motor cells. *FEBS Letters* **581**: 2337-2347.

Morsomme P, Boutry M. 2000. The plant plasma membrane H^+-ATPase: Structure, function and regulation. *BBA – Biomembr.* **1465**: 1-16.

Morth JP, Pedersen BP, Buch-Pedersen MJ, Andersen JP, Vilsen B, Palmgren MG, Nissen P. 2011. A structural overview of the plasma membrane Na^+,K^+-ATPase and H^+-ATPase ion pumps. *Nature Rev. Mol. Cell. Biol.* **12**: 60-70.

Neumann PM. 1993. Rapid and reversible modifications of extension capacity of cell walls in elongating maize leaf tissues responding to root addition and removal of NaCl. *Plant, Cell Environ.* **16**: 1107-1114.

Neves-Piestun BG, Bernstein N. 2001. Salinity-induced inhibition of leaf elongation in maize is not mediated by changes in cell wall acidification capacity. *Plant Physiol.* **125**: 1419-1428.

O'Neal ME, Landis DA, Isaacs R. 2002. An inexpensive, accurate method for measuring leaf area and defoliation through digital image analysis. *J. Econ. Entom.* **95**: 1190-1194.

Oecking C, Eckerskorn C, Weiler EW. 1994. The fusicoccin receptor of plants is a member of the 14-3-3-superfamily of eukaryotic regulatory proteins. *FEBS Letters* **352**: 163-166.

Olivari C, Meanti C, De Michelis MI, Rasi-Caldogno F. 1998. Fusicoccin binding to its plasma membrane receptor and the activation of the plasma membrane H^+-ATPase. IV. Fusicoccin induces the association between the plasma membrane H^+-ATPase and the fusicoccin receptor. *Plant Physiol.* **116**: 529-537.

Paál Á. 1918. Über phototropsche Reizleitungen. *Jehrb. wiss. Bot.* **58**: 406-458.

Palmgren MG. 1991. Acridine-orange as a probe for measuring pH gradients across membranes - mechanism and limitations. *Anal. Biochem.* **192**: 316-321.

Palmgren MG. 2001. Plant plasma membrane H^+-ATPases: Powerhouses for nutrient uptake. *Ann. Rev. Plant Physiol. Plant Mol. Biol.* **52**: 817-845.

Palmgren MG, Sommarin M, Serrano R, Larsson C. 1991. Identification of an autoinhibitory domain in the C-terminal region of the plant plasma membrane H^+-ATPase. *J. Biol. Chem.* **266**: 20470-20475.

Pedersen BP, Buch-Pedersen MJ, Morth JP, Palmgren MG, Nissen P. 2007. Crystal structure of the plasma membrane proton pump. *Nature* **450**: 1111-1119.

Perrot-Rechenmann C. 2010. Cellular responses to auxin: Division versus expansion. *Cold Spring Harbor Persp. Biol.* **2**: a001446; 1-15.

Peters WS. 2004. Growth rate gradients and extracellular pH in roots: How to control an explosion. *New Phytol.* **162**: 571-574.

Peters WS, Felle HH. 1999. The correlation of profiles of surface pH and elongation growth in maize roots. *Plant Physiol.* **121**: 905-912.

Peters WS, Luthen H, Bottger M, Felle H. 1998. The temporal correlation of changes in apoplast pH and growth rate in maize coleoptile segments. *Austr. J. Plant Physiol.* **25**: 21-25.

Peters WS, Richter U, Felle HH. 1992. Auxin-induced H^+-pump stimulation does not depend on the presence of epidermal-cells in corn coleoptiles. *Planta* **186**: 313-316.

Pfaffl MW. 2001. A new mathematical model for relative quantification in real-time RT-PCR. *Nucl. Acids Res.* **29**: e45.

Philippar K, Büchsenschütz K, Edwards D, Löffler J, Lüthen H, Kranz E, Edwards K, Hedrich R. 2006. The auxin-induced k^+ channel gene *ZMK1* in maize functions in coleoptile growth and is required for embryo development. *Plant Mol. Biol.* **61**: 757-768.

Philippar K, Fuchs I, Lüthen H, Hoth S, Bauer CS, Haga K, Thiel G, Ljung K, Sandberg G, Böttger M, Becker D, Hedrich R. 1999. Auxin-induced K^+ channel expression represents an essential step in coleoptile growth and gravitropism. *PNAS* **96**: 12186-12191.

Philippar K, Ivashikina N, Ache P, Christian M, Lüthen H, Palme K, Hedrich R. 2004. Auxin activates KAT1 and KAT2, two K^+-channel genes expressed in seedlings of *Arabidopsis thaliana*. *Plant J.* **37**: 815-827.

Pitann B, Kranz T, Muhling KH. 2009a. The apoplastic pH and its significance in adaptation to salinity in maize (*Zea mays* L.): Comparison of fluorescence microscopy and ph-sensitive microelectrodes. *Plant Sci.* **176**: 497-504.

Pitann B, Schubert S, Muhling KH. 2009b. Decline in leaf growth under salt stress is due to an inhibition of H+-pumping activity and increase in apoplastic pH of maize leaves. *J. Plant Nutr. Soil Sci.* **172**: 535-543.

Pollock CJ, Tomos AD, Thomas A, Smith CJ, Lloyd EJ, Stoddart JL. 1990. Extension growth in a barley mutant with reduced sensitivity to low-temperature. *New Phytol.* **115**: 617-623.

Pope AJ, Leigh RA. 1988. Dissipation of ph gradients in tonoplast vesicles and liposomes by mixtures of acridine orange and anions: Implications for the use of acridine orange as a pH probe. *Plant Physiol.* **86**: 1315-1322.

Pritchard J. 1994. The control of cell expansion in roots. *New Phytol.* **127**: 3-26.

Rayle DL. 1973. Auxin-induced hydrogen-ion secretion in avena coleoptiles and its implications. *Planta* **114**: 63-73.

Rayle DL, Cleland R. 1970. Enhancement of wall loosening and elongation by acid solutions. *Plant Physiol.* **46**: 250-253.

Rayle DL, Cleland RE. 1992. The acid growth theory of auxin-induced cell elongation is alive and well. *Plant Physiol.* **99**: 1271-1274.

Reidy B, McQueen-Mason S, Nösberger J, Fleming A. 2001. Differential expression of α- and β-expansin genes in the elongating leaf of festuca pratensis. *Plant Mol. Biol.* **46**: 491-504.

Richardson A, Wojciechowski T, Franke R, Schreiber L, Kerstiens G, Jarvis M, Fricke W. 2007. Cuticular permeance in relation to wax and cutin development along the growing barley (*Hordeum vulgare*) leaf. *Planta* **225**: 1471-1481.

Rodriguez-Navarro A, Rubio F. 2006. High-affinity potassium and sodium transport systems in plants. *J. Exp. Bot.* **57**: 1149-1160.

Rubio F, Santa-María GE, Rodríguez-Navarro A. 2000. Cloning of *Arabidopsis* and barley cDNAs encoding HAK potassium transporters in root and shoot cells. *Physiol. Plant.* **109**: 34-43.

Sabirzhanova IB, Sabirzhanov BE, Chemeris AV, Veselov DS, Kudoyarova GR. 2005. Fast changes in expression of expansin gene and leaf extensibility in osmotically stressed maize plants. *Plant Physiol. Biochem.* **43**: 419-422.

Sakurai N, Masuda Y. 1978. Auxin-induced changes in barley coleoptile cell-wall composition. *Plant Cell Physiol.* **19**: 1217-1223.

Santi S, Cesco S, Varanini Z, Pinton R. 2005. Two plasma membrane H^+-ATPase genes are differentially expressed in iron-deficient cucumber plants. *Plant Physiol. Biochem.* **43**: 287-292.

Sarkadi B, Price EM, Boucher RC, Germann UA, Scarborough GA. 1992. Expression of the human multidrug resistance cdna in insect cells generates a high-activity drug-stimulated membrane ATPase. *J. Biol. Chem.* **267**: 4854-4858.

Schopfer P. 1989. pH-dependence of extension growth in *Avena*-coleopiles and its implications for the mechanism of auxin action. *Plant Physiol.* **90**: 202-207.

Schulte D, Close TJ, Graner A, Langridge P, Matsumoto T, Muehlbauer G, Sato K, Schulman AH, Waugh R, Wise RP, Stein N. 2009. The international barley sequencing consortium - At the threshold of efficient access to the barley genome. *Plant Physiol.* **149**: 142-147.

Senn ME, Rubio F, Bañuelos MA, Rodríguez-Navarro A. 2001. Comparative functional features of plant potassium hvhak1 and hvhak2 transporters. *J. Biol. Chem.* **276**: 44563-44569.

Shen H, He LF, Sasaki T, Yamamoto Y, Zheng SJ, Ligaba A, Yan XL, Ahn SJ, Yamaguchi M, Sasakawa H, Matsumoto H. 2005. Citrate secretion coupled with the modulation of soybean root tip under aluminum stress. Up-regulation of transcription, translation, and threonine-oriented phosphorylation of plasma membrane H^+-ATPase. *Plant Physiol.* **138**: 287-296.

Slayman CL. 1965. Electrical properties of *Neurospora crassa*. *J. General Physiol.* **49**: 69-92.

Spalding EP, Hirsch RE, Lewis DR, Qi Z, Sussman MR, Lewis BD. 1999. Potassium uptake supporting plant growth in the absence of AKT1 channel activity: Inhibition by ammonium and stimulation by sodium. *J. Gen. Physiol.* **113**: 909-918.

Speth C, Jaspert N, Marcon C, Oecking C. 2010. Regulation of the plant plasma membrane H^+-ATPase by its c-terminal domain: What do we know for sure? *European J. Cell Biol.* **89**: 145-151.

Stahlberg R, Van Volkenburgh E. 1999. The effect of light on membrane potential, apoplastic pH and cell expansion in leaves of *Pisum sativum* L. var. Argenteum. - role of the plasma-membrane H^+-ATPase and photosynthesis. *Planta* **208**: 188-195.

Steudle E. 2000. Water uptake by roots: Effects of water deficit. *J. Exp. Bot.* **51**: 1531-1542.

Stiles K, McClintick A, Volkenburgh E. 2003. A developmental gradient in the mechanism of K^+ uptake during light-stimulated leaf growth in *Nicotiana tabacum* L. *Planta* **217**: 587-596.

Stiles KA, Van Volkenburgh E 2004. Role of K^+ in leaf growth: K^+ uptake is required for light-stimulated H^+ efflux but not solute accumulation. *Plant, Cell Environ***. 27:** 315-325.

Stoddart JL, Lloyd EJ. 1986. Modification by gibberellin of the growth-temperature relationship in mutant and normal genotypes of several cereals. *Planta* **167**: 364-368.

Szczerba MW, Britto DT, Kronzucker HJ. 2006. Rapid, futile K^+ cycling and pool-size dynamics define low-affinity potassium transport in barley. *Plant Physiol.* **141**: 1494-1507.

Szczerba MW, Britto DT, Kronzucker HJ. 2009. K^+ transport in plants: Physiology and molecular biology. *J. Plant Physiol.* **166**: 447-466.

Sze H, Li X, Palmgren MG. 1999. Energization of plant cell membranes by H+-pumping ATPases: Regulation and biosynthesis. *Plant Cell* **11**: 677-690.

Tang AC, Boyer JS. 2008. Xylem tension affects growth-induced water potential and daily elongation of maize leaves. *J. Exp. Bot.* **59**: 753-764.

Tang C, Drevon JJ, Jaillard B, Souche G, Hinsinger P. 2004. Proton release of two genotypes of bean (*Phaseolus vulgaris* L.) as affected by N nutrition and P deficiency. *Plant Soil* **260**: 59-68.

Taylor G, Davies WJ. 1985. The control of leaf growth of betula and acer by photoenvironment. *New Phytol.* **101**: 259-268.

Tode K, Lüthen H. 2001. Fusicoccin- and IAA-induced elongation growth share the same pattern of K^+ dependence. *J. Exp. Bot.* **52**: 251-255.

Ullrich CI, Novacky AJ. 1990. Extracellular and intracellular ph and membrane-potential changes induced by K^+, Cl^-, $H_2PO_4^-$, and NO_3^- uptake and fusicoccin in root hairs of limnobium-stoloniferum. *Plant Physiol.* **94**: 1561-1567.

Van Volkenburgh E, Boyer JS. 1985. Inhibitory effects of water deficit on maize leaf elongation. *Plant Physiol.* **77**: 190-194.

Van Volkenburgh E, Cleland RE. 1980. Proton excretion and cell expansion in bean *Phaseolus vulgaris* leaves. *Planta* **148**: 273-278.

Vera-Estrella R, Barkla BJ, Higgins VJ, Blumwald E. 1994. Plant defense response to fungal pathogens (activation of host-plasma membrane H^+-ATPase by elicitor-induced enzyme dephosphorylation). *Plant Physiol.* **104**: 209-215.

Vesper MJ, Evans ML. 1979. Nonhormonal induction of H^+ efflux from plant tissues and its correlation with growth. *PNAS* **76**: 6366-6370.

Villalba JM, Lützelschwab M, Serrano R. 1991. Immunocytolocalization of plasma-membrane H^+-ATPase in maize coleoptiles and enclosed leaves. *Planta* **185**: 458-461.

Vogelstein B, Kinzler KW. 1999. Digital PCR. *PNAS* **96**: 9236-9241.

Volkov V, Boscari A, Clément M, Miller AJ, Amtmann A, Fricke W. 2009. Electrophysiological characterization of pathways for K^+ uptake into growing and non-growing leaf cells of barley. *Plant, Cell Environ.* **32**: 1778-1790.

Volkov V, Hachez C, Moshelion M, Draye X, Chaumont F, Fricke W. 2007. Water permeability differs between growing and non-growing barley leaf tissues. .*J. Exp. Bot.* **58**: 377-390.

Vysotskaya LB, Arkhipova TN, Timergalina LN, Veselov SY, Dedov AV, Kudoyarova GR. 2003. Effect of partial root excision on shoot water relations. *J. Plant Physiol.* **160**: 1011-1015.

Wakeel A, Hanstein S, Pitann B, Schubert S. 2010. Hydrolytic and pumping activity of H+-ATPase from leaves of sugar beet (*Beta vulgaris* L.) as affected by salt stress. *J. Plant Physiol.* **167**: 725-731.

Wei WX, Alexandersson E, Golldack D, Miller AJ, Kjellborn PO, Fricke W. 2007. HvPIP1;6, a barley (*Hordeum vulgare* L.) plasma membrane water channel particularly expressed in growing compared with non-growing leaf tissues. *Plant Cell Physiol.* **48**: 1132-1147.

Wieczorek H, Putzenlechner M, Zeiske W, Klein U. 1991. A vacuolar-type proton pump energizes K^+ / H^+ antiport in an animal plasma-membrane. *J. Biol. Chem.* **266**: 15340-15347.

Würtele M, Jelich-Ottmann C, Wittinghofer A, Oecking C. 2003. Structural view of a fungal toxin acting on a 14-3-3 regulatory complex. *EMBO J.* **22**: 987-994.

Yan F, Feuerle R, Schaffer S, Fortmeier H, Schubert S. 1998. Adaptation of active proton pumping and plasmalemma ATPase activity of corn roots to low root medium pH. *Plant Physiol.* **117**: 311-319.

Yan F, Zhu Y, Muller C, Zorb C, Schubert S. 2002. Adaptation of H^+-pumping and plasma membrane H^+ ATPase activity in proteoid roots of white lupin under phosphate deficiency. *Plant Physiol.* **129**: 50-63.

Zhu Y, Tingjun DI, Guohua XU, Xi C, Houqing Z, Feng YAN, Qirong S. 2009. Adaptation of plasma membrane H^+-ATPase of rice roots to low pH as related to ammonium nutrition. *Plant, Cell Environ.* **32**: 1428-1440.

Zoccarato F, Cavallini L, Alexandre A. 1999. The pH-sensitive dye acridine orange as a tool to monitorexocytosis/endocytosis in synaptosomes. *J. Neurochem.* **72**: 625-633.

Zörb C, Stracke B, Tramnitz B, Denter D, Sümer A, Mühling KH, Yan F, Schubert S. 2005. Does H^+ pumping by plasmalemma ATPase limit leaf growth of maize *Zea mays* during the first phase of salt stress? *J. Plant Nutr. Soil Sci.* **168**: 550-557.

7 Appendix

7.1 Processing of qPCR data

(i) Total cell volume was considered to equal the total water content of plant tissue (neglecting any water in intercellular space). The water content was calculated from the fresh weight of the samples:

$$m_w = m_{FW} \cdot w_{\%} \text{ [g]}$$

$$V_{cell} = m_w \cdot 10^{12} \text{ [µm}^3\text{]}$$

where: m_w: amount of water in the tissue (g); m_{FW}: fresh weight of tissue (g) and $w_{\%}$: percentage water content of the tissue, $100 \cdot \left(\frac{m_{FW} - m_{DW}}{m_{FW}} \right)$; m_{DW}, dry weight); V_{cell}: total cell volume (µm^3).

(ii) From water content, from the proportion of leaf volume occupied by epidermis (0.26) and mesophyll (0.646) and from the cell sizes (99,372 µm^3 for epidermis cells in elongation zone; 461,552 µm^3 for epidermis cells in emerged blade; 6,620 µm^3 for mesophyll cells in elongation zone and 14,830 for mesophyll cells in emerged leaf blade) the number of epidermal cells, mesophyll cells and total number of the cells were calculated:

Elongation zone: $N_{Epcell} = \frac{V_{cell} \cdot 0.260}{99{,}372}$; $N_{Mcell} = \frac{V_{cell} \cdot 0.646}{6{,}620}$ [piece]

Emerged Blade: $N_{Epcell} = \frac{V_{cell} \cdot 0.296}{461{,}552}$; $N_{Mcell} = \frac{V_{cell} \cdot 0.653}{14{,}830}$ [piece]

Total cell number: $N_{cell} = N_{Epcell} + N_{Mcell}$ [piece]

where: N_{Epcell}: number of epidermal cells; N_{Mcell}: number of mesophyll cells and N_{cell}: total cell number.

(iii) Plasma membrane surface was calculated as:

Elongation zone: $A = N_{Epcell} \cdot 19{,}704 + N_{Mcell} \cdot 1{,}632$ [µm^2]

Emerge blade: $A = N_{Epcell} \cdot 50{,}004 + N_{Mcell} \cdot 2{,}855$ [µm^2]

where: A: plasma membrane surface of the sample (µm^2).

(iv) Calculation of the PM-H$^+$-ATPase copy number in the sample was carried out with the help of calibration curve using PM-H$^+$-ATPase DNA standard. This calibration curve was different for each qPCR measurement. An example of this calculation may be found in Fig. 7.1.

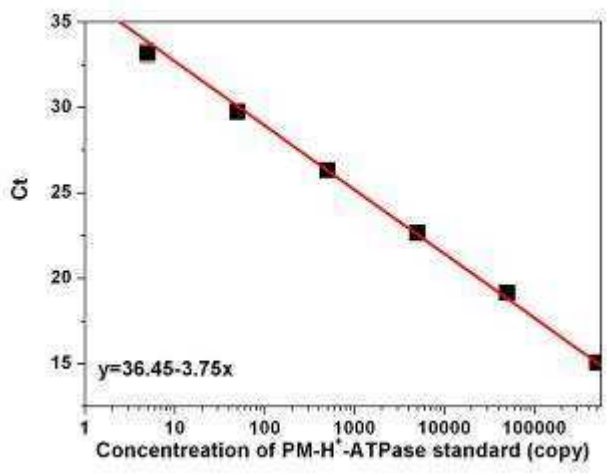

Figure 7.1 Typical calibration curve for converting Ct values into transcript copy number

For calibration three replicates were used and r^2 of the fitted line was always higher than 0.98.

From the calibration curve Ct values were converted into copy number of PM-H$^+$-ATPase transcript. For example, using the above calibration curve resulted in the following:

$$N_{PM-H^+-ATPase} = 10^{\frac{36.45-\overline{Ct}}{3.75}} \text{ [copy]}$$

where: $N_{PM-H^+-ATPase}$: copy number of PM-H$^+$-ATPase in the PCR sample (typically 250 pg); $\overline{Ct}$: average Ct values of 3 technical replicates.

(v) From the copy number of PCR reaction the total copy number in 1 μg RNA could easily be calculated through multiplying the results with respective dilution factors; these were typically 4,000 using 250 pg template in each reaction:

$$N_{copy1\mu g} = N_{PM-H^+-ATPase} \cdot 4{,}000 \text{ [copy]}$$

where: $N_{copy1\mu g}$ is the PM-H$^+$-ATPase copy number in 1 μg RNA

(vi) The copy number of transcript in 1 μg RNA could then be multiplied by the total RNA content of the leaf sample used for extraction of RNA:

$$N_{totalcopy} = N_{copy1\mu g} \cdot m_{RNA} \text{ [copy]}$$

where: $N_{totalcopy}$: the total PM-H^+-ATPase mRNA copy in the sample; m_{RNA} is amount of total RNA (μg) in the sample.

(vii) Finally, this total copy number of PM-H^+-ATPase transcripts could then be realted to the total number of cells or the total plasma membrane surface area in the leaf sample:

$$c_{copy \cdot cell^{-1}} = \frac{N_{totalcopy}}{N_{cell}} \text{ [copy cell}^{-1}\text{]}$$

$$c_{copy \cdot A^{-1}} = \frac{N_{totalcopy}}{A} \cdot 10^6 \text{ [copy mm}^{-2}\text{]}$$

where: $c_{copy \cdot cell^{-1}}$: PM-H^+-ATPase copy number in a single cell; $c_{copy \cdot A^{-1}}$: PM-H^+-ATPase copy number in 1 mm^2 plasma membrane.

Example for these calculations can be found on Table 7.1 for Golf and Table 7.2 for Jersey barley cultivar.

Table 7.1 Example for qPCR calculation of Golf cultivar. S1 - 3 label different batches

	Elongation zone			Emerged blade		
	S1	**S2**	**S3**	**S1**	**S2**	**S3**
Fresh weight (mg)	56.6	57.7	50.0	53.5	50.7	48.7
Water content (mg)	52.1	51.3	46.0	46.4	44.0	42.3
Number of epidermis cells (x 10^4)	13.6	13.4	12.0	2.98	2.82	2.71
Number of mesophyll cells (x 10^6)	5.08	5.00	4.49	2.04	1.94	1.86
Total number of cells (x 10^6)	5.22	5.14	4.61	2.07	1.97	1.87
Total membrane surface of epidermis cells (mm^2 x 10^3)	2.69	2.64	2.37	1.49	1.41	1.36
Total membrane surface of mesophyll cells (mm^2 x 10^3)	8.30	8.17	7.33	5.84	5.53	5.31
Total membrane surface of the sample (mm^2 x 10^3)	10.9	10.8	9.70	7.32	6.94	6.67
Total RNA in the sample (µg)	123	106	105	61.3	51.9	40.9
PM-H^+-ATPase copy in 1 µg RNA (x 10^6)	14.8	11.5	13.7	9.91	6.63	14.1
PM-H^+-ATPase copy in the sample (x 10^9)	1.83	1.21	1.43	0.607	0.344	0.577
PM-H^+-ATPase copy in a cell	350	236	312	293	175	306
PM-H^+-ATPase copy per mm^2 plasma membrane (x 10^4)	166	112	148	83.0	49.6	86.6

Table 7.2 Example for qPCR calculation of Jersey cultivar. S1 - 3 label different batches

	Elongation zone			Emerged blade		
	S1	**S2**	**S3**	**S1**	**S2**	**S3**
Fresh weight (mg)	69.2	57.6	58.7	77.1	74.9	62.2
Water content (mg)	64.9	54.0	55.1	68.5	66.5	55.2
Number of epidermis cells (x 10^4)	17.0	14.1	14.4	4.39	4.27	3.54
Number of mesophyll cells (x 10^6)	6.33	5.27	5.37	3.01	2.93	2.43
Total number of cells (x 10^6)	6.50	5.41	5.52	3.06	2.97	2.47
Total membrane surface of epidermis cells (mm^2 x 10^3)	3.35	2.79	2.84	2.20	2.13	1.77
Total membrane surface of mesophyll cells (mm^2 x 10^3)	10.3	8.60	8.77	8.61	8.36	6.94
Total membrane surface of the sample (mm^2 x 10^3)	13.7	11.4	11.6	10.8	10.5	8.71
Total RNA in the sample (µg)	161	119	121	24.7	108	26.8
PM-H^+-ATPase copy in 1 µg RNA (x 10^6)	5.90	4.76	4.45	4.52	4.13	5.56
PM-H^+-ATPase copy in the sample (x 10^9)	9.49	5.65	5.34	1.11	4.47	1.49
PM-H^+-ATPase copy in a cell	146	104	97	36	150	60
PM-H^+-ATPase copy per mm^2 plasma membrane (x 10^4)	6.94	4.97	4.60	1.03	4.26	1.71

Table 7.3 Example for qPCR calculation of Jersey protoplasts. S1 - 3 label different batches

	Elongation zone			Emerged blade		
	S1	**S2**	**S3**	**S1**	**S2**	**S3**
Protoplast No (x 10^6)	5.13	5.05	5.51	5.57	3.84	7.85
Surface (mm^2 x 10^{10})	8.37	8.24	9.00	1.59	1.10	2.24
Total RNA(□g)	26.5	28.2	37.9	31.6	29.2	65.3
PM-H^+-ATPase copy in 1 µg RNA (x 10^6)	5.34	3.95	7.02	3.09	2.06	5.60
PM-H^+-ATPase copy in the sample (x 10^7)	14.1	11.1	26.6	9.75	6.00	36.6
PM-H^+-ATPase copy in a cell	27.6	22.0	48.3	17.5	15.6	46.6
PM-H^+-ATPase copy in 1 mm^2 plasma membrane (x 10^4)	1.69	1.35	2.96	0.613	0.548	1.63

7.2 List of chemicals

$(NH_4)_2HPO_4$	M&B
5(6)carboxyfluorescein	Sigma
Acetic acid	Reanal, BDH
Acridine orange	BDH
Acylamide (C_3H_5NO)	Sigma-Aldrich
Agarose	Bioline
Ammonium molibdate	M&B
APS (ammonium persulfate; $(NH_4)_2S_2O_8$)	Sigma-Aldrich
APTES (3-aminopropyltriethoxysilane)	Sigma-Aldrich
Ascorbic acid	Szkarabeusz
ATP (adenosine 5′-triphosphate disodium salt hydrate)	Sigma
Bis acrylamide (N,N′-methylenebis(acrylamide), $C_7H_{10}N_2O_2$)	Sigma
BIS-TRIS propane ($CH_2[CH_2NHC(CH_2OH)_3]_2$)	Sigma
Boric acid	BDH
Brij^{TM}58	Sigma
Bromocresol purple	DIFCO
Bromophenol blue ($C_{19}H_{10}Br_4O_5S$)	Reanal
BSA (bovine serum albumin fraction V)	Sigma-Aldrich
$Ca(NO_3)_2x4H_2O$	Reanal, BDH
$CaCl_2$	Reanal, BDH
$CaSO_4$	BDH
Cellulase	Worthington
Coomassie brilliant blue R-250 ($C_{45}H_{44}N_3NaO_7S_2$)	Reanal
CsCl	Gibco BLR
$CuSO_4x5H_2O$	BDH
Dextran T-500	Sigma-Aldrich
Driselase	Sigma
DTT (dithiothreitol, $C_4H_{10}O_2S_2$)	Sigma, Fluka
EDTA	Reanal, BDH
Entellan®	Merck
Ethanol	Merck
Ethidium bromide	Sigma
Fe^{III}NaEDTA	BDH
Formalin	BDH

Fusicoccin	Sigma
Glycerol	Reanal, Fluka
Glycine	Reanal
H_2SO_4	Molar
H_3BO_3	BDH
HCl	BDH
HEPES ($C_8H_{18}N_2O_4S$)	Sigma
Hydrogen Ionophore II Cocktail A	Fluka
K_2HPO_4	Reanal, BDH
KCl	Reanal, BDH
KH_2PO_4	Reanal, BDH
KNO_3	Reanal, BDH
KOH	Reanal, BDH
MES (2-[N-morpholino]ethanesulfonic acid, $C_6H_{13}NO_4S$)	Sigma
Methanol	Reanal, BDH
$MgSO_4x7H_2O$	Reanal, BDH
$MnSO_4xH_2O$	BDH
MOPS (3-[N-morpholino]propanesulfonic acid, $C_7H_{15}NO_4S$)	Sigma
$Na_2HPO_4x2H_2O$	BDH
$Na_2MoO_4x2H_2O$	BDH
Na_3VO_4	Sigma
NAA (1-naphthaleneacetic acid, $C_{12}H_{10}O_2$)	Sigma
Na-ascorbate	Fluka
NaCl	BDH
$NaH_2PO_4x2H_2O$	BDH
NaN_3	Sigma
NaOH	BDH
Neo-clear®	Merck
$NH_4H_2PO_4$	M&B
Nitrocellulose	Sigma
Non soluble PVP (polyvinylpyrrolidone)	Serva
Paraffin wax	BDH
Pectolyase	Sigma
PEG-3350	Sigma
Phtalate buffer	Sigma

PMSF (phenylmethylsulfonyl fluoride, $C_7H_7FO_2S$)	Sigma
Potassium antimony (III) oxid tartrate	BDH
Potassium hydrogen phthalate ($KHC_8H_4O_4$)	Sigma-Aldrich
PVC (high molecular weight polyvinyl chloride)	Fluka
PVP K30 (polyvinylpyrrolidone)	Sigma
SDS (Sodium dodecyl sulfate, $CH_3(CH_2)_{11}OSO_3Na$)	Sigma
Sorbitol	Sigma
Sucrose ($C_{12}H_{22}O_{11}$)	Reanal, Sigma
TAPS (N-tris[Hydroxymethyl]methyl-3-amino-propanesulfonic acis)	Sigma
TEMED (*N*,*N*,*N*′,*N*′-tetramethylethylenediamine, $C_6H_{16}N_2$)	Fluka
THF (tetrahydrofuran, C_4H_8O)	Sigma-Aldrich
Toluidine blue	Sigma
TRIS (tris(hydroxymethyl)aminomethane, $NH_2C(CH_2OH)_3$)	Reanal, IBI
Triton®X-100	Reanal, Sigma
Tween®20	Sigma
$ZnCl_2$	BDH
β-mercapto ethanol ($HSCH_2CH_2OH$)	Sigma
α-Naphthaleneacetic acid (NAA)	Sigma